Geochemistry and Tectonic Setting of Some Proterozoic Rocks in the Pedernal Hills and Manzano Mountains, New Mexico

Christopher G. McKee

Sumitted in Partial Fulfillment
of the Requirements for the Degree of
Master of Science in Geology

New Mexico Institute of Mining and Technology

Socorro, New Mexico

January, 1988

ABSTRACT

Variably deformed, early Proterozoic successions of bimodal volcanic rocks and associated volcaniclastic sediments occur in the Pedernal Hills and in the Manzano Mountains, central New Mexico. The Manzano succession is in fault contact with a somewhat younger Proterozoic succession and the Pedernal succession appears to overlie a group of massive quartzites and mica schists.

Felsic volcanics and volcaniclastic sediments dominate in both successions and include ash flow tuffs and hypabyssal intrusives. Felsic units are calc-alkaline, range in composition from rhyodacite to high-silica rhyolite and are similar in trace element distributions to modern continental-arc felsic volcanics. They exhibt light-REE enriched patterns with negative Eu anomalies and show notable depletions in Sr, P, Ta, Nb, and Ti. Felsic magmas can be produced by two-stage fractional crystallization of an andesitic parent. Andesites and basalts are minor in abundance and are chiefly tuffs and breccias with some dikes and sills. Geochemically, they include calc-alkaline (CAB) and tholeiitic (TH) groups. CAB are light-REE enriched (La/Yb = 6-10) with relatively high contents of high field strength elements (HFSE). TH have nearly flat REE patterns (La/Yb = 1-3) and exhibt low contents of HFSE. TH appear to have been derived from a depleted lherzolite source and CAB from an enriched

lherzolite source.

Data are consistent with a tectonic setting for this early Proterozoic volcanic association in a continental-margin arc system in which two mantle sources are available for basalt production. Central New Mexico appears to represent the southernmost exposure of this early Proterozoic arc association which underlies portions of northern New Mexico.

I would like to thank Dr. Kent Condie for suggesting this study and also for his help and support that made this project possible. The staff at Sandia National Laboratory Reactor and Paul Wieg helped greatly with the neutron activation analysis. Kathleen B. Faris is thanked for her help with the X-ray fluorescence analysis. Finally, I would like to thank all my collegues especailly G. Patrick Bowling, Mike N. B. Knoper, and Charles Ferguson, for their help and comments. The research was partially supported by NSF grant EAR 8313735.

TABLE OF CONTENTS

LIST OF TABLES

LIST OF FIGURES

INTRODUCTION

GENERAL STATEMENT

Early Proterozoic rocks are exposed in various mountain ranges and uplifts of the southwestern United States. Basically two assemblages are found in early Proterozoic terranes of the Southwest: a quarzite-schist assemblage commonly overlies, conformably or unconformably, a bimodal metavolcanic assemblage (Condie, 1982a and 1986). The bimodal assemblage is present throughout southern Colorado and extends south into central New Mexico (Boardman, 1976; Condie and Budding, 1979; Condie, 1980; Condie and Nuter, 1981; Roberston, 1981; and Condie and Shadel, 1984). Some terranes contain rocks having calc-alkaline characteristics such as the Gold Hill-Wheeler Peak area, New Mexico (Condie and McCrink, 1982), but most terranes are tholeiitic in character (Condie, 1982a). The quartzite-schist assemblage occurs in the Manzano Mountains, Pedernal Hills, and San Andres Mountains of central New Mexico (Stark, 1956; Condie and Budding, 1979; Grambling, 1982; Bauer, 1982a and 1982b; and Bauer and Williams, 1985) (Fig. 1).

Tectonic evolution of early Proterozoic terranes of the southwestern United States is open to interpretation. Both continental rift and arc models have been proposed (Silver, 1978; Condie and Budding, 1979; and Van Schmus and

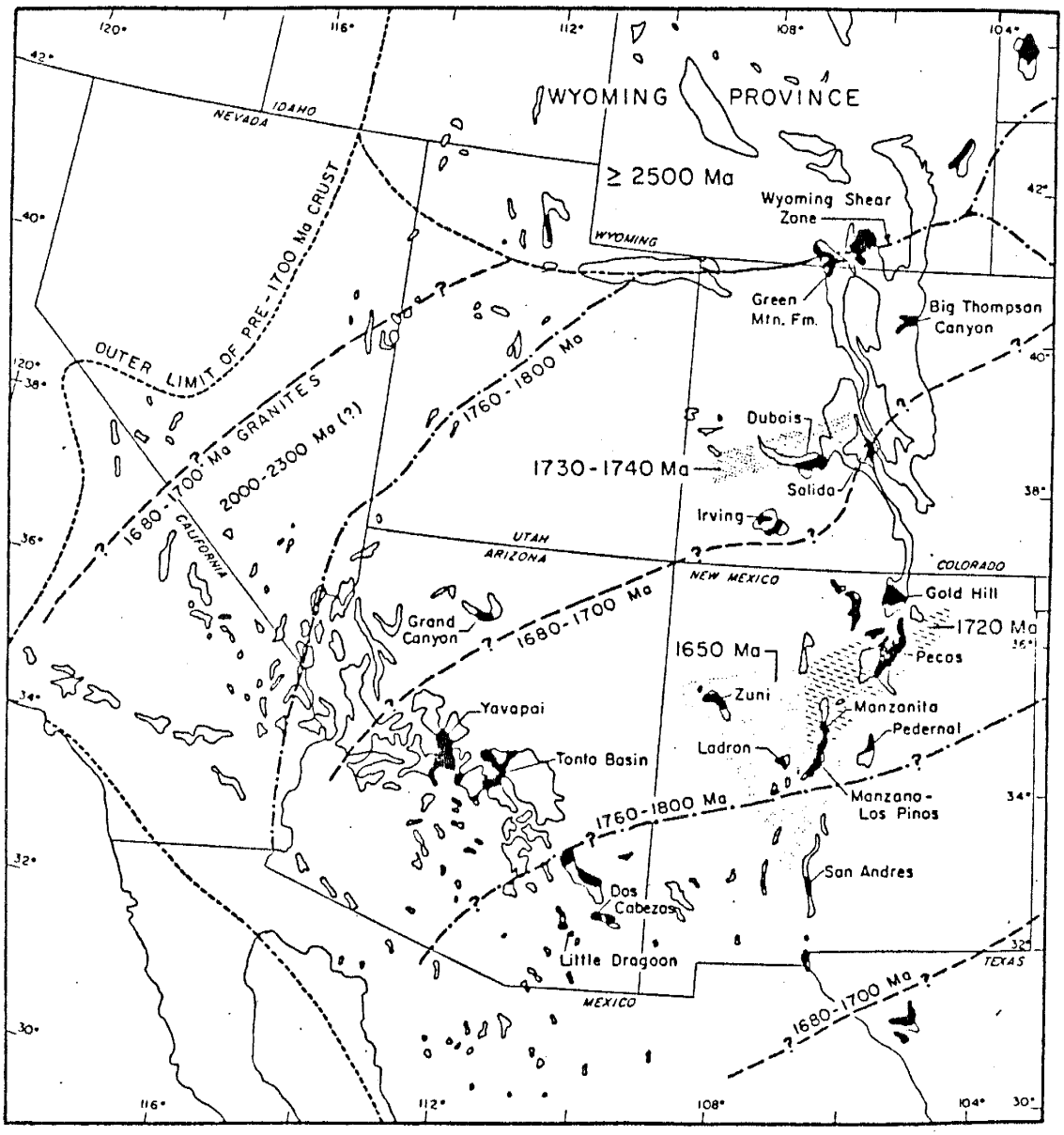

Figure 1. Map of age provinces for Precambrian supracrustal rocks of the Southwest (after Condie, 1986).

Bickford, 1981), but there are problems with both models. Continental rift models require older crust to act as basement, but isotopic data suggest that most of the Precambrian rocks in the Southwest formed around 1700-1800 Ma (DePaolo, 1981 and Stacey and Hedlund, 1983). However, there is no isotopic evidence for substantially older crust to act as a basement for rifting. The lack of calc-alkaline rocks, especially of intermediate composition, thick graywacke sequences, and blueschist metamorphic rocks are problems for arc models. A model combining elements of rift and arc models seems to accommodate most data (Condie, 1982a and 1986).

Proterozoic supracrustal rocks in the Southwest young southward from the Wyoming shear zone (Engel, 1963; Van Schmus and Bickford, 1981; Thomas, et al., 1984; and Nelson and DePaolo, 1985) and can be divided into five age provinces: 1760-1800 Ma, 1730-1740 Ma, 1720 Ma, 1680-1700 Ma, and 1650 Ma (Fig. 1: Condie, 1986). Two successions in the 1680-1700 Ma province were studied as part of a continuing investigation of Proterozoic rocks of Southwest. The two sections are located in central New Mexico: one area near the Pedernal Hills and the other area in the central Manzano Mountains (Fig. 2). The successions will be referred to as the Pedernal and the Manzano sections, respectively.

The early Proterozoic rocks in the southern Manzano Mountains have been interpreted as having formed in a

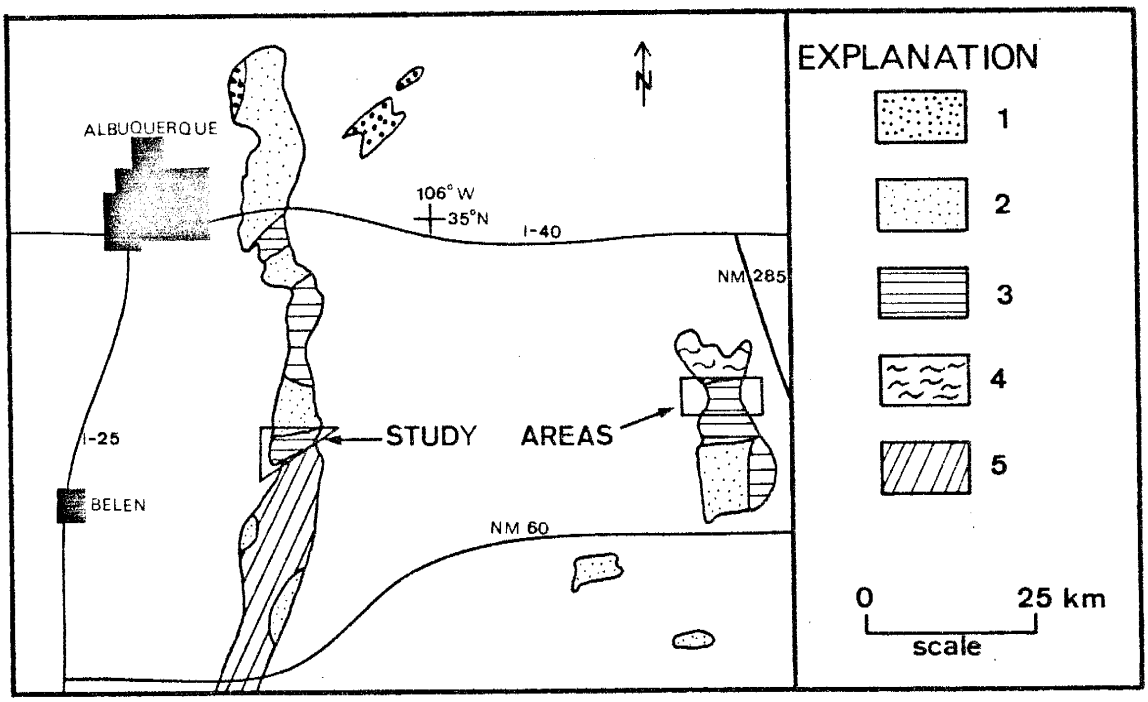

Figure 2. Map of exposed supracrustal rocks and granitoids of early to mid-Proterozoic age in central New Mexico. The two outlined areas are the two sections studied in this investigation. 1 is undifferentiated metamorphic rocks; 2, granitic rocks; 3, volcanic-dominated supracrustal rocks; 4, quartzite; and 5, sediment-dominated supracrustal rocks.

continental rift tectonic setting (Condie and Budding, 1979), but one problem with this model is the lack of exposed basement. The Manzano section was studied as the first step to asses the possiblity that it served as basement for the overlying proposed rift succession in the southern Manzanos. General geologic descriptions exist for the Manzano and Pedernal sections and structural data are avaible for the Pedernal Hills (Armstrong and Holcombe, 1982 and Bauer and Williams, 1985), but there is a lack of detailed geochemical work for either succession.

PURPOSE

The purpose of this study is divided into three parts. The first is to describe, both petrographically and geochemically, the rocks of the Pedernal and the Manzano sections in order to classify and characterize them. The second is to compare the two successions to Phanerozoic successions and discuss possible tectonic affinities for each section. Comparision will also be made to the early Proterozoic rocks of the southern Manzano Mountains. Finally, possible magma genesis models of the metavolcanic rocks will be presented and discussed.

LOCATION

The two sections are located in central New Mexico

(Fig. 2). The Manzano section occurs along the west flank of the central Manzano Mountains, just south of Bosque Peak and north of Comanche Canyon (Fig. 3). County gravel roads and roads built by Horizon Corporation provide access to the study area. The Manzano section is within the boundaries of the Manzano Wilderness Area.

The northern boundary of the Manzano section is the intrusive contact of the Ojita Pluton located on the northern edge of Encino Canyon, sections 7, 8, and 9 of T6N, R5E (Fig. 3). The western boundary is the limit of outcrops, sections 7 and 30 of T6N, R5E. The eastern boundary meets the western boundary at section 30 of T6N, R5E and continues northward to section 9 of T6N, R5E. Most of the eastern boundary is in contact with overlying Proterozoic rocks and the rest of the boundary is in contact with Paleozoic limestones.

The Pedernal section is located south of the Pedernal Hills in sections 28, 29, 32, and 33 of T7N, R12E (Fig. 4), on the Harral Ranch. Gravel and dirt roads on the Harral Ranch were used for access to the Pedernal section. The Harral Ranch is located approximately 12.5 miles north of Encino along State Highway 285. The northern boundary is defined by the contact with a thick Proterozoic quartzite-mica schist unit, the southern boundary by a change in structural style, and the eastern and western boundaries by the limits of outcrops.

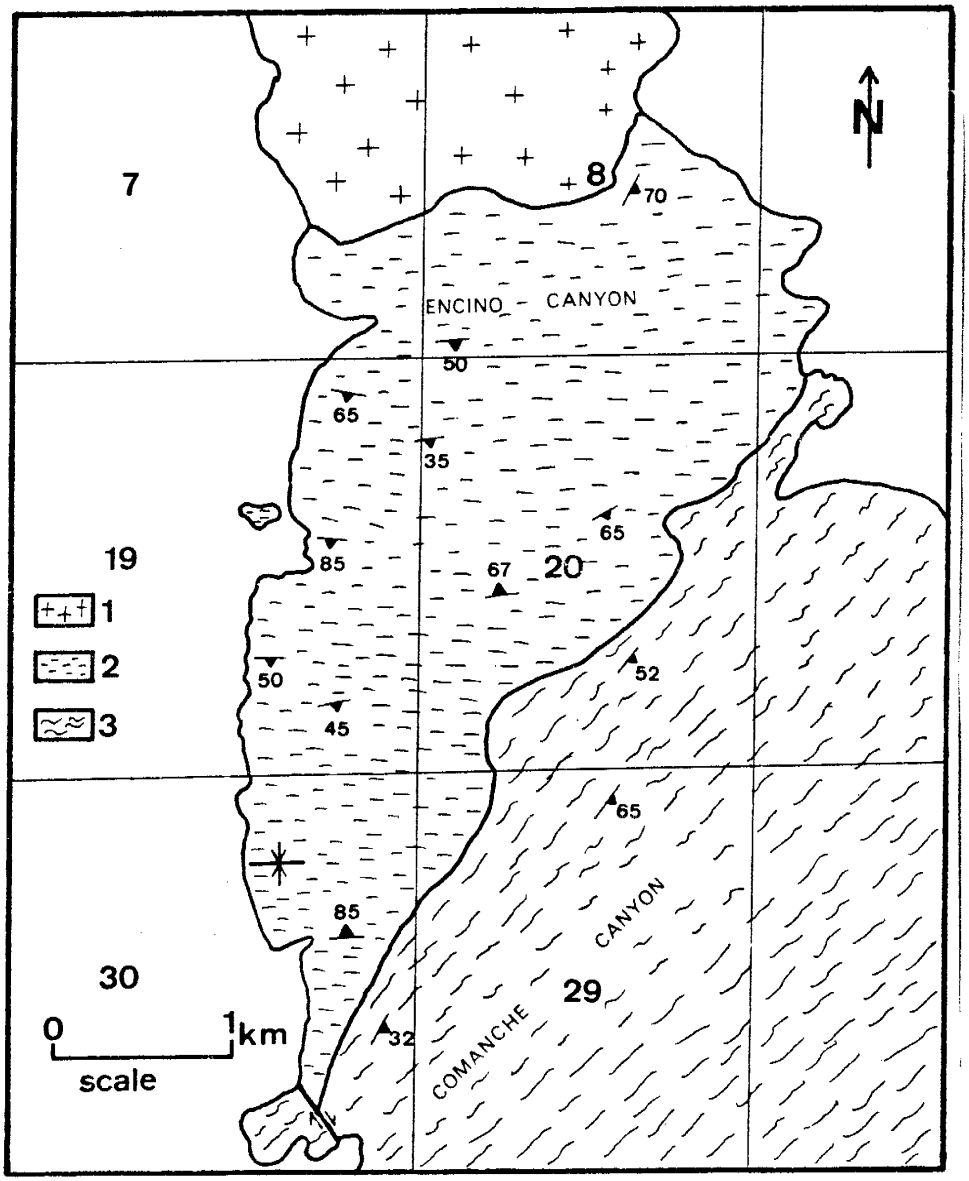

Figure 3. Generalized geologic map of the Manzano section (modified from Myers and McKay, 1971 and 1972). 1, Ojito Pluton; 2, volcanic-dominated succession; and 3, sediment-dominated succession.

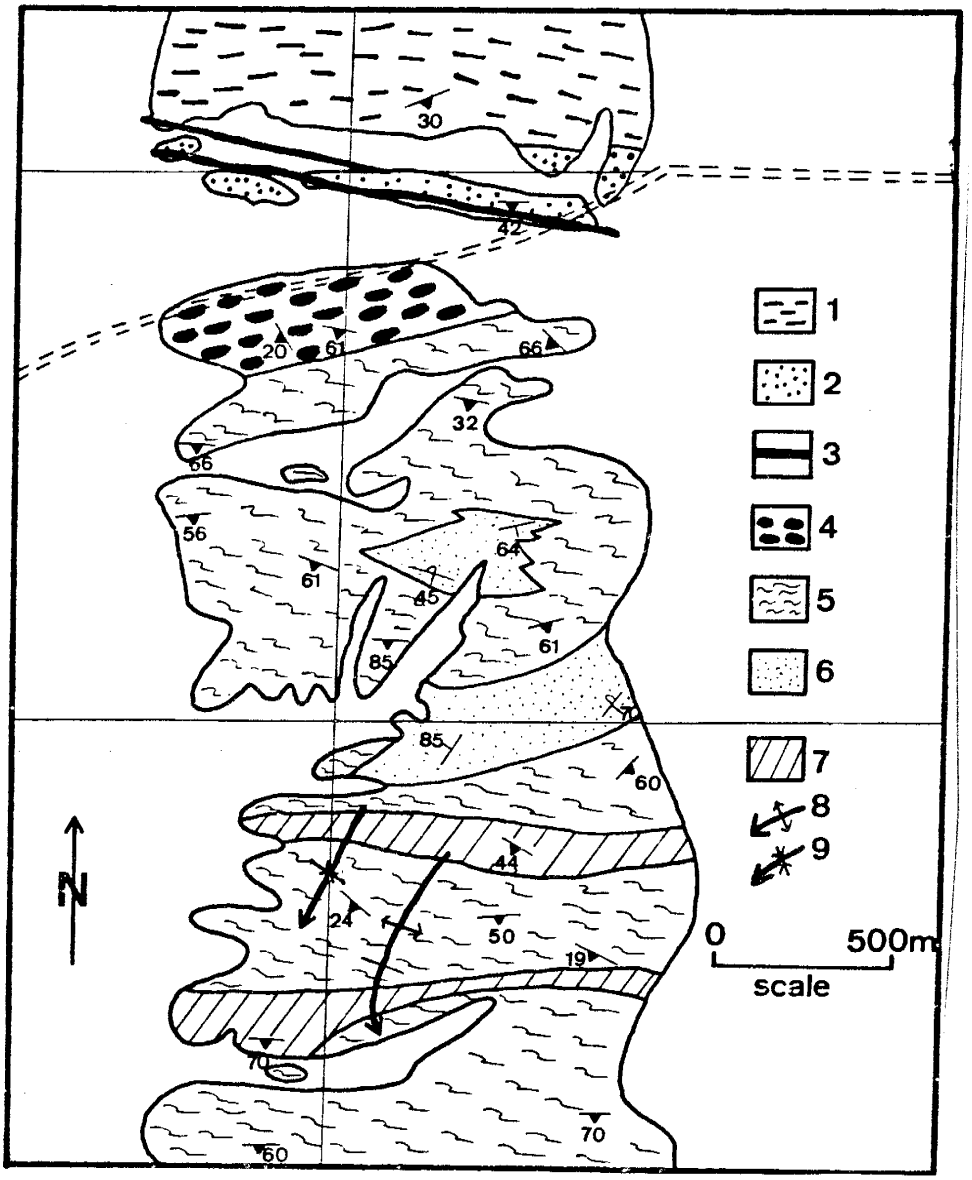

Figure 4. Generalized geologic map of the Pedernal section (modified after Armstrong, 1977 and Armstrong and Holcombe, 1982). 1, quartzite and mica schist; 2, northern boundary terrane; 3, syenite dikes; 4, coarse mafic volcaniclastic rocks; 5, pyroclastic rocks; 6, epiclastic rocks; 7, ash flow tuffs, 8, syncline, and 9, anticline.

PREVIOUS WORK

The earliest mention of Precambrian rocks in the Pedernal Hills and Manzano Mountains is only brief accounts (Johnson, 1902; Meinzer, 1911; Darton, 1928; Smith, 1957; Fitzsimmons, 1961; and Titus, 1963). The first detailed work in the Manzano Mountains was by Rieche (1949), in which he describes the general geology, stratigraphy, and structure of Precambrian rocks in the Manzanita and northern Manzano Mountains. The Manzano section (figure 3) represents the southern part of the Lower Metaclastic Series map unit of Rieche (1949). Myers and McKay (1971 and 1972) mapped Bosque Peak and Capilla Peak quadrangles, but their maps generalized the Precambrian lithologies and structures. The Manzano section is part of their Metaclastic map unit. The Ojita Pluton has been described and dated by Rb-Sr whole rock isochron method at 1527 +/- 39 Ma by White (1978). Maxwell and Wobus (1982a and 1982b) and Maxwell (1982) review evidence for economic potential of the Manzano Mountains. Structural work is presented by Johnson (1986a, b).

The first important geological studies in the Pedernal Hills are by Fallis (1958) and Gonzalez (1968), two unplublished master theses from Uiversity of New Mexico, in which the petrology, metamorphism, and structure of the Precambrian rocks are described. Woodward and Fitzsimmons (1967), Woodward (1969), Gonzalez and Woodward (1972), and

Kelley (1972) review and discuss the Precambrian rocks in the Pedernal Hills and related areas. The Pedernal pluton which intrudes the succession described in this report, has been dated by Mukhopadhyay, et al., (1975) by Rb-Sr whole rock isochron method at 1471 +/- 97 Ma. More recently, Armstrong and Holcombe (1982) studied the petrology and structure of the schists just south of the Pedernal Hills and the Pedernal section (Fig. 4) is included in this area. Bauer and Williams (1985) studied the structure of the northern quartzite unit of the Pedernal Hills.

There are several general papers dealing with Precambrian rocks of New Mexico and the Southwest. Brookins (1974 and 1982) reviews the geochronology of Precambrian rocks of central New Mexico. Condie (1978) presents compositional data for the Proterozoic granitoids of New Mexico and discusses their petrogenetic characteristics. Condie and Budding (1979) describe the petrology, structure, metamorphism, geochemistry, and other aspects of the Precambrian rocks of central New Mexico. Condie (1982a) presents a map of Precambrian terranes of the Southwest, including central New Mexico. The geochemistry and tectonic setting of the early Proterozoic rocks in the Southwest is reviewed by Condie (1986).

METHOD

Different lithologies and their physical

characteristics are identified and described in the field and representative samples of compositional and textural varietes present were collected for labratory studies. Over 100 samples from the Manzano section and more than 200 from the Pedernal section were collected. Of the samples brought back, 32 were selected for geochemical studies (Manzanos 10 and Pedernals 22) and 27 for detailed thin section descriptions (Manzanos 8 and Pedernals 22).

Geochemical samples were analyzed for major and trace elements by instumental neutron activation analysis (see Appendix E) and X-ray fluorescence techniques (see Appendix D). The results are plotted on various two and three component diagrams and MORB-normalized diagrams in order to classify, characterize, and interpret geochemical trends.

GENERAL GEOLOGY

Manzano Section

The Manzano Mountains occur along the east flank of the Rio Grande rift and are in part comprised of early Proterozoic rocks. The western margin of the Proterozoic rocks are high-angle normal faults of Tertiary age buried by peidmont fans, while the eastern margin consists of either high-angle Laramide thrusts or a Phanerozoic unconformity (Rieche, 1949 and Condie and Budding, 1979). The Proterozoic rocks consist of metavolcanics,

metasediments, and syntectonic to post-tectonic intrusives.

There are three rock packages in the central and southern Manzano Mountains: granitic intrusives, the Lower Metaclastic unit of Rieche (1949), and a southern unit composed of the Sais, Blue Springs, White Ridge, Sevilleta, and basic schist formations (Stark, 1956). These southern units extend into the Los Pinos Mountains and form a quarzite-schist assemblage (Sais, Blue Spring, and White Ridge formations) and a bimodal metvolcanic assemblage (Sevilleta and basic schist formations) (Stark and Dapples, 1946; Stark, 1956; Condie and Budding, 1979; Grambling, 1982; and Bauer, 1982a and 1982b). The bimodal metavolcanics overlie the quartzite-schist assemblage, a relationship that is opposite to that found in most early Proterozoic terranes of the Southwest (Bauer, 1982b).

The northern boundary of the Manzano study area is the Ojita Pluton, a medium-grained, biotite granodiorite (White, 1978). The intrusive ranges from quartz gabbro to quartz monzonite to granodiorite with mafic inclusions of unknown parentage and roof pendants of country rock (Rieche, 1949; Myers and McKay, 1971; and Condie and Budding, 1979). The contact with the country rock is concordant to disconcordant with silicification occurring in the country rock near the contact (Rieche, 1949 and Condie and Budding, 1979). The Ojita Pluton has been dated at 1527 +/- 39 Ma by whole rock, Rb-Sr isochron method by

White (1978).

The western margin of the study area consists of piedmont fans composed of Proterozoic rock debris shed from the Manzano Mountains. Part of the eastern boundary is an unconformity with the Sandia Formation of Pennsylvannian age (Myers and McKay, 1971 and 1972 and Condie and Budding, 1979) and the rest is the contact with the southern early Proterozoic terrane. This contact has previously been interpreted as an unconformity (Rieche, 1949 and Condie and Budding, 1979), but recent structural analysis of the southern terrane has led to a new interpretation of the contact as a fault, as previously discussed (Cavin, et al., 1982 and Johnson, 1986a and 1986b).

The rocks of the Manzano study area are comprised of bimodal metavolcanic rocks, associated metavolcaniclastic rocks, and metasedimentary rocks. Felsic metavolcanic rocks are common and usually have associated metavolcaniclastic rocks. Mafic metavolcanic rocks are rare and appear to be discontious flows, dikes, and/or sills. Metasedimentary rocks dominate the area and commonly have relict graded bedding preserved. Younging directions in the metasedimentary rocks indicate isoclinal folding has occurred. An axial plane foliation, associated with this isoclinal folding, dominates the outcrops in the study area. This foliation (S1) is defined by alignment of micas and is generally parallel to bedding (So) in most outcrops. S1 is poorly developed in the metavolcanic and

metavolcaniclastic rocks, but well developed in the metasedimentary rocks. Some outcrops show a second foliation (S2) which is a crenulation cleavage. The intersection of S1 and S2 has produced a lineation where both foliation occur in the same outcrop. Porphyroblasts occur randomly orientated within the plane of S1 in the fine-grained metasedimentary rocks.

Pedernal Section

Exposure of the early Proterozoic rocks of the Pedernal Hills has produced a plateau in the schist dominated area and low round hills in the more resistant quartzites. Where exposed, the Yeso Formation (Permian) unconformably overlies the Precambrian rocks of the Pedernals (Condie and Budding, 1979). The Precambrian terrane is composed of four basic rock assemblages: quartzite and schist, metavolcanic rocks and associated metasedimentary rocks, the Pedernal pluton, and cataclastite.

The Pedernal Hills are composed of quartzite with interbedded muscovite-quartz and specularite-quartz schists (Gonzalez, 1968; Woodward, 1969; and Gonzalez and Woodward, 1972). Original sedimentary textures are not preserved, but traces of rounded zircon, tourmaline, and apatite are consistent with a clastic origin for the quartzites (Gonzalez, 1968 and Gonzalez and Woodward, 1972). The

contact with the quartzite succession defines the northern boundary of the Pedernal section. This zone, which is poorly exposed, is comprised of schists, phyllites, and quartzites. There are no stratigraphic up indicators near the boundary, but structurally, it appears that the northern quartzite terrane is the lowest unit (Fig. 3). Also, small quartzite clasts that are similar to the northern quartzites occur in the large northern mafic volcaniclastic unit. Bauer and Williams (1985) used both field evidence and similarity of structural styles in the quartzite with the structural styles in the metavolcanics and metasediments to the south, to arrive at the same conclusion. Two syenite dikes intrude the Precambrian rocks in this boundary zone. The syenites are described and dated at 469 +/- 7 Ma by the Rb-Sr whole rock isochron method (Loring and Armstrong, 1982).

South of the study area, the Pedernal pluton intrudes the exposed Precambrian rocks. The intrusive consists of quartz monzonite, alkali granite, and granite, with an average composition of granite (Gonzalez, 1968; Woodward, 1969; Gonzalez and Woodward, 1972; and Condie and Budding, 1979). The contact with the surrounding schists is concordant to disconcordant (Condie and Budding, 1979).

In the southern part of the metavolcanic terrane and extending into the granite is a cataclastic zone (Fig. 3). The cataclastic zone is composed of highly sheared granite and schists with only minor recrystallization

(Gonzalez, 1968; Gonzalez and Woodward, 1972; and Condie and Budding, 1979). It may have formed during late stages of emplacement of the granite (Gonzalez, 1968 and Gonzalez and Woodward, 1972).

The southern boundary of the study area is the boundary between the M-2 and Crab Hill map units of Armstrong (1977) and Armstrong and Holcombe (1982). The boundary between these two units is gradational, but there is a change in structural style, with an increase in the amount of shearing in the Crab Hill suite.

The study area consists of the T-phase and M-2 map units of Armstrong (1977) and Armstrong and Holcombe (1982). Included in the succession are bimodal metvolcanic rocks and associated hypabyssal intrusives, mafic and felsic metavolcaniclastic rocks, and related metasedimentary rocks. Three folding events are identified in the study area (F1, F2, and F4) while a fourth (F3) occurs only in the Crab Hill unit (Armstrong and Holcombe, 1982). Structural complexity increases from north to south. In the northern part, large isoclinal folds with axial plane foliation parallel to bedding dominate (Armstrong and Holcombe, 1982). The southern part of the study area is dominated by second generation folds that rotate and transpose So and S1 (Armstrong and Holcombe, 1982). A further folding event, F4 is identified in some outcrops in the southern part of the study area (Armstrong and Holcombe, 1982).

F2 folds, F2, F4 interference folds, and some asymetric folds are present in the field in the southern part of the study area. Asymetric folds and mineral lineations are visible in the northern boundary zone and asymetric folds are present in the northern part of the study section. Foliation is poorly to well developed and is usually defined by the alignment of micas and elongation of quartz in quartz rich rocks.

FIELD STUDIES

INTRODUCTION

Lithologic descriptions are based on outcrops, hand samples, and standard thin sections (Manzanos, 8 thin sections and Pedernals, 27 thin sections). This section reviews field data for the different rock types and thin section descriptions are given in the petrography section. Both the Manzano and Pedernal successions are metamorphosed to upper-greenschist to lower-amphibolite facies. Since most of the rocks have been metamorphosed, the prefix meta- will be dropped for the remainder of this report.

The Manzano succession is well exposed along the flanks and noses of ridges while exposure is poor on the tops of ridges and in the bottoms of canyons. Five rock types are recognized in the Manzano section. Four are metamorphosed and include felsic pyroclastics, felsic volcaniclastics, mafic volcanics, and sedimentary rocks. Post-tectonic, unmetamorphosed, mafic intrusives are the fifth rock type. The metamorphic rocks strike east-west to southwest-northeast, while the post-tectonic intrusives have variable strikes and crosscut the foliation.

In the Pedernal section, the outcrops are poorly exposed and discontinous. Some units can be correlated from one outcrop to the next, but most beds cannot be followed between outcrops due to poor exposure and the structural complexity. The rocks consist of mafic and

felsic volcanics, mafic and felsic hypabyssal intrusives, mafic and felsic volcaniclastics, epiclastic rocks, and post-tectonic syenite dikes. The overall strike of the section is east-west to southwest-northeast. The metamorphic rocks have steep, variable dips to the south and the syenite dikes appear to be vertical.

FELSIC VOLCANIC ROCKS

Felsic volcanic rocks occur in both the Pedernal and Manzano sections. In the Pedernal succession, the felsic volcanics dominate in the southern third, but occur throughout the section. Two distinct types of felsic volcanics are recognized in the Pedernal section: ash flow tuffs and hypabyssal intrusives. The other felsic volcanics lack characteristic features to further classify them. Felsic volcanics occur only in the northern half of the Manzano succession and include ash flow tuffs. Again, most units lack distinctive textures or fabrics useful for classification beyond volcanic or pyroclastic. Recognizable felsic intrusives are not present in the Manzano section.

The felsic volcanics generally are massive, poorly to moderately foliated with the foliation defined by the alignment of micas. Some units have what appear to represent welded zones with faint, parallel laminations. Also, some units contain elongated to irregular-shaped rock

fragments that have their long axes parallel to the foliation and may be flatten pumice fragments. These fragments are 7 to 20 mm long and composed of aphanitic to fine-grained feldspar, quartz, and muscovite in the Manzano section. In the Pedernal section, the rock fragments are 10 to 140 mm long and 5 to 60 mm wide and are composed of feldspar, quartz, and biotite. Since most of these fragments occur within the middle of the units, it is believed that they represent recrystallized pumice or lithic fragments.

The felsic pyroclastics are phenocryst poor, generally contain 5 % phenocrysts, which are euhedral to anhedral and in some cases broken. The euhedral phenocrysts are evidence that these units are not sedimentary in origin (Fisher and Schmincke, 1984) and the broken phenocrysts are common features in pyroclastic rocks (Fisher and Schmincke, 1984).

Ash Flow Tuffs

Ash flow tuffs with local evidence of welding occur in both the Manzano and Pedernal sections. These units contain euhedral phenocrysts, broken phenocrysts, possible recrystallized pumice and/or lithic fragments, and in some cases, relict eutaxitic texture, all of which are common features of welded ash flow tuffs (Smith, 1960; Ross and Smith, 1961; and Fisher and Schmincke, 1984). They

comprised of what appears to be welded and unwelded zones. The boundaries between welded and unwelded zones can only be approximated due to poor exposure. Such boundaries are normally transitional in modern rocks (Smith, 1960).

The tuffs interpreted as being welded are black on fresh surfaces and weather to shades of gray, brown, and red. The rocks are porphyritic and composed of up to 2 % plagioclase phenocrysts and traces of quartz phenocrysts in a black, aphanitic groundmass. The plagioclase is clear to white, anhedral to euhedral, lath shaped, and ranges up to 4 mm in size. The quartz is clear, equant, anhedral, and averages 1.5 mm in size.

The partially welded zones vary from dark red to black on fresh surfaces and weather to various shades of red, brown, orange, and gray. The rocks are composed of traces of quartz phenocrysts and up to 3 % plagioclase phenocrysts in aphanitic to fine-grained matrices. The quartz phenocrysts are clear, equant, anhedral and average 1 mm in size. Plagioclase phenocrysts are white, anhedral to subhedral, lath shaped, and 1 to 4 mm in size. The matrix is composed of black, red-gray to dark red colored, aphanitic, welded matrix and dark gray to dark red colored, fine-grained, nonwelded matrix. The two types of matrix are intermixed, generally occur in elongated patches with the long axes parallel to the foliation, and occur in ratios of 1:4 to 4:1. The nonwelded matrix is composed of quartz, feldspar, mica, and opaques.

The nonwelded zones are dark gray to dark tan on fresh surfaces and weather to brown, orange-brown, or orange-tan. They are composed of traces of quartz phenocrysts, traces to 5 % plagioclase phenocrysts, and up to 15 % metamorphic biotite (Pedernal section) or muscovite (Manzano section) set in a fine-grained matrix of quartz, feldspar, biotite, muscovite, and opaques. Plagioclase occurs as white to light green, anhedral to euhedral phenocrysts, 0.5 to 4 mm in size, and slightly elongated to bladed in shape. Quartz is equant, anhedral, clear, and 0.5 to 1.5 mm in size and biotite and muscovite occur as subhedral flakes, 0.5 to 2 mm in size and define the foliation.

Other Felsic Pyroclastic Rocks.

Other felsic pyroclastic rocks are light tan, brown, dark red-brown, light gray, or red-gray on fresh surfaces and weather to shades of gray and brown. They are composed plagioclase phenocrysts (5 to 20 %), quartz phenocrysts (trace), metamorphic biotite (Pedernal section) or muscovite (Manzano section), and the remainder is fine-grained matrix composed of quartz, feldspar, micas, and opaques. The plagioclase is white to light green, lath shaped, anhedral to euhedral, and 1 to 3 mm in size. Quartz occurs as clear, equant, anhedral phenocrysts which are 0.5 to 2 mm in size. The biotite and muscovite are

subhedral flakes, 0.5 to 2.5 mm in size and comprise up to 10 % of the rocks.

Some of these felsic volcanics may represent fall or surge deposits which are typically associated with flow deposits (Ross and Smith, 1961; Sparks, et al., 1973; Sparks, 1976; Fisher, 1979; and Fisher and Schmincke, 1984). Fall and surge deposits can form before or after deposition of ash flows and generally do not have internal fabrics. Surge deposits are characterized by bedforms (Sparks, 1976; Fisher, 1979; Wright, et al., 1980; Wohletz and Sherridan, 1979; and Fisher and Schmincke, 1984), but may be poorly formed and not preserved (Sparks, 1976). Fall deposits are well sorted and tend to mantle topography (Sparks, 1976; Wright, et al., 1980; and Fisher and Schmincke, 1984), but these characteristics are not likely to be preserved in metamorphic rocks. These units may be parts of unwelded ash flow tuffs or the outer zones of welded ash flow tuffs. There are no distinguishing characteristics present in the Precambrian exposures of the Pedernals.

Felsic Intrusives

Felsic intrusive rocks are recognized only in the Pedernal succession. These units have intrusive, cross-cutting contacts with the surrounding rocks. Other similar rock types that do not have exposed contacts may also be

intrusives.

The intrusive rocks are red to gray on fresh surfaces which darkens with weathering. They are 1 to 3 m thick and usually elongated in shape with the long axes subparallel to the foliation.

MAFIC VOLCANIC ROCKS

Mafic volcanic rocks occur in both the Manzano and Pedernal sections. In the Manzano section, the mafic rocks are poorly exposed and comprise a minor component of the succession. They may represent flows, dikes, and/or sills. Exposures are highly weathered, 1 to 3 m in size and contacts with the surrounding rocks are covered. They are composed of 20 to 30 %, green, anhedral amphibole 2 to 5 mm in size; 20 % green, saussuritized, anhedral plagioclase, 1 to 3 mm in size; and a dark green, aphanitic matrix.

Mafic volcanics occur throughout the Pedernal section, but are most common in the northern part of the succession and generally occur as small discontinous outcrops. The mafic volcanics can be divided into three types: fine- to medium-grained rocks interpreted as pyroclastic rocks, porphyritic volcanics, and hybabyssal intrusives.

Fine- To Medium-grained Volcanic Rocks.

The fine- to medium-grained volcanics are massive to moderately foliated and may be associated with volcaniclastics. They are medium to dark green or gray on fresh surfaces and weather to dark green. The volcanics contain saussurtized plagioclase laths in a fine-grained to aphanitic matrix. Some of the medium-grained units contain elongated fragments that may be recrystallized scoriae or lithic fragments. The medium-grained volcanics also contain plagioclase laths that are euhedral and up to 5 mm in length. The matrix of the fine- to medium-grained volcanics is composed of epidote, chlorite, biotite, quartz, feldspar, muscovite, and opaques.

Hypabyssal Intrusive Rocks

Porphyritic units have sharp, intrusive, cross-cutting contacts with the surrounding rocks and may represent sills, dikes, or both. These units are 15 to 40 cm thick and can be traced for up to 10 meters. The intrusive rocks are porphyritic and contain subhedral to euhedral, randomly oriented, sausuritized plagioclase laths, 1 to 8 mm in length that comprise 30 to 60 % of the rock. They also exhibt relict subophitic textures, with chlorite, epidote, and amphibole pseudomorphs (?) of pyroxenes.

Porphyritic Volcanic Rocks

There are some single, small outcrops of porphyritic volcanics in which contact relationships are not exposed. They have the same appearance as the mafic intrusive rocks discussed above. Most occurrences are believed to represent sills and/or dikes, but since contacts are not exposed, some or all exposures could represent submarine lava flows, though pillows are not present.

VOLCANICLASTIC ROCKS

Volcaniclastic rocks occur in the Pedernal and the Manzano successions. There are numerous units of mafic and felsic volcaniclastic rocks throughout the Pedernal section, with a thick mafic unit dominating the northern part of the succession. Felsic volcaniclastic rocks occur in the northern part of the Manzano section. These units show evidence of secondary transport by the rounding of clasts. Primary textures or structures are not preserved in either the mafic or felsic volcaniclastic rocks. The volcaniclastic rocks have clasts ranging in size from coarse sand to boulder with most clasts in the pebble to cobble size range.

Volcaniclastic rocks are generally coarse-grained, dominanted by volcanic clasts or subangular to angular mineral grains, and lack any internal textures or fabrics.

These features distinquish volcaniclastic rocks from epiclastic rocks which range from very fine- to coarse-grained, are dominanted by rounded to subrounded mineral grains, and usually display partial Bouma sequences.

Mafic Volcaniclastics-Pedernal Section

The mafic volcaniclastic rocks are light to dark green or gray and weather to dark green. The matrix is green, gray or black and ranges from aphanitic to fine-grained. The most common clast type are aphanitic clasts that range from brown to gray to green in color. These clasts are elongated, range from angular to rounded, and are of variable size (3 X 1 to 30 X 20 mm).

The next most common rock type has relict diabasic texture. These clasts appear similar to some of the diabasic intrusives in the study area and are believed to be clasts of similar intrusives. The clasts are elongated to irregular in shape and range from subangular to rounded. They range in size from 5 X 3 to 12 X 8 mm, but some are as large as 150 X 70. The clasts are composed of saussuritized plagioclase in a black-gray matrix. The plagioclase is green, generally lath shaped, anhedral to euhedral, ranges in size from 0.5 to 5 mm long, and can compose 25 to 80 % of the clasts. The rest of the clast is matrix and some of this matrix has what appear to be pyroxene pseudomorphs.

Other less common rock types present as clasts are chert, quartzite, and amphibolite. The chert occurs only in the central part of the study section. The chert clasts are subangular, have blocky shapes, range in size from 2 to 10 mm, and are medium to dark purple to almost black in color. The quarzite clasts occur only in the northern breccia unit. They are fine- to medium-grained, white to clear in color, angular to subangular, and are about 15 mm in size. These quartzites appear similar to the rocks in the northern quartzite terrane. The amphibolite clasts are dark green to black and almost exclusively composed of fine- to medium-grained amphibole. These clasts are equant to elongated, angular to rounded, range in size from 5 to 50 mm, and most clasts have secondary veins of chlorite and epidote.

Felsic Volcaniclastic Rocks

Manzano Section

In the Manzano section, felsic volcaniclastic rocks occur only in the northern part of the succession and are generally associated with felsic volcanic rocks. This section lacks mafic volcaniclastic rocks. Felsic volcaniclastic rocks are poorly foliated, green to light brown on a fresh surface and weather to shades of green and brown. They are composed of fine- to coarse-grained sand-

sized plagioclase and quartz grains. Some units have relict graded bedding, but most units are massive.

Pedernal Section

Felsic volcaniclastic rocks are restricted to the central and southern parts of the Pedernal area. They are especially common on either side of the the two ash flow tuffs (Fig. 4) and are commonly associated with other felsic pyroclastics. Some felsic volcaniclastics are similar to mafic volcaniclastics with green weathered surfaces. These green felsic volcaniclastics are the dominante type of felsic volcaniclastic. Other felsic volcaniclastics have reddish brown weathered surfaces.

The green felsic volcaniclastics have a black to green or red-brown unweathered surface color. They have a fine-grained matrix composed of quartz (40 %), plagioclase (10 %), biotite (15 %), and small, black, aphanitic volcanic clasts (30 %). Minerals are 2 mm and less in size and are anhedral. Epidote and chlorite occur as patches in the matrix.

The clast population tends to be monolithic with most clasts being gray, aphanitic, and rounded to subrounded in shape with a few subangular clasts. They range in size from 50 X 40 to 5 X 3 mm in size. Parts of clasts may be replaced or are altered to pseudomatrix.

The reddish brown volcaniclastics have a gray or brown

unweathered color. The matrix is composed of anhedral to subhedral sausseritized plagioclase (60 %), anhedral quartz (15 %), anhedral to subhedral biotite (5 %), possibly some anhedral K-feldspar (3 %), and black to white aphanitic volcanic clasts (17 %). The plagioclase is lath shaped and 3 to 5 mm long, but ranges up to 15 mm. Quartz is 3 mm and less, biotite 2 mm and less, and the potassium feldspar 6 mm and less in size. There is a trace of 2 to 5 mm, anhedral chalcopyrite and/or euhedral pyrite in some units. Clasts are rounded and elongated. Some units lack clasts and are composed of coarse sand size grains of plagioclase, quartz, and K-feldspar with opaques and metamorphic biotite.

EPICLASTIC ROCKS

Epiclastic rocks occur in both the Pedernal and Manzano successions and include units that have relict graded beds, planar beds and cross laminations. These occur throughout the Pedernal section, but dominate in two areas near the center of the study section and one area in the northern boundary zone. The Manzano section is dominated by epiclastic rocks.

Manzano Section

Epiclastic rocks in the Manzano section are medium

bedded with relict graded beds and are laterally continous in large exposures. Some units are ungraded, with massive or planar bedded textures. The rocks are gray, green, or light-brown on fresh surface and weather to gray or brown with some units having a phyllitic sheen. Muscovite and elongated quartz define the foliation.

Beds range from 5 to 35 cm thick and in large exposures, they extend for tens of meters before pinching out. Most outcrops are composed of 5 to 20 individual beds. The beds are composed of clear quartz, altered feldspars, muscovite, and opaques. The beds range from very fine- to coarse-grained.

The fine- to very fine-grained tops of beds have porphyroblasts of chloritoid (?) or pseudomorphic andalusite (?) randomly orientated within the plane of S1. The chloritoid is green, spindle shaped, and up to 40 mm long with most grains 5 to 10 mm long. It comprises up to 35 % of the top layer, but decrease in size and abundance as the beds increase in grain size. The pseudomorphic andalusite is ovoid shaped to euhedral, 6 to 60 mm long, dark brown, bronze, or dark green in color and is replaced by sericite. These porphyroblats comprise up to 40 % of the top layer of graded beds and decrease in size and abundance with downward coarsening of the beds. Porphyroblasts do not occur in all of the epiclastic rocks.

Pedernal Section

Graded Epiclastic Rocks

In the middle of the section, green to gray epiclastic rocks occur with relict planar beds, 1 to 10 mm thick and with graded beds, 10 to 50 mm thick. Rarely do the planar beds contain low angle crossbeds. The rocks range from fine-grained to coarse-grained sandstones. They are composed of subangular to subrounded plagioclase (15 to 45 %), subangular quartz (trace to 30 %), and very fine-grained matrix. The matix is dominated by chlorite, quartz and feldspar with traces of biotite. Foliation in the sedimentary rocks is defined by the alignment of micas and is parallel to bedding or at an angle up to 20 degrees to bedding planes. Small scale, outcrop size, asymmetric folds occur in some units.

Northern Boundary Zone Sedimentary Rocks

The northern boundary zone is composed of various phyllites, schists and quartzite beds. The phyllites and schists are green, brown, gray, or red and are highly foliated while the quartzites are white and poorly foliated.

POST-TECTONIC INTRUSIVE ROCKS.

Post-tectonic intrusive rocks occur in both sections. In the Pedernal succession, two syenite dikes are exposed in the northern boundary zone (Fig. 4). Small mafic dikes and/or sills occur throughout the Manzano section.

Syenite.

Syenite dikes occur in the northern boundary zone of the Pedernal succession and are exposed in small outcrops and prospect pits. The dikes are light to dark brick red on fresh and weathered surfaces, average 50 cm wide and can be traced for about 0.7 km along strike. The rocks are massive and have blocky outcrops.

Mafic Intrusives.

Mafic intrusives of the Manzano section range from 10 to 35 cm thick and extend for up to 25 m along strike. The rocks are dark green to black massive units that crosscut foliation and structural trend. They have variable dips and strikes. These units are composed of 1 mm subhedral to euhedral plagioclase phenocrysts (traces to 10 %), in a green, aphanitic matrix.

PETROGRAPHY

INTRODUCTION

Lithologic descriptions are based on outcrops, hand samples, and standard thin sections (Manzanos, 8 thin sections and Pedernals, 27 thin sections). Petrographic summaries are given below for each rock type and individual sample descriptions are located in Appendix B.

FELSIC VOLCANIC ROCKS

Felsic pyroclastic rocks are prophyritic with minor plagioclase and traces of quartz phenocrysts set in a fine-grained to aphanitic matrix (Table 1). The plagioclase phenocrysts are lath shaped, anhedral to subhedral, altered, and show recrystallized grain boundaries. The laths are 0.5 to 4 mm long and up to 1 mm wide with pericline, albite, and Carlsbad twins and compositions falling in the range of An9-30. The quartz phenocrysts average 0.75 mm in size, are anhedral, equant, and show undulatory extinction. One thin section (P718) has an opaque, subhedral phenocryst that is 1.5 mm long and 0.5 mm wide and may represent an altered pyroxene or amphibole phenocryst.

In the matrix, the micas and amphiboles are idioblastic to xenoblastic and usually lepidoblastic, while the rest of the matrix minerals are generally xenoblastic

TABLE 1. MINERAL PERCENTAGES FOR THE FELSIC VOLCANIC ROCKS.

	Felsic Pyroclastic Rocks				
	P710	P714	P718	P735	P793
Phenocrysts					
Plag	1	2	5	--	2
Qtz	tr	tr	--	--	--
Matrix					
Q+F	53	65	57	--	72
Qtz	--	--	--	54	--
Plag	--	--	--	9	--
Musc	33	1	32	21	--
Biot	8	10	1	10	tr
K-spar	--	15	--	--	17
Opaq	tr	1	4	5	7
Chl	4	1	1	--	tr
Epid	tr	2	1	1	tr
Gar	--	tr	--	--	tr
Amp	tr	--	--	--	--
Zir	--	tr	--	--	--

	Felsic Intrusive Rocks.	
	P769	P719
Phenocrysts		
Plag	2	50
Opaq	tr	--
Matrix		
Q+Feld	55	--
Qtz	--	33
Plag	--	9
Musc	20	--
Biot	10	1
Epid	10	tr
Opaq	2	5
Chl	--	1
Amp	--	1
Zir	--	tr

Plag = plagioclase, Qtz = quartz, Biot = biotite, Opaq = opaques including hematite, Epid = epidote, Gar = garnet, Q+F = modally indistinguishable quartz and fe;dspar, K-spar = all K-feldspar, Musc = muscovite and sericite, Chl = chlorite, Amp = amphibole, Zir = zircon, Carb = carbonate minerals, Tour = tourmaline, and tr = trace amount.

and granoblastic. The stained thin sections suggest about 15 to 17 % K-feldspar is present in the matrix. The matrix minerals are 0.05 to 0.5 mm in size and may represent recrystallized glassy material.

FELSIC INTRUSIVES

One of the intrusive rocks has a glomeroporphyritic texture with crystal clots 1 to 2 mm in size composed of 2 to 4 plagioclase crystals and sometimes 1 or 2 opaque crystals. Also, plagioclase and opaque phenocrysts are present (Table 1). The plagioclase phenocrysts are anhedral to euhedral, 0.4 to 2 mm in size, equant to lath shaped, and show Carlsbad twinning. There are equant, euhedral to anhedral, opaque phenocrysts that are 0.3 to 1 mm in size. The matrix (grains 2 mm in size) is composed of quartz, feldspar, micas, epidote, and opaques. Matrix micas are idioblastic to xenoblastic and generally lepidioblastic and other matrix minerals are granoblastic and xenoblastic, with some of the quartz and feldspar elongated parallel to the foliation.

Another intrusive rock has plagioclase phenocrysts that are lath shaped, 0.5 to 2.1 mm long, subhedral to euhedral, and contain albite, pericline, and Carlsbad twins (Table 1). The plagioclase is highly altered (65-100 %) to very fine-grained mosaics of muscovite, sericite, and other minerals. The matrix of the rock is composed of hypidiomorphic quartz, plagioclase, opaques, biotite,

chlorite, amphibole, and zircon. Quartz is equant, anhedral, and 0.1 to 0.5 mm is size and plagioclase is highly altered (80-100 %), anhedral, equant to elongated, and 0.03 to 0.2 mm in size. Opaques are euhedral to anhedral, equant, and 0.01 to 1 mm in size and other minerals are idioblastic to xenoblastic, granoblastic, and 0.03 to 0.5 mm in size.

MAFIC VOLCANIC ROCKS

Fine- To Medium-grained Volcanic Rocks.

Mafic volcanic rocks are composed of plagioclase, epidote, chlorite, amphiboles, biotite, muscovite, quartz, and opaques (Table 2). The plagioclase crystals are 0.2 to 0.35 mm in length, anhedral, and range from equant to elongated and appear to be phenocrysts. Individual phenocrysts are comprised of 70 to 90 % of a mosaic of alternation products including sericite, muscovite, epidote, chlorite, and opaques. Matrices are composed of epidote, chlorite, amphibole, biotite, quartz, muscovite, and opaques and matrix minerals are xenoblastic to idioblastic, granoblastic to lepidioblastic, and 0.02 to 0.4 mm in size. Some of the opaque crystals are embayed to skeletal shaped and may be phenocrysts of magnetite or ilmenite.

TABLE 2. MINERAL PERCENTAGES FOR THE MAFIC VOLCANIC ROCKS.

	P740	P765	P774	P792
Phenocrysts				
Plag	tr	--	tr	--
Matrix				
Q-Feld	58	42	20	30
Epid	20	18	20	20
Amp	3	20	22	10
Chl	15	9	5	10
Biot	1	tr	27	tr
Opaq	1	7	tr	3
Musc	tr	--	tr	5
Carb	--	--	--	3

See table 1 for explanation of abbreviations.

VOLCANICLASTIC ROCKS

Mafic Volcaniclastics-Pedernal Section

Petrographically, the mafic volcaniclastic rocks are composed of 26 % to 67 % lithic fragments and the rest is matrix composed of chlorite, epidote, sericite, muscovite, quartz, feldspar, and traces of biotite, carbonate, and opaques (see appendix I). The fragments are dominated by unstable lithic grains that have been recrystallized to a very fine-grained mosaic of chlorite, epidote, amphibole, sericite, muscovite, quartz, and feldspar. The unstable lithic fragments are equant to elongated, subangular to rounded, and 0.5 mm to 10 mm wide and 0.5 mm to 2.5 cm long. The unstable lithic fragments range from quartz-feldspar dominated to chlorite-epidote dominated with the chlorite-epidote variety the most common. The other lithic fragments are polycrystalline quartz grains interpreted to be recrystallized chert grains. The quartz in the chert grains is very fine-grained, equant, has polygonal to interlobate crystal boundaries, and has undulatory extinction. The quartzose lithic grains are angular to subrounded, equant to elongated in shape, range in size from 0.2 to 2 mm wide and 1 to 4 mm long and have corroded grain boundaries. Some of the quartzose grains are embayed and replaced by matrix.

Felsic Volcaniclastic Rocks-Manzano Section

Felsic volcaniclastic rocks are composed of detrital quartz and feldspar grains in a fine-grained matrix (Table 3). The quartz grains are angular to subangular, equant to elongated, dominantly monocrystalline, and show moderate to extreme undulatory extinction.Some quartz grains have recrystallized grain boundaries. One sample (M734) has a large (4.5 mm) rounded quartz grain that shows undulatory extinction, and is replaced by matrix along the grain boundary. This particular grain may have come from a granitic rock.

Feldspar grains are angular to rounded, elongated to equant, 0.2 to 4 mm in size, and are altered (30-100 %) to very fine-grained sericite, epidote, and opaques. The feldspars are dominantly plagioclase which has pericline, albite, and Carlsbad twins. The matrix of the volcaniclastic rock is dominated by quartz and feldspar, but includes sericite, muscovite, epidote, opaques, rutile (?), and amphibole. One stained section shows about 9 % K-feldspar in the matrix.

EPICLASTIC SEDIMENTARY ROCKS

Manzano Section

The epiclastic rocks are composed of detrital quartz

TABLE 3. MINERAL PERCENTAGES FOR THE VOLCANICLASTIC ROCKS.

	M100-Fine	M100-Coarse	M734	BOS-3
Clastic Grains				
Qtz	5	12	60	50
Plag	--	15	10	8
Matrix				
Q+F	43	42	5	15
Musc	50	--	5	15
Amp	10	5	--	--
Biot	--	tr	tr	10
Chl	--	tr	1	tr
Opaq	tr	tr	tr	tr
Epid	--	5	--	tr
Gar	--	--	--	tr

See table 1 for explanation of abreviations.

and feldspar grains in a matrix of quartz, feldspar, opaques, muscovite, epidote, sericite, amphibole, chlorite, biotite, hematite, and garnet (Table 4). Quartz grains are angular to subrounded, monocrystalline and show undulatory extinction. The grains are 0.2 to 3.5 mm in size and some have recrystallized grain boundaries. Feldspar grains are chiefly subangular to rounded plagioclase that have Carlsbad and albite twins, are altered (50-95 %) to fine-grained sericite and muscovite, and are 0.2 to 2.1 mm in size. The matrix crystals are 0.01 to 0.6 mm in size, xenoblastic to idioblastic, granoblastic to lepidioblastic, and dominated by quartz and feldspar.

Pedernal Section-Northern Boundary Zone Rocks

Petrographically, the schists contain quartz, epidote, muscovite, red-brown or green biotite, chlorite, and opaques (Table 4). Quartz crystals are xenoblastic, equant to elongated parallel to the foliation, 0.05 to 1.5 mm in size, and have polygonal, interlobate, or sutured grain boundaries. Epidote occurs as xenoblastic crystals that are 0.05 to 0.3 mm in size and rarely twinned. Micas are idioblastic to xenoblastic, lepidoblastic, and 0.05 to 4 mm in size. In one thin section (P749), the micas are bent by microscopic folds. In some cases, biotite (red-brown) is intergrown with chlorite. The opauqe minerals are

TABLE 4. MINERAL PERCENTAGES FOR THE SEDIMENTARY ROCKS.

	Manzano Section Rocks				
	M601	M732	M753	BOS-1	BOS-6
Clastic Grains					
Qtz	20	40	--	--	10
Plag	20	10	--	--	tr
Chert	--	tr	--	--	--
Matrix					
Q-F	50	39	70	68	66
Musc	tr	1	15	20	7
Opaq	1	8	tr	7	3
Chl	--	1	--	5	1
Biot	2	--	5	--	--
Amp	tr	--	--	--	2
K-spar	--	--	9	--	--
Epid	tr	tr	tr	--	tr
Zir	--	--	tr	--	tr
Carb	--	tr	--	--	--

	Pedernal Section-Northern Boundary Zone					
	P745	P746	P748	P749	P83	P84
Qtz	35	40	55	43	90	97
Epid	30	25	15	--	4	--
Biot	5	30	10	20	--	tr
Chl	30	1	10	--	5	--
Opaq	tr	5	8	2	tr	1
Musc	--	--	2	35	--	1
Zir	--	--	--	--	tr	tr
Tour	--	--	--	--	tr	tr
Carb	--	--	--	--	tr	--

See table 1 for explanation of abbreviations.

xenoblastic, and 0.05 to 1.8 mm in size. One sample (P745) has red spots in hand speciemen and these red spots contain about 5 % hemetite in thin section.

Quartzites in the northern boundary zone appear similar to the quartzites in the northern quartzite terrane. These quartzites contain quartz, chlorite, epidote, and trace of opaques, zircon, carbonate, and tourmaline (Table 4). The quartz crystals are xenoblastic, show undulatory extinction, have polygonal, interlobate, or sutured grain boundaries, are equant to elongated parrallel to the foliation, and are 0.05 to 1 mm in size. Chlorite occurs as idioblastic to xenoblastic, lepidoblastic crystals that are 0.05 to 0.5 mm in size. Epidote crystals are xenoblastic, and 0.05 to 0.3 mm in size that occur dominately in thin bands which are 0.5 mm thick and are parrallel to the foliation. Zircon, carbonate, and tourmaline occur as small (<0.1 mm), xenoblastic, equant to elongated grains. Most of the quartzites in the northern boundary zone have less quartz than those of the northern quartzite unit (90 vs 97 %, respectively). The lower quartz content may reflect higher input of very fine-grained material (clay) into the basin of deposition.

Also, one thin section of northern quartzite unit was studied. It contains quartz grains, 0.01 to 1 mm in size that are serriated and have polygonal to interlobate grain boundaries and some show motar texture. The grains are equant to elongated parallel to foliation and have

undulatory extinction. Chlorite and muscovite, 0.01 to 0.5 mm in size, in part define foliation. Also, traces of opaques, zircon, and tourmaline (?) are present.

POST-TECTONIC SYENITE DIKES

One section of the syenite was studied. It is composed of 85 % altered alkali feldspar, showing trachytic texture, 10 % hypidiomorphic quartz, and 5 % hematite. The feldspars are highly altered to clays with minor sericite and hematite.

ALTERATION

PEDERNAL SECTION

Quartz veins and aphanitic veins occur throughout the Pedernal section. The quartz can also occur along fractures and in pockets. It is generally clear to white, but can also be red brown, tan, or green. Veins are 5 mm thick and extend up to 1 m. Quartz crystals range from anhedral to subhedral, equant to elongated, and 7 mm in size. Pockets of quartz are up to 20 by 60 mm in size.

Aphanitic veins are usually less than 1 mm wide, 20 to 50 cm long, and are some shade of green, red, brown, or black. Some are dominated by chlorite and epidote dominated. There is also minor clay alteration, secondary calcite, caliche and small euhedral pyrite crystals. Malachite and azurite occur in small crystal groups no more than 3 mm in size in various units throughout the study area.

MANZANO SECTION

Silicifiaction has occurred along the contacts with the Ojita Pluton and the boundary with the southern Manzano terrane. Also present are white, medium-to coarse-grained quartz veins that are 1 mm to 3 cm wide and extend for up to 20 cm; they may show ptygmatic folded patterns. Minor

chlorite and epidote veins, 1 mm wide and up to 10 cm long are present in some outcrops.

GEOCHEMISTRY

INTRODUCTION

Thirty two samples were chosen for chemical analysis. Analyses were performed by X-ray flourescence (see Appendix D) and instrumental neutron activation analysis (see Appendix E). Samples were selected to represent the various lithologies encountered in the two study areas and show no visible signs of alteration in hand specimen or outcrop. All weathering rinds were removed from the samples in the field. The chemical composition of the rocks are used to assign rock names, to quantify chemical trends, to aid in tectonic interpretations, and for geochemical modeling.

Compositions of each sample are listed in Appendix F and averages of the various rock types from each area are listed in Table 5. Since the rocks from both successions are metamorphosed to greenschist facies, secondary alteration must be taken into account in discussing the compositions of the rocks.

ALTERATION

Alteration can occur during diagenesis, metamorphism, metasomatism, hydrothermal activity, or during other secondary processes. It can destroy original minerals and

TABLE 5. AVERAGE COMPOSITION OF ROCKS FROM THE PEDERNALS AND THE MANZANOS.

ROCK TYPE	THOLEIITE	CAB	HIGH-MG# ANDESITE	LOW-MG# ANDESITE
	PEDERNAL	PEDERNAL	PEDERNAL	PEDERNAL
N	2	1	1	4
SiO2	49.7	50.7	52.9	55.3
TiO2	0.64	0.54	0.70	0.84
Al2O3	14.8	19.5	15.0	16.6
Fe2O3-T	10.9	8.78	9.08	10.1
MgO	8.17	4.86	6.78	4.37
CaO	10.0	8.46	5.86	5.42
Na2O	2.72	2.87	1.71	3.34
K2O	0.15	0.86	2.31	1.28
MnO	0.16	0.12	0.13	0.14
P2O5	0.074	0.11	0.16	0.15
Mg No.	63	55.4	62.8	49.0
Sr	113	287	264	206
Ba	137	334	403	353
Rb	5.1	29	119	53
Th	2.0	4.6	9.1	8.4
U	ND	1.2	2.1	1.8
Pb	8.7	16	22	17
Cs	0.24*	1.2	0.72	2.2
Zr	52	99	149	138
Hf	1.5	2.9	4.6	4.5
Nb	5.2	7.4	11	10
Ta	ND	0.6	1.8	1.2
Y	23	28	33	34
Sc	47	31	28	34
V	269	201	199	222
Cr	58	11	48	21
Co	60	13	55	46
Ni	23	9.3	21	11
La	10	41	51	37
Ce	25	75	107	91
Sm	3.6	7.2	8.2	8.8
Eu	1.1	1.8	1.8	2.1
Tb	0.68*	0.87	1.1	1.4
Yb	2.6	2.8	3.1	3.5
Lu	0.43	0.40	0.44	0.53
Ga	14	16	15	18
Zn	88	77	101	102
Cu	153	23	118	195*

TABLE 5. CONTINUED.

ROCK TYPE	RHYODACITE	HIGH-SILICA RHYOLITE	RHYOLITE	HIGH-SILICA RHYOLITE
	PEDERNAL	PEDERNAL	MANZANO	MANZANO
N	2	2	3	1
SiO2	70.0	76.4	73.0	77.7
TiO2	0.41	0.15	0.33	0.28
Al2O3	13.8	12.0	13.1	11.2
Fe2O3-T	4.03	2.56	3.69	2.92
MgO	0.96	0.15	0.86	0.61
CaO	1.30	0.78	2.16	2.24
Na2O	4.06	3.85	3.32	3.21
K2O	2.49	3.86	2.25	1.03
MnO	0.069	0.059	0.11	0.11
P2O5	0.09	0.016	0.08	0.006
Mg No.	40.4	14	39.8	35.5
Sr	95	51	239	340
Ba	638	731	813	443
Rb	113	140	99	41
Th	19	19	12	8.6
U	3.1	4.3	2.6	1.7
Pb	18	22	24	20
Cs	3.5	1.6	3.2	1.7
Zr	254	323	272	231
Hf	9.0	10	9.2	7.9
Nb	14	16	12	8.4
Ta	2.2	2.4	1.5	1.1
Y	52	85	52	39
Sc	15	8.6	18	16
V	35	ND	27	22
Cr	5.0	ND	1.6*	ND
Co	7.3	0.38	6.1	5.2
Ni	ND	ND	ND	ND
La	83	97	77	57
Ce	158	191	153	115
Sm	13	17	14	9.7
Eu	2.6	2.9	4.6	4.1
Tb	1.8	2.7	1.9	1.4
Yb	6.4	8.8	5.3	3.8
Lu	0.86	1.5	0.8	0.56
Ga	ND	ND	14*	ND
Zn	ND	ND	98*	ND
Cu	ND	ND	10*	ND

TABLE 5. CONTINUED.

ROCK TYPE	SEDIMENT
	MANZANO
N	4
SiO2	73.0
TiO2	0.60
Al2O3	13.0
Fe2O3-T	4.79
MgO	1.01
CaO	1.02
Na2O	1.93
K2O	2.55
MnO	0.079
P2O5	0.083
Mg No.	---
Sr	93
Ba	517
Rb	127
Th	17
U	3.6
Pb	26
Cs	3.8
Zr	251
Hf	9.3
Nb	15
Ta	2.4
Y	41
Sc	13
V	59
Cr	7.6
Co	14
Ni	3.8
La	82
Ce	151
Sm	12
Eu	2.2
Tb	1.6
Yb	4.0
Lu	0.67
Ga	20*
Zn	91*
Cu	23*

N, the number of samples used in the averages

*, not all of the analyses were used in the average.

Fe2O3-T, total Fe as Fe2O3.

Major elements in weight percent and trace elements in ppm.

Mg No., (MgO/40.32)/(MgO/40.32) +(FeO/71.85); molecular proportions; Fe2O3/FeO= 0.15 for mafic rocks and 0.50 for felsic rocks.

physical characteristics.

Chemical alteration occurs by one or more processes. First, an element can be leached from or added to a rock with a constant volume maintained. A second possibility is that an element may be immobile, but diluted by addition of other elements. Also, the concentration of an immobile element may be increased by leaching of other elements.

Studies of secondary alteration generally follow one of three approaches. One method is to experimentally alter rocks with seawater in the laboratory (Bischoff and Dickson, 1975; Hajash, 1975; Seyfried and Bischoff, 1977 and 1981; Mottl and Holland, 1978; Menzies and Seyfried, 1979; Hajash and Archer, 1980; Hajash and Chandler, 1981; Seyfried and Mottl, 1982; Mottl, 1983; and Hajash, 1984). A second approach is to compare fresh and altered volcanic rocks (Hart, 1969 and 1970; Philpotts, et al., 1969; Cann, 1970; Thompson, 1973; Hart, et al., 1974; Hellman and Henderson, 1977; Humphries and Thompson, 1978; Ludden and Thompson, 1978 and 1979; Staudigel, et al., 1981; and Nystrom, 1984). The third method evaluates variation of element concentrations as a function of increasing metamorphic grade (Elliot, 1973; Field and Elliot, 1974; Smith and Smith, 1976; Wood, et al., 1976; Condie, et al., 1977; Hellman, et al., 1979; Hynes, 1980; Gelinas, et al., 1982; Ludden, et al., 1982; and Dostal and Strong, 1983). The coherence of some trace elements (Zr, Y, Ti, Hf, and Ta) imply that these elements are immobile (Cann, 1970;

Smith and Smith, 1976; Wood, et al., 1976; and Gelinas, et al., 1982). This coherence may be due to coherent alteration patterns of elements (Hellman, et al., 1977; Hellmen, et al., 1979; and Nystrom, 1984). Since ratios of some elements do not change during alteration (such as Zr/Y, Ti/Zr, and Hf/Ta), these ratios can still be used for tectonic interpretation (Cann, 1970 and Nystrom, 1984).

Studies have shown that large ion lithophile (LIL) elements (K, Sr, Ba, Rb, Cs) are very mobile during alteration. Also, most major elements can be modified by secondary processes. Some trace elements appear to be immobile, though there is contradiction in some studies. The least mobile elements are Ti, Zr, Nb, Hf, Ta, Y, Sc, and heavy REE (Cann, 1970; Pearce and Cann, 1973; Floyd and Winchester, 1975; Smith and Smith, 1976; Condie, et al., 1977; and Nystrom, 1984).

It is preferable to eleminate altered samples by screening analyses. One method is to use known igneous fractionation trends as suggested by Beswick and Soucie (1978) (Fig. 5). Most of the volcanic samples from both the Pedernal and Manzano sections fall in or near the defined igneous rock trends. M601, M742, M758, and P753 consistently plot outside of the magmatic field for most plots and this may be due to secondary alteration.

Other methods of screening include high LOI (>2.5 %),

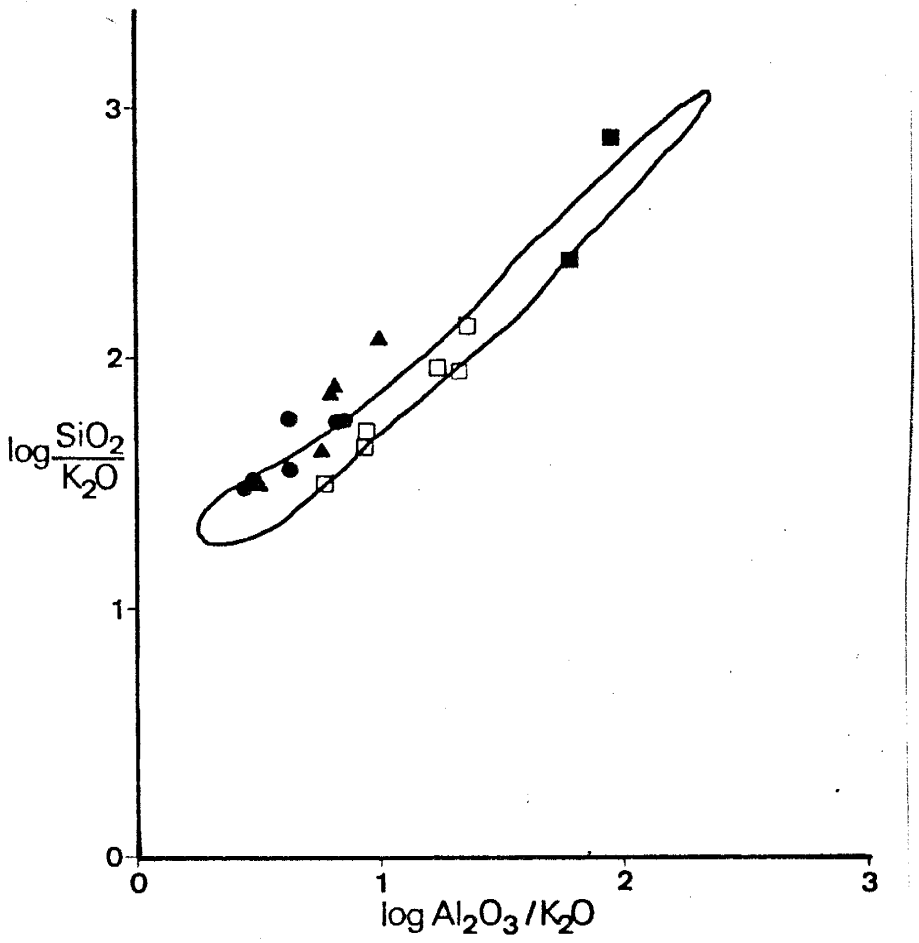

Figure 5. Molecular proportion (SiO2/K2O)-(Al2O3/K2O) diagram with all of the volcanic rock samples from both the Pedernal and the Manzano successions plotted. This diagram is used to detect significantly altered samples which plot outside of the deliniated area. The igneous rock trend is from Beswich and Soucie (1978).

extensive alteration in thin section, and unusual compositions. Most of the mafic samples have high LOI values (1.77-3.97 %), one felsic sample has a high SiO2 content (M743), one felsic volcanic sample has secondary quartz veins (P769), and three samples have unusual major element contents (P719, P753, and P765) (Appendix F). The positive Eu anomaly and low HFS element content of P719 may be related to its high modal content of plagioclase.

CLASSIFICATION

Various rock classification schemes are used by different authors. Classification subdivisions are arbritrary, while natural rocks form a chemical continuum. In this investigation, several classifications are used to better describe the rocks and are discussed in Appendix E. Some problems occur when classifying rocks. One problem is the overlap of various fields due to the different criteria for rock classification. Geochemical criteria should allow for inconsistences (Winchester and Floyd, 1977). Confusion also occurs because different authors have used different terminology to describe the same rock types.

The terms alkalic and subalkaline are used in this report. Subalkaline is further divided into tholeiitic and calc-alkaline groups based on the presence or absence of iron enrichment trends, respectively (Nockolds and Allen, 1953, 1954, and 1956). These divisions are similar to

those of Miyashiro (1974), except for subalkalic, which Miyashiro refers to as non-alkalic. In the classification systems used, the original terminology was converted to the above terms in order to be consistent.

Volcanic rocks from the Pedernal section are divided into felsic and mafic groups and define a bimodal suite (Table 5). This is apparent in the field and in thin section. Only felsic volcanics are analyzed from the Manzano section (Table 6), but minor mafic volcanics also occur in the section. Again, the Manzano section is bimodal. Other Proterozoic terranes of the Southwest also have bimodal volcanic rocks (Condie and Budding, 1979; Condie and Nuter, 1981; Roberston, 1981; and Condie and Shadel, 1984). The bimodal nature of the volcanic rocks is unexplained and is still one of the important questions for the Proterozoic geology of the Southwest. This is especially true of terranes interpreted as arc environments.

Application of different classification schemes to each of the volcanic groups from the Manzano and the Pedernal sections are given is Table 6. The mafic rocks are subalkaline and can further be divided into tholeiitic and calk-alkaline groups. Two mafic volcanic samples are tholeiitic basalts (P760 and P762). The rest of the Pedernal mafic volcanics are calc-alkaline and range from basalt to andesite in composition (P740, P765, P772,

TABLE 6. CLASSIFICATION OF THE VOLCANIC SAMPLES FROM BOTH PEDERNAL AND MANZANO SECTIONS.

Classification	P760	P762	P792	P740	P765
Na2O+K2O-SiO2	SA	SA	SA	SA	SA
Q-Ne-Ol	SA	SA	SA	SA	SA
Cpx-Opx-Ol	SA	SA	---	---	---
Or-Ab-An	T-B	T-B	CA-B	CA-B	T-B
Al2O3-Norm.An	T	T	CA	CA	T
Norm. CI-An	B	B	B	B	B
Middlemost Class	B	B	B	An	An
Type	SA	SA	SA	SA	SA
Rock	T-B	T-B to High Al-B	High Al-B	I	I
FeO*/MgO-SiO2	CA	CA	T	CA	T
Na2O+K2O-SiO2	SA	SA	SA	SA	SA
Alkalinity Index-SiO2	SA	SA	SA	SA	SA
Alkali Index-DI	Low-K	Low-K	Low-K	Low-K	Low-K
DI-Na2O+K2O	SA	SA	SA	SA	SA
Cation Plot	T-B	T-B	CA-An	CA-B	T-B
TiO2-Zr/P2O5	SA	SA	SA	SA	SA-A
Nb/Y-Zr/P2O5	SA	SA	SA	SA	SA
AFM	T	T	CA	CA	T
K2O-SiO2	Low-K B	Low-K BA	BA	Low-K An	Low-K BA
Zr/TiO2-Nb/Y	BA	BA	An	An	BA
SiO2-Nb/Y	B	B	B	An	An
SiO2-Zr/TiO2	B	B	B	An	An

A, alkalic.
SA, subalkalic.
T, tholeiitic.
CA, calc-alkaline.
B, basalt.
BA, basaltic andesite.
An, andesite.
D, dacite.
RD, rhyodacite.
R, rhyolite.

For details of each classification system used, see Appendix F.
Norm. An, normative plagioclase composition.
Norm. CI, normative color index calculated from CIPW norms.
DI, differentiation index.

TABLE 6. CONTINUED.

Classification	P772	P774	P775	P901	P719
Na2O+K2O-SiO2	SA	SA	SA	SA	SA
Q-Ne-Ol	SA	SA	SA	SA	SA
Cpx-Opx-Ol	---	---	---	---	---
Or-Ab-An	CA-B	CA-B		CA-An	T-D
Al2O3-Norm.An	CA	CA	T	CA	---
Norm. CI-An	B	B	B	An	D-An
Middlemost Class	An	An		An	R
Type	SA	SA		SA	High-Ca
Rock	An	I		An	R
FeO*/MgO-SiO2	T	CA	CA	T	T
Na2O+K2O-SiO2	SA	SA	SA	SA	SA
Alkalinity Index-SiO2	SA	SA	SA	SA	SA
Alkali Index-DI	High-K	Low-K	High-K	Low-K	Low-K
DI-Na2O+K2O	SA	SA	SA	SA	SA
Cation Plot	CA-B	CA-B	T-B	CA-An	T-R
TiO2-Zr/P2O5	SA	SA	SA	SA	
Nb/Y-Zr/P2O5	SA	SA	SA	SA	
AFM	T-CA	CA	CA	CA	T
K2O-SiO2	High-K BA	An	High-K An	An	R
Zr/TiO2-Nb/Y	BA	An	An	An	D
SiO2-Nb/Y	An	An	An	An	RD
SiO2-Zr/TiO2	An	An	An	An	RD

A, alkalic.
SA, subalkalic.
T, tholeiitic.
CA, calc-alkaline.
B, basalt.
BA, basaltic andesite.
An, andesite.
D, dacite.
RD, rhyodacite.
R, rhyolite.

For details of each classification system used, see Appendix F.
Norm. An, normative plagioclase composition.
Norm. CI, normative color index calculated from CIPW norms.
DI, differentiation index.

TABLE 6. CONTINUED.

Classification	P767	P710	P769	P720	P969
Na2O+K2O-SiO2	SA	SA	SA	SA	SA
Q-Ne-Ol	SA	SA	SA	SA	SA
Cpx-Opx-Ol	---	---	---	---	---
Or-Ab-An	T-An	CA-D	CA-D	CA-R	CA-R
Al2O3-Norm.An	---	---	---	---	---
Norm. CI-An	An	D	D	R	R
Middlemost Class	R	R	R	R	R
Type	High-Ca	Low-Ca	High-Ca	Low-Ca	Low-Ca
Rock	R	R	R	R	R
FeO*/MgO-SiO2	CA	CA	CA	T	T
Na2O+K2O-SiO2	SA	SA	SA	SA	SA
Alkalinity Index-SiO2	SA	A	SA	A	A
Alkali Index-DI	High-K	High-K	Low-K	High-K	High-K
DI-Na2O+K2O	SA	SA	SA	SA	SA
Cation Plot	CA-D	CA-D	CA-D	T-R	T-R
TiO2-Zr/P2O5					
Nb/Y-Zr/P2O5					
AFM	CA	CA	CA	---	---
K2O-SiO2	R	R	R	R	R
Zr/TiO2-Nb/Y	RD	RD	R	R	R
SiO2-Nb/Y	R	RD	RD	R	R
SiO2-Zr/TiO2	R	RD	RD	R	R

A, alkalic.
SA, subalkalic.
T, tholeiitic.
CA, calc-alkaline.
B, basalt.
BA, basaltic andesite.
An, andesite.
D, dacite.
RD, rhyodacite.
R, rhyolite.

For details of each classification system used, see Appendix F.
Norm. An, normative plagioclase composition.
Norm. CI, normative color index calculated from CIPW norms.
DI, differentiation index.

TABLE 6. CONTINUED.

Classification	P753	M601	M723	M758	M743
Na2O+K2O-SiO2	SA	SA	SA	SA	SA
Q-Ne-Ol	SA	SA	SA	SA	SA
Cpx-Opx-Ol	---	---	---	---	---
Or-Ab-An	CA-D	CA-D	CA-D	CA-D	CA-R
Al2O3-Norm.An	---	---	---	---	---
Norm. CI-An	D	D	D	D	R
Middlemost					
Class	R	R	R	R	R
Type	Low-Ca	High-Ca	High-Ca	High-Ca	High-Ca
Rock	R	R	R	R	R
FeO*/MgO-SiO2	CA	CA	CA	CA	CA
Na2O+K2O-SiO2	SA	SA	SA	SA	SA
Alkalinity					
Index-SiO2	SA	SA	SA	SA	A
Alkali Index-					
DI	High-K	Low-K	High-K	Low-K	Low-K
DI-Na2O+K2O	SA	SA	SA	SA	SA
Cation Plot	CA-B	CA-D	CA-D	CA-D	CA-R
TiO2-Zr/P2O5					
Nb/Y-Zr/P2O5					
AFM	CA	CA	CA	CA	---
K2O-SiO2	R	Low-K R	R	Low-K R	Low-K R
Zr/TiO2-Nb/Y	D	RD	RD	RD	R
SiO2-Nb/Y	R	R	R	R	R
SiO2-Zr/TiO2	R	R	R	R	R

A, alkalic.
SA, subalkalic.
T, tholeiitic.
CA, calc-alkaline.
B, basalt.
BA, basaltic andesite.
An, andesite.
D, dacite.
RD, rhyodacite.
R, rhyolite.

For details of each classification system used, see Appendix F.
Norm. An, normative plagioclase composition.
Norm. CI, normative color index calculated from CIPW norms.
DI, differentiation index.

P774, P775, P792, and P901). The felsic volcanics from both successions are calc-alkaline and range in composition from rhyodacite to high-silica rhyolite.

FELSIC VOLCANIC ROCKS

The felsic volcanic rocks from both the Pedernal and Manzano sections range in composition from rhyodacite to high-silica rhyolite. In these rocks, there is a general decrease in TiO2, Al2O3, Fe2O3-T, and MgO with increasing SiO2. Sample P753 is the major with low Al2O3, K2O, and Na2O and high MgO and Fe2O3-T at high SiO2. P753 consistently plots off the igneous rock trends (Fig. 5) and maybe altered.

CaO, Na2O, K2O, MnO, and P2O5 behave erratically with increasing SiO2 (see Appendix F). Considering the low LOI values (0.24-1.78 %), the present compositions may reflect the original compositions. P753, with its unusual composition, and P769 and M743, which are silicified, are exceptions.

Felsic volcanics from both sections have light REE enriched patterns with La/Yb ranging from 4.4 to 10.2. In the Pedernals, all but two (P719 and P753) of the felsic volcanics have negative Eu anomalis (Figs. 6 and 7). The positive Eu anomaly of P719 can be explained by the high modal plagioclase content and Eu is preferentially partitioned into plagioclase.

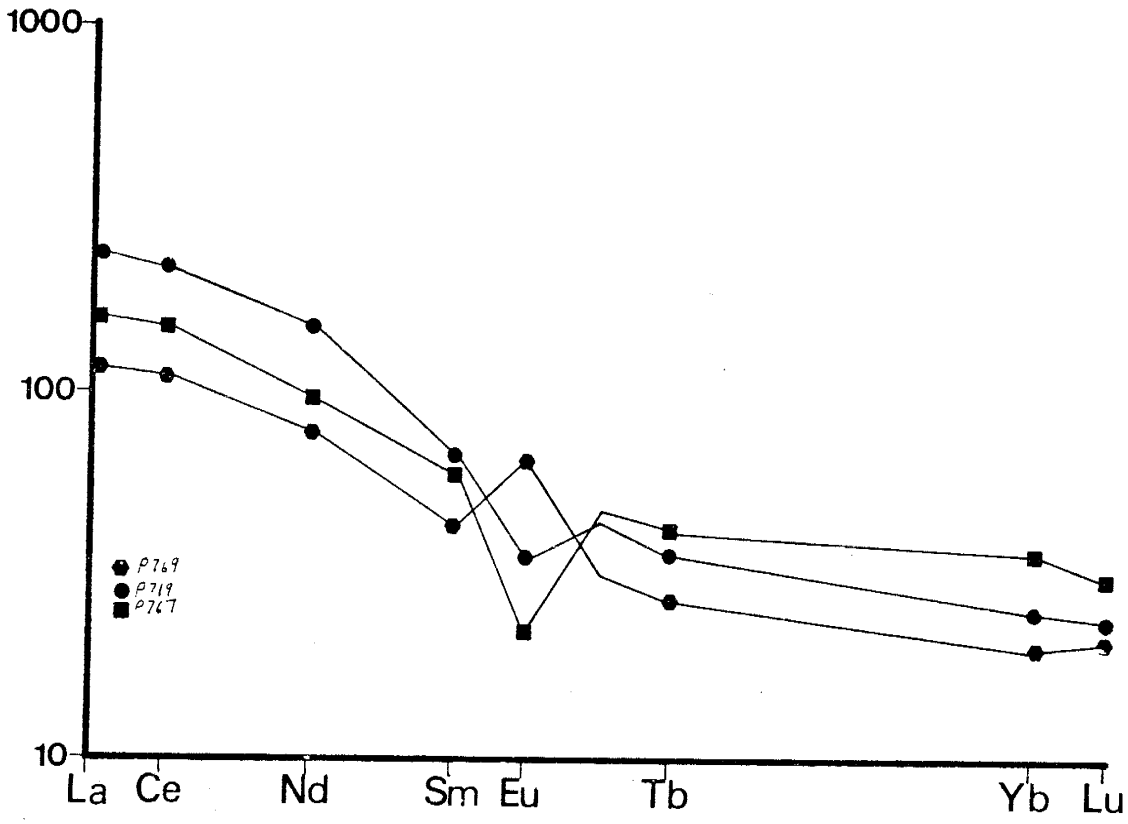

Figure 6. Chondrite normalized REE diagram of three of the felsic volcanic rocks from the Pedernal succession. Normalizing values are given in Appendix F.

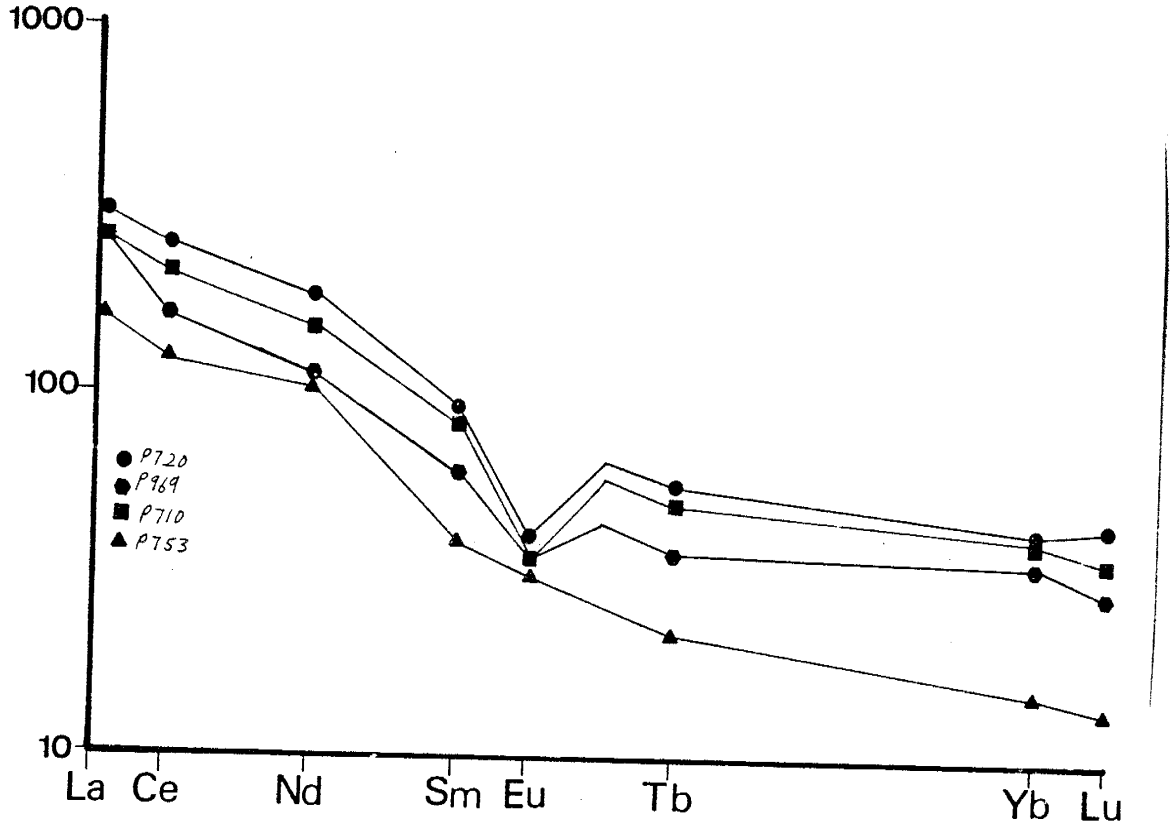

Figure 7. Chondrite normalized REE diagram of four of the felsic volcanic rocks from the Pedernal succession.

P753 has no Eu anomaly (Eu/Eu*=1; Fig. 7). The heavy REE are also depleted compared to other felsic volcanics from the Pedernals. The high Mg number (55.7) is similar to the mafic volcanics.

The Manzano samples show a variable Eu anomaly, with both negative (Eu/Eu*=0.58) and positive (Eu/Eu*=1.4) Eu anomalies (Figs. 8 and 9). Although the positive Eu anomalies may be due to plagioclase accumulation, there is no petrographic evidence to support this idea.

Compatible elements (Sc, V, Cr, Co, and Ni) have low concentrations in felsic volcanics from both the Pedernal and Manzano sections and in some cases, the concentrations are below detectability limits. The concentration of these elements is in the range reported for modern calc-alkaline felsic volcanics (Ewart, 1979).

LIL elements have variable concentrations in the felsic volcanics. This variation is, at least, in part related to magmatic fractionation overprinted by alteration. These elements are not very useful for tectonic interpretation or magma modeling due to their mobile nature.

The high field strength (HFS) elements have variable to uniform concentrations in the felsic samples. Zr and Hf have variable concentrations in the Pedernal samples with less variation in the Manzano samples. This may reflect different amounts of zircon in the rocks. Nb, Y, and Ta have uniform concentrations in felsic rocks within each

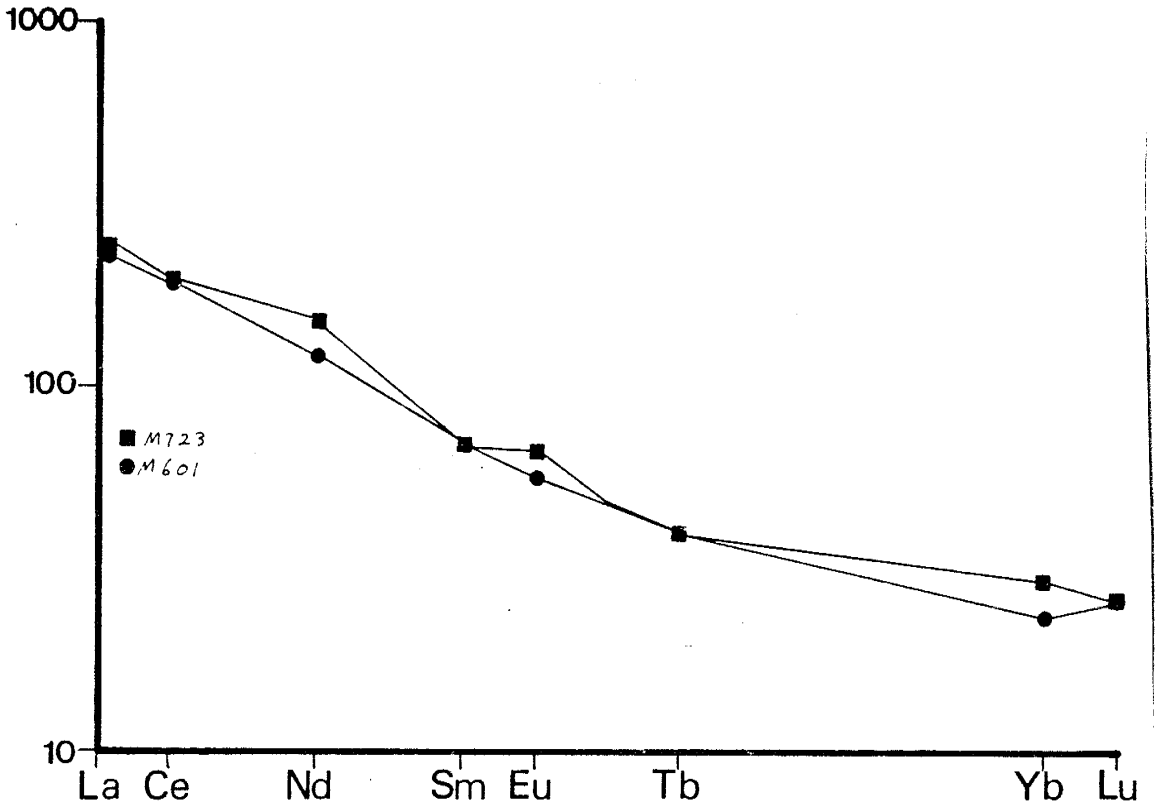

Figure 8. Chondrite normalized REE diagram of two of the felsic volcanic rocks from the Manzano succession.

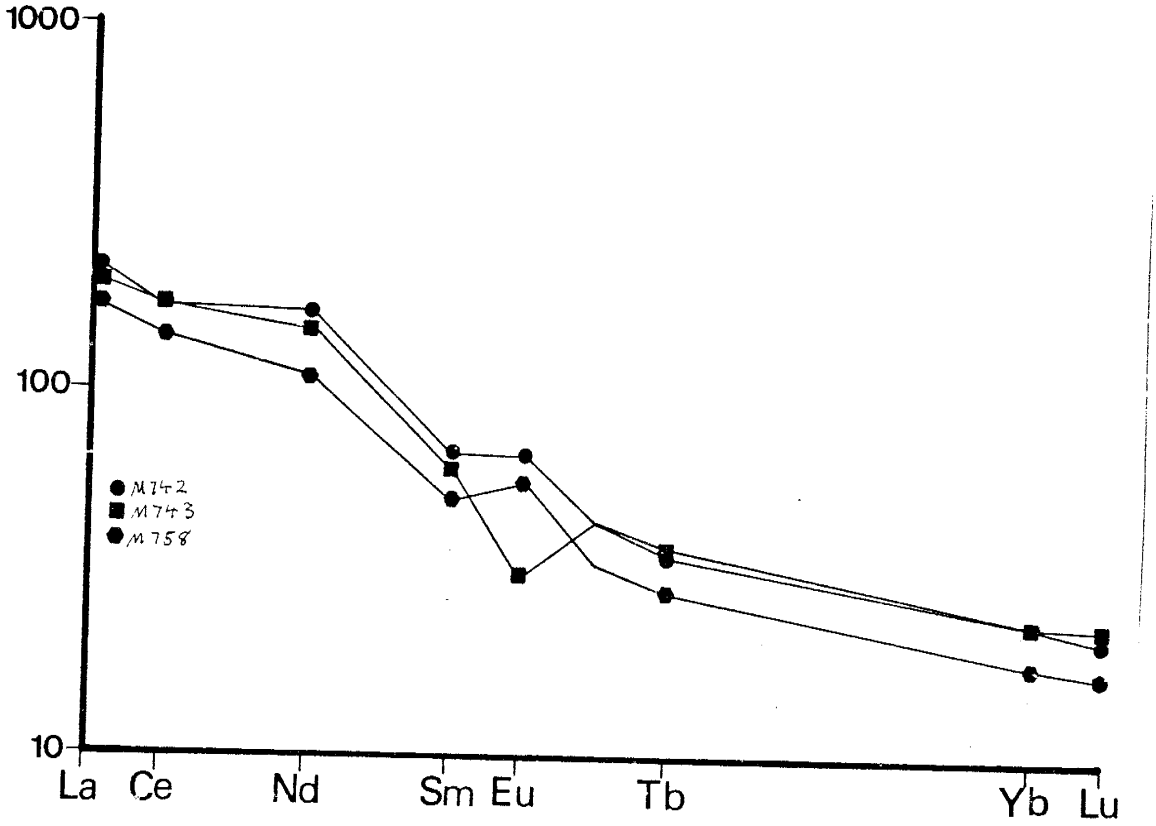

Figure 9. Chondrite normalized REE diagram of three of the felsic volcanic rocks from the Manzano succession.

section, but vary between sections. Nb, Y, and Ta have higher concentrations in the Pedernal samples than the Manzano samples.

MAFIC VOLCANIC ROCKS

Mafic volcanics were analyzed from the Pedernal section only. The Manzano section contains mafic volcanics, but they are of minor importance. Although there are larger occurrences of mafic volcanics north of the Ojita Pluton (Rieche, 1949 and Condie and Budding, 1979), they may or may not be related to the Manzano section.

The mafic volcanics from the Pedernal section range from 50 to 58 % SiO2 and can be divided into tholeiitic and calc-alkaline groups using conventional AFM and MgO/FeO plots (see Appendix E). Samples P760 and P762 are tholeiitic basalts. P760 has a flat REE pattern while P762 has a slighyly light REE enriched pattern (Fig. 10) and neither has an Eu anomaly, so plagioclase was probably not an important phase in their petrogenesis.

For comparison, modern tholeiites are also given in Table 7. Cr is lower and Co is higher while V, Sc, and Mn have roughly the same concentrations in the Pedernal tholeiites as in modern tholeiites. Ni is relatively low in the Pedernal samples but is similar to Ni in IAB. The low Cr and Ni contents in the Pedernal basalts may be

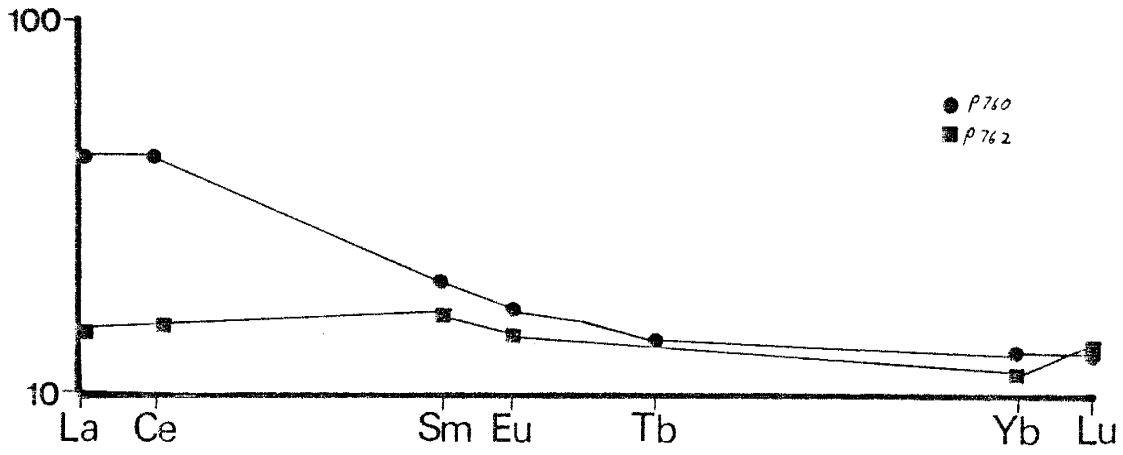

Figure 10. Chondrite normalized REE diagram of the tholeiitic basalts from the Pedernal succession.

TABLE 7. COMPARISION OF MODERN THOLEIITES AND P760 AND P762

	N-MORB	ISLAND	RIFT	CAB	IAB	P762	P760
SiO2	51.5	50.5	51.5	51.6	51.7	50.4	51.9
TiO2	1.6	2.2	2.3	1.0	0.85	0.57	0.74
Al2O3	16.2	16.0	16.6	17.4	17.5	16.4	13.9
FeO-T	8.8	9.8	8.9	9.1	9.4	9.00	11.1
MgO	6.5	7.2	6.5	6.8	7.0	8.81	8.01
CaO	11.9	9.8	9.5	9.7	10.2	11.1	9.49
Na2O	3.0	3.1	3.0	2.7	2.6	2.38	3.20
K2O	0.12	0.90	1.2	1.2	0.49	0.10	0.21
MnO	0.18	0.18	0.17	0.18	0.18	0.15	0.18
P2O5	0.16	0.30	0.35	0.30	0.09	0.088	0.063
Rb	1.0	15	35	20	8	2.7	7.4
Ba	12	315	400	350	125	91	182
Sr	130	375	385	525	260	139	87
Zr	110	150	262	140	55	56	48
Y	33	40	35	25	21	22	23
Nb	3	15	19	5	2.0	5.4	5.0
Hf	3.6	3.8	5.0	2.5	1.0	1.7	1.2
Th	0.2	2.5	3.5	1.5	0.50	2.3	1.7
La	3.5	20	27	10	3.0	15	4.9
Sm	2.9	8.5	9	3.5	1.5	4.0	3.1
Yb	2.6	2.2	2.8	2.5	2.0	2.8	2.4
V	275	240	250	226	253	227	311
Sc	42	30	41	30	34	48	45
Cu	80	46	62	80	90	121	185
Zn	75	80	82	80	81	77	99
Ni	80	100	75	50	30	25	21
Co	35	40	32	30	32	63	57
Cr	225	220	200	100	145	66	49

FeO-T is total iron as FeO.
ND is not determined or below the detectability limit.
Analyses recalculated to 100 %, volatile free.
N-MORB, ISLAND, RIFT, CAB, AND IAB are averaged data from Condie (1985).
ISLAND is average oceanic island basalt, RIFT is average continental rift basalt, CAB is average continental arc basalt, and IAB is average island arc basalt.

related to one or more of three possiblities. 1) Ni and Cr are preferentially partitioned into ferromagnesium minerals in basalts, but olivine and pyroxene are not present and may have broken down during metamorphism. Therefore, Ni and Cr could have been leached from the samples during metamorphic recrystallization. Mn and Co are also preferentially partitioned into ferromagnesium minerals and if leaching were the primary reason for lower Ni and Cr, then Mn and Co should also be lower. The fact they are not lower, however, suggests that leaching was not the primary mechanism for low Ni and Cr.

2) Differences in crystallization history of samples P760 and P762 compared to modern tholeiites. A possible difference in crystallization history may be related to the amount of olivine and Cr-spinel removed. Cr-spinel has a high Kd for Cr and lower Kds for Sc, V, Ni, and Co (Irving, 1978). Extensive crystallization of Cr-spinel from the parental magmas of P760 and P762 (compared to modern tholeiitic magmas) could explain the low Cr, but not the low Ni and high Co. The depletion of Cr and Ni relative to Co may be explained by crystallization of pyroxenes and magnetite. The Kds for Cr and Ni are higher than the Kd for Co in both pyroxenes and magnetite (Ewart, et al., 1973). The large depletion of Cr relative to Ni could be explained by the larger Kd for Cr relative to Ni in pyroxenes and magnetite (Ewart, et al., 1973). Support for magnetite crystallization is evident in terms of low TiO2

in both P760 and P762 compared to the modern tholeiites. The high total Fe and V contents, however, do not support significant magnetite crystallization. P760 and P762 also have high MgO contents compared to modern tholeiites, and Al2O3 and Fe2O3-T contents for P760 are also high. The HFS elements, REE, Th, Rb, Sr, and Ba concentrations in P760 and P762 are within the range of average modern tholeiites.

Calc-alkaline rocks range in composition from basalt to andesite and have light REE enriched patterns (La/Yb=4.3 to 10.3: Figs. 11 and 12). La is 85-155 X chondrites and Yb is 13-20 X chondrites. Eu anomalies (Eu/Eu*) range from 0.65 to 0.95 and do not vary with SiO2 content, Mg number, or other compositional measures of differentiation. The rocks generally have high Al2O3, which together with the small Eu anomalies indicates only a limited role for plagioclase in the petrogenesis.

The HFS element contents of the calc-alkaline volcanics fall in the range of modern subalkaline rocks (Condie, 1985). HFS elements, Th, and U increase while MgO and Sc decrease with increasing SiO2.

Sr, Ba, Rb, V, Sc, and Mn contents of the calc-alkaline rocks are generally within the range of modern subalkaline volcanics (Condie, 1985). Cr and Ni are low and Co is quite variable in the these samples compared to modern average subalkaline rocks (Condie, 1985). The Cr, Ni, and Co values may be explained by the more evolved

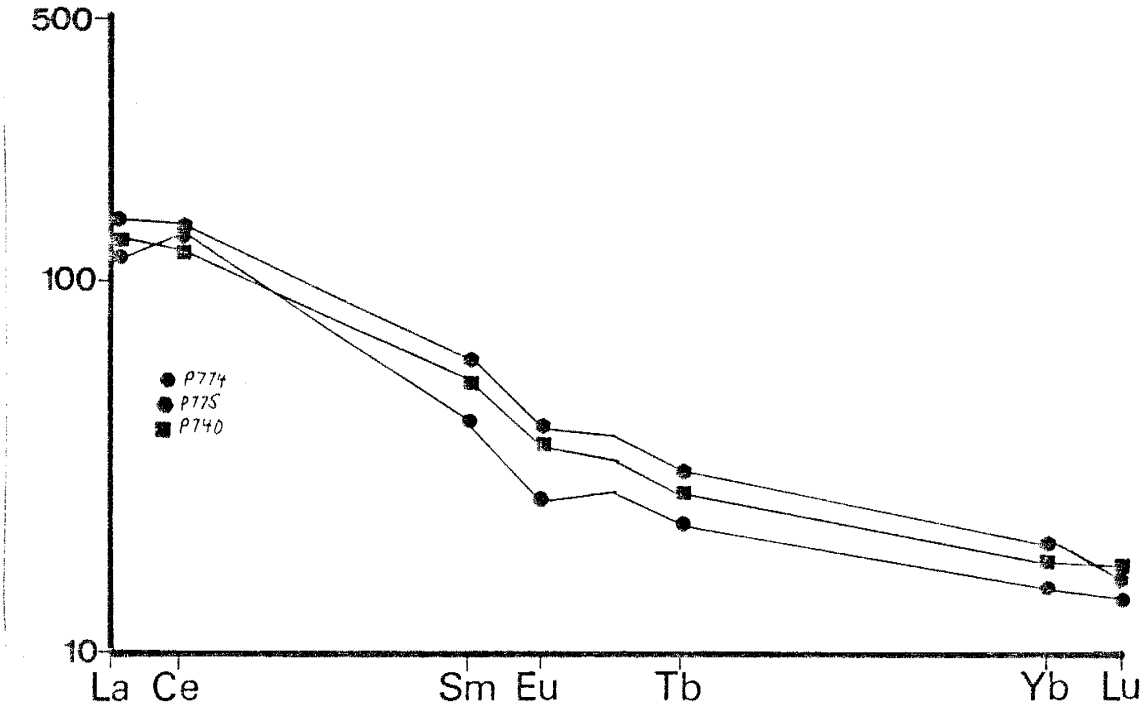

Figure 11. Chondrite normalized REE diagram of one calc-alkaline basalt and two calc-alkaline andesites from the Pedernal succession.

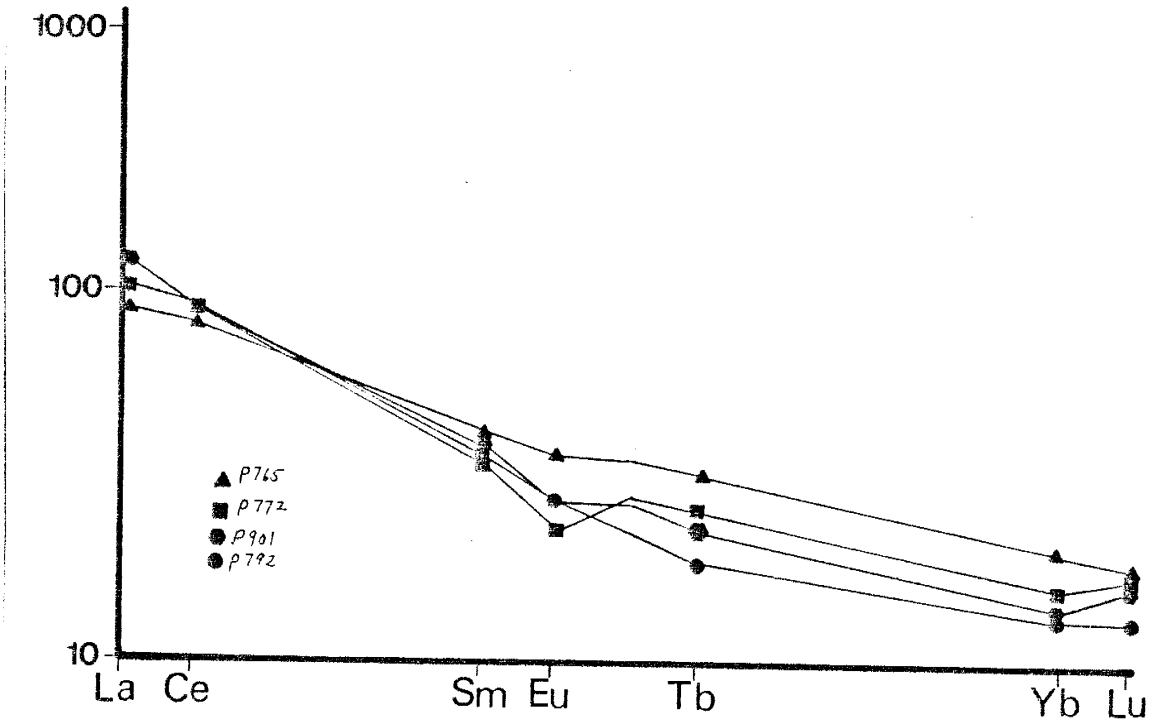

Figure 12. Chondrite normalized REE diagram of four of the calc-alkaline andesites from the Pedernal succession.

nature of the calc-alkaline magmas, by alteration, or differences in crystallization history (see discussion under tholeiites for more details).

VOLCANICLASTIC ROCKS

Clast-Matrix Pairs, Pedernal Section

One clast and a coexisting matrix sample from three volcaniclastics were analyzed from the Pedernal section. These analyses were made to evaluate how closely the composition of the clasts in volcaniclastic units match the compositions of the corresponding matrices. Also, some Proterozoic rocks of the Southwest have been identified as andesites using major element compositions. These andesitic units in some cases are breccias and the major element compositions may be due to mixing of mafic and felsic rock material.

In choosing the volcaniclastic samples for analyses, areas that contained a diverse clast population, had obvious secondary alteration, or contain unusual clasts (quartzite, chert, and some meduim- to coarse-grained mafic clasts) were avoided. This limits the possibility that the composition of the matrix is influenced by unusual clast types or alteration. The dominate clast type in each volcaniclastic sample was chosen for analysis. In separating the matrix, not all of the small clasts could be

removed. The matrix of each sample may in part be composed of clasts similar to the ones analyzed, either as clasts that could not be removed or as secondary matrix formed by recrystallization.

One of the volcaniclastics is mafic (P742) and the other two (P739 and P900) are felsic (see appendix D). Figure 13 shows the compostion of each clast divided by the compostion of its corresponding matrix. The compostion of the clasts is similar to the compostion of the corresponding matrix, with variations generally less than a factor of 0.5.

For both of the clast-matrix pairs from the felsic volcaniclastics, the matrix contains more than twice the concentration of P2O5, Cs, and Co than the coexisting clast which may be due to secondary alteration during or after deposition. Sample P739 has higher Hf, U, and Yb and lower Zn and TiO2 concentrations in the clast than the coexisting matrix. Sr, Th, Zr, Ta, Yb, and Lu have higher concentrations in the clast compared to the matrix in sample P900. The high Sr could be due to alteration or a larger modal content of plagioclase in the clast compared to the matrix, while the high Zr and Ta may be due to a larger modal zircon content in the clast.

Samples P900 and P739 have similar compositions to the felsic volcanics from the Pedernal section. Compared to the felsic volcanics, they have higher Al2O3, Sr, and CaO contents and lower Ba and Rb concentrations and this may be

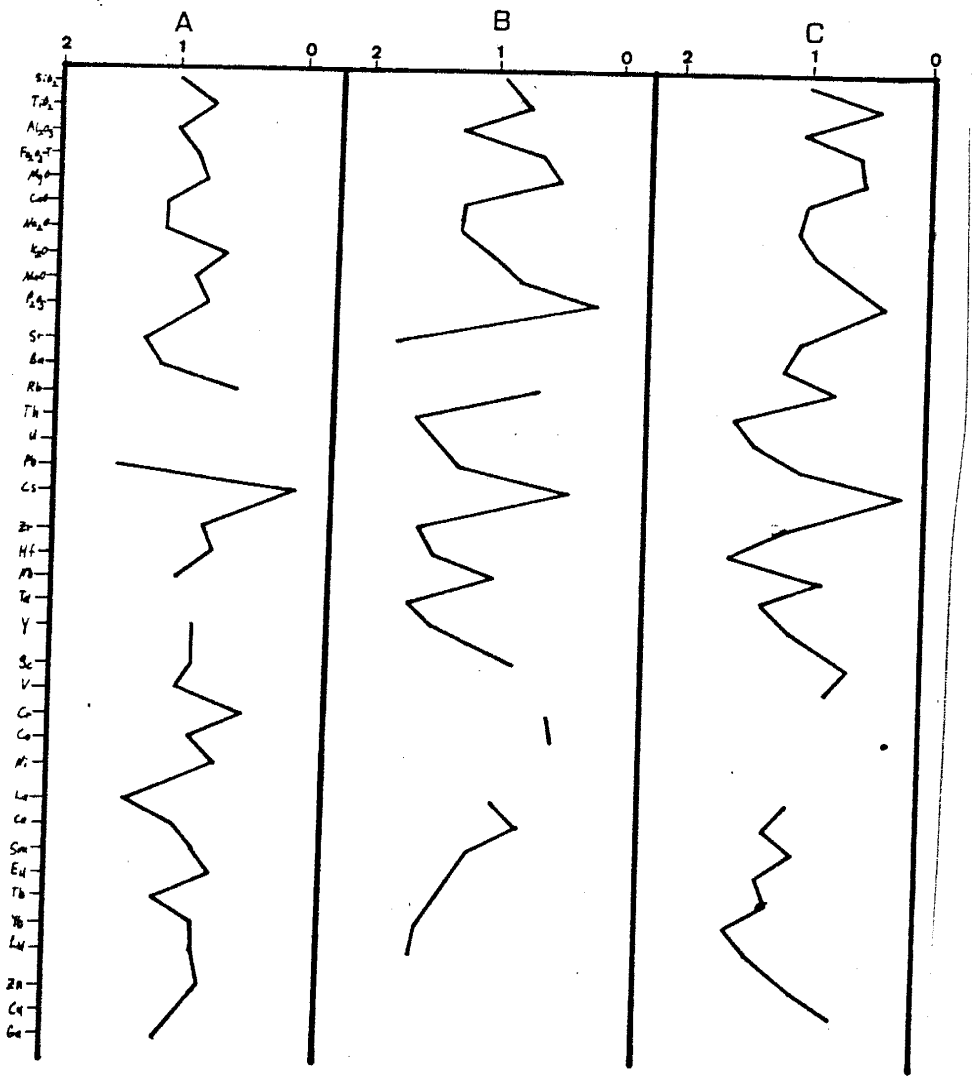

Figure 13. Composition of volcanic clasts divided by the composition of the coexisting matrix for each of the volcaniclastic pairs. A is P742, B is P900, and C is P739.

due to alteration. Also, the higher Al2O3, CaO, and Sr may be explained by the higher modal contents of plagioclase in the volcaniclastic rocks compared to the felsic volcanics. This is supported by the generally low content of plagioclase phenocrysts in the volcanics and the high content of plagioclase observed in the felsic volcaniclastics.

In sample P742, Pb is higher and Cs and Cr lower in the clast than in the coexisting matrix. This rock has a similar composition to the tholeiitic volcanics. It has a flat REE pattern with no Eu anomaly (Fig. 14), similar to sample P760. REE and Sc contents are slightly higher while Ba and Ni are lower in P742 than in P760.

Manzano Section

After inspection of thin sections from the Manzano succession, one sample (M734) originally identified as a felsic volcanic is in fact a volcaniclastic rock. It has high content of LIL elements and HFS elements, low concentrations of compatible elements, and a light REE pattern with a positive Eu anomaly (Fig. 15). Compared to felsic volcanics from the Manzano section, M734 has lower SiO2 and higher concentrations of TiO2, Al2O3, Sr, Pb, Zr, Hf, and Eu. The higher Al2O3, Sr, and Eu contents are problably due to the high modal plagioclase. The high TiO2, Zr, and Hf could be related to higher modal Fe-Ti

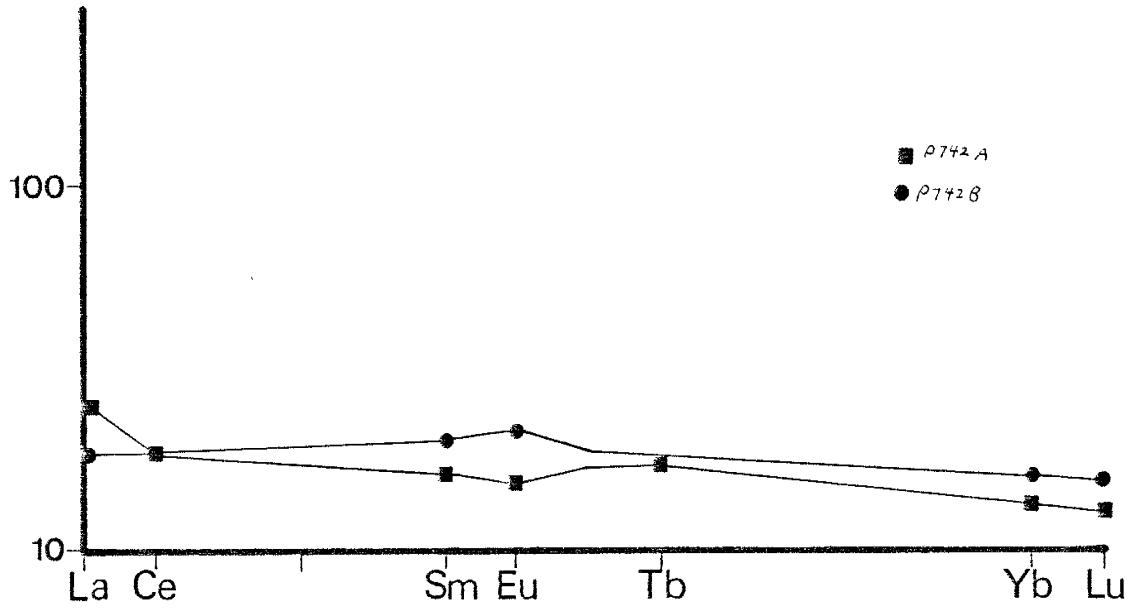

Figure 14. Chondrite normalized REE diagram of the mafic volcaniclastic rock from the Pederanl succession.

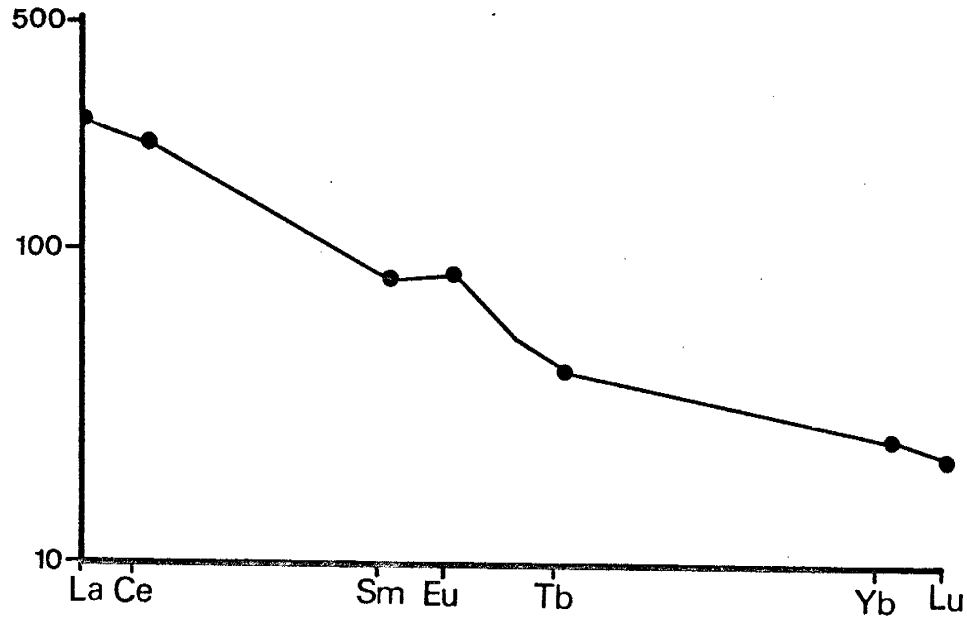

Figure 15. Chondrite normalized REE diagram of the felsic volcaniclastic rock from the Manzano succession.

oxides and zircon, but there is no petrographic evidence to support this. Another possible explanation is alteration, but Ti, Zr, and Hf are believed to be relatively immobile.

Since M734 has a similar composition to felsic volcanic rocks from the Manzano section, it is believed to have been derived from the felsic volcanics. In thin section, it has one large quartz grain probable derived from a granitic source.

SEDIMENTARY ROCKS

Sedimentary rocks in the Manzano section are felsic in major-element composition. They are enriched in TiO2, Fe2O3-T, MgO, Nb, Ta, Cr, Co, U, Th, and V relative to the associated felsic volcanic rocks. Although such enrichment suggests high ferromagnesium mineral contents, petrographic studies do not support such an inference. The low CaO in the sedimentary rocks relative to that in the felsic volcanics may reflect losses during plagioclase alteration and supporting this possibility is the fact that plagioclase is commonly altered. The enrichment of Th, U, Nb, Ta, Co, Cr, V, TiO2, and Fe2O3-T in the sedimentary rocks compared to associated felsic volcanic rocks could be due to enrichment of heavy minerals in the sediments during weathering, transportation, and deposition, but petrographic evidence to support this idea is lacking. The higher TiO2, Co, Cr, U, and Th in the sedimentary rocks may

be due to concentration of these elements in clays during weathering (Pettijohn, 1963; Bhatia and Crook, 1986; and van de Kamp and Leake, 1986). The high modal abundance of sericite in the matrices is evidence for clays in the original sediments. The sedimentary rocks are believed to have been derived by penecontemporary erosion of the interbedded felsic volcanics.

TECTONIC INTERPRETATIONS

INTRODUCTION

Tectonic environmental interpretations are based on rock types and rock associations along with geochemical characteristics. Phanerozoic-type tectonic settings are used as models for the Proterozoic terranes. It is possible that Proterozoic tectonics may have been different than Phanerozoic tectonics. In fact, Proterozoic tectonics may have been transitional from Archean tectonics to Phanerozoic tectonics (Greenberg and Brown, 1983), though "modern-type" arc environments may have begun just after 2.0 Ga (Condie, 1985) with the Wopmay orogen as an example (Hoffman, 1980). Terranes 1.7 -1.9 Ga in age appear to have a large percentage of igneous rocks formed in both island arcs and continental margin arcs (Condie, 1986 and Patchett and Arndt, 1986).

GEOCHEMICAL CHARACTERISTICS

Published tectonomagmatic diagrams which employ relatively immobile trace elements are used along with MORB normalized spider diagrams to assess possible tectonic environments for both the Manzano and Pedernal sections. Comparison of overall compositions of volcanic rocks from both sections with various modern rock types is also

presented. There may be problems comparing two different sets of data based on silica content because the data sets may not have the same degree of differentiation at the same silica content (Gill, 1981) and also the possibility of silicification during metamorphism. In order to limit differences due to differentiation among mafic and andesitic rocks, comparisons are made with modern volcanics that have similar Mg numbers to the samples studied.

Phenocryst accumulation or removal can change a magma's composition. One possible way to screen rocks that have accumulated phenocrysts is to use the Al2O3/TiO2 and Cr/Ti ratios (Pearce and Norry, 1979). Pearce and Norry (1979) state (p 37) that cumulate rocks can be differentiated from noncumulate rocks by using the Al2O3/TiO2 and Cr/Ti ratios (Pearce and Flowers, 1977). Inspection of the diagrams proposed by Pearce and Flowers (1977) show overlap of cumulate and noncumulate rocks. So the distinction of cumulates from noncumulates cannot be made solely by use of the Al2O3/TiO2 or Cr/Ti ratios. The ability to distinguish cumulate from noncumulate rocks is critical to the tectonic interpretations of Pearce and Norry (1979).

There are problems with tectonomagmatic discrimination diagrams. Some use mobile elements (Sr, Rb, K, and others) which can lead to incorrect interpretations. Also, not all diagrams can distinguish between many recognized modern tectonic environments. Scatter on a diagram may be

attributed to fractional crystallization of a suite of rocks (Prestvik, 1982). There are problems in other studies showing that tectonic interpretation must also be consistent with field data (Morrison, 1978; Thompson, et al., 1980; and Holm, 1982).

Mafic and Andesitic Rocks

Most work on tectonic discrimination has dealt with basalts. Mafic and andesitic rocks from the Pedernals plot in areas corresponding to arc volcanics, back-arc basin volcanics, and MORB on the Ti-V diagram (Fig. 16) (Shervias, 1982). The rocks have low TiO2 concentrations, a typical feature of arc rocks. On a La-Ta diagram (Fig. 17) the calc-alkaline basalt and andesites fall in or near the arc field. These rocks have low Ta, a characteristic of arc volcanics. The tholeiites are not plotted since Ta concentrations are below the detectablilty for INAA (<0.2 ppm). On figure 18, the calc-alkaline basalt and andesites plot in the continental arc field. This diagram separates island-arc volcanic rocks from continental-arc voclanic rocks since Ta is enriched only in continental-arc volcanic rocks.

The Zr/Y-Zr diagram is not definitive in terms of mafic and andesitic volcanics from the Pedernals (Fig.

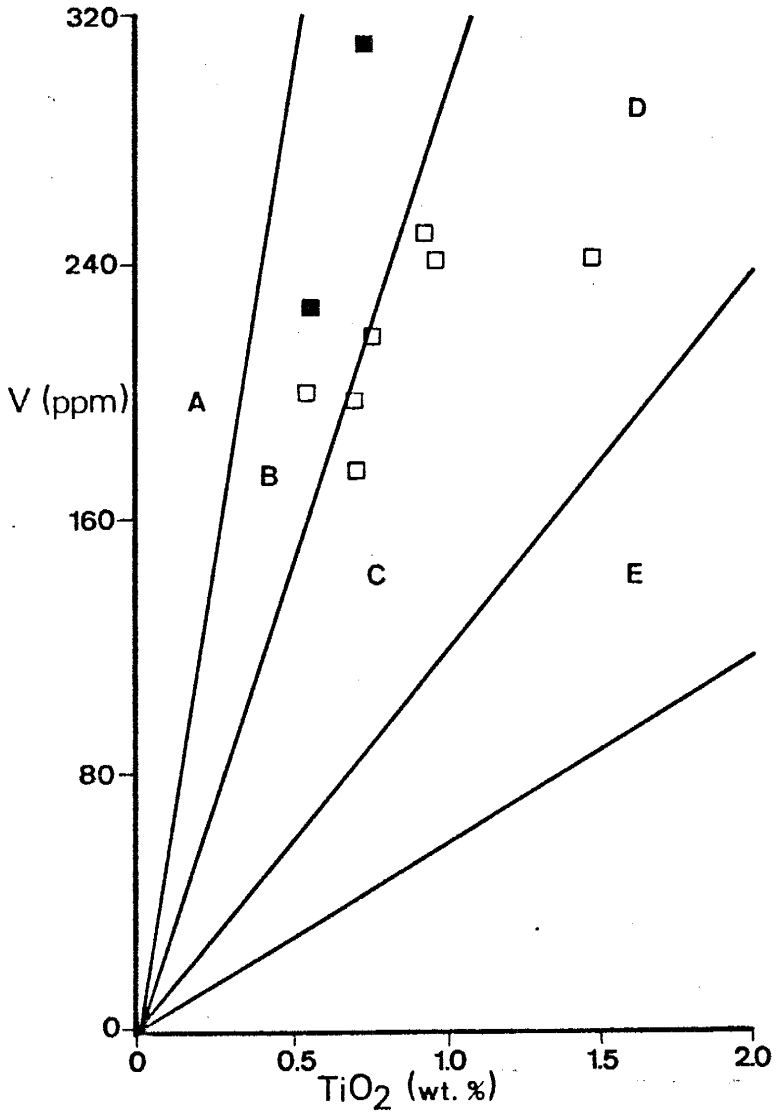

Figure 16. TiO2-V diagram showing the distribution of basalts and andesites from the Pedernal succession. Open squares are calc-alkaline volcanics and closed squares are tholeiitic volcanics. Fields are A and B, arc basalts; B, back-arc basin basalts; C, MORB and within plate basalts; and D, within plate basalts.

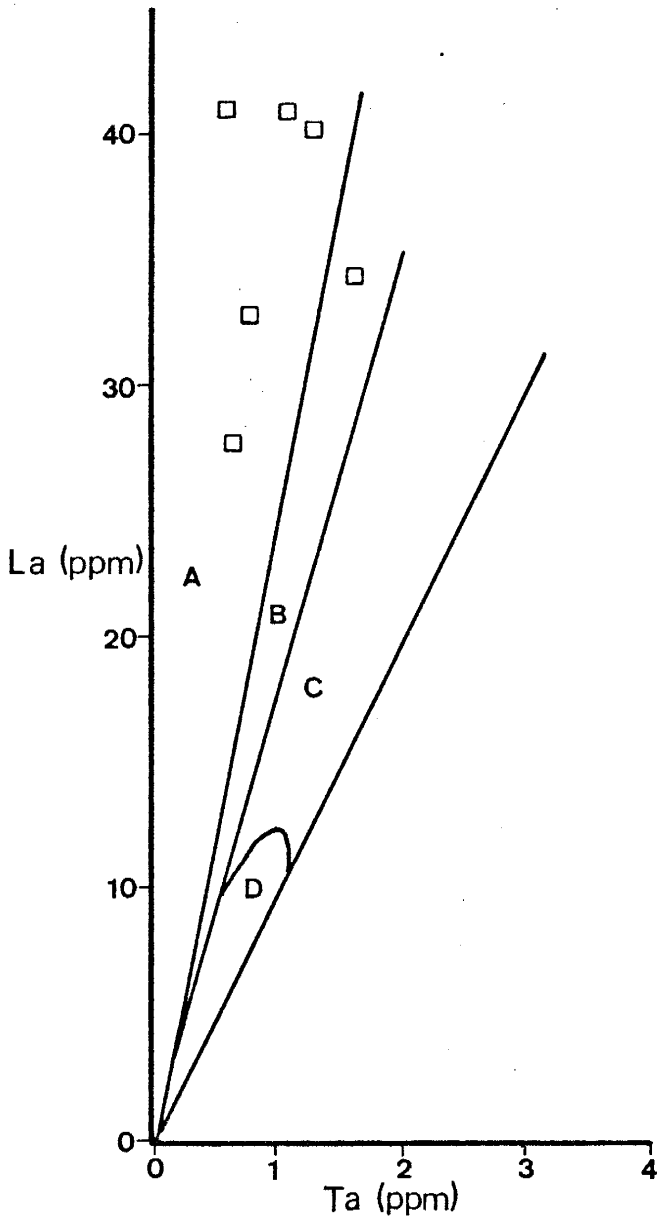

Figure 17. Ta-La diagram showing the distribution of basalts and andesites rock from the Pedernal succession. Fields modified from Drury (1983). CRB, continental rift basalts and OIB, oceanic island basalts. Symbols as in Fig. 16. Fields are A, arc basalts; B, mixed; C, MOR, oceanic island, and continental rift basalts; and D, MORB.

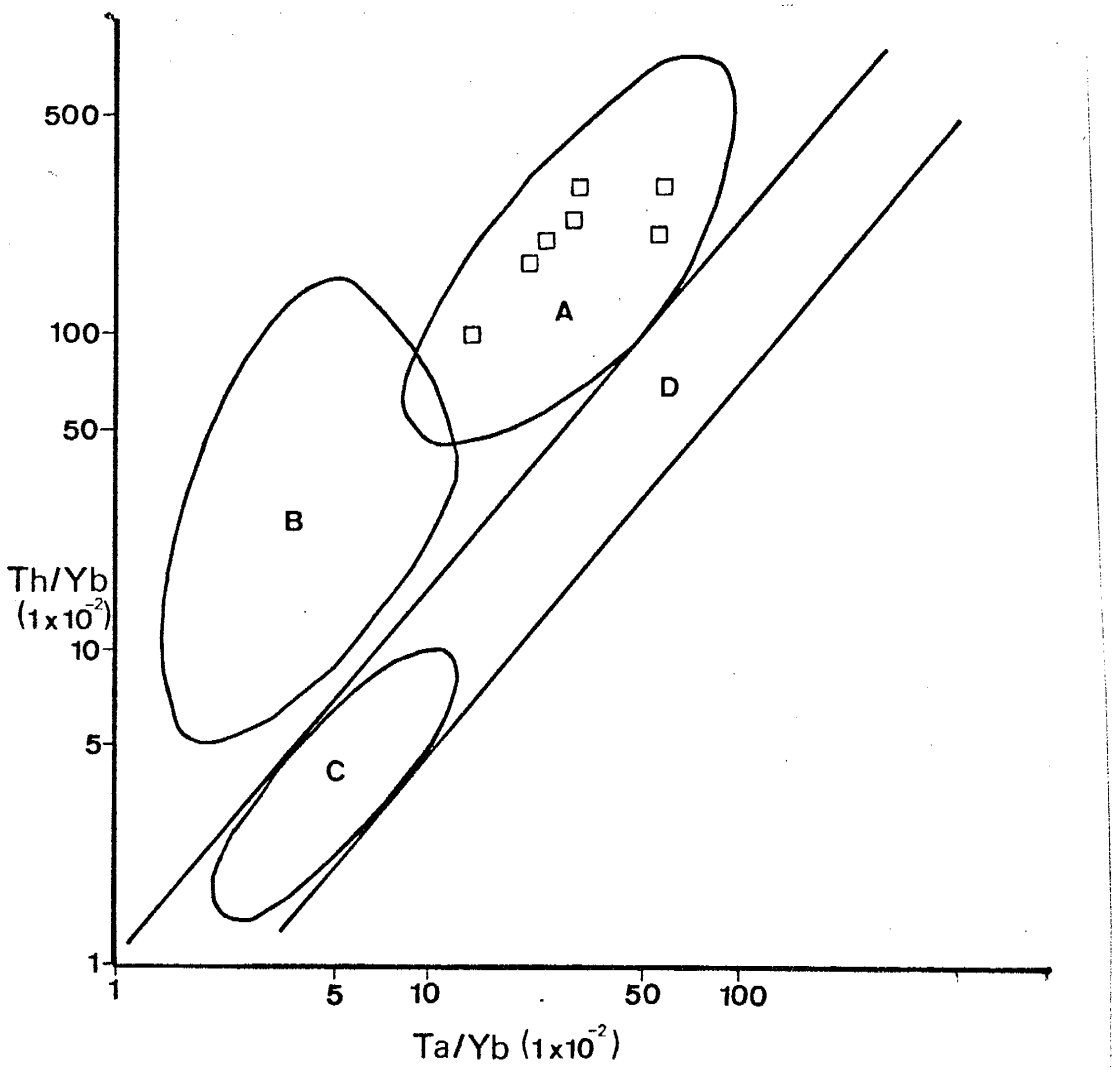

Figure 18. Ta/Yb-Th/Yb diagram showing the distribution of basalts and andesites from the Pedernal succession. Fields from Pearce (1983). Symbols as in Fig. 16. Fields are A, continental arc; B, island arc; C, MORB; and D, within plate.

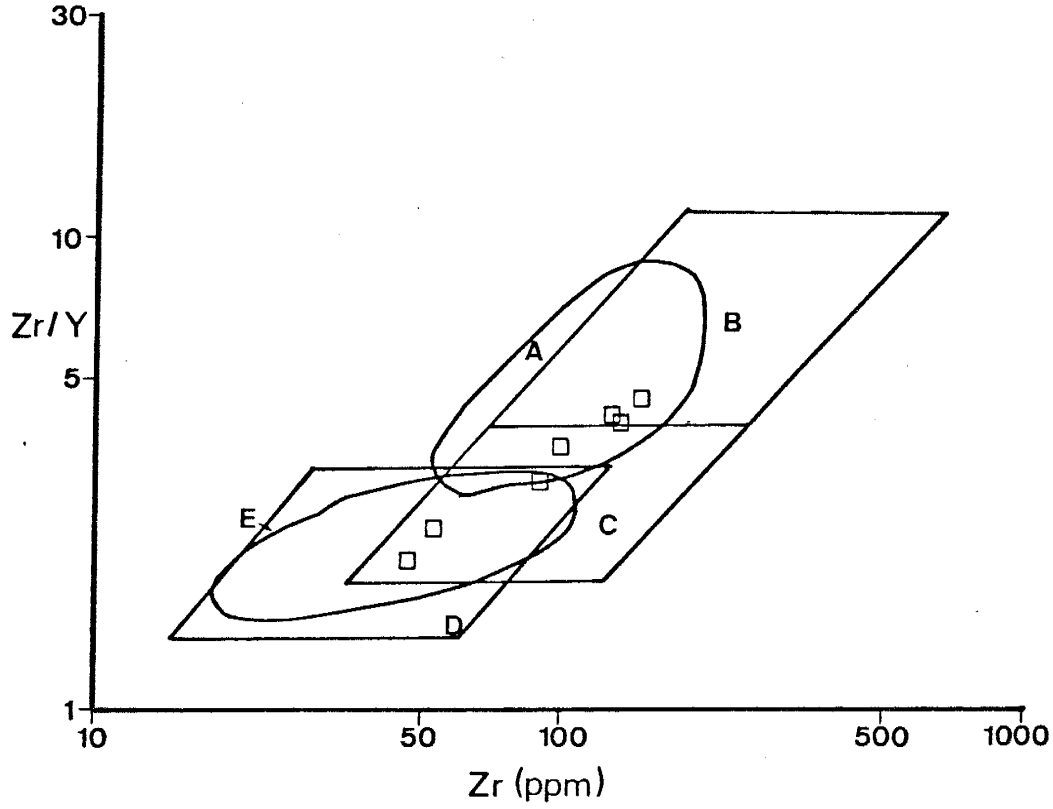

Figure 19. Zr-Zr/Y diagram showing the distribution of basalts and andesites form the Pedernal succession. Fields from Pearce (1983). Symbols as in Fig. 16. Fields are A, continental arc; B, oceanic island; C, MORB; and D and E, island arc.

19). There is considerable overlap of the fields on this diagram, but the data are consistent, though not conclusive, with an arc environment. The mafic and andesitic rocks plot in the island-arc field on a Ti-Cr digram (Fig. 20), a feature consistent with their low Cr and Ti.

Pearce (1983) proposes MORB-normalized spider diagrams to distinguish samples from different tectonic environments. Selected modern samples from different tectonic environments are plotted on MORB-normalized diagrams and compared to the results of Pearce (Appendix H). The reference samples plotted are from the literature and are discussed in appendix H. The fields proposed by Pearce are slightly expanded, but the conclusions of Pearce are still valid. The data base used to construct the diagrams includes only modern mafic volcanic rocks, but it appears that Proterozoic basalts can be compared to modern basalts (Pharaoh and Pearce, 1984).

Samples P760 and P762 have spidergrams similar to those of modern island-arc basalts (Figs. 21 and 22). Sr, K, Rb, and Ba are all low in P762 compared to island-arc basalts, but this may be due to alteration. The calc-alkaline basalt and andesites have spidergrams similar to continental-arc mafic volcanics (Figs. 23 and 24). Some of the Pedernal samples are andesites as indicated on the figures. Pearce (1983) suggests that andesites also can be plotted on MORB-normalized diagrams, since fractional

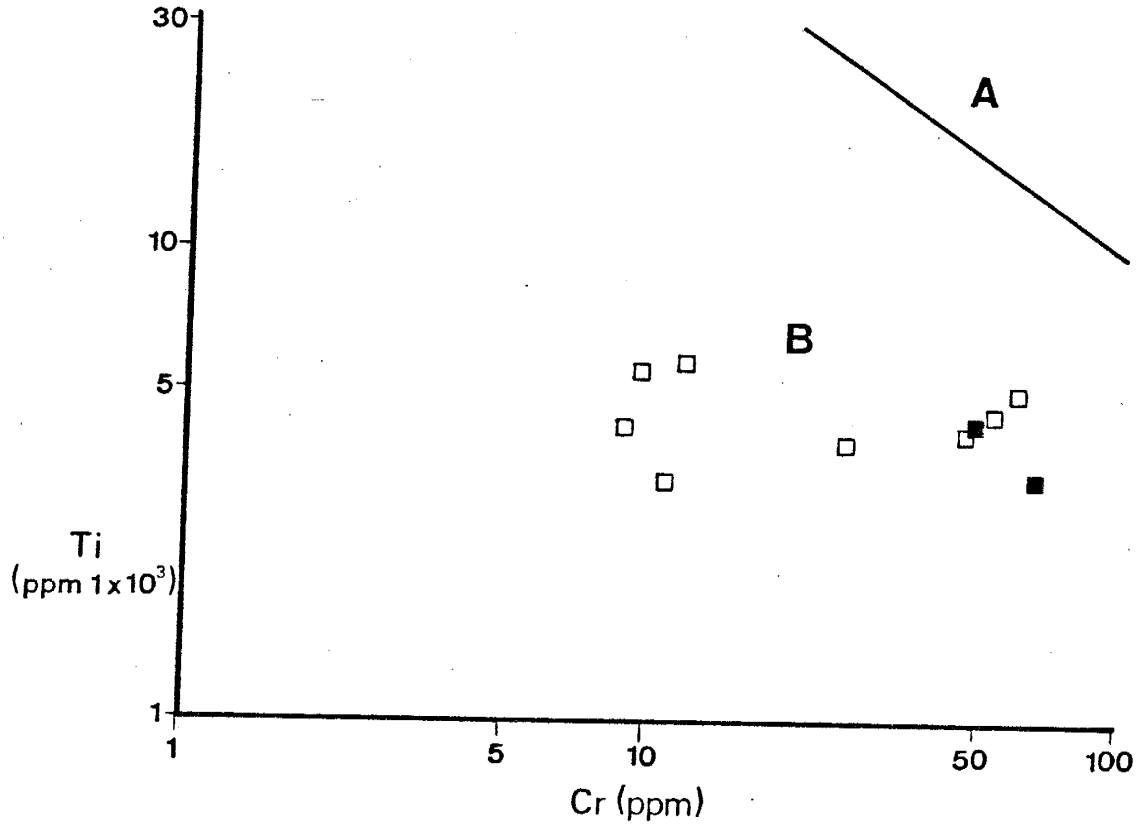

Figure 20. Cr-Ti diagram showing the distribution of basalts and andesites from the Pedernal succession. Fields from Garcia (1978). Symbols as in Fig. 16. Fields are A, ocean floor basalts and B, island arc tholeiites.

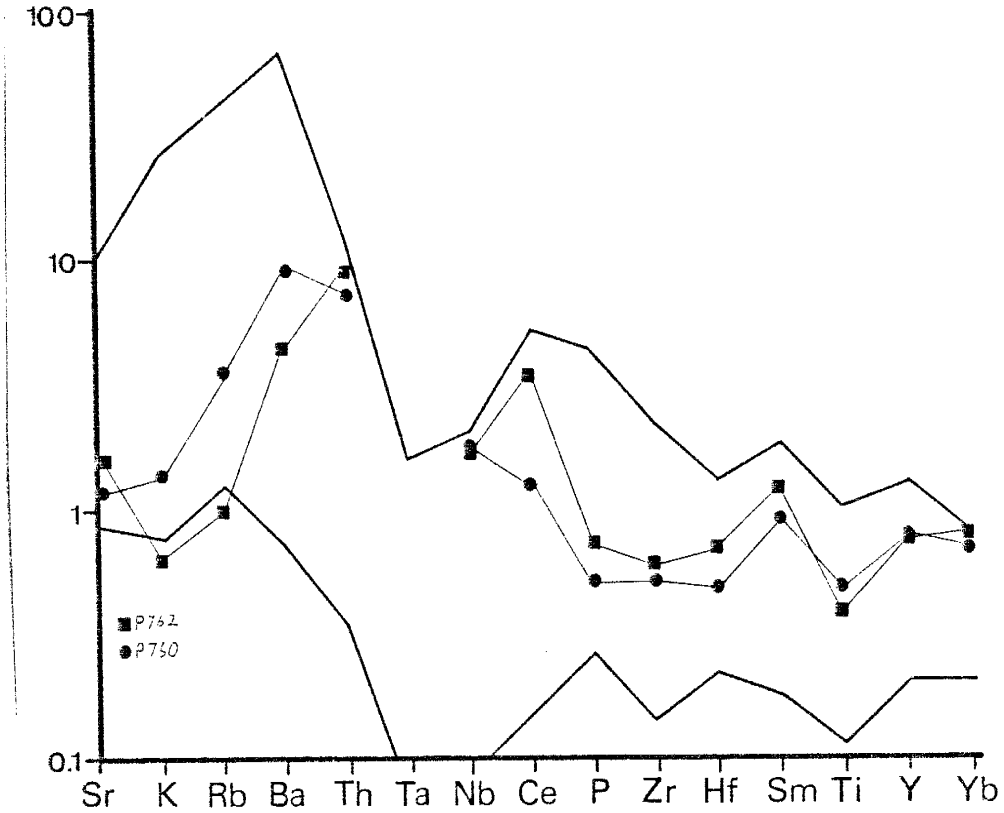

Figure 22. MORB-normalized spider diagram for samples P762 (square) and P760 (circle). Field for island-arc basalts is based on Pearce (1983) and data in Appendix H.

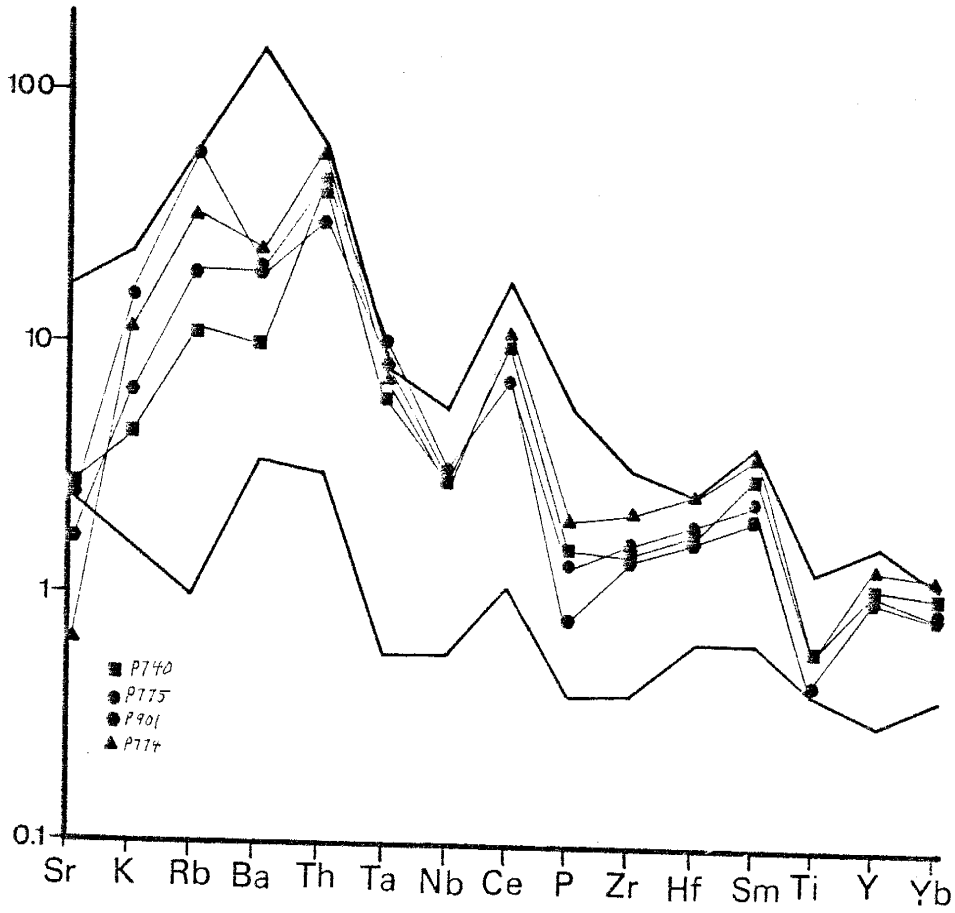

Figure 23. MORB-normalized spider diagram for samples P740, P774, P775, and P901. Field for continental-arc basalts is based on Pearce (1983) and data in Appendix H.

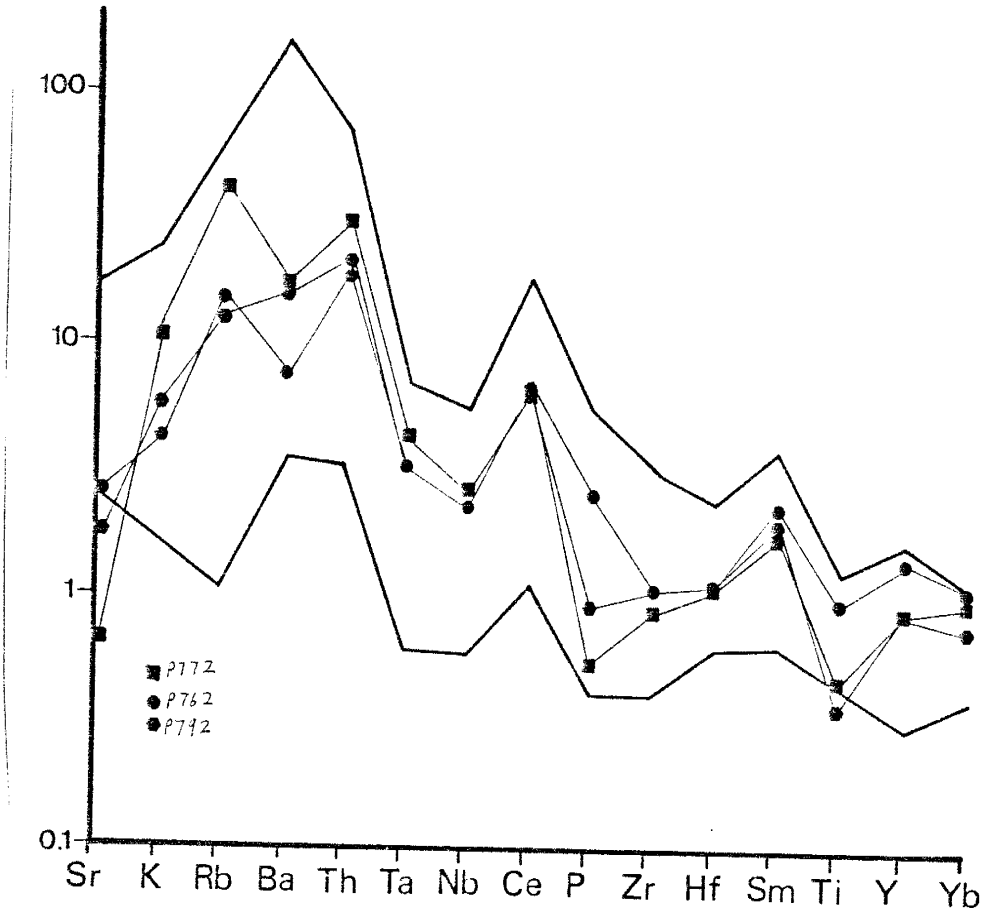

Figure 24. MORB-normalized spider diagram for P765, P772, and P792. Field for continental-arc basalts is based on Pearce (1983) and data in Appendix H.

crystallization does not change the shape of the element pattern, but only the magnitude of the element concentrations. Sr values for some samples are lower than typical for continental-arc volcanics. This may reflect alteration or a more evolved nature of the Pedernal samples, with plagioclase representing an important phase in their petrogenesis.

A Hf-Th-Ta diagram is presented in Fig. 25 and includes all of the volcanic samples from the Pedernal and Manzano sections. Theses samples fall within or near the convergent plate margin field as they also do on a Ti-Zr plot (Fig. 26).

Pedernal andesites are plotted on two diagrams from Bailey (1981) in Fig. 29. Most of the samples fall in or near the continental-arc and evolved island-arc fields. Only P775 falls in the Andean field. Samples P774 and P775 have high Th and plot off the diagram Fig. 27b. The Pedernal andesites plot in or near the evolved island-arc field on Fig. 28 and in or near the continental-arc field on Fig. 29. The andesites as a group are consistent with a continental-arc or an evolved island-arc tectonic setting. Both primitive island-arc and Andean arc settings are unlikely for the Pedernal section.

Considering all of the tectonomagmatic diagrams, a continental-arc environment seems to be the most plausible for the Pedernal section. As a further check, the overall compositions of the mafic volcanic samples are compared to

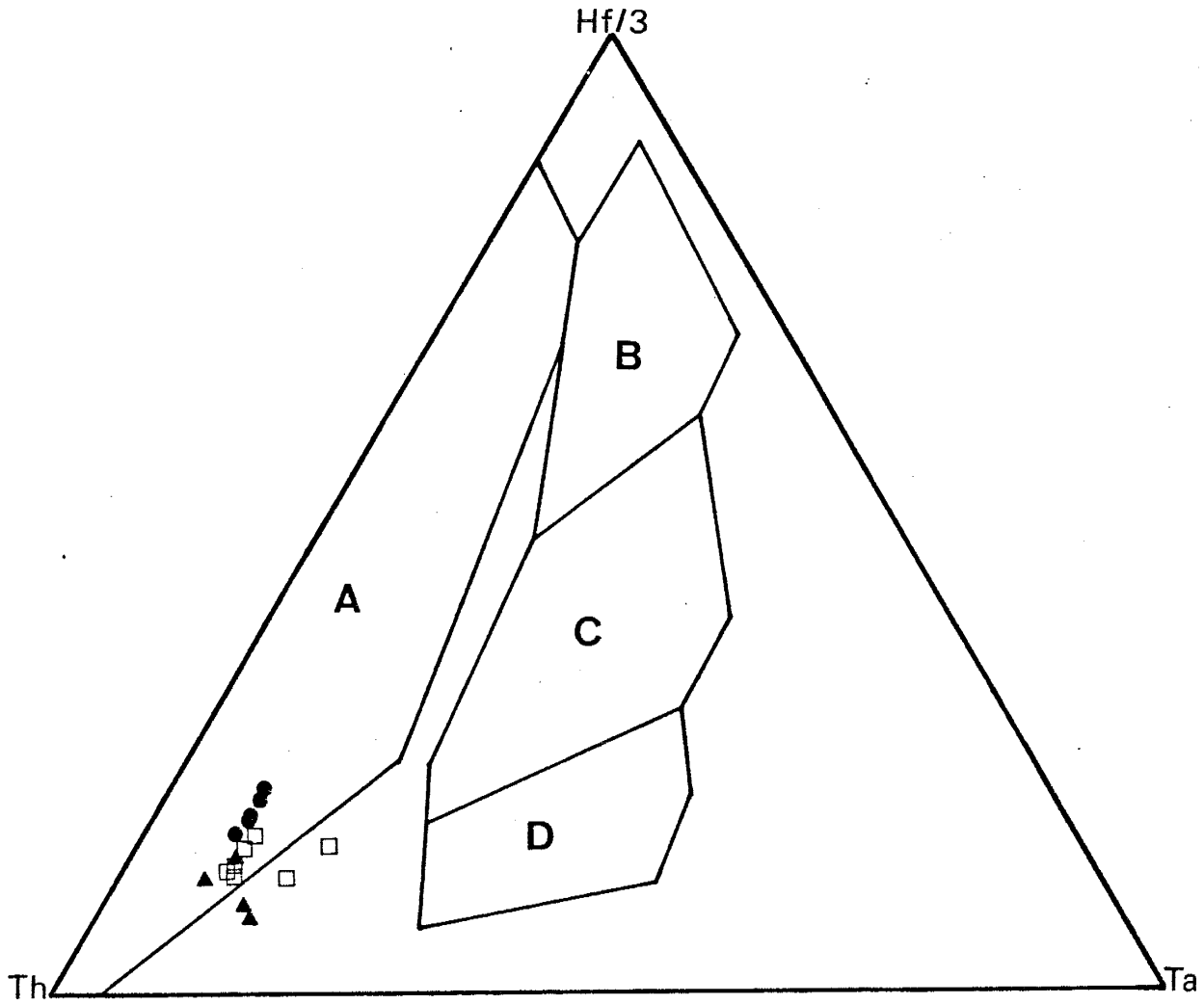

Figure 25. Hf-Ta-Th diagram showing the distribution of volcanic rocks from both the Pedernal and the Manzano successions. Fields from Wood (1980). Open squares are calc-alkaline basalt and andesites, closed squares are tholeiitic basalts, and circles are felsic volcanics, all from the Pedernal section and triangles are felsic volcanics from the Manzano succession. Fields are A, convergent plate; B, N-MORB; C, E-MORB; and D, within plate.

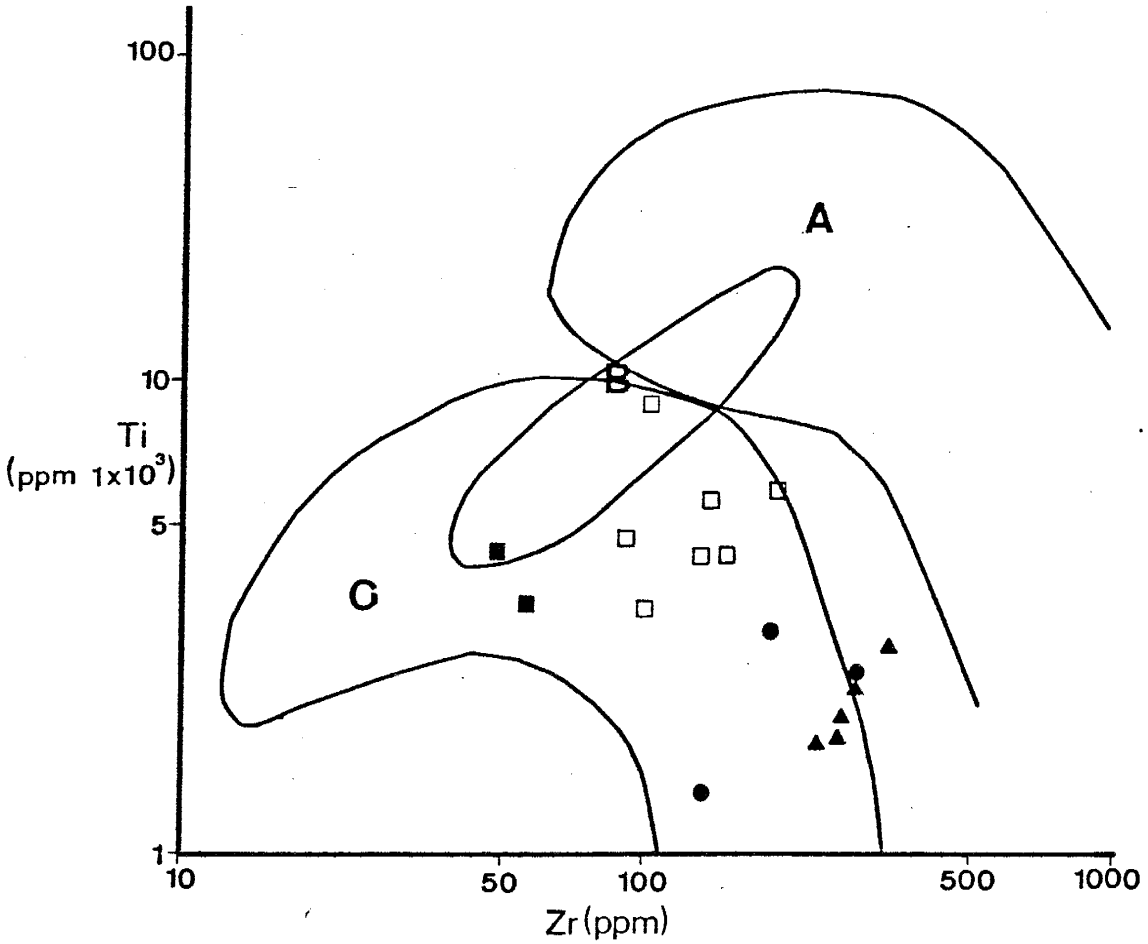

Figure 26. Zr-Ti diagram showing the distribution of all the volcanic rocks from both the Pedernal and the Manzano successions. Fields from Alabastar, et al. (1982). Symbols as in Fig. 25. Fields are A, within plate; B, MORB; and C, arc.

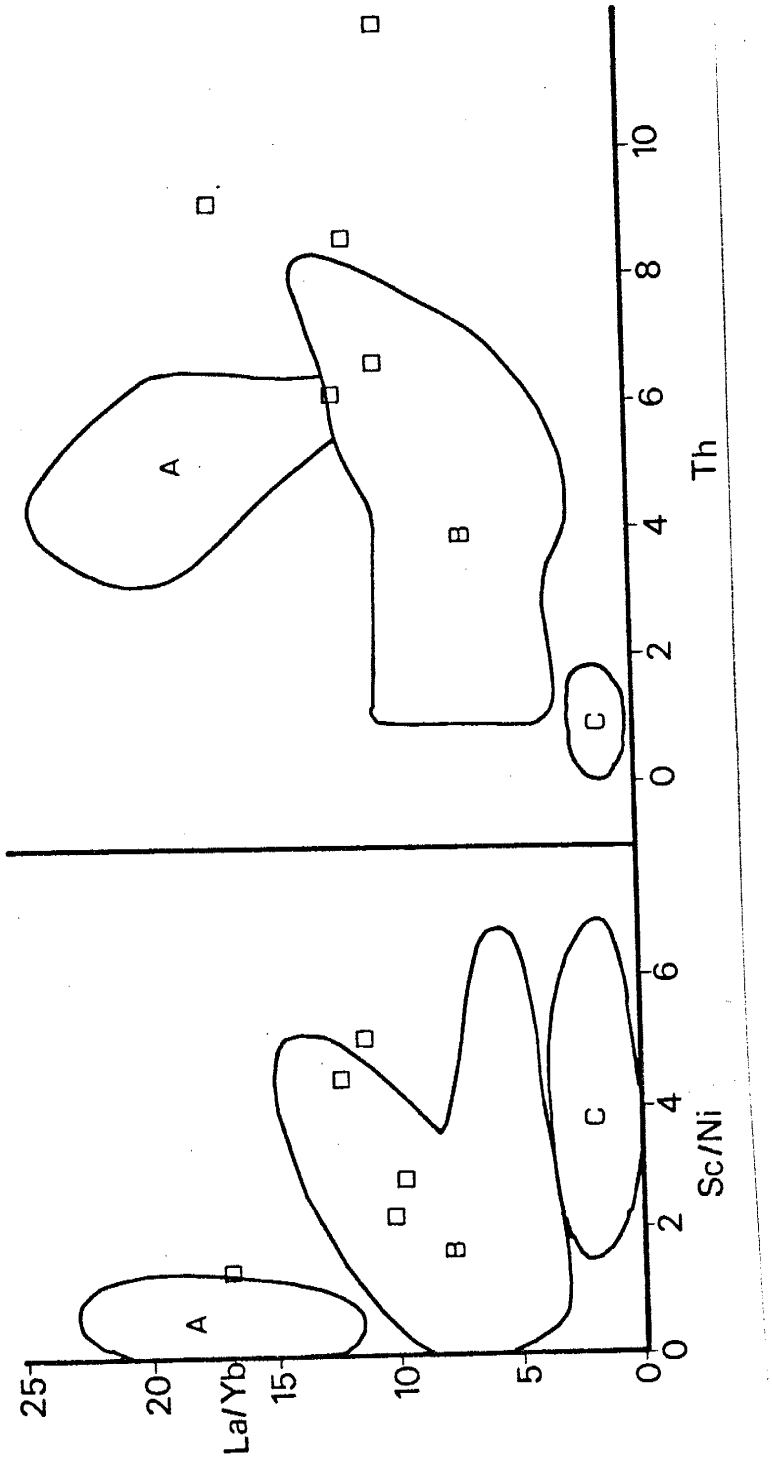

Figure 27. a.) Sc/Ni-SiO2 diagram. b.) Th-SiO2 diagram. Both diagrams show the distribution of calc-alkaline andesites from the Pedernal succession. Fields modified from Bailey (1981). Symbols as in Fig. 25. Fields are A, andean arc; B, continental arc and evoloved island arc; and C, primitive island arc.

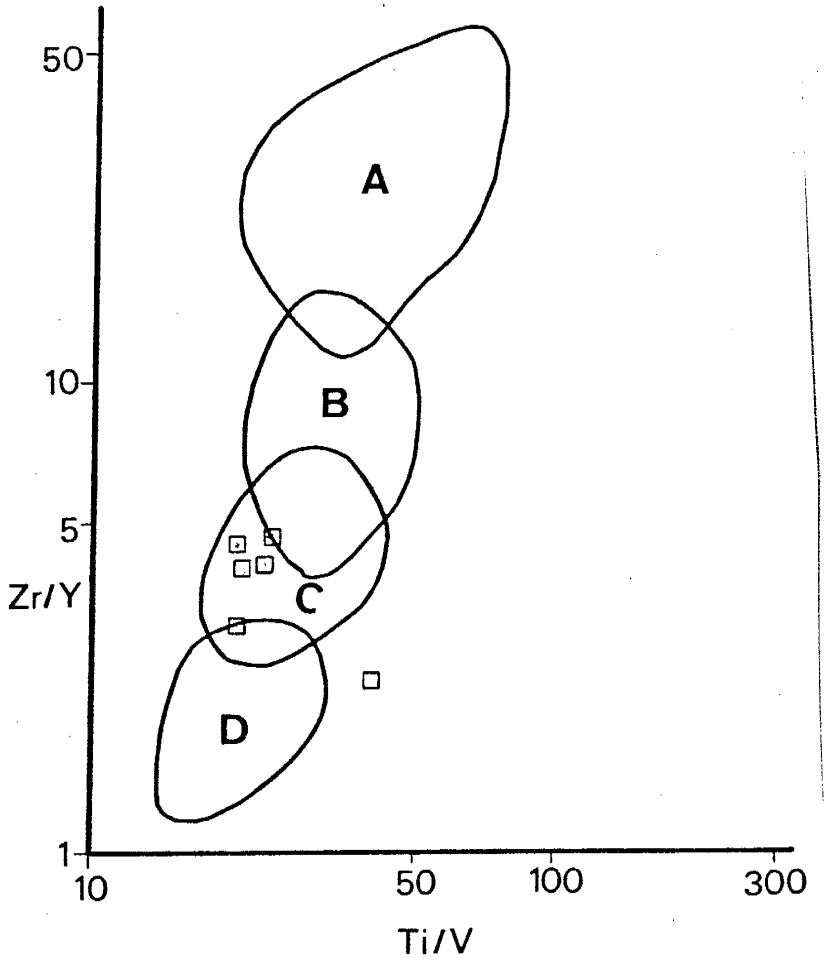

Figure 28. Zr/Y-Ti/V diagram showing the distribution of calc-alkaline andesites from the Pedernal section. Fields are A, Andean; B, Continental-Arcs; C, Evolved Island-Arcs; and D, Primitive Island-Arcs (Condie, personal communication, 1986).

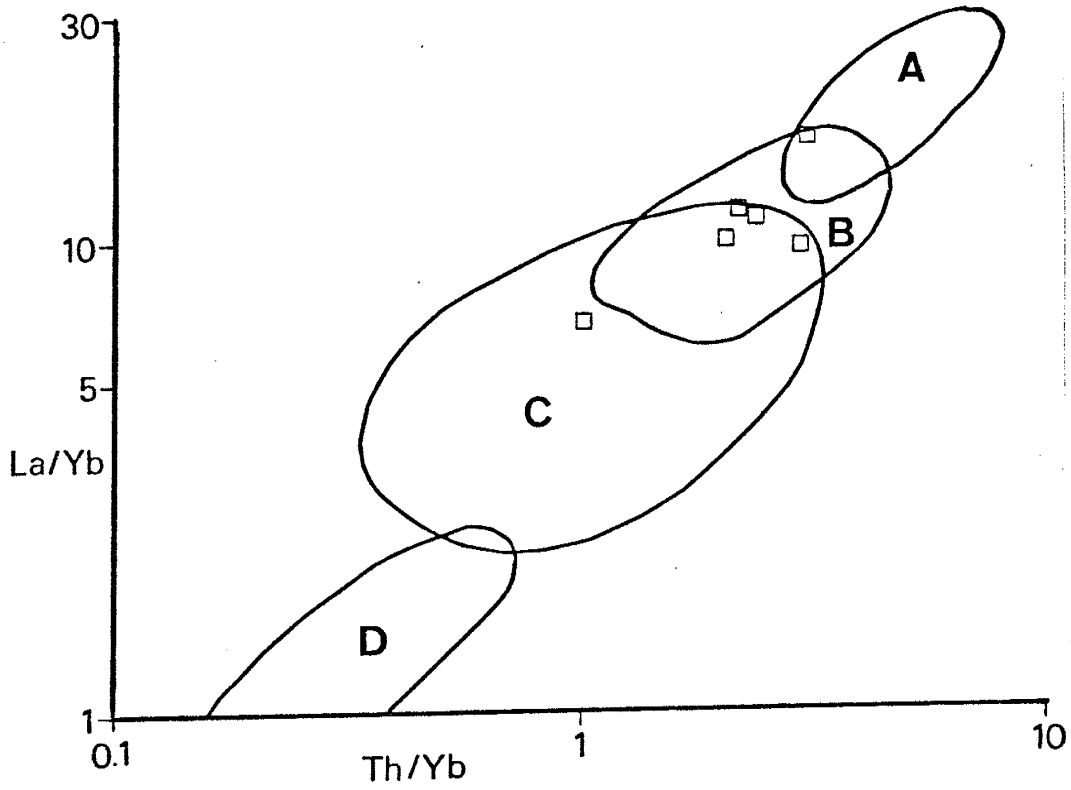

Figure 29. La/Yb-Th/Yb diagram showing the distribution of calc-alkaline andesites from the Pedernal section. Fields are A, Andean; B, Continental-Arcs; C, Evolved Island-Arcs; and D, Primitive Island-Arcs (Condie, personal communication, 1986).

modern equivalents in Tables 8-11. The mafic rocks from the Pedernal section are divided into two groups: Group I has Mg numbers from 59 to 66 and Group II has Mg numbers from 49 to 55.

Group I samples are similar to orogenic samples with the same Mg number (Table 8), but there are some differences. TiO2, Ni, and Co concentrations are lower and Th contents are higher in group I samples compared to corresponding contents in orogenic basalts. Also, P775 has higher contents of light REE and Y, and P760 has a lower concentration of Al2O3 and a higher content of Fe2O3-T than orogenic volcanics.

Boninites are unique rocks that occur in some arcs (Dietrich, et al., 1978). Group I samples are compared to average boninite from the inner wall of the Mariana trench in table 9. Boninites have lower concentrations of TiO2, Al2O3, Zr, Hf, REE, V, and Cu and higher contents of Ni, Cr, and MgO, and higher Mg numbers than the group I samples.

Group II samples have similar trace element contents to orogenic volcanic rocks with similar Mg numbers, but have higher contents of REE, Y, Nb, Ni, and Cr (Table 10). Boninites have lower concentrations of TiO2, Al2O3, P2O5, Zr, Hf, V, and REE and higher contents of MgO, Ni, and Cr, and higher Mg numbers than the group II samples (Table 11).

From Tables 8-11, group I and II samples are most

TABLE 8. COMPARISION OF HIGH MG NUMBER SAMPLES WITH OROGENIC ROCKS THAT HAVE SIMILAR MG NUMBERS.

	P762	P760	P775	SWP	ANDES	IAB-C	IAB-JW
SiO2	50.4	51.9	55.9	51.09	55.11	51.7	52.4
TiO2	0.57	0.74	0.73	0.84	1.36	0.85	0.81
Al2O3	16.4	13.9	15.9	17.50	16.86	17.5	16.2
Fe2O3-T	10.0	12.3	9.59	9.34	7.81	9.4	8.69
MgO	8.81	8.01	7.16	7.02	5.25	7.0	6.84
CaO	11.1	9.49	6.19	11.59	7.38	10.2	11.9
Na2O	2.38	3.20	1.80	2.07	3.74	2.6	2.44
K2O	0.10	0.21	2.44	0.26	1.95	0.49	0.44
MnO	0.15	0.18	0.13	0.19	0.14	0.18	0.17
P2O5	0.088	0.063	0.16	0.09	0.41	0.09	0.11
Mg No.	66	60	63	63	60	63	64
Rb	2.7	7.4	119	4.1	49.4	8	5.0
Ba	91	182	403	90.2	690	125	75
Sr	139	87	264	224	629	260	200
Th	2.3	1.7	9.1			0.50	0.5
Zr	56	48	149	30.8	199	55	70
Nb	5.4	5.0	11	1.7	11.4	2.0	
Hf	1.7	1.2	4.6	0.86	3.8	1.0	1.0
Y	22	23	33	15.8	16.8	21	
La	15	4.9	51	2.95	22.2	3.0	1.1
Ce	36	13	107	7.77	46.2		2.6
Yb	2.8	2.4	3.1	2.26	2.5	2.0	1.4
V	227	311	199	286	168	253	270
Ni	25	21	21	35.5	68.7	30	30
Co	63	57	55	35.7	29.8	32	
Cr	66	49	48	82.4	198	145	50
Zn	77	99	101	78.2	97.6	81	

SWP, average island arc tholeiitic basalt from the soutwest Pacific and ANDES, average andesite of 54-56 wt. % SiO2 from the Andes (Ewart, 1982a). Fe2O3 and FeO are recalculated to Fe2O3-T.

IAB-C, average immature island arc tholeiitic basalt from Condie (1985). FeO-T is recalculated to Fe2O3-T.

IAB-JW, average island arc tholeiite of Jakes and White (1972). FeO-T is recalculated to Fe2O3-T.

All averages and analyses are recalculated to 100% on a volatile free basis. Major elements in weight percent and trace elements in ppm. Fe2O3-T is total iron as Fe2O3.

TABLE 9. COMPARISION OF HIGH MG NUMBER SAMPLES WITH AVERAGE BONINITES FROM THE MARIANA TRENCH.

	P762	P760	P775	A
SiO2	50.4	51.9	55.9	57.20
TiO2	0.57	0.74	0.73	0.20
Al2O3	16.4	13.9	15.9	10.61
Fe2O3-T	10.0	12.3	9.59	9.57
MgO	8.81	8.01	7.16	13.94
CaO	11.1	9.49	6.19	5.68
Na2O	2.38	3.20	1.80	1.82
K2O	0.10	0.21	2.44	0.77
MnO	0.15	0.18	0.13	0.18
P2O5	0.088	0.063	0.16	0.03
Mg No.	66	60	63	81
Rb	2.7	7.4	119	26
Sr	139	87	264	116
Zr	56	48	149	31
Hf	1.7	1.2	4.6	0.6
La	15	4.9	51	1.2
Ce	36	13	107	1.7
Sm	4.0	3.1	8.2	0.4
Yb	2.8	2.4	3.1	0.6
V	227	311	199	163
Sc	48	45	28	30
Ni	25	21	21	280
Co	63	57	55	48
Cr	66	49	48	821
Cu	121	185	118	87
Zn	77	99	101	72

A, average of five boninites from the inner wall of the Mariana Trench (Dietrich, et al., 1978). Fe2O3-T recalculated from Fe2O3 and FeO.

The average boninite and analyses are recalculated to 100% on a volatile free basis. Major elements are in weight percent. Trace elements are in ppm. Fe2O3-T is total iron as Fe2O3.

TABLE 10. COMPARISION OF LOW MG NUMBER SAMPLES WITH OROGENIC ANDESITES THAT HAVE SIMILAR MG NUMBERS.

	P792	P772	P740	P774	NWP	A	B
SiO2	52.9	54.5	56.7	57.8	51.02	55.31	57.29
TiO2	0.56	0.78	0.94	0.98	0.87	0.91	0.80
Al2O3	20.3	17.4	16.5	16.1	18.30	18.05	17.79
Fe2O3-T	8.23	12.9	10.1	9.04	10.38	8.51	7.85
MgO	5.05	6.00	4.32	4.06	5.65	4.38	3.97
CaO	8.84	3.91	7.04	6.55	11.24	8.40	7.85
Na2O	2.98	2.28	3.41	3.41	1.98	3.01	3.01
K2O	0.91	1.91	0.66	1.70	0.27	1.08	1.11
MnO	0.12	0.19	0.14	0.11	0.19	0.17	0.15
P2O5	0.11	0.07	0.19	0.25	0.10	0.19	0.16
Mg No.	55	51	49	50	55	54	53
Rb	29	88	22	64	2.4	42.5	22.2
Ba	334	371	196	466	195	369	254
Sr	287	68	324	248	247	350	263
Zr	99	90	136	189	313	121	147
Nb	7.4	9.3	9.6	12		3.4	2.7
Hf	2.9	3.1	4.4	6.1	0.90	2.1	2.6
Y	28	30	34	40	17	22.1	20.5
La	41	33	41	40	2.40	10.6	9.3
Ce	75	75	99	116	7.34	25.1	22.8
Yb	2.8	3.3	3.7	4.1	1.81	2.2	2.4
V	201	219	251	243	240	221	194
Ni	9.3	22	6.9	10	38	45.9	43.3
Co	13	71	45	36	40.8	34.6	37.7
Cr	11	53	9.4	12	30.6	66.8	92.5
Zn	77	120	95	88	74.4	75.5	77.5

NWP, average island arc tholeiitic basalt from the northwest Pacific; A, average andesite of 54-56 wt. % SiO2 from northwestern Pacific; B, average andesite of 56-58 wt. % SiO2 from northwestern Pacific (Ewart, 1982a). Fe2O3-T are recalculated from Fe2O3 and FeO.

All analyses and averages are recalculated to 100 % on a volatile free basis. Major elements in weight percent and trace elements in ppm. Fe2O3-T is total iron as Fe2O3.

TABLE 11. COMPARISION OF LOW MG NUMBER SAMPLES WITH AVERAGE BONITITE FROM THE MARIANA TRENCH.

	P792	P772	P740	P774	A
SiO2	52.9	54.5	56.7	57.8	57.20
TiO2	0.56	0.78	0.94	0.98	0.20
Al2O3	20.3	17.4	16.5	16.1	10.61
Fe2O3-T	8.23	12.9	10.1	9.04	9.57
MgO	5.05	6.00	4.32	4.06	13.94
CaO	8.84	3.91	7.04	6.55	5.68
Na2O	2.98	2.28	3.41	3.41	1.82
K2O	0.91	1.91	0.66	1.70	0.77
MnO	0.12	0.19	0.14	0.11	0.18
P2O5	0.11	0.07	0.19	0.25	0.03
Mg No.	55	51	49	50	81
Rb	29	88	22	64	26
Sr	287	68	324	248	116
Zr	99	90	136	189	31
Hf	2.9	3.1	4.4	6.1	0.6
La	41	33	41	40	1.2
Ce	75	75	99	116	1.7
Yb	2.8	3.3	3.7	4.1	0.6
V	201	219	251	243	163
Ni	9.3	22	6.9	10	280
Co	13	71	45	36	48
Cr	11	53	9.4	12	821
Zn	77	120	95	88	72

A, the average of Five boninites from the inner wall of the Mariana Trench (Dietrich, et al., 1978). FeO and Fe2O3 recalculated to Fe2O3-T.

Analyses and the average boninite are recalculated to 100% on a volatile free basis. Major elements are in weight percent and trace elements are in ppm. Fe2O3-T is total iron as Fe2O3.

similar to orogenic volcanics. This is the same conclusion reached from the tectonomagmatic diagrams for the mafic volcanics from the Pedernals Hills. Both groups are dissimilar to boninites, which is an unique rock type that occurs in some arcs.

Table 12 lists the FeO*/MgO ratios of the mafic and andesitic volcanic samples and most are less than 2. Exceptions are P765 and P901. Subalkalic basalts and andesites with the FeO*/MgO ratio less than 2 are rare from tectonic environments other than arcs (Ewart, 1981).

Only convergent plate margin andesites have high Cu contents (above 70 ppm: Gill, 1981). The calc-alkaline andesites from the Pedernals have greater than 70 ppm Cu, but there are occurrences of secondary azurite and malachite in the Pedernals. The samples analyzed did not show evidence of secondary Cu mineralization, but the high Cu content could be due to alteration.

Felsic Volcanics

Until recently, few geochemical studies of felsic volcanics have been made in relation to ancient tectonic settings. Felsic volcanics are common in both continental arcs and rifts, but are not very common in other tectonic environments. The compositions of felsic volcanics from both the Manzano and Pedernal sections are similar to averages of continental-arc felsic volcanics (Ewart,

TABLE 12. FEO-T/MGO RATIOS OF THE MAFIC METAVOLCANIC ROCKS

	P762	P760	P792	P772	P775	P765	P740	P901	P774
FeO-T/MgO	1.02	1.39	1.63	1.94	1.21	3.53	2.10	2.43	2.01

1979).

In terms of V-Zr contents, all of the Manzano samples and all but one of the Pedernal samples are similar to felsic volcanics from evolved island-arcs and continental-arcs (Fig. 30). Only one sample (P767), which is altered, falls in the primitive island-arc field. On a TiO2-Zr diagram (Fig. 31), most of the Manzano samples plot in or near the continental-arc field, but the Pedernal samples are scattered. The two diagrams suggest that felsic volcanics from both successions formed in evolved island-arc or continental-arc environments. For the Pedernals, this is the same conclusion reached for the mafic calc-alkaline volcanics.

Sedimentary Rocks

Two methods are used for tectonic environment classification of sedimentary rocks: geochemical and petrographic. Following the classification scheme of Crook (1974), the Manzano sedimentary rocks are quartz-intermediate graywackes (15-65 % quartz and 68-74 % SiO2). Quartz-intermediate graywackes are related to evolved island arcs and continental margin arcs (Crook, 1974).

Figure 32 is a TiO2-FeO*+MgO diagram showing the distribution of Manzano sedimentary rock samples. Three samples plot in the continental island arc field and one in the active continental margin field. A similar distribution is apparent on the Fe/Mg-Al/Si diagram (Fig.

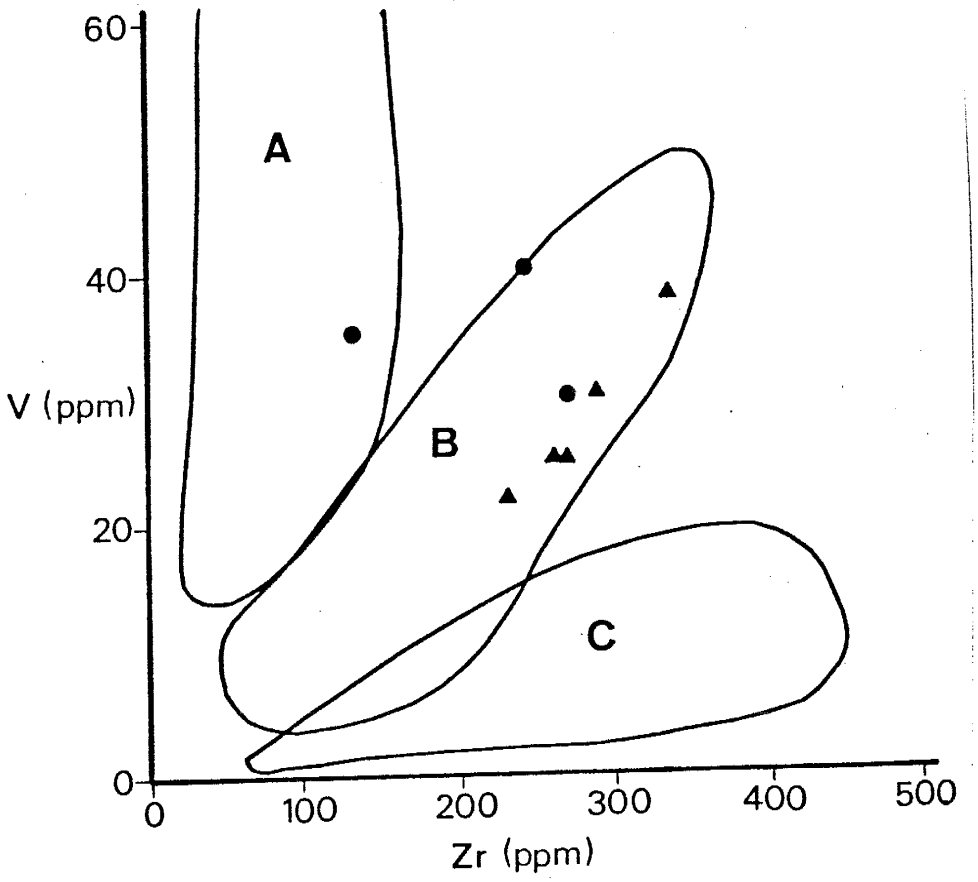

Figure 30. Zr-V diagram showing the distribution of felsic volcanic rocks from both the Pedernal and the Manzano successions. Circles are Pedernal felsic volcanic rocks and triangles are Manzano felsic voclanic rocks. Fields are A, immature island arc; B, evoloved island and continental arc; and C, rifts (Condie, personal communication, 1986).

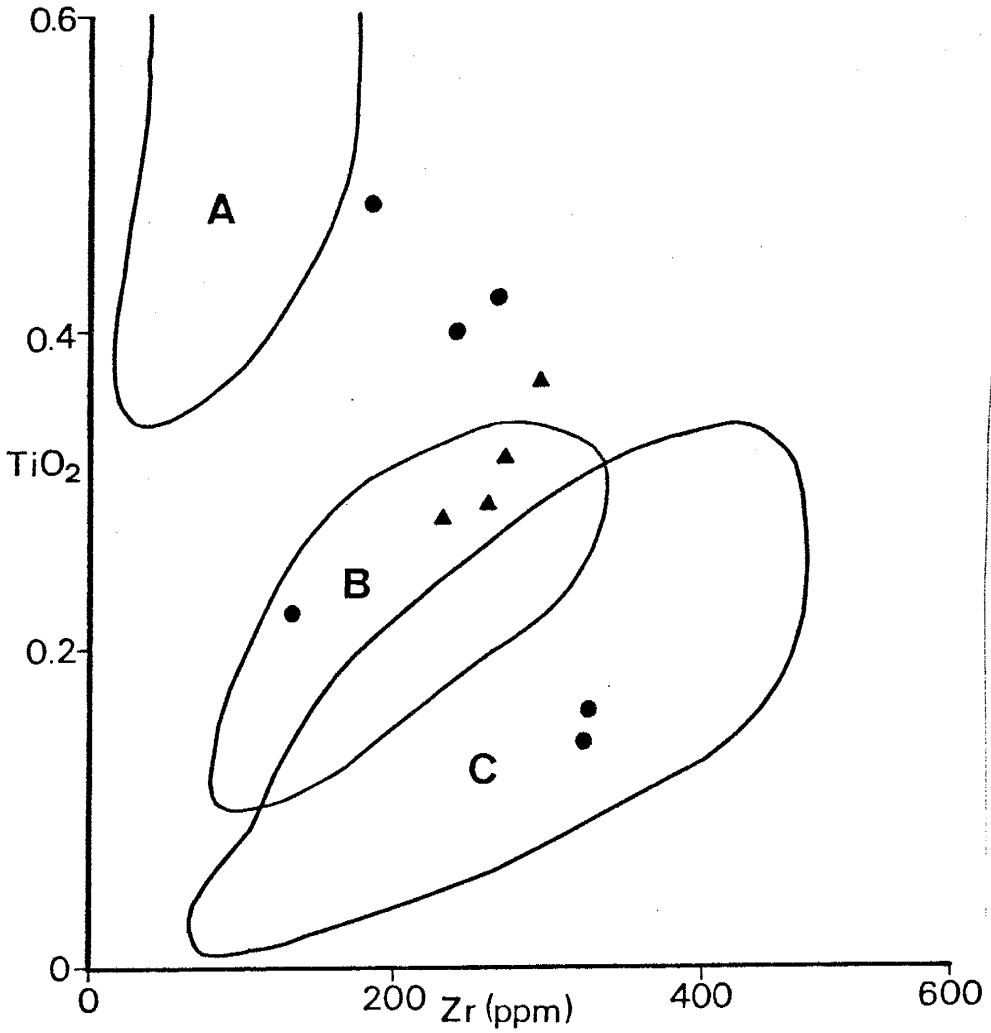

Figure 31. Zr-TiO2 diagram showing the distribution of felsic volcanic rocks from both the Pedernal and the Manzano successions. Symbols as in Fig. 30. From Condie, personal communication, 1986.

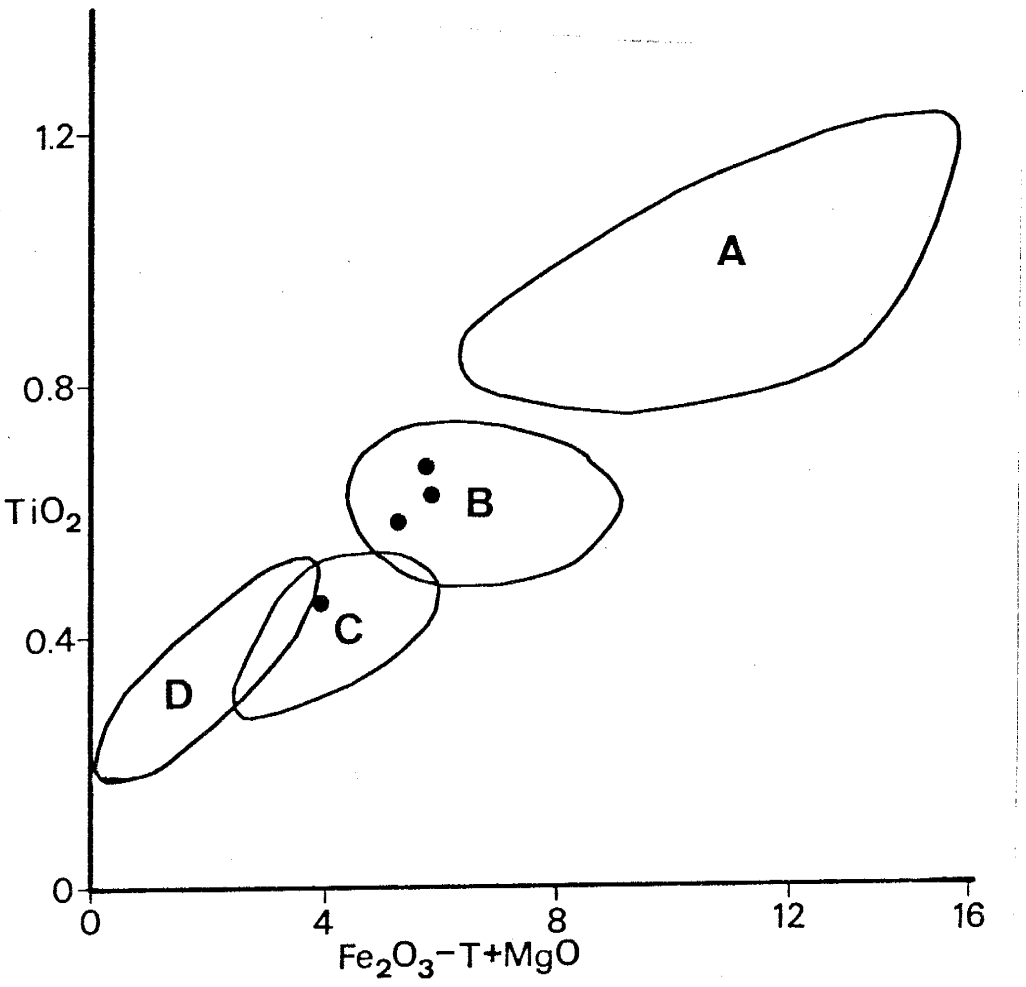

Figure 32. Fe203-T+MgO-Ti02 diagram showing the distribution of sedimentary rocks from the Manzano succession. Fields modified from Bhatia (1983) are A, island-arc field; B, continental-arc field; C, active continental margin field; and D, passive margin field.

33). Figures 34 and 35 are two triangular diagrams for sedimentary rocks that use trace elements and again the Manzano samples plot in the continental-arc field. These four diagrams support the conclusions from the felsic volcanics of the Manzano section for formation in a continental-arc or evolved island-arc environment.

Modal analysis of standard thin sections with a point counter was performed on four volcaniclastic samples from the Pedernal section (see Appendix I). QFL diagrams constructed for use with modal data are based on fine- to medium-grained sandstones that had less than 25 % matrix (Dickinson, 1970; Dickinson and Suczek, 1979; and Bhatia, 1983). The Pedernal samples are pebble to cobble conglomerates and have more than 25 % matrix, so the diagrams cannot be strictly applied. Also, weathering and/or sedimentary processes may modify sandstone compositions such that the samples have an anomalous composition for a particular tectonic setting (Breyer and Ehlmann, 1981; Potter, 1984; and Valloni, 1985) or the source areas for the sandstones may be unrelated to the tectonic setting of the basin of deposition (Mack, 1984 and Velbel, 1985). On the QFL diagram, modern sands from different tectonic environments overlap (Valloni and Mezzadri, 1984 and Valloni, 1985).

Not all of the matrix present in the Pedernal samples is primary since diagenesis and metamorphism can convert unstable mineral grains and fine-grained rock fragments

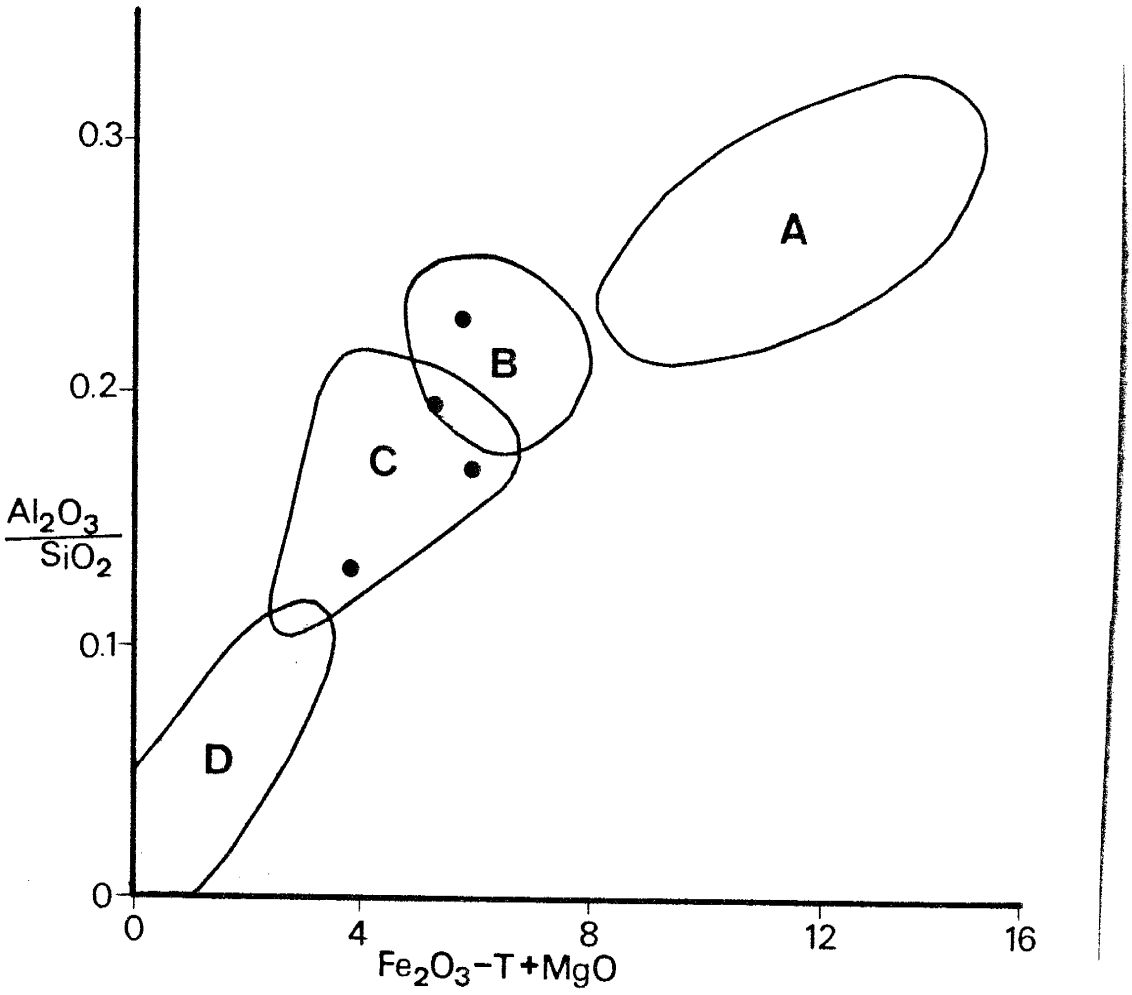

Figure 33. Fe2O3-T+MgO-Al2O3/SiO2 diagram showing the distribution of sedimenatry rocks from the Manzano succession. Symbols as in Fig. 32. From Bhatia (1983).

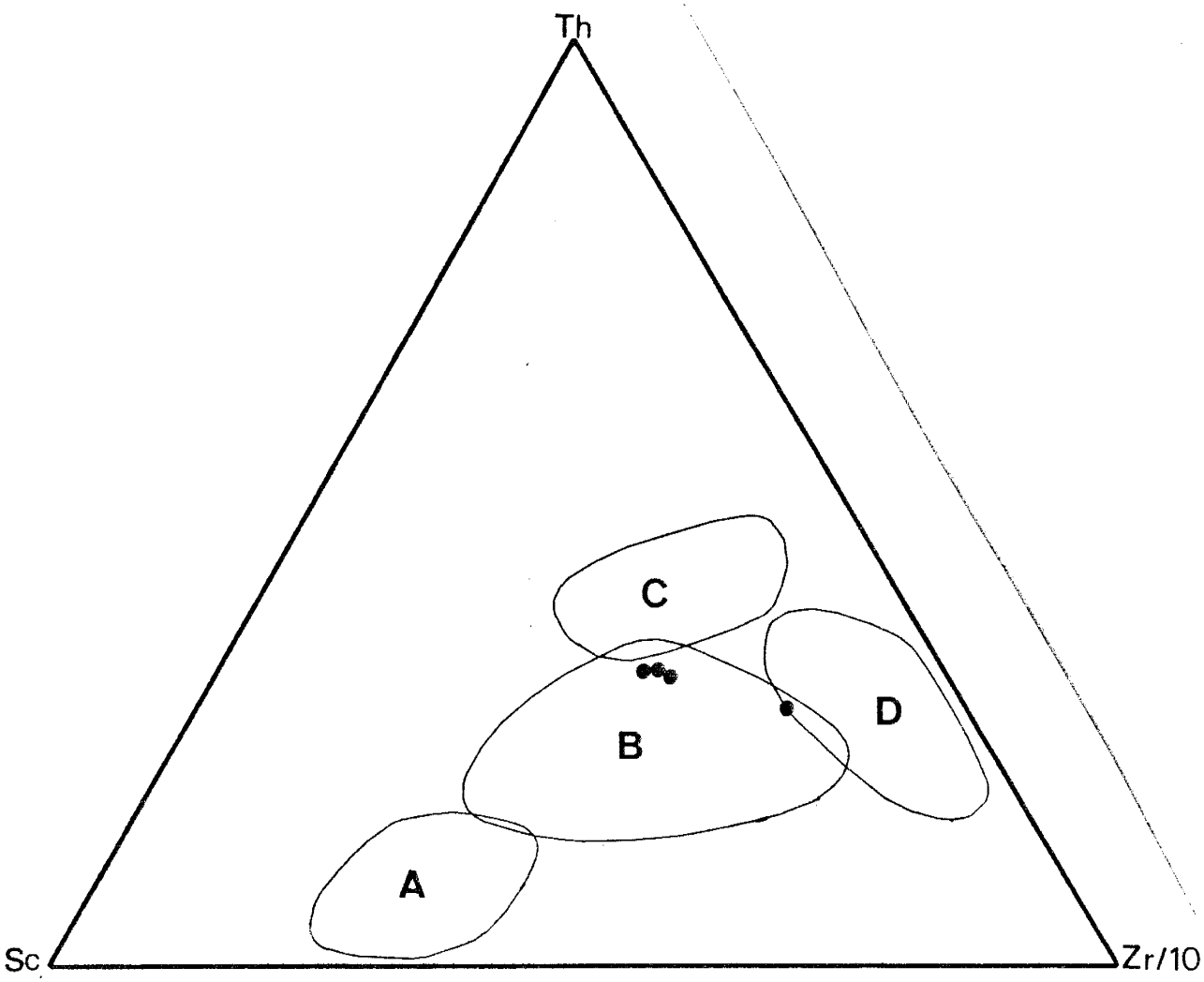

Figure 34. Th-Sc-Zr diagram showing the distribution of seddimentary rocks from the Manzano succession. Fields modified from Bhatia, 1986. Symbols as in Fig. 32.

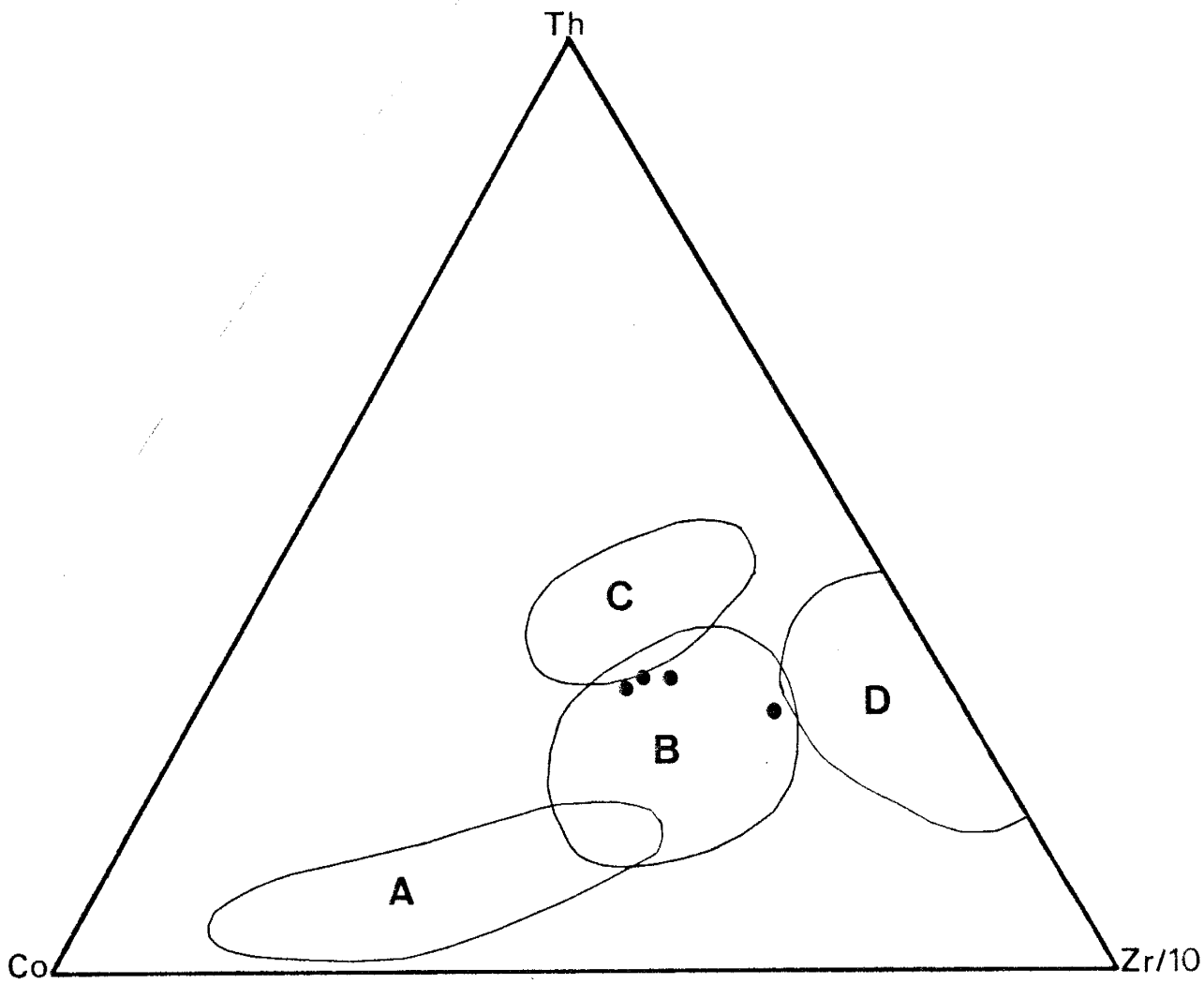

Figure 35. Th-Co-Zr diagram showing the distribution of sedimentary rocks from the Manzano succession. Fields modified from Bhatia, 1986. Symbols as in Fig. 32.

into secondary or pseudomatrix (Brenchley, 1969; Hawkins and Whetten, 1969; Whetten and Hawkins, 1970; Maynard, et al., 1982; and Bhatia, 1983). Also, the feldspar content may be low since grain-size affects the modal content of feldspars (Field and Pilkey, 1969) with most feldspar grains falling in the coarse silt to very fine sand range (Odom, 1975). Differentiation of lithic grains into sedimentary and volcanic types is not possible since all lithic grains are completely recrystallized to amphibole, chlorite, epidote, and quartz mosaics.

QFL and QmFLt modal parameters for the Pedernal sediments are given in Table 13. These samples plot near the L (Fig. 36) and Lt (Fig. 37) apices and indicate an undissected arc setting. While the Qp-Ls-Lv diagram cannot be used, most of the clasts observed in the field are volcanic in origin and samples should plot towards the Lv apex, which would again indicate an arc environment.

ROCK ASSOCIATIONS

Condie (1982b) divided early to middle Proterozoic supracruatal successions into three groups and assigned the groups to possible tectonic enviroments. Assemblage I is a quartzite-carbonate-shale assemblage and the northern quartzite-schist succession in the Pedernal Hills appears to be representative of this assemblage. Assemblage II is a bimodal volcanic-quartzite-arkose rock package and

TABLE 13. MODAL ANALYSES OF PEDERNAL VOLCANICICLASTICS.

SYMBOL	P743 COUNTS	P743 PERCENT	P744 COUNTS	P744 PERCENT
Qm	3	0.2	0	0.0
Qp	17	1.4	43	4.2
L	315	25.3	644	62.7
P	0	0.0	0	0.0
MP	0	0.0	0	0.0
Bi	14	1.1	0	0.0
Amp	507	42.8	62	6.0
Ch	52	4.2	15	1.5
Ep	59	4.7	95	9.3
Sr	125	10.0	23	2.2
Op	5	0.4	3	0.3
Ma	147	11.8	130	12.7
TOTAL	1244	99.9	1027	100.0

SYMBOL	P86 COUNTS	P86 PERCENT	P10 COUNTS	P10 PERCENT
Qm	1	0.1	0	0.0
Qp	150	14.9	0	0.0
L	380	37.8	416	40.0
P	4	0.4	0	0.0
MP	0	0.0	7	0.7
Bi	5	0.5	0	0.0
Amp	263	26.2	126	12.1
Ch	38	3.8	138	13.7
Ep	35	3.5	242	23.3
Sr	0	0.0	0	0.0
Op	20	2.0	11	1.1
Ma	109	10.8	75	7.2
TOTAL	1005	100	1039	100

Qm, monocrystalline quartz grains; Qp, polycrystalline quartz grains; L, unstable polycrystalline lithic grains; P, monocrystalline plagioclase grains; MP, metamorphic plagioclase; Bi, biotite; Ch, chlorite; Amp, amphibole; Ep, epidote; Sr, sericitic matrix; Op, opaques; and Ma, quartzose-feldspathic matrix.

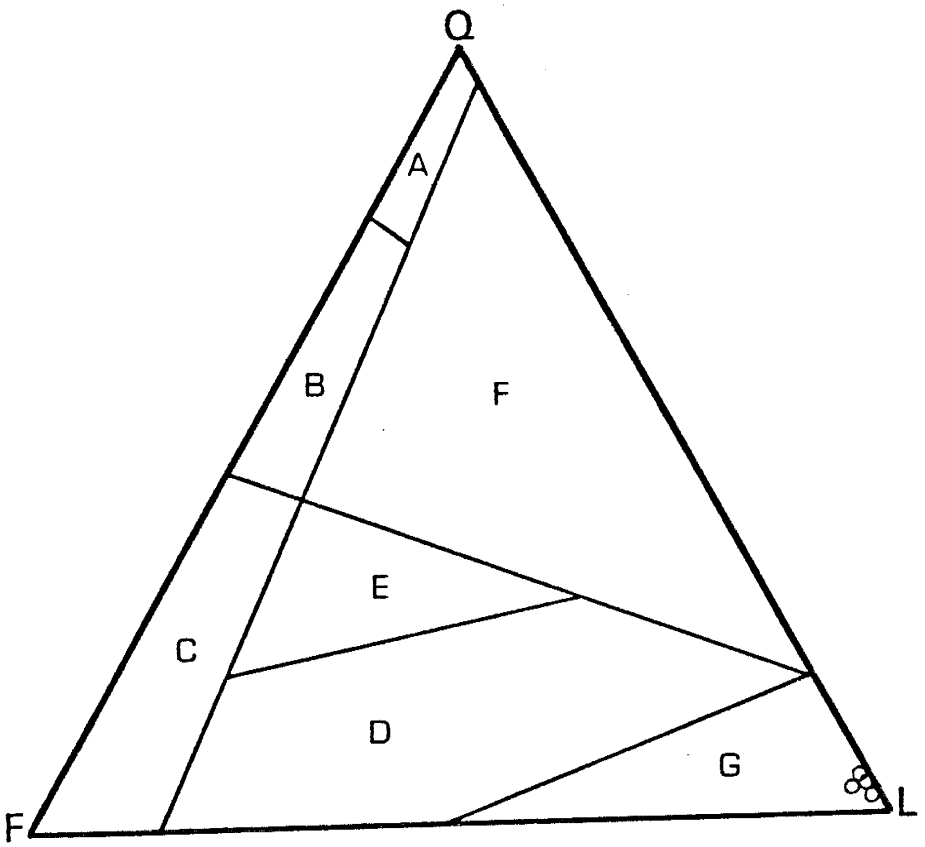

Figure 36. QFL diagram showing the distribution of mafic volcaniclastic rocks from the Pedernal succession. Q, total quartzose grains; F, monocrystalline feldspar grains; and L, unstable lithic grains. Fields are A, cratonic interior; B, transitional continental; C, basement uplift; D, transitional arc; E, dissected arc; F, recycled; and G, undissected arc (Dickinson, 1983).

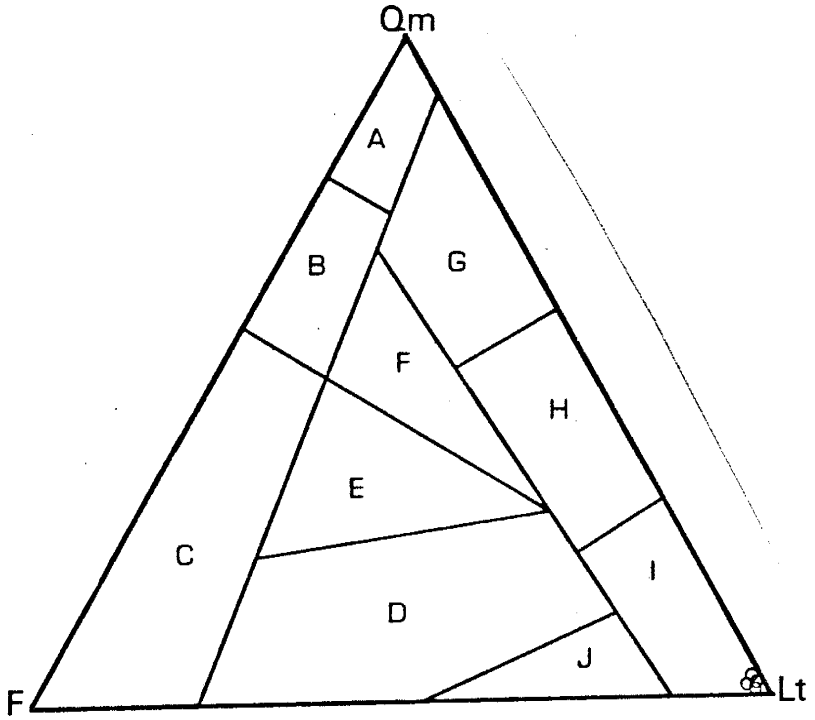

Figure 37. QmFLt diagram showing the distribution of mafic volcaniclastic rocks from the Pedernal succession. Qm, monocrystalline quartz grains; F, monocrystalline feldspar grains; and Lt, total lithic grains. Fields are A, cratonic interior; B, transitional continental; C, basement uplift; D, transitional arc; E, dissected arc; F, mixed; G, quartzose recycled; H, transitional recycled; I, lithic recycled; and J, undissected arc (Dickinson, 1983).

assemblage III is a continous volcanic-greywacke suite. The Manzano and Pedernal sections are similar to assemblages II and III of Condie (1982b). While the volcanics are bimodal in the Pedernal and Manzano successions, both sections are most similar to assemblage III. Some bimodal volcanic successions are included in assemblage III (Condie, 1982b). Since both the Manzano and Pedernal sections are similar to assemblage III and assemblage III is similar lithologically to Phanerzoic arc environments (Condie, 1982b), the Pedernal and Manzano sections would appear to have formed in an arc environment. This is the same conclusion arrived at using the chemical compositions of the volcanic and sedimentary rocks. A continental-arc is favored over an island-arc due to the relative abundance of felsic volcanics, especially welded ash flow tuffs which are rare in island arcs (Miayshiro, 1974 and Baker, 1982).

The occurence of both tholeiitic and calc-alkaline rocks in the Pedernal section could represent an evolution with time from tholeiitic to calc-alkaline volcanism within one volcano. This is a common feature in some modern arc systems (Miyashiro, 1974). Another possibility is that volcanic rocks from the Pedernal section were erupted from more than one volcanic center. Zonation of rock types in arcs is has been noted for a number of years (Kuno, 1959; Jakes and White, 1972; De Boer, et al., 1980; and Gill, 1981). The zones from the trench to the back-arc are

tholeiitic, calc-alkaline and shonshonitic to alkalic. Since there are both tholeiitic and calc-alkaline rocks present in the Pedernals, the rocks probably formed toward the front of the arc.

Paired metamorphic belts, thick sequences of greywacke and interbedded mudstone, and tectonic melanges are characteristic features of modern arcs (Mitchell and Reading, 1971 and Garcia, 1978). None of these features has been identified in the Pedernal Hills or in the Manzano Mountains. These features may not have been preserved in the rock record or are not exposed at present. High pressure blueschists may not develop when underthrusting is not rapid enough to produce the unusually low geothermal gradient required and so paired metamorphic belts may not always be produced at subduction zones (Miyashiro, 1972).

In conclusion, both the Pedernal and the Manzano sections appear to have formed in an arc environment. For both sections, a continental-arc is favored over an island-arc, both on geochemical and lithological grounds.

MAGMAGENESIS MODELING

INTRODUCTION

Simple fractional crystallization and partial melting models are used to test possible petrogenetic schemes for the volcanic rocks from both the Pedernal and Manzano sections. Trace elements are modeled by the Rayleigh fractionation equation using distribution coefficients compiled from published sources. Major elements are modeled by a mass balance equation and Ti and K are modeled both as trace elements and as major elements.

For purposes of partial melting models, it is assumed that equilibrium is always reached. Also, trace elements are assumed to follow Henry's Law, a requirement for use of the Rayleigh fractionation equations. Some authors contend that Henry's Law is not obeyed in some geological systems (Wood, 1976; Mysen, 1977, 1978a, and 1978b; and Harrison, 1981a), but Watson (1985) has reviewed the literature and concludes that Henry's Law is obeyed in most geological situations for trace elements.

Another assumption in this study is that certain elements that are essential structural constituents behave according to Henry's Law: Zr in zircon, REE in allanite, Ti in magnetite and ilmenite, and K in biotite and potassium feldspar. Zircon and allanite are accessory phases that usually comprise less than 1 % of the mode.

Also, Zr and REE obey Henry's Law in all other phases used in the modeling, so it appears to be appropriate to model Zr and REE as though they always obey Henry's Law.

Partition coefficients vary depending on several factors: pressure, bulk composition, temperature, and other factors (Watson, 1976 and 1977; Hart and Davis, 1978; Irving and Frey, 1978; Mysen, 1978a and 1978b; and Mysen and Kushiro, 1979). The most important factor for incompatible elements appears to be bulk composition (Watson, 1977; Hart and Davis, 1978; Irving, 1978; Irving and Frey, 1978; Mysen and Virgo, 1979 and 1980; and Mysen, et al., 1979). Partition coefficients are assumed to be constant for any given stage in any model, even though some trace elements have highly variable Kds (i.e., Sr and Eu). Partition coefficients used and references are listed in Appendix J.

A final assumption made is that the present compositions of the volcanic samples closely approximates the compositions of the magmas from which the rocks crystallized. Most of the volcanic rocks are pyroclastics and include pyroclastic flows. During eruption and emplacement of pyroclastic flows, crystals and lithic fragments may be enriched in the flows and possible fractionation of elements. Thus, pyroclastic flows may not always be of the same composition as their parent magmas (Fisher and Schmincke, 1984). Also, alteration may have changed the concentrations of some elements.

MAFIC VOLCANIC ROCKS

Intersample Relationships

Recent volcanoes have erupted both tholeiitic and calc-alkaline magmas from the same vent (Sakuyama, 1981 and 1983) and the mafic tholeiitic and calc-alkaline volcanics from the Pedernal section may represent such mixed eruptions. If the Pedernal mafic volcanics were erupted from a single volcanic vent, one or more parental magmas may have existed. Both single and multiple parent models have been proposed for modern volcanics (Kuno, 1960 and 1968; Kushiro and Sato, 1978; and Masuda and Aoki, 1979). The other possibility, is multiple volcanic structures existed and produced rocks from multiple parental magmas. Both single parental and multi-parental magma models are tested in this study.

One difference between the tholeiitic and calc-alkaline series is the iron enrichment in tholeiites. This iron enrichment is due to delayed magnetite crystallization related to low fO2 in tholeiitic magmas (Kennedy, 1955; Osburn, 1962; and Miyashiro and Shido, 1975). Differences in fO2 during eruption of a single parental magma could lead to two different trends: one calc-alkaline and the other tholeiitic.

Calc-alkaline magmas may develop from tholeiitic magmas by closed system fractional crystallization (Bowen,

1928 and Coulon and Thorpe, 1981). Attempts to model the mafic calc-alkaline volcanics by fractional crystallization using the associated tholeiitic volcanics as parental magmas are unsuccessful, especially for compatible elements and the REE. Compatible elements in some of the mafic calc-alkaline volcanics have about the same concentrations as in the tholeiites, so olivine and pyroxenes cannot be important crystallizing phases. Likewise, TiO2 and Fe2O3-T have the same contents in both the tholeiites and calc-alkaline rocks and thus, Fe-Ti oxides also cannot be important phases. The light REE are enriched in the mafic calc-alkaline volcanics compared to the tholeiites, with heavy REE having about the same concentration levels in both groups. Amphibole and garnet will fractionate the light REE from heavy REE. Garnet however, depletes the heavy REE too much in resulting daughter liquids for even small amounts of cystallization (up to 15 %). The bulk distribution coefficient for models involving amphibole are less than one and the light REE are not fractionated from the heavy REE. If only amphibole is crystallized, unrealistically high amounts of crystallization are needed to fractionate the REE and the calculated composition departs significantly from observed compositions. Poldervaart and Elston (1954) and Green and Ringwood (1968) object to deriving calc-alkaline magmas from tholeiitic magmas by fractional crystallization on the basis of different trends on AFM diagrams and major element

variation. Sakuyama (1981 and 1983) and Wada (1981) have shown that simple fractional crystallization of a tholeiitic magma will not yield a calc-alkaline magma in terms of 1) different mineral phases in fresh volcanics, 2) different contents of Ni, Cr, Rb, Ba, and Th, and 3) different variation of Mg, Ca, Na, and Si relative to K. Since Pedernal tholeiitic rocks cannot be related to the calc-alkaline rocks, two or more parental magmas are needed for Pedernal mafic rocks. Two different sources for younger tholeiitic and calc-alkaline rocks have been proposed by Donnelly and Rodgers (1980) and Gill (1984).

Attempts to relate calc-alkaline basalts to calc-alkaline andesites and andesites to each other by closed system fractional crystallization failed to produce statisfactory results. TiO2 increases in the more evolved rocks, so an Fe-Ti oxide cannot be used. In some cases, compatible transitional elements have the same contents in the parent and daughter compositions and this restricts ferromagnesium minerals to unrealistically small amounts. Since the trace elements have similar concentrations in the mafic calc-alkaline volcanic rocks, these volcanics may have been derived form a similar source. More than one parental magma may have formed In the Pedernal succession. Variations in degree of melting of the mantle source and differing crystallization histories may account for the observed differnces in the compositions of the rocks.

It is desirable to use igneous rocks that represent

primary or at least relatively undifferentiated magmas for modeling. Primary basalts should contain 235-400 ppm Ni (Sato, 1977), have a FeO*/MgO ratio less than 1.0 (Tatsumi, et al., 1983), and have Mg numbers between 70-75 (Green, 1971 and Gill, 1984).

For the Pedernal mafic rocks, the highest Ni value is 25 ppm, all FeO*/MgO ratios are greater than 1.0, and all of the Mg numbers are less than 73. On an MgO-FeO diagram (Fig. 38) all of the mafic volcanic samples from the Pedernal section plot below the field of primary melts produced from a pyrolite parent, indicating fractional crystllization of olivine and probably other phases. The distribution of data on a Zr-Ni diagram (Fig. 39) shows the same relations.

MgO, Ni, and Cr in Pedernal basalts are too depleted for the rocks to represent primary melts. Alumina usually increases with differentiation (Prefit, et al., 1980; Uto, 1981; Kay, et al., 1982; and Luhr and Carmichael, 1985) and in fact, high Al2O3 may be evidence that fractional crystallization occurred (Green and Ringwood, 1967; Lewis, 1971; and Holloway and Burnham, 1972). This is consistent with the observation that most high-Al basalts have undergone significant fractional crystallization (Lopes-Escobar, et al., 1977 and 1981; Nicholls, 1978; and Prefit, et al., 1980) with olivine and spinel as important residual phases (Luhr and Carmichael, 1985). From these considerations, it appears that none of the mafic rocks in

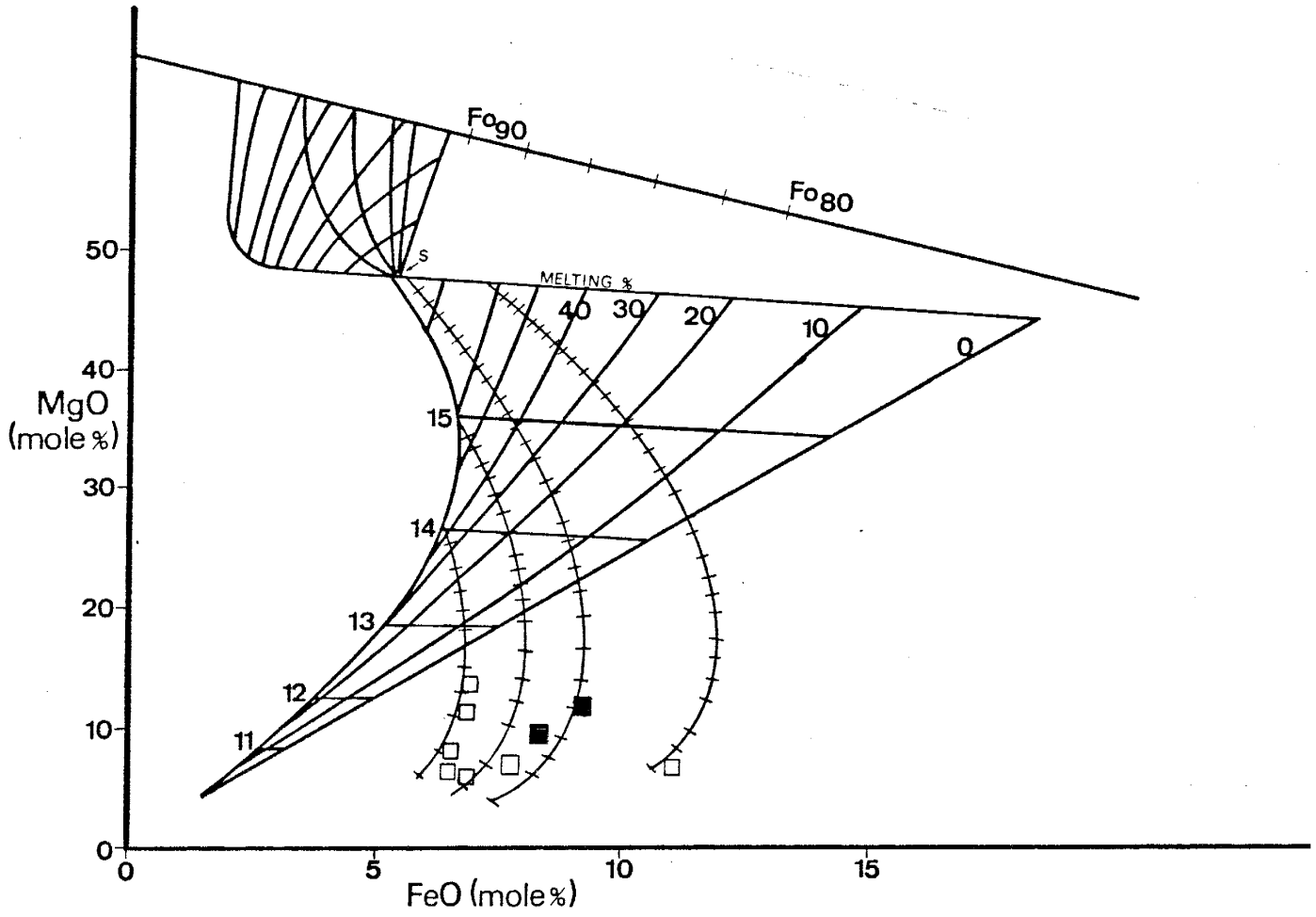

Figure 38. FeO-MgO diagram showing the distribution of basalts from the Pedernal succession. Curved lines with tick marks are olivine fractionation paths with each tick mark representing 5 % olivine removal. The diagram is constructed for 1 atm pressure. Modified from Hansen and Langmuir (1978). Open square is calc-alkaline basalt and Closed squares are tholeiitic basalts.

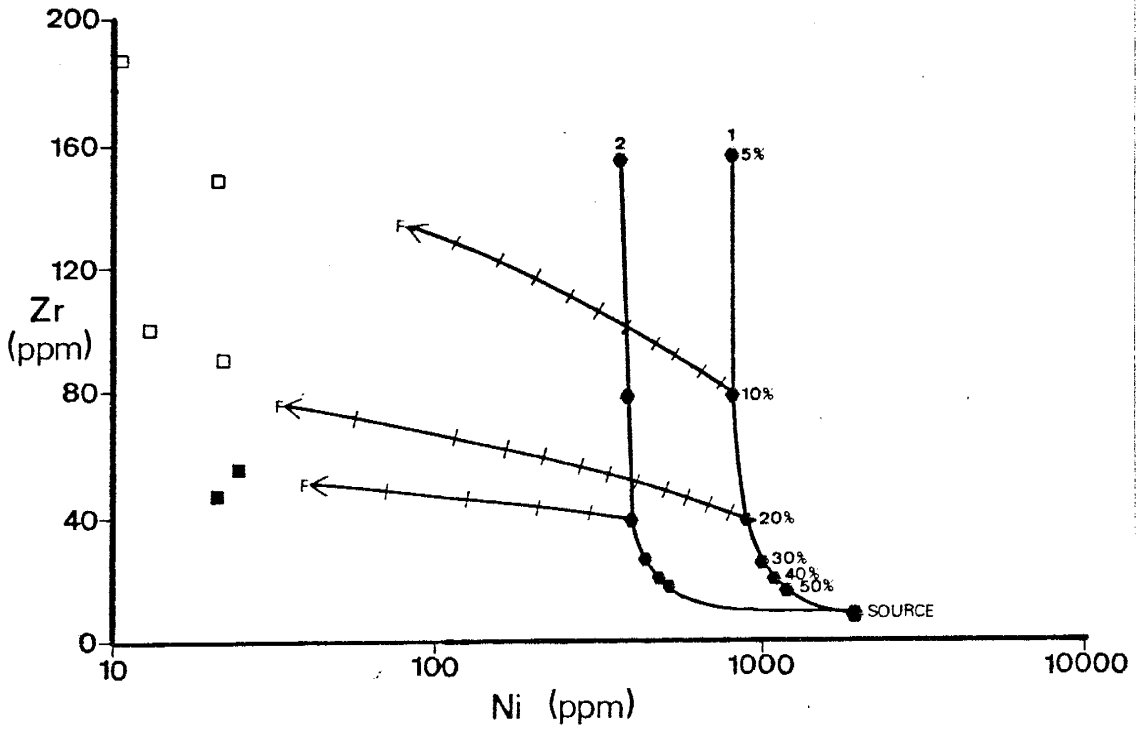

Figure 39. Ni-Zr diagram showing the distribution of basalts and andesites from the Pedernal succession plotted. Curved lines with tick marks are olivine fractionation paths with each tick mark representing 5 % olivine removal. The source has a mode of ol:opx:cpx in the ratio of 55:25:20 and the melt has a ratio of 20:25:55. Modified from Rajamani, et al. (1985). Symbols as in Fig. 38. Line 1 is for 1500 C and line 2 is for 1250 C.

the Pedernal section represent primary melts.

The origin of calc-alkaline rocks has been explained by several models: fractional crystallization involving olivine, clinopyroxene, and magnetite (Osburn, 1959 and 1962; and Miyashiro and Shido, 1975) or amphibole (Cawthorn and O'Hare, 1976 and Boettcher, 1977); partial melting of a subducted slab (Green and Ringwood, 1968); hydrous partial melting of peridotitic mantle above the slab (Kushiro, 1972 and 1974 and Green, 1973); contamination of a parental magma with crustal material (Tilley, 1950; Wilcox, 1954; Coats, 1962; Coulon and Thorpe, 1981; and Gill, 1981); or magma mixing (Eichelberger, 1978; Sakuyama, 1979, 1981, and 1983; Luhr and Carmiachael, 1980; Heiken and Eichelberger, 1980; and Wada, 1981).

LIL elements and light REE are enriched in calc-alkaline rocks compared to NMORB and this is illustrated on the MORB normalized diagrams (Figs. 23 and 24). Provided calc-alkaline rocks are not contaminated by crustal material, the source of calc-alakline rocks is enriched in LIL elements and light REE compared to NMORB. This enrichment has been attributed to a subduction component by Pearce (1983) caused by dehydration of the subducted slab (Ringwood, 1974; Best, 1975; Thope, et al., 1976; Hawkesworth, et al., 1977; Hawkesworth, et al., 1979; Mysen, 1979; Saunders and Tarney, 1979; Wendlandt and Harrison, 1979; Hawkesworth and Powell, 1980; Saunders, et al., 1980; and Hole, et al., 1984) or hydrous partial

melting of the slab (Frey and Green, 1974 and Ringwood, 1977). This enrichment could also be a primary feature of the source and the source of calc-alkaline rocks could be similar to sources of alkalic basalt (Tarney and Saunders, 1979), ocean island basalts (Morris and Hart, 1983), or a combination of oceanic island basalt source and a subduction component (Saunders, et al., 1980; Gill, 1984; and White and Pathett, 1984). Selective contamination of primary magma by continental crustal material could cause enrichment of LIL elements and light REE, but isotopic evidence supports the idea that most of the enrichment is subcrustal (Margaritz, et al., 1978 and Cameron and Cameron, 1985).

Dehydration of a subducted slab is supported by experimental work which shows that H2O fluid-mineral distribution coefficients are high for light REE (Mysen, 1977, 1979, and 1981). An H2O-fluid would also carry high contents of LIL elements. Hawkesworth (1979) believes that trace element characteristics of calc-alkaline rocks are more consistent with enrichment from a hydrous fluid than with partial melting of a descending slab.

Hawkesworth, et al. (1984) studied mantle xenoliths and found two types of metasomatism. One type of metasomatism is characterized by low Ti/K ratios and high Rb/Ba and Rb/Sr ratios and appears to be subduction related (Holm and Munksgaard, 1982 and Hawkesworth, et al., 1984). This enrichment involves a H2O- and alkali-rich fluid from

the subducted slab (Hawkesworth, et al., 1984). The Pedernal calc-alkaline basalt and andesites have enriched LIL elements and light REE. Some of this enrichment could be due to alteration since LIL elements and light REE are considered mobile.

The HFS elements are depleted relative to the LIL elements or REE and are best illustrated on the MORB-normalized diagrams (Figs. 24 and 25). This especially evident for Ti. Low TiO2 is consistent with phlogopite, amphibole, or an Fe-Ti oxide phase occurring as a fractionating phase (Prefit, et al., 1980). Briqueu, et al. (1984) related Ti (+/- V) depletion to fractional crystallization of an Fe-Ti oxide. They compared Ti and V concentrations to several fractionation indices. The Pedernal calc-alkaline basalt and andesites have variable Ti and V with respect to several differentiation indices (Zr, Fe2O3-T, Mg number, and Sm). The failure of the Pedernal rocks to follow a trend similar to that displayed by as Brique, et al. (1984) may be due to one of four reasons. 1) An Fe-Ti oxide may not have crystallized out. An Fe-Ti oxide is indicated by decreasing Fe2O3-T and TiO2 with increasing silica (Kuno, 1968 and Anderson and Gottfried, 1971). The Pedernal calc-alkaline basalt and andesites have variable Fe2O3-T and TiO2 with increasing SiO2. 2) An Fe-Ti oxide may have accumulated in some and/or been depleted in other samples. 3) The rocks are not co-magmatic. 4) There has been alteration, even though

Ti is considered to be immobile. The low Ti (and other HFS elements) may be a source characteristic which is typical of arc rocks.

Source Charateristics

Bougault, et al. (1980) used incompatible element ratios to show mantle inhomogenieties. Source incompatible element ratios are not significantly affected by fractional crystallization (Bougault, et al., 1980). Table 14 lists several incompatible ratios. Y/Tb ratios are about the same for all the mafic volcanics. The Y/Tb ratio is lower than primordial mantle ratio or the NMORB ratio. This could indicate slight enrichment of Tb in the source since Y is believed to be insenitive to mantle enrichments and depletions (Alabaster, et al., 1982). The Zr/Nb ratios are all lower than NMORB or primordial mantle and appears to indicate enrichment of Nb relative to Zr. This is supported by the NMORB-normalized diagrams. The other ratios vary between samples and may indicate mantle inhomogenieties (Bougault, et al., 1980), but some of the scatter in the La/Ta, La/Yb, and Ta/Th ratios may be related to the mobility of La and Th. All of the La/Ta and La/Yb ratios are higher and all the Ta/Th ratios are lower than NMORB or primordial mantle ratio. This is consistent with enrichment of light REE and LIL elements relative to some HFS elements in arc rocks. The Ti/Zr ratio is less

TABLE 14. INCOMPATIBLE ELEMENT RATIOS FOR THE MAFIC VOLCANIC ROCKS FROM THE PEDERNAL SECTION.

SAMPLE	P760	P762	P792	P775	P772	P740
Y/Tb	21	34	32	30	17	26
Zr/Hf	39	32	34	32	29	31
La/Ta	---	---	68	28	41	37
Ta/Th	---	---	0.13	0.20	0.12	0.13
Ti/Zr	59	90	33	28	51	41

	P765	P774	P901	A	B
Y/Tb	31	27	29	44	37-47
Zr/Hf	36	31	31	31	34-44
La/Ta	48	31	21	17	16
Ta/Th	0.14	0.11	0.26	0.45	0.90
Ti/Zr	96	31	32	139	100

A is primordial mantle from Wood (1979).
B is N-MORB values (Bougault, et al., 1980 and Pearce, 1983).

than primordial mantle or NMORB. Inspection of the MORB normalized spider diagrams indicates the low Ti/Zr ratios are caused by depletion of Ti.

Enrichments can be illustrated on the Th/Yb-Ta/Yb diagram (Fig. 40). A trend for within plate depletion and enrichment has a slope of unity and affects both Th and Ta, with depletion creating a NMORB type source and enrichment creating a within plate type source. Within plate enrichment has been related to a CO2-rich fluid or an intersitial melt (Frey and Green, 1974; Lloyd and Bailey, 1975; O'Nions, et al., 1977; and Wood, et al., 1979). The second type of enricment affects only Th and has been related to a H2O-rich fluid in a subduction zone (Hawkesworth, 1979 and Hawkesworth, et al., 1979). The mafic and andesitic calc-alkaline rocks from the Pedernals plot in the Th-enriched field. Two types of enrichment can be interpreted from this diagram. These are within plate enrichment were Th and Ta are both enriched and a subduction zone enrichment were only Th is enriched. The Zr/Y-Zr diagram (Fig. 41) also illustrates enrichment and depletion due to the empirical observation that Zr is affected more than Y by processes that cause mantle heterogeneity (Alabaster, et al., 1982). From this diagram, it appears that the tholeiites were produced from a depleted source and the calc-alkaline volcanics from an enriched source relative to chondritic values.

Three components may contribute to arc magmas:

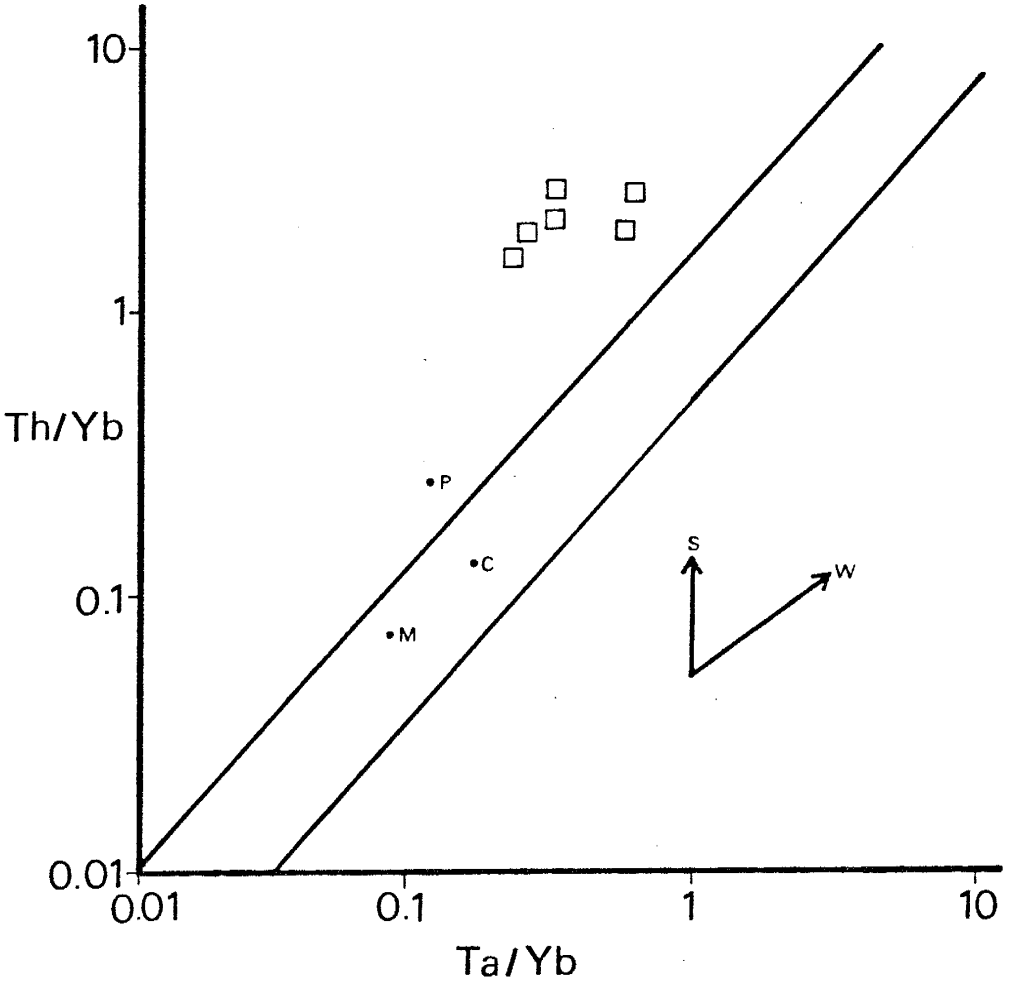

Figure 40. Th/Yb-Ta/Yb diagram showing fields of within plate enrichment and depletion and an arrow representing typical subduction zone enrichment. Fields from Pearce (1983). Symbols as in Fig. 38. W is within plate enrichment; s, subduction zone enrichment; M, average MORB; C, chondrite; and P, primordial mantle.

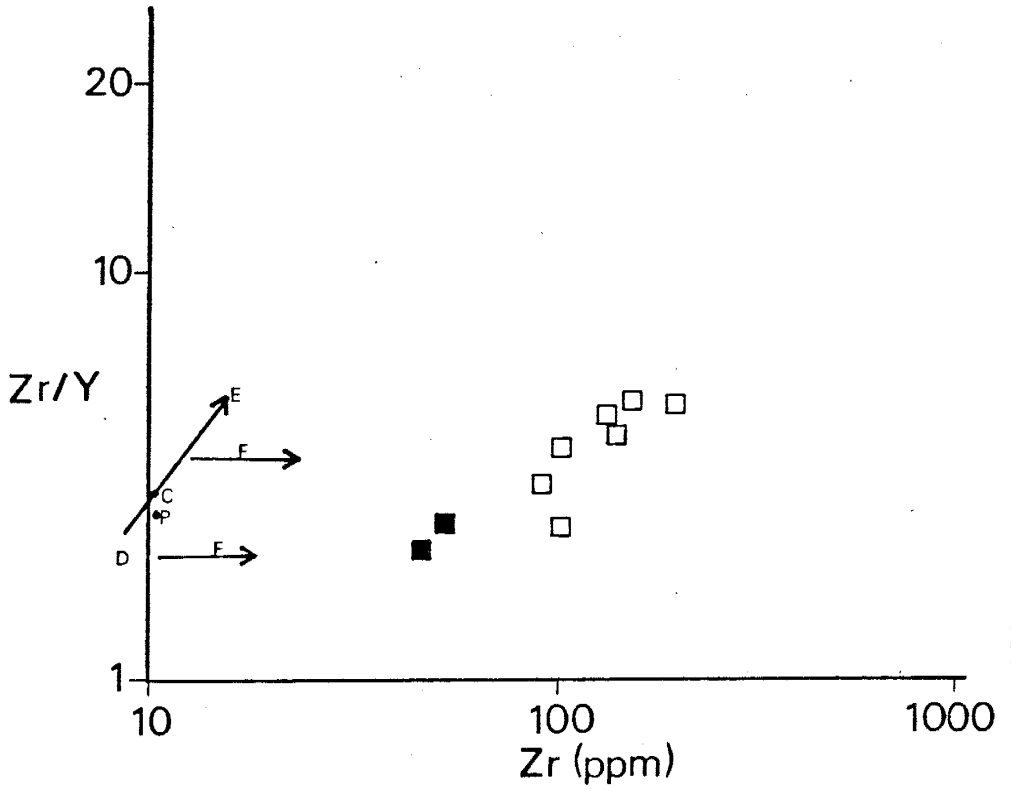

Figure 41. Zr/Y-Zr diagram showing C3 primordial mantle value (C on the diagram) and areas of enriched (E) and depleted sources (D). The arrows (F) represent the paths of partial melting (p. m.). Based on diagram from Pearce (1982). Symbols as in Fig. 38.

depleted mantle similar to NMORB source, subduction zone component, and enriched mantle. Using the procedures of Pearce (1983), the mafic volcanic samples are plotted on MORB normalized spidergrams and percent contribution of the three components for each sample are calculated with results presented in Tables 15 and 16. The procedures include assuming the primary source of the volcanics was a depleted source similar to that of NMORB and that changes in the shape of the plots is due to enrichment and depletion of the mantle sources and not to degree of partial melting or differentiation (Pearce, 1983). Y and Yb are assumed to be unaffected by enrichment processes and so a horizontal line is drawn through Y and Yb. This line represents the contribution of a depleted mantle component which is similar to N-MORB source. Enrichments are due to the subduction zone and the within plate processes.

Sample P760 has a spidergram similar to island arc basalts (figure 22). Only the depleted mantle and subduction zone components contibute to P760 (table 15). P, Zr, Hf, and Ti values are below the depleted mantle line and are assumed to have 100 % contribution from the depleted mantle. These low values probably indicate mantle source depletion. Less likely, they may reflect alteration, though Zr, Hf, and Ti are thought to be immobile.

Sample P762 has a spidergram similar to island arc basalts (figure 23). K and Rb are low, but this could be

TABLE 15. SOURCE COMPONENTS FOR THE THOLEIITIC VOLCANICS FROM THE PEDERNAL SECTION.

	P760		P762	
	m %	sz %	m %	sz %
Sr	65	35	48	52
K	58	42	100	---
Rb	21	79	80	20
Ba	8	92	18	82
Th	11	89	8	92
Ta	ND	ND	ND	ND
Nb	43	57	48	52
Ce	60	40	23	77
P	100	---	100	---
Zr	100	---	100	---
Hf	100	---	100	---
Sm	80	20	67	33
Ti	100	---	100	---
Y	100	---	100	---
Yb	100	---	100	---

m is the contribution from a depleted mantle source.
sz is the contribution from the subduction zone component.
ND is below the detectability limit for INAA.

TABLE 16. SOURCE COMPONENTS FOR THE MAFIC CALC-ALKALIC VOLCANICS FROM THE PEDERNAL SECTION.

	P792			P772		
	m %	wp %	sz %	m %	wp %	sz %
Sr	38	37	25	100	---	---
K	16	24	60	8	15	77
Rb	7	14	79	2	6	92
Ba	6	12	82	5	14	81
Th	4	9	87	3	8	89
Ta	26	74	---	22	78	---
Nb	37	63	---	37	63	---
Ce	12	12	76	13	16	71
P	100	---	---	100	---	---
Zr	82	18	---	100	---	---
Hf	75	25	---	77	23	---
Sm	42	9	49	53	5	42
Ti	100	---	---	100	---	---
Y	100	---	---	100	---	---
Yb	100	---	---	100	---	---

	P775			P765		
	m %	wp %	sz %	m %	wp %	sz %
Sr	45	55	---	82	18	---
K	6	20	74	33	29	38
Rb	2	9	89	9	9	82
Ba	5	27	68	19	20	61
Th	2	13	85	7	7	86
Ta	10	90	---	42	58	---
Nb	31	69	---	56	44	---
Ce	10	15	75	10	25	65
P	74	26	---	52	26	22
Zr	59	41	---	100	---	---
Hf	50	50	---	100	---	---
Sm	40	28	32	58	13	29
Ti	100	---	---	100	---	---
Y	100	---	---	100	---	---
Yb	100	---	---	100	---	---

TABLE 16. CONTINUED.

	P740			P901		
	m %	wp %	sz %	m %	wp %	sz %
Sr	41	41	18	63	37	---
K	26	58	16	15	41	44
Rb	10	31	59	5	26	69
Ba	11	34	55	5	26	69
Th	2	8	90	3	16	81
Ta	18	82	---	11	89	---
Nb	39	61	---	35	65	---
Ce	11	11	78	13	17	70
P	71	29	---	100	---	---
Zr	73	27	---	68	32	---
Hf	61	39	---	54	46	---
Sm	36	17	47	45	26	29
Ti	100	---	---	100	---	---
Y	100	---	---	100	---	---
Yb	100	---	---	100	---	---

	P774		
	m %	wp %	sz %
Sr	100	---	---
K	11	25	64
Rb	4	13	83
Ba	5	18	77
Th	2	7	91
Ta	16	84	---
Nb	34	66	---
Ce	10	16	74
P	48	52	---
Zr	57	43	---
Hf	46	54	---
Sm	33	35	32
Ti	100	---	---
Y	100	---	---
Yb	100	---	---

m is the contribution from a depleted mantle source.
wp is the contribution from an enriched mantle source or subcontinental mantle.
sz is the contribution from the subduction zone component.

due to alteration. Again, only depleted mantle and a subduction zone component contribute to P762 with P, Zr, Hf, and Ti values less than the depleted mantle line (Table 15).

The calc-alkaline basalts and andesites from the Pedernals have three mantle components: depleted mantle, subduction zone, and within plate (Table 16). Ti and, in some cases P, are less in the Pedernal rocks than the depleted mantle. This may indicate depletion in the mantle, retention of an Fe-Ti oxide phase for Ti and apatite for P in the mantle, or fractionation of these phases. Also, the low P values may be due to alteration. The Sm values and some Ce values are obtained by interpolation of a line between Hf and Nb (see Pearce, 1983, for disscussions). Sr and P are also less than the within plate values for some samples and both of these elements are affected by within plate enrichments. The low values could be due to alteration or fractionation of plagioclase (Sr) and apatite (P and Sr).

FELSIC VOLCANIC ROCKS

For both sections, the trace element contents of the felsic volcanics are similar. P753, P719, P767, and M743 are not included in the modeling since they may not represent liquid compositions. P719 has a high modal plagioclase content and the other three (P753, P767, and

M743) have been altered. Both fractional crystallization and batch melting models are tested.

The first step is to try to relate the felsic volcanics within each section to each other by closed system fractional crystallization. For the Manzano section, M743 is excluded since it has been silicified. The fractionation sequence is determined by increasing silica contents: M742-M601-M723-M758. Table 17 summarizes the model for M742 to M601. The first column lists the assumed composition of the parental magma (M742), the second column the phases, and their corresponding amounts removed from the parental magma to produce the daughter liquid. The value for F is the percent of parental magma left after fractional crystallization has occurred. The calculated composition of the daughter liquid (for M601) is listed in column three and the observed composition (for M601) in column four. Major differences characterize elements that are easily mobilized, such as Mg, Ca, Na, K, Rb, Ba, K, and Sr. M742 has a positive Eu anomaly and may indicate plagioclase accumulation. Higher Kds for Sr (5) and Eu (4) in plagioclase would also lower the calculated values of Sr and Eu, bringing them close to the observed values.

Table 18 lists the model for M723 derived from M601. Again, Na, K, Rb, Ba, Sr, and Eu have significantly different values between those calculated and those observed and this may be due to alteration. M723 has a

TABLE 17. FRACTIONAL CRYSTALLIZATION MODEL OF M742 TO M601.

	M742	Model		M601 Calculated	M601 Observed
SiO2	72.2	F = 90		73.0	73.2
Al2O3	13.7			13.5	13.1
Fe2O3-T	3.87	Opx	5	3.51	3.59
MgO	1.03	K-spar	8	0.98	0.79
CaO	2.48	Mgt	5	2.43	2.02
Na2O	3.52	Plag	57	3.33	4.06
K2O	1.62	Biot	5	1.63	1.49
TiO2	0.37	Qtz	19.5	0.34	0.29
P2O5	0.08	Apat	0.5	0.07	0.061
		Zir	0.18		
		All	0.01		
Rb	70			76	55
Ba	811			815	908
K	13452			14214	12373
Sr	353			297	210
Th	11			12	13
U	2.4			2.7	2.7
Zr	288			259	260
Hf	9.4			9.3	8.4
Nb	11			12	12
Ta	1.4			1.5	1.6
Y	47			49	51
Ti	2220			2244	1740
V	30			21	25
Sc	18			17	18
La	73			78	77
Ce	140			147	155
Sm	13			14	14
Eu	4.9			4.8	4.1
Tb	1.8			1.9	1.9
Yb	4.9			5.1	4.8
Lu	0.75			0.78	0.82

TABLE 18. FRACTIONAL CRYSTALLIZATION MODEL OF M601 TO M723.

	M601	Model		M723 Calculated	M723 Observed
SiO2	73.2	F = 90		73.6	73.7
Al2O3	13.1			12.7	12.5
Fe2O3-T	3.59	Opx	5	3.72	3.62
MgO	0.79	K-spar	8	0.73	0.75
CaO	2.02	Plag	60	1.91	1.98
Na2O	4.06	Biot	4	3.90	2.38
K2O	1.49	Qtz	22.5	1.49	3.63
TiO2	0.29	Zir	0.05	0.31	0.32
P2O5	0.061	All	0.016	0.07	0.070
Rb	55			60	172
Ba	908			912	721
K	12373			13070	30129
Sr	210			175	155
Th	13			14	13
U	2.7			3.0	2.6
Zr	260			269	269
Hf	8.4			9.0	9.7
Nb	12			13	12
Ta	1.6			1.8	1.5
Y	51			56	57
Ti	1740			1891	1920
V	25			21	25
Sc	18			18	19
La	77			81	80
Ce	155			163	164
Sm	14			15	14
Eu	4.1			4.0	4.9
Tb	1.9			2.0	2.0
Yb	4.8			5.2	6.2
Lu	0.82			0.89	0.84

positive Eu anomaly and differences in Eu may be due to some plagioclase accumulation in M723 relative to M601. Sr can be modeled by increasing the Sr Kd in plagioclase to 6. There are also differences in Yb and Hf that cannot be explained.

The last step for the Manzano section rocks is to test M758 as a residual liquid derived by fractional crystallization of M723. Both rhyolitic and high-silica rhyolite Kds produce unsuccessful models. Table 19 lists one of the models using the high-silica rhyolite Kds. M758 may have been altered or it is not co-magmatic with the other felsic volcanics from the Manzano section. A third possibility, is that M758 formed by differentiation as proposed by Hildreth (1979 and 1981), with diffusion or a fluid phase having been important during fractionation. It should be noted that M601, M742, and M758 consistently plot off the igneous rock trends on diagrams proposed by Beswich and Soucie (1978), which may indicate alteration.

In modeling the felsic volcanics from the Pedernals, three samples were not included: P719 has high modal plagioclase content and P767 and P753 are altered. P720 and P969 are from the same unit and have very similar compositions, so their compositions are averaged for purposes of modeling. The sequence of modeling is again determined by increasing SiO2 contents: P769-P710-P720,P969. Table 20 lists the model for P769 to P710. There are significant differences for some elements such as

TABLE 19. FRACTIONAL CRYSTALLIZATION MODEL OF M723 TO M758.

	M723	Model		M758 Calculated	M758 Observed
SiO2	73.7	F = 70		77.8	77.7
Al2O3	12.5			10.2	11.2
Fe2O3-T	3.62	Opx	5	2.87	2.92
MgO	0.75	K-spar	13	0.41	0.61
CaO	1.98	Plag	56	1.63	2.24
Na2O	2.38	Biot	3	1.14	3.21
K2O	3.63	Qtz	14	4.32	1.03
TiO2	0.32	Gar	8	0.29	0.28
P2O5	0.070	Ilm	0.3	0.06	0.066
		Apat	0.2		
		Zir	0.12		
Rb	172	All	0.09	234	41
Ba	721			688	443
K	30129			36886	8553
Sr	155			80	340
Th	13			11	8.6
U	2.6			3.7	1.7
Zr	269			230	231
Hf	9.7			11	7.9
Nb	12			15	8.4
Ta	1.5			2.0	1.1
Y	57			26	39
Ti	1920			1623	1680
V	25			14	22
Sc	19			11	16
La	80			49	57
Ce	164			112	115
Sm	14			11	9.7
Eu	4.9			3.6	4.1
Tb	2.0			0.74	1.4
Yb	6.2			2.4	3.8
Lu	0.84			0.43	0.56

TABLE 20. FRACTIONAL CRYSTALLIZATION MODEL OF P769 TO P710.

	P769	Model		P710 Calculated	P710 Observed
SiO2	69.4	F = 90		70.4	70.5
Al2O3	14.3			14.0	13.2
Fe2O3-T	3.86	Opx	5	3.20	4.19
MgO	0.81	K-spar	15	0.74	1.11
CaO	1.66	Plag	55	1.53	0.94
Na2O	4.42	Biot	5	4.33	3.69
K2O	2.02	Qtz	11.5	1.99	2.94
TiO2	0.42	Mag	8	0.36	0.40
P2O5	0.11	Apat	0.5	0.10	0.071
		Zir	0.18		
		All	0.17		
Rb	78			85	147
Ba	678			652	599
K	16774			17533	24413
Sr	117			95	72
Th	20			16	18
U	3.3			3.7	2.8
Zr	267			239	240
Hf	9.1			9.0	8.9
Nb	14			15	14
Ta	2.1			2.2	2.2
Y	44			45	59
Ti	2520			2427	2400
V	30			19	40
Sc	14			13	16
La	81			57	85
Ce	181			136	135
Sm	13			11	12
Eu	2.6			2.2	2.6
Tb	1.8			1.7	1.8
Yb	5.4			5.5	7.3
Lu	0.79			0.81	0.93

Fe, Mg, Ca, Na, K, P, Rb, Ce, Sr, Yb, Y, U, Lu, and V. Many of these differences may reflect alteration. V, Y and the heavy REE are considered immobile and their differences can not be readily explained.

Modeling of P710 to derive both P720 and P969 was not successful using either rhyolitic or high-silica rhyolitic Kds. The model that produces the best match between calculated composition and observed composition is listed in Table 21. The most significant feature of this model is the unrealistically high magnetite content (40 %) used to drastically reduce the Ti (Kd = 100) content. Modeling using ilmenite, which has a higher content of Ti than magnetite, is also unsuccessful. P720 and P969 may have been altered or are not co-magmatic with the other felsic volcanics from the Pedernal section. P720 and P969 could also have formed by a mechanism similar to the model Hildreth (1979 and 1981) proposed were diffusion or a fluid phase was important in the differentiation process.

Rhyolitic magmas can be produced by partial melting of the crust or by fractional crystallization of a more mafic parent (Pichler and Zeil, 1972; Fernandez, et al., 1973; Wyllie, et al., 1976; Thorpe, et al., 1979; Burt, et al., 1982; James, 1982; and Christiansen, et al., 1983). Primary rhyolitic magmas cannot be produced directly from the mantle (see Wylie, et al., 1976 for a review). A possible explanation for the origin of the felsic volcanics is that they are products of partial melting of the crust.

TABLE 21. FRACTIONAL CRYSTALLIZATION MODEL OF P710 TO P720 AND P969.

	P710	Model		Average of P720 and P969 Calculated	Observed
SiO2	70.5	F = 85		76.5	76.4
Al2O3	13.2			13.3	12.0
Fe2O3-T	4.19	Opx	5	0.0	2.56
MgO	1.11	Plag	54	1.15	0.15
CaO	0.94	Mag	40	0.57	0.78
Na2O	3.69	Apat	0.5	3.50	3.85
K2O	2.94	All	0.01	3.40	3.86
TiO2	0.40			0.0	0.15
P2O5	0.71			0.01	0.016
Rb	147			172	140
Ba	599			686	730
K	24413			28470	32053
Sr	72			59	51
Th	18			20	19
U	2.8			3.3	4.3
Zr	240			265	323
Hf	8.9			10	10
Nb	14			14	16
Ta	2.2			1.9	2.4
Y	59			56	85
Ti	2400			1243	900
V	40			6.4	ND
Sc	16			11	8.6
La	85			96	97
Ce	135			147	190
Sm	12			13	17
Eu	2.6			2.6	2.9
Tb	1.8			1.9	2.7
Yb	7.3			8.1	8.8
Lu	0.93			1.0	1.5

An excellent example of partial melting of the crust to produce rhyolitic magmas is the Taupo Volcanic Field (Ewart, et al., 1968; Ewart and Taylor, 1969; Cole, 1979 and 1981; and Reid, 1983).

There are numerous possible sources in the crust with variable compositions and mineralogies. For purposes of modeling, source compositions and mineral abundances are assumed. Partial melting of the crust involves quartz, feldspars, micas, hornblende, and other minor phases (Brown and Fyfe, 1970). Seven different sources were selected for modeling (Table 22). The first four represent possible sources in island arcs and the last three possible sources in the lower to middle continental crust.

Watson (1979) studied zircon saturation in felsic magmas. If partial melting of the crust occurs with zircon in the residue and the source has more than 100 ppm Zr, the magma will have less than 100 ppm Zr. All of the felsic volcanics from both the Manzano and Pedernal sections have greater than 100 ppm Zr. This indicates that zircon started to crystallize or was entrained by the magma during partial melting.

The first four sources are modeled with the modes listed in Table 23. The modes are varied within a small range and represent lower to middle crustal levels. Felsic Kds are used, but may not be strictly applicable since felsic Kds are arrived at using felsic phenocrysts in

TABLE 22. CRUSTAL SOURCE COMPOSITIONS FOR FELSIC VOLCANIC MODELLING.

	1	2	3	4	5	6	7
SiO2	52.8	51.5	47.7	51.6	67.9	65.6	65.6
TiO2	0.56	0.74	0.45	1.0	0.43	0.58	0.53
Al2O3	20.3	13.8	9.93	17.4	16.0	15.79	15.9
Fe2O3-T	9.14	12.3	11.2	9.1	3.50	4.76	5.33
MgO	5.06	7.94	18.0	6.8	1.39	2.08	2.37
CaO	8.80	9.41	9.25	9.7	3.61	4.56	4.48
Na2O	2.99	3.18	1.69	2.7	5.02	4.49	4.22
K2O	0.90	0.20	1.07	1.2	1.61	1.51	1.21
MnO	0.12	0.17	0.20	0.18	0.05	0.06	0.07
P2O5	0.11	0.061	0.29	0.30	0.16	0.20	0.17
Rb	29	7.4	15	20	45	41	13
Ba	334	182	92	350	567	475	499
Sr	287	87	501	525	635	534	586
Th	4.6	1.7		1.5	4.7	2.9	1.4
Zr	99	48	24	140	153	158	134
Nb	7.4	5.0	1.6	5	7.5	8.1	5.3
Ta	0.6				1.1	1.6	0.17
Hf	2.9	1.2		2.5	4.2	4.2	3.5
Y	28	23	11	25	12	13	13
Co	13	57	90	30	12	22	16
V	201	311	217	226			
Sc	31	45	35	30	5.4	9.7	11
La	41	4.9		10	29	36	31
Ce	75	13			55	65	60
Sm	7.2	3.1		3.5	3.8	4.9	5.1
Eu	1.8	1.0			1.3	1.5	1.3
Tb	0.87				0.44	0.58	0.47
Yb	2.8	2.4		2.5	0.94	1.1	1.1
Lu	0.40	0.43			0.15	0.18	0.18

1 P792, 2 P760, 3 average of 6 arc picrites from Ramsay, et al. (1984), 4 average CAB from Condie (1985), and 5 average tonalite, 6 average low-pressure granulite, and 7 average medium- to high-pressure granulite, all from Allen (1985).
All averages are recalculated to 100 % on a volatile free basis.
Major elements in weight percent. Trace elements in ppm.
Fe2O3-T is total iron as Fe2O3.

TABLE 23. SOURCE MINERALOGY USED FOR PARTIAL MELTING OF MAFIC SOURCES FOR THE MODELLING OF THE FELSIC VOLCANIC ROCKS.

Garnet Granulite	Mode	Melt
Plagioclase	58	64
Clinopyroxene	22	5
Garnet	10	5
Quartz	8	25
Magnetite	2	1
Garnet Amphibolite		
Amphibole	35	5
Plagioclase	32	60
Clinopyroxene	17	4
Garnet	9	5
Quartz	5	25
Magnetite	2	1
Amphibolite		
Plagioclase	54	69
Amphibole	39	12
Quartz	5	18
Magnetite	2	1

Mode, percent that the phases occurs in the parent before partial melting.
Melt, percent that the phases contribute to the liquid upon partial melting.

volcanic rocks. Partial melting of the first four sources involves mafic phenocrysts in equilibrium with a felsic magma and the Kds may be different for such a system.

For sources 1 through 4, none of the models tested produced an acceptable fit of calculated compositions to observed compositions. The La/Yb ratio can be produced with garnet in the residue, but the calculated REE concentrations are depleted relative to the observed values for the felsic volcanics from both sections. Also, the calculated HFS elements did not match the observed contents in the felsic volcanics.

For numbers 5, 6, and 7, the source modes are dominated by plagioclase with potassium feldspar, biotite, garnet, clinopyroxene, amphibole, magnetite, ilmenite, apatite, zircon, and allanite. Again, none of the models tested are reasonable. The REE can be matched, but the major elements and the HFS elements are dissimilar to the observed values for the felsic volcanics. So, it seems the felsic volcanics cannot be produced by partial melting of these crustal sources.

Since partial melting models cannot explain the felsic volcanics from both sections, closed system fractional crystallization of the calc-alkaline basalt and andesites from the Pedernals was tested. Comparision of primordial mantle normalized diagrams of the calc-alkaline basalt and andesites from the Pedernals with the felsic volcanics from both the Pedernal and Manzano sections show the same

negative anomalies of Nb, Ta, Sr, P, and Ti (Figs. 42, 43, and 44). This could be explained by fractional crystallization with the felsic volcanics inheriting the anomalies from the mafic magmas.

There is a general decrease of TiO2, Al2O3, Fe2O3-T, MgO, CaO, and P2O5 from the mafic to felsic calc-alkaline rocks and such trends are typical of calc-alkaline suites (Gill,1981) and may indicate fractional crystallization. Since the Al2O3/CaO ratio increases from 2 to 15, clinopyroxene and/or amphibole may play a significant role in the fractionating phases. Lowering of Fe, Mg, and Mn requires ferromagnesium minerals and steepening of REE patterns suggests that amphibole has played a significant role. Apatite is needed to lower P, feldspars to lower Al, and amphibole and/or an Fe-Ti oxide to lower Ti. Apatite usually occurs as small crystals in volcanic rocks which may be difficult to settle out of a magma. One possible mechanism for removing apatite from a magma is for the apatite to occur as inclusions in other fractionating phases which provides a mechanism for locally saturating the melt in apatite (Luhr and Carnichael, 1980 and Harrison and Watson, 1984). Zircon probably is a fractionating phase, since Zr is staturated in the the felsic volcanics considering the high Zr contents and the work of Watson (1979). Poldervaart (1956) presents petrographic evidence for early crystallization of zircon.

Since very few primary phenocrysts survived

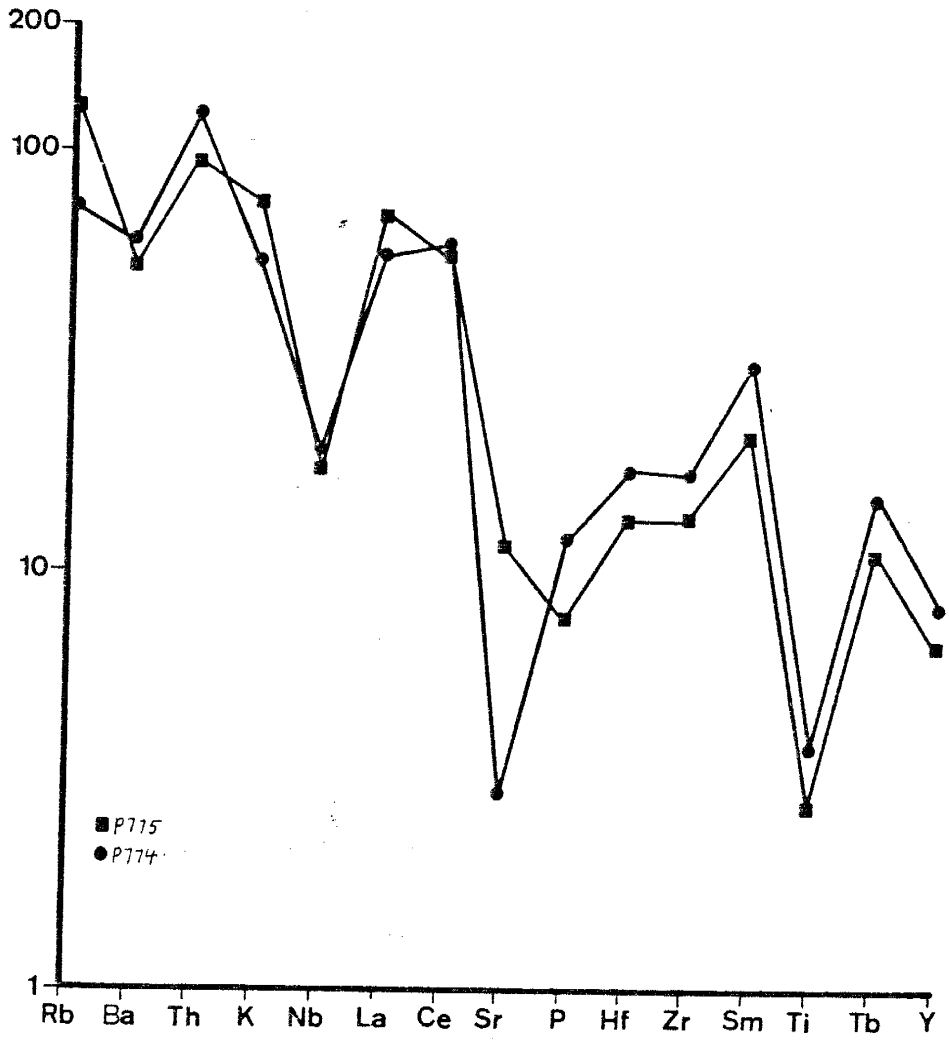

Figure 42. Primordial mantle normalized spider diagram of some calc-alkaline andesites from the Pedernal succession. Normalizing values from Wood (1979).

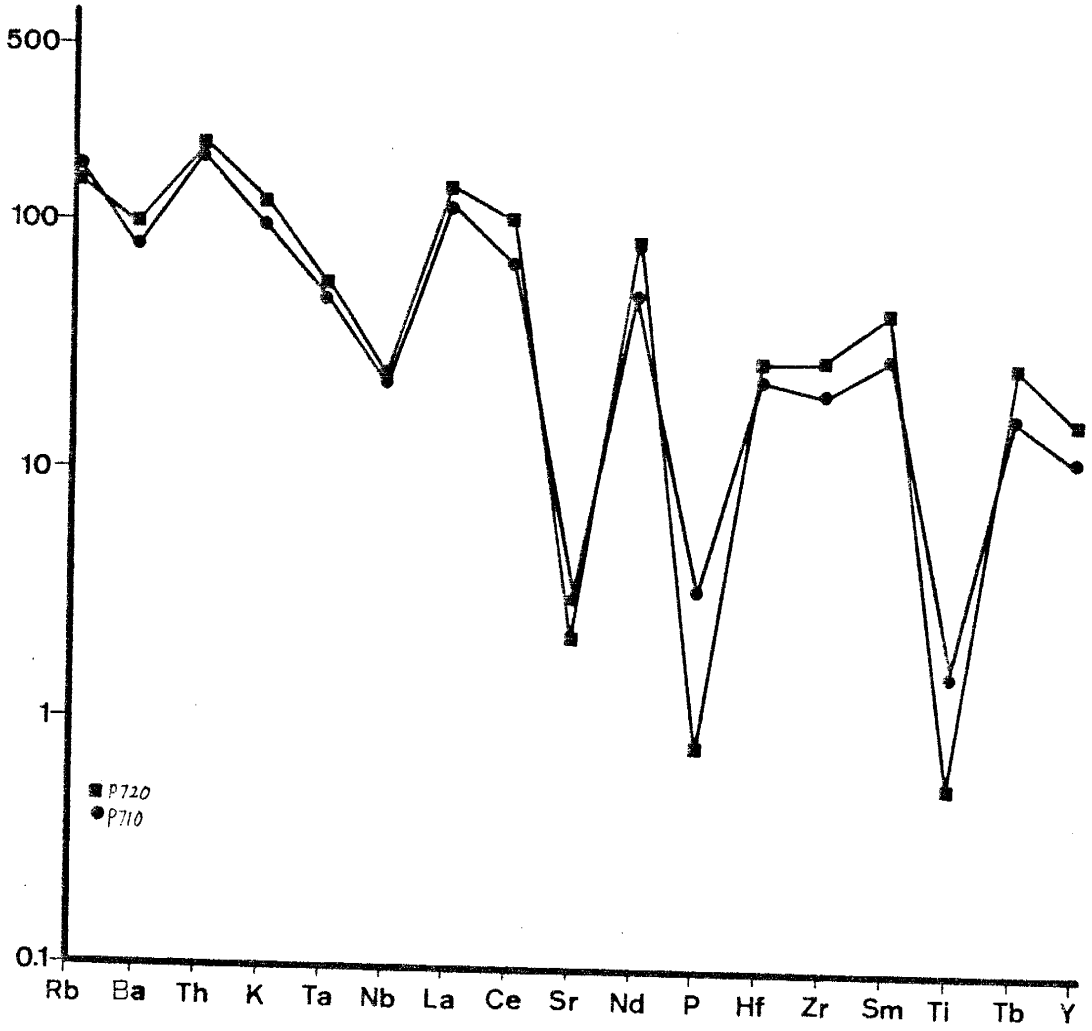

Figure 43. Primordial mantle normalized spider diagram of some of the felsic volcanic rocks from the Pedernal succession.

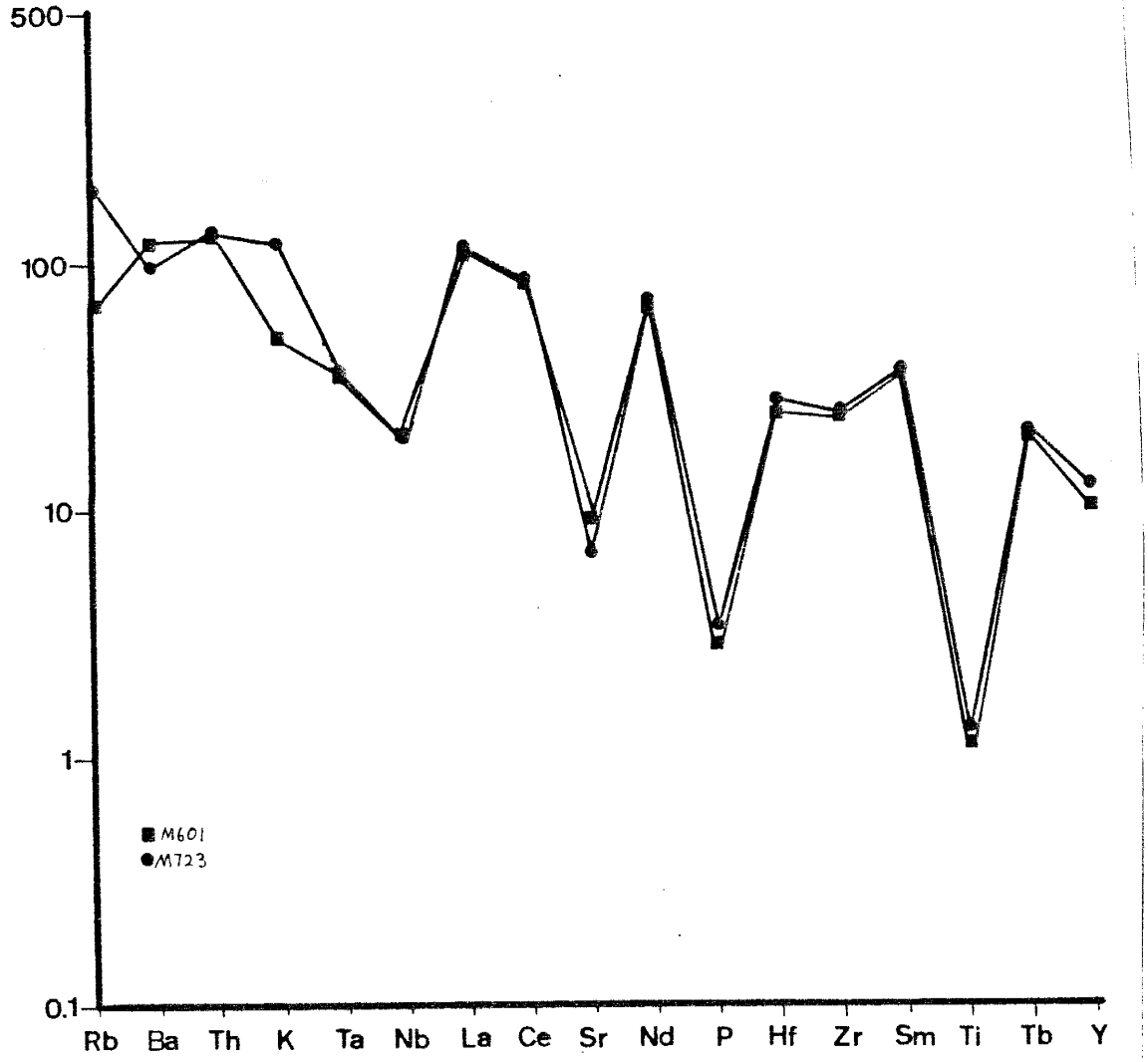

Figure 44. Primordial mantle normalized spider diagram of some of the felsic volcanic rocks from the Manzano succession.

metamorphism and recrystallization in the Pedernal calc-alkaline basalt or andesites, the minerals used and their modes are estimated from fresh calc-alkaline volcanics from the literature.

A two stage fractional crystallization model is presented that explains both the major and trace element distributions. Stage 1 produces a high-silica andesitic magma by fractionation of plagioclase, clinopyroxene, olivine, and magnetite from a magma assumed to have the same composition as sample P774. Stage 2 produces the felsic magmas by fractionation of the high silica andesitic magma by removal of plagioclase, amphibole, orthopyroxene, magnetite, ilmenite, apatite, and zircon. This model is similar to the model proposed for the Medicine Lake volcanics (Grove and Donnelly-Nolan, 1986). Table 24 summarizes the composition of P774 (column 2), the high-silica andesitic magma (column 3), the calculated felsic magma (column 4), and sample P769 (column 5). Most of the LIL elements and La, Nb, V, and Cr show significant differences between the calculated rhyolite and sample P769. These differences could be due to alteration (LIL elements and La), poorly known Kds (U), or the assumption of constant Kds is wrong (Cr). The other elements are reasonably matched.

This model can explain the felsic volcanics and the compositional gap in the volcanic rocks. The compositional gap in the volcanics can be explained by the shallow slope

TABLE 24. FRACTIONAL CRYSTALLIZATION MODEL OF P774 TO FELSIC VOLCANIC ROCKS.

	P710	Calculated Andesite	Calculated Rhyolite	P769
SiO2	57.9	60.7	71.5	71.6
Al2O3	16.1	16.6	13.8	14.7
Fe2O3-T	9.05	8.11	4.07	3.98
MgO	4.06	1.97	0.65	0.84
CaO	6.56	5.68	1.81	1.71
Na2O	3.42	3.85	4.33	4.56
K2O	1.70	2.04	3.23	2.08
TiO2	0.99	0.77	0.39	0.43
P2O5	0.25	0.29	0.13	0.11
Rb	64	76	130	78
Ba	466	549	948	678
K	13863	16467	28508	13448
Sr	248	253	139	117
Th	12	14	23	20
U	2.3	2.8	4.8	3.3
Zr	189	226	267	267
Hf	6.1	7.2	9.4	9.1
Nb	12	14	19	14
Ta	1.3	1.6	2.0	2.1
Y	40	47	46	44
Ti	5820	4991	3533	2520
V	243	240	17	30
Sc	28	30	12	14
La	40	47	71	81
Ce	116	138	183	181
Sm	12	14	15	13
Eu	2.8	3.2	2.7	2.6
Tb	1.5	1.8	1.8	1.8
Yb	4.1	4.8	5.1	5.4
Lu	0.52	0.61	0.65	0.79

of the cotectic on a temperature-composition diagram (Fig. 45), were a small temperature change produces a large change in the composition of the residual liquid (Grove and Donnelly-Nolan, 1986). The change in the fractionating phases from stage 1 to stage 2 is due to a reaction when the shallow sloping cotectic is reached and olivine and clinopyroxene react with the liquid and are replaced by amphibole and orthopyroxene. This type of model is supported by experimental work (Wyllie, 1963; Holloway and Burnham, 1972; Helz, 1976; Spulber and Rutherford, 1983; and Rutherford, et al., 1985) and field observations at Mt. Mazama (Smith, 1979; Ritchey, 1980; and Bacon, 1983), Aso Caldera, Japan (Lipman, 1967), and Shikotsu, Japan (Katsui, 1963).

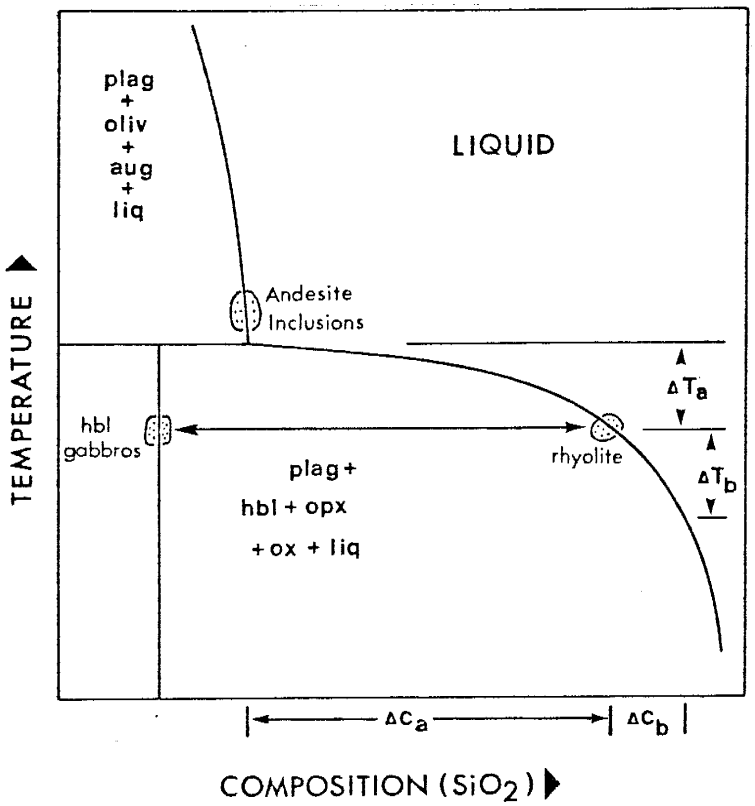

Figure 45. Temperature-composition diagram. The shallow slope of the cotectic results in a large percentage of crystals being removed over a small temperature interval. This can generate a compositionsl gap (modified from Grove and Donnelly-Nolan, 1986).

DEPOSITIONAL MODEL

MANZANO SECTION

There are four rock types in the Manzano study section: minor mafic rocks, felsic pyroclastic rocks, felsic volcaniclastic rocks, and graded epiclastic rocks. Graded bedded epiclastic sediments occur in numerous depositional environments and are therefore not diagnositic of depositional environment. The graded sedimentary rocks are laterally continous in large exposures, medium bedded, have nonerosive to scoured contacts, do not show signs of substantial reworking, and do not contain channel deposits. For these reasons, the graded epiclastic rocks are believed to represent turbidites. Most individual beds do not contain all of the Bouma sequence, but not all Phanerozoic turbidites display complete Bouma sequences (Walker, 1976). Similar types of sediments have been described from the bottom of Crater Lake, Oregon (Nelson, et al., 1986).

Some of the felsic volcanics show evidence of welding, which can form during either submarine or subaerial eruption. Welded subaqueous pyroclastics have been reported by several authors (Francis and Howells, 1973; Wright and Coward, 1977; Rudnick, 1983; Kokelaar, et al., 1984; Kokelaar, et al., 1984; Yamada, 1984; and Howells, et al., 1985). Entrance of a pyroclastic flow into the water

and its subsequent welding has been modeled by Sparks, et al. (1980). Using this model, the pyrolcastic flows are erupted subaerially, but continue under water only if they have a higher density than water (Sparks, et al., 1980). It is possible for flows to be emplaced below the wave base, with subaqueous deposition promoting welding (Sparks, et al., 1980). A boundary zone forms between the flow and water, where water is incorporated into the flow (Sparks, et al., 1980). If enough turbulence develops in the boundary zone, depletion of light glassy material and pumice fragments and enrichment of phenocrysts may occur, producing the volcaniclastic rocks. The volcaniclastic rocks in the Manzanos have a large content of phenocrysts with very little if any primary matrix, with primary matrix representing glassy material or pumice fragments. Emplacement of the flows may initiate turbidity currents, thus, explaining the graded bedded sedimentary rocks. The nongraded epiclastic rocks probably formed by normal deposition of suspended clastic material.

Interbedded turbidites and felsic pyroclastic flows have been described by Busby-Spera (1985 and 1986) from the Mineral King roof pendant, California. The turbidites in the Mineral King area were formed in a sandstone rich fan environment (Busby-Spera, 1985). Comparison of the Manzano section to the Mineral King turbidites indicates the Manzano turbidites may have formed in an outer fan environment. Some of the Mineral King pyroclasitc units

are bedded, but bedded deposits only account for 5 to 15 % of the exposed outcrops of felsic volcanics in the Mineral King section (Busby-Spera, 1986). The general lack of bedded deposits in the Manzano section could be due to slightly different depositional environment.

The site of deposition for the Manzano section within a continental arc is problematic. The basin may have been a fore-arc, intra-arc, or back-arc basin. The lack of large quantities of mafic epiclastic material may indicate a distal fore-arc or back-arc basin setting.

PEDERNAL SECTION

There are several rock types in the Pedernal section including pyroclastic rocks and epiclastic sedimentary rocks. Associated with the ash flow tuffs are coarse-grained volcaniclastic rocks which may represent reworked ash flow tuffs.

There are epiclastic rocks with relict graded beds, associated planar beds and possibly some cross laminations. All of these type of beds can occur in several depositonal environments. The exposures of the graded bedded sediments are poor and individual beds can not be traced from one outcrop to the other. Abundant grading, poor sorting, possible Bouma sequences, and the lack of shallow water structures leads to the interpretation that these rocks are turbidites.

The mafic rocks are composed of pyroclastics and hypabyssal intrusives, with no evidence of pillow basalts, pillow breccias, or hyloclastites. This indicates the pyroclasitcs may have been subaerially erupted. Since mafic pyroclatics do not travel far, the source or sources must have been near by. Associated with the mafic pyroclastics are pebble to cobble volcaniclastic rocks. The volcaniclastic rocks are unsorted and ungraded, heterolithic, massive, have subangular to subrounded clasts, and the clasts do not have glassy margins or vesicular margins. Glassy or vesicular margins may not have been preserved. The lack of glassy margins indicates the deposits are not pillow breccias. Most of these volcaniclastic rocks are framework supported, but some matrix supported units do occur. The rounding of the clasts, lack of any stratification or gradation and the occurence of both framework and matrix supported breccias are evidence that these deposits did not form by direct volcanic eruption. The heterolithic nature of the units and rounding indicate the deposits are epiclastic. The poor sorting and lack of internal fabric or structure indicates a lack of strong currents during deposition. Lack of evidence for reworking of the volcaniclastics, especially the matrix supported units, indicates subaerial deposition and quick burial or subaqueous deposition below the wave base. These breccias are similar to facies E from Mitchell (1970) which are interpreted to be cool submarine

lahars. Just to the south of the study area is a group of schists the author interpretes to be sedimentary rocks. Included in this area is a ferroginous quartzite bed that Armstrong and Holcombe (1982) interpret to be an exhalitive.

All the rock types in the Pedernal section are consistent with a subaqueous environment. The lack of mature sediments indicates minimal reworking. The lack of bedded cherts or deep-sea type mudstones may indicate deposition was not in the deeper parts of a basin or the basin did not reach sufficient size to allow these types of rocks to form.

The northern quartzite-schist succession could represent a shelf environment similar to the Ortega Quarzite of northern New Mexico (Soegaard and Eriksson, 1985 and 1986). The schists of the northern boundary zone may represent the first input of volcanic detritus. A submarine volcanic structure or structures may have gradually become emergent. The first mafic pyroclastics and the northern volcanic breccia were erupted from these structures, the pyroclastics being subaerially erupted. A period of erosion with intermitiant eruptions produced the sediments and pyroclastics of the central part of the study section. Fractional crystallization produces the felsic magmas and these are erupted subaerially and then are deposited subaqueously. Both mafic and felsic magmas are intruded within the section producing the hypabyssal

intrusives.

Since both tholeiitc and calc-alkaline rocks occur within the section, a fore-arc or intra-arc basin on the front side of the arc seems most reasonably. This is due to the general restriction of tholeiitic rocks to the front of an arc (Gill, 1981).

CONCLUSIONS

MANZANO SECTION

The Manzano section is dominated by graded sedimentary rocks interpreted as turbidites. The sedimentary rocks are interbedded with felsic pyroclastic rocks which include welded ash flow tuffs and volcaniclastic rocks. Minor mafic rocks are present and may represent flows, dikes, and/or sills.

The sedimentary rocks are quartz rich, felsic in composition, and appear to have been derived from the felsic pyroclastics by turbidity currents and deposited on the outer part of a submarine fan.

The felsic volcanics range from rhyodacite to high-silica rhyolite, are calc-alkaline, have light REE enriched patterns, and have trace element contents similar to modern continental-arc volcanics. The felsic volcanics appear to have evolved by closed system fractional crystallization from a basaltic parent and not by partial melting of the crust.

The Manzano section formed in a subaqueous environment in a continental-arc setting. The basin of deposition may have been a fore-arc, an intra-arc, or a back-arc basin. After deposition, the rocks were deformed at least twice and were than intruded by the Ojita Pluton and minor mafic dikes.

The southern Manzano terrane has been interpreted as a continental rift succession (Condie and Budding, 1979). The southern Manzano terrane may represent a back-arc basin formed after the arc travelled southward of the Manzano section.

PEDERNAL SECTION

The Pedernal section is composed of bimodal volcanic rocks, associated volcaniclastic rocks and sedimentary rocks. Both tholeiitic and calc-alkaline mafic rocks occur in the section. The tholeiites are basaltic, have flat to slightly light REE enriched patterns, and are derived from a slightly enriched mantle source. The calc-alkaline volcanics range in composition from basalt to andesite, have light REE enriched patterns, and are derived from an enriched mantle source. The Pedernal Hills are one of the few exposures of Proterozoic rocks in the Southwest that contain andesites. The calc-alkaline andesites are not co-magmatic with each other or the calc-alkaline basalt, but are derived from a similar source. The mafic rocks have trace element contents similar to modern arc volcanic rocks.

The felsic volcanic rocks are calc-alkaline, range in composition from rhyodacite to high-silica rhyolite, and include welded ash flow tuffs. They have light REE enriched patterns and have negative anomalies of Sr, P, and

Nb on primordial normalized diagrams similar to the mafic volcanics. From modeling, the felsic voclanics cannot be derived from the crust by partial melting, but can be produced by closed system fractional crystallization of a basaltic magma. They have trace element contents similar to modern continental-arc volcanics.

Graded epiclastic sedimentary rocks are believed to represent turbidites. The volcaniclastic rocks have features similar to cool, submarine lahars. All of the rock types present in the Pedernal section are consistent with subaqueous deposition.

The contact with the northern quartzite-schist terrane is not well exposed, but the Pedernal section appears to overlie the quartzite-schist terrane. The Pedernal section may have formed subaqueously in a continental-arc setting. The basin of deposition may have been a fore-arc, intra-arc, or back-arc basin. After deposition, the Pedernal section was deformed several times (Armstrong and Holcombe, 1982) and then intruded by the mid-Proterozoic Pedernal Pluton and Cambrian-Ordovician syenites.

APPENDIX A
ACCESS AND SAMPLE LOCATION

The access to the Manzano succession is poor, but excellent for the Pedernal succession, using a two wheel drive car. The Manzano section is within the Manzano Wilderness area and no roads go thourgh the area. County roads, U S Forest Service roads, and roads built by Horizon Corporation on the Tome Land Grant are used for access to the Manzano section. All of these roads end about 1 to 1.5 miles from the Manzano section. Access to the Pedernal succession was through the Harral Ranch. Several roads cut accross or parrallel the exposures in the Pedernal section and in several cases, the car can be parked next to outcrops.

Sample locations for both petrographic and geochemical samples are presented in figure A1 (Manzano section) and A2 (Pedernal section). See Appendix C for description of sample collecting and preparation techniques.

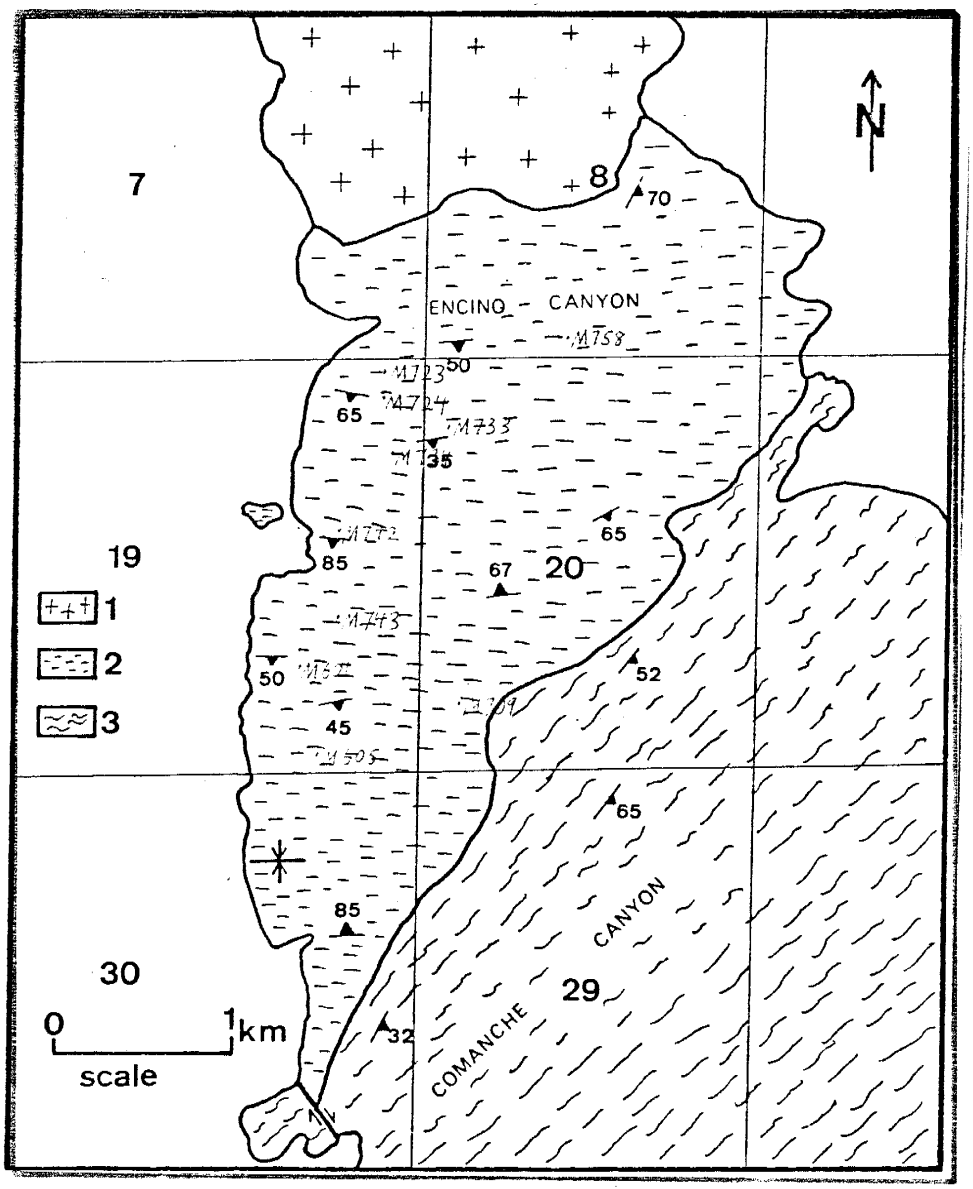

Figure A1. Generalized geologic map of the Manzano section showing sample locations. Symbols as in figure 3.

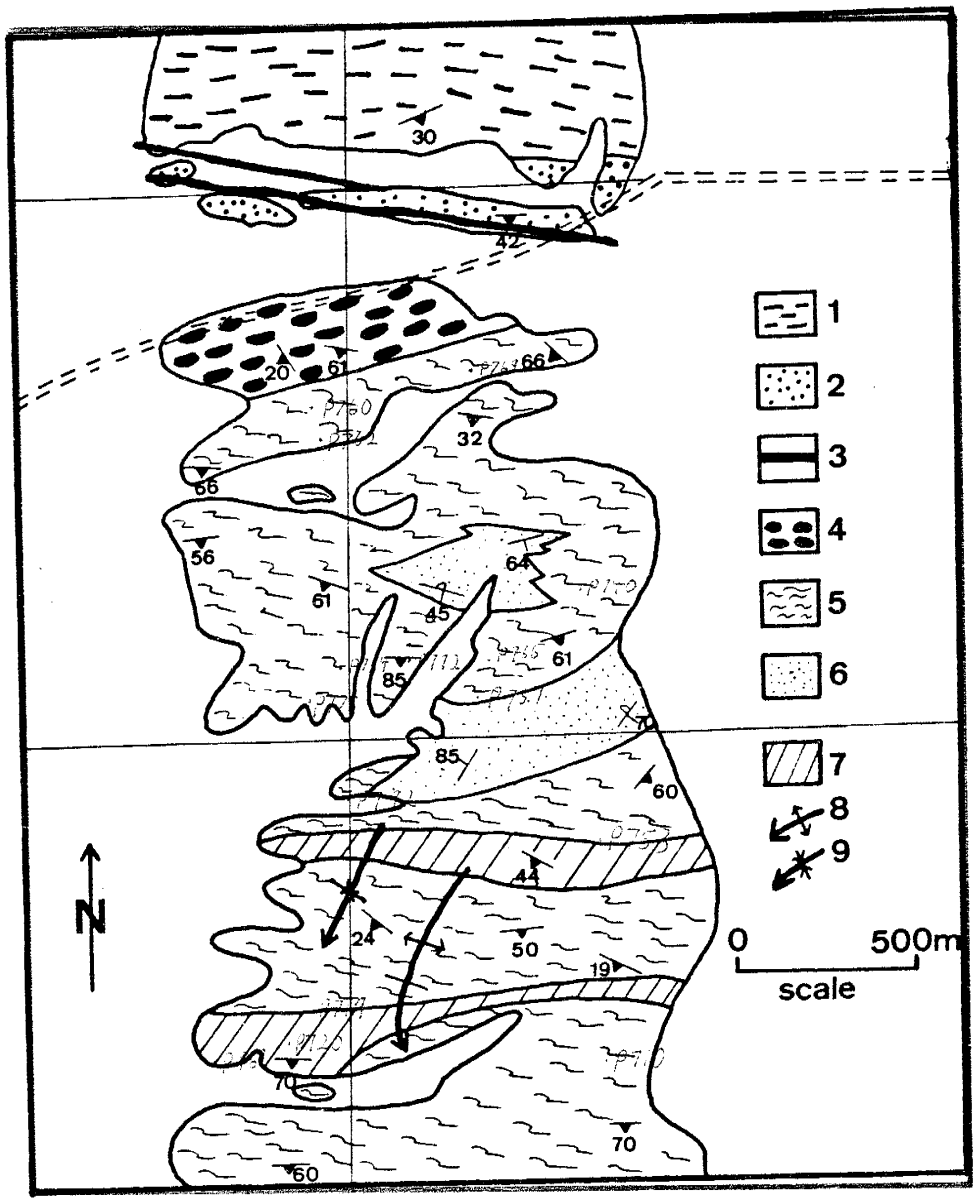

Figure A2. Generalized geologic map of the Pedernal section showing sample locations. Symbols as in figure 4.

APPENDIX B
PETROGRAPHIC DESCRIPTIONS

INTRODUCTION

This appendix gives the detailed petrography of each thin section studied. Sample localities are given in Appendix A. See the Field Studies section in the main text for a disscussion of the rocks in the field and their relationship to each other.

Plagioclase compositions are estimated by the Michel-Levy method using the high temperature curve of Jones and Bloss (1980). Since the extinction angles are low (less than 20 degrees), positive and negative angles need to be determined. In all cases, the {001} cleavage trace could not be identified, so the relief of plagioclase is compared to quartz when ever possible.

Some of the thin sections are stained to help identify K-feldspar crystals. For the sedimentary rocks, the elongation classes follow Folk (1965) and the sorting classification is based on Pettijohn, et al. (1972). The four mafic volcaniclastic rocks were point counted and techniques are discussed in Appendix I.

FELSIC VOLCANIC ROCKS

Pyroclastic Rocks

P710

The rock is brown, holocrystalline, and composed of 1 % plagioclase phenocrysts, traces of quartz phenocrysts, and the remainder a matrix of quartz, feldspars, muscovite, sericite, biotite, amphibole, chlorite, opaques, and epidote. The plagioclase phenocrysts are anhedral, equant to elongated, 0.4 to 1.6 mm in size, show albite and Carlsbad twins, are recrystallized to matrix minerals along grain boundaries, and are altered to sericite and muscovite within the crystals. The quartz phenocrysts are anhedral, elongated to equant, range from 0.4 to 1.0 mm in size, show undulatory extinction, and are altered and embayed by matrix minerals. The matrix is dominated by modally indistinguisalbe quartz-feldspar (53 % of the rock) which oocur as 0.03 to 0.3 mm sized crystals with some of the feldspar grains showing albite twins and some of the feldspar grains are altered to sericite and muscovite. The muscovite and sericite comprise 33 % of the rock and occur as idioblastic to xenoblastic flakes, 0.2 mm and less in size. Biotite (8 %) occurs as idioblastic to xenoblastic flakes, 0.03 to 0.08 mm in size and is red-brown in color. The chlorite (4 %) occurs as idioblastic to xenoblasitc crystals, 0.01 to 0.05 mm in size. The amphibole (trace) is xenoblastic to lipidioblastic, granoblastic, and 0.05 to 0.2 mm in size. Opaques (trace) are xenoblastic, granoblastic, and 0.01 to 0.25 mm in size. Epidote occurs as small (0.2 and less), anhedral, equant cyrstals in trace amounts. The quartz-feldspar, epidote, and opaques are xenoblastic and granoblastic while the chlorite, biotite, and muscovite-sericite are idioblastic to xenoblastic with the chlorite and biotite having lepidoblastic textures.

P714

The rock is brownish-green, holocrystalline and porphyritic with 2 % plagioclase phenocrysts, traces of quartz phenocrysts and a matrix of quartz, plagioclase, K-feldspar, biotite, epidote, opaques, chlorite, muscovite, sericite, garnet, and zircon. The plagioclase phenocrysts are subhedral to anhedral, equant to lath shaped, 0.3 to 1.6 mm in size, show albite and Carlsbad twins, have fractures, are replaced by matrix minerals along grain boundaries and within phenocrysts, and range in composition from An10 to An30. The quartz phenocrysts are equant to elongated, anhedral, 0.4 to 0.5 mm in size, and show undulatory extinction which has produced polycrystalline aggregates of 0.1 mm size crystals. The matrix minerals are 0.4 mm and less in size, anhedral to subhedral, and

equant to platy in shape. Some of the plagioclase in the matrix has albite and/or carlsbad twins and most are altered to muscovite and sericite. The biotite occurs mainly as crystal aggregates which are altered to muscovite, epidote, chlorite, and opaques. The quartz-feldspar and epidote are xenoblastic and granoblastic while the biotite, chlorite, and muscovite-sericite are idioblastic to xenoblastic and the biotite is lepidoblastic. The garnet (trace) is euhedral to subhedral and 0.1 to 0.2 mm in size. The zircon (trace) is equant to elongated, andhedral, and 0.05 mm and less in size.

P718

The rock is reddish-gray to greenish gray, holocrystalline, and porphyritic with 5 % plagioclase phenocrysts, and a matrix of quartz, feldspar, muscovite, sericite, opaques, biotite, epidote, chlorite, and carbonate. The plagioclase phenocrysts are subhedral to anhedral, lath shaped, 0.6 to 1.7 mm long and up to 0.6 mm wide in size, replaced by sericite and muscovite along grain boundaries, fractures, and within the crystals, have pericline and albite twins, and range in composition from An8 to An15. The quartz-feldspar in the matrix is anhedral, equant to slightly elongated, 0.05 to 0.9 mm in size, and some feldspar grains show albite and carlsbad twins and/or are altered to sericite, muscovite, epidote, and carbonate. Muscovite occurs as subhedral crystal aggregates up to 0.8 mm in size and as very fine-grained crystals with sericite that are less than 0.1 mm in size. The biotite occurs as brown and green colored, equant, subhedral flakes, 0.1 to 0.75 mm in size and many are altered to epidote, muscovite, sericite, chlorite, and opaques. The opaques are anhedral, equant, embayed, or skeletal, and normally 0.1 mm and less in size (one crystal is 1 mm). The chlorite and epidote occur as anhedral, equant flakes less than 0.1 mm in size. The epidote, opaques, and quartz-feldspar are xenoblastic and granoblastic while the chlorite and muscovite-sericite are idioblastic to xenoblastic. The carbonate and epidote are xenoblastic, granoblastic, and 0.05 to 0.5 mm in size.

P735

The rock is gray, holocrystalline, fine-grained, and composed of 54 % quartz, 10 % biotite, 9 % plagioclase, 5 % opaques, 1 % muscovite, 1 % epidote and 20 % muscovite-sericite. The quartz is anhedral, equant, has undulatory extinction, and ranges in size from less than 0.2 to 0.9 mm. Normally the quartz occurs in slightly elongated polycrystal aggregates of 10 to 25 crystals. The grain sizes in the polycrystal aggregates can be bimodal with 1 or 2 large crystals and the rest smaller crystals. Quartz also occurs as single crystals. The biotite is anhedral,

0.05 to 0.15 mm in size, and usually is associated with opaques and muscovite. Some biotite grains are replaced by epidote in the center of grains. The plagioclase is anhedral, equant to elongated, 0.1 to 1 mm in size, and altered to sericite. The opaques are anhedral, equant to embayed, 0.05 to 0.6 mm in size, occur as single crystals usually associated with chlorite and muscovite, and may have a hematite alteration around the crystal boundary. The muscovite occurs as clear, anhedral to subhedral, crystal aggregates with individual crystals 0.05 to 0.15 mm in size. The matrix is dominated by sericite-muscovite, with anhedral crystals less than 0.05 mm in size. Some matrix occurs as pacthes, 0.3 to 0.6 mm in size and may represent plagioclase replaced by sericite-muscovite. The quartz, plagioclase, opaques, and epidote are xenoblastic and granoblastic while the chlorite and muscovite-sericite are xenoblastic to idioblastic. The epidote is granoblastic, xenoblastic, and 0.02 to 0.35 mm in size.

P733

The rock is reddish-gray, holocrystalline and prophyritic with 2 % plagioclase phenocrysts and a matrix of quartz, plagioclase, K-feldspar, opaques, biotite, epidote-zoisite, chlorite, and garnet. The plagioclase phenocrysts are euhedral to anhedral, equant to lath shaped, 0.5 to 2.8 mm in size, altered, show albite and Carlsbad twins, and are about An10 in composition. About 17 % of the matrix is K-feldspar which occurs as equant, anhedral crystals, 0.03 to 0.55 mm in size. The quartz-plagioclase in the matrix comprise 72 % of the rock and occur as equant to slightly elongated, anhedral crystals, 0.1 mm and less in size. Some of the plagioclase in the matrix have albite twins. The opaques (7 % of the rock) are equnat, skelatal, or embayed, anhedral, and 0.1 mm and less in size. Biotite (trace) occurs as anhedral, skeletal shaped crystals, 0.1 mm in size, and are altered to chlorite and epidote. The chlorite (trace) and epidote-zoisite (trace) occur as equant, anhedral crystals, 0.1 mm and less in size. The quartz, feldspar, opaques, and epidote are xenoblastic and granoblastic while the biotite and chlorite are idioblastic to xenoblastic. The garnet is euhedral to subhedral, equant, and 0.02 to 0.07 mm in size.

Felsic Intrusive Rocks

P719

The rock is greenish-gray, holocrystalline, and composed of 50 % plagioclase phenocrysts, hypidiomorphic quartz (33 %), plagioclase (9 %), opaques (5 %), and chlorite (1 %), biotite (1 %), amphibole (1 %), epidote

(trace), and zircon (trace). The plagioclase phenocrysts are 0.7 to 3.2 mm in size, subhedral to anhedral, lath shaped, show albite twinning, have opaques inclusions, and are altered (20-100 %) to mosaics of sericite, epidote, chlorite, and opaques. The quartz and opaques are xenoblastic, granoblastic, and 0.05 to 0.65 mm in size. The matrix plagioclase is anhedral, equant to elongated, and altered (80-100 %) to mosaics of sericite, epidote, chlorite, and opaques. The biotite is green in color, subhedral to anhedral, equant to elongated, 0.03 to 1.0 mm in size, and some grains are altered to chlorite, epidote, and sericite. The chlorite, epidote, and amphibole (green-brown) are xenoblastic, generally granoblastic, and 0.03 to 0.3 mm in size. The zircon is subhedral, elongated, and 0.05 mm in size.

P768

The rock is reddish-gray, holocrystalline, glomeroporphyritic, and very fine-grained with 1 % plagioclase crystal clots, 1 % plagioclase phenocrysts, traces of opaque phenocrysts, and the remainder is matrix composed of quartz-feldspar (55 %), muscovite and sericite (20 %), epidote-zoisite (10 %), biotite (10 %), opaques (2 %), and hematite (trace). The crystal clots are composed of 2 to 4, subhedral to anhedral plagioclase phenocrysts with some clots having 1, euhedral opaque phenocryst. The plagioclase phenocrysts are anhedral to euhedral, equant to elongated, 0.4 to 1.8 mm in size, have carlsbad twins, and are altered to and embayed by matrix. The opaque phenocrysts are 0.4 to 0.55 mm in size and are euhedral to anhedral. The matrix minerals are euhedral to anhedral, equant to platy in shape, and generally less than 0.2 mm in size. The quartz, feldspar, epidote-zoisite, opaques and hematite in the matrix are xenoblastic and granoblastic while the muscovite, sericite, and biotite are idioblastic to xenoblastic and lepidoblastic. Both green and red-brown biotite occurs with the green colored variety dominating. There are quartz veins, 0.02 to 0.45 mm wide composed of quartz crystals that are xenoblastic, granoblastic, and 0.02 to 0.45 mm in size.

MAFIC VOLCANIC ROCKS

P740

The sample is dark green, holocrystalline, fine-grained, and composed of plagioclase phenocrysts (trace) and a matrix of quartz-feldspar (58 %), epidote (20 %), chlorite (15 %), amphibole (3 %), biotite (1 %), opaques (1 %), and muscovite (trace). The plagioclase phenocrysts

average 1.2 mm, are anhedral, elongated, show carlsbad and albite twins, and are highly altered to epidote, chlorite, biotite, and opaques. The quartz-feldspar are xenoblastic, granoblastic, and 0.05 mm and less in size. The epidote is xenoblastic, granoblastic, and 0.02 to 0.1 mm in size. The chlorite occurs as xenoblastic to idioblastic crystals that are 0.03 to 0.1 mm in size. Biotite is 0.05 to 0.4 mm in size, green in color, and xenoblastic to idioblastic. Both the chlorite and biotite commonly occur in crystal aggregates containing both chlorite and biotite. The opaques and quartz are xenoblastic, granoblastic, and 0.02 to 0.4 mm in size. The muscovite is 0.05 to 0.4 mm and xenoblastic.

P765

The sample is dark green, holocrystalline, fine-grained, and composed of quartz-feldspar (42 %), amphibole (20 %), epidote (18 %), chlorite (8 %), opaques (7 %) and biotite (trace). The quartz-feldspar, epidote, chlorite, amphibole, and biotite occur as small (0.1 mm and less in size) crystals that are xenoblastic to idioblastic, and generally granoblastic. The opaques are anhedral to euhedral, skeletal, embayed, or have corroded crystal boundaries, some have hematitic alteration halos, and are 0.02 to 0.6 mm in size.

P774

The sample is dark green, holocrystalline, fine-grained, and composed of plagioclase phenocrysts (trace) and a matrix of amphibole (22 %), epidote (20 %), biotite (27 %), quartz-feldspar (20 %), chlorite (5 %), muscovite (trace), zoisite (trace), and opaques (trace). The plagioclase phenocrysts are 1.0 to 1.6 mm in length and 0.5 to 0.7 mm wide, elongated, anhedral, may show carlsbad twins, and are highly altered (70-90 %) to mosaics of epidote, chlorite, and biotite. The epidote and zoisite occur as xenoblastic crystals that are 0.05 to 0.2 mm in size and have granoblastic texture. The bioite is 0.05 to 0.1 mm in size, idioblastic to xenoblastic, and some have an oxidized halo around them. The chlorite and muscovite are 0.05 to 0.1 mm in size and idioblastic to xenoblastic. The quartz-feldspar and opaques are xenoblastic, granoblastic, and 0.05 to 0.2 mm in size.

P792

The sample is dark green, holocrystalline, fine-grained, and composed of quartz-feldspar (30 %), epidote-zoisite (20 %), amphibole (10 %), chlorite (10 %), sericite (5 %), carbonates (3 %), hematite (2 %), opaques (1 %), and biotite (trace). The plagioclase is 0.05 to 1 mm in size, equant to elongated, anhedral, and altered. The quartz-

feldspar are 0.05 to 0.2 mm in size, xenoblastic and granoblastic. Quetz and feldspar also occur in a vein as 0.5 to 1.2 mm crystals that are xenoblastic, have polygonal, interlobate, or sutured grain counderies, and show undulatory extinctions. The feldspar crystals are altered to epidote, chlorite, opaques, and other matrix minerals and some crystals show carlsbad twins. The epidote is 0.05 to 0.2 mm in size, xenoblastic, and granoblastic. The chlorite occurs as 0.1 mm, idioblastic to xenoblastic crystals. The quartz is xenoblastic, granoblastic, show undulatory extinction, and are 0.1 to 0.5 mm in size. The sericite is xenoblastic and 0.05 and less in size. The opaques occur as anhedral crystals that are 0.02 to 0.07 mm in size and are altered to a cryptocrystalline material and as xenoblastic crystals in the matrix that are 0.05 to 0.1 mm in size. The carbonate is xenoblastic, granoblastic, and 0.1 mm in size. Biotite is 0.05 to 0.1 mm in size and idioblastic to xenoblastic. The hematite is xenoblastic, idioblastic to granoblastic, and 0.02 to 0.05 mm in size.

VOLCANICLASTIC ROCKS

Manzano Section - Felsic Rocks

M100

The rock is a gray to greenish gray, holocrystalline, graded bedded rock and the thin section contains two domains: one is fine-grained and the other is coarse-grained. The fine-grained domain is composed of quartz grains (5 %) and a matrix of muscovite-sericite (50 %), quartz-feldspar (43 %), actinolite (10 %), and traces of hematite. The quartz grains are moderately sorted, very elongated to very equant, angular to subround, 0.1 to 0.2 mm in size, equant, and show moderate to extreme undulatroy extinction. The micas are idioblastic to xenoblastic and 0.05 to 0.3 mm in size. The quartz-feldspar are xenoblastic, granoblastic, and 0.05 to 0.1 mm in size. The actinolite is xenoblastic, nemoblastic, and 0.05 to 0.3 mm in size. The hematite is anhedral, 0.05 mm in size, and dark red in color.

The coarse-grained domain is very poorly sorted and composed of very elongated to very equant plagioclase grains (15 %), quartz grains (12 %), and a recrystallized matrix of quartz-feldspar (42 %), epidote (5 %), actinolite (5 %), green biotite (trace), chlorite (trace), hematite (trace), and opaques (trace). The quartz grains are 0.2 to 1.2 mm in size, angular to subangular, show moderate to extreme undulatory extinction which in some cases has produced polycrystalline grains, and have corroded grain boundaries that have been recrystallized to matrix. The

plagioclase grains show pericline, albite, and carlsbad twins, are angular to subround, 0.2 to 2.1 mm in size, are equant to elongated, and are altered (80-95 %) to mosaics of muscovite-sericite, epidote, and opaques. Some cores of feldspar grains are altered more than the rims. The quartz-feldspar and epidote in the matrix are xenoblastic, granoblastic, and 0.05 to 0.1 mm in size. The actinolite is xenoblastic, elongated, and 0.05 to 0.1 mm in size. The biotite is idioblastic to xenoblastic, and 0.05 to 0.1 mm in size. Chlorite occurs as polycrystalline aggregates associated with opaques and is xenoblastic to idioblastic and averages 0.1 mm in size. The opaques are xenoblastic, elongated, 0.05 to 0.1 mm in size, and are associated with chlorite. The hematite is xenoblastic, granoblastic, and 0.05 mm in size.

M734

The sample is greenish-gray, holocrystalline, fine-grained, very poorly sorted, and composed of very elongated to very equant grains of plagioclase (60 %), quartz (10 %), chert (trace), and a recrystallized matrix of quartz-feldspar (5 %), sericite (5 %), chlorite (1 %), brown biotite (trace), muscovite (trace), and opaques (trace). The plagioclase grains are 0.2 to 4.0 mm in size, show carlsbad, albite, and pericline twins, are subangular to round, equant to elongated, and altered (20-100 %) to sericite, muscovite, and opaques. The quartz grains are 0.1 to 2.5 mm in size, with one 4.7 mm grain, equant to elongated, angular to round, and altered along grain boundaries to and embayed by matrix. The quartz grains show moderate to extreme undulatory extinction and deformation may have produced polycrystalline grains. One grain has been fractured with matrix occurring between the fragments. The chert grains are 0.8 mm in size, angular, equant, and altered to matrix along the grain boundaries. The quartz-feldspar and sericite are less than 0.05 mm in size. The chlorite occurs as xenoblastic to idioblastic crystals, 0.05 to 0.2 mm in size and usually associated with opaques. The opaques are xenoblastic, granoblastic, and 0.05 to 0.4 mm in size. The biotite and muscovite are xenoblastic and 0.05 to 0.2 mm in size. The epidote is xenoblastic, granoblastic, and 0.05 to 0.1 mm in size.

BOS-3

The rock is holocrystalline, fine-grained, and composed of feldspar grains (50 %), quartz grains (8 %), and a matrix of quartz-feldspar (15 %), muscovite (10 %), biotite (10 %), sericite (5 %), opaques (trace), chlorite (trace), epidote (trace), and garnet (trace). The feldspar grains appear to be dominated by plagioclase and are 0.4 to 2 mm in size, angular to subround, very equant to very elongated, show carlsbad, albite, and pericline twins, and

are replaced (40-100 %) by sericite, muscovite, quartz, and other minerals. The quartz grains are 0.2 to 2.2 mm in size, angular to round, very equant to very elongated, and embayed and corroded along grain boundaries by matrix. All quartz grains show undulatory extinction and deformation may have produced the polycrystalline grains from monocrystalline grains. The quartz-feldspar, opaques, and epidote are xenoblastic, granoblastic, and 0.05 to 0.1 mm in size. The micas are xenoblastic to idioblastic, 0.05 to 0.3 mm in size, and some of the biotite is chloritized. The sericite is 0.05 mm and less in size. The garnet is 0.15 mm in size, equant, and subhedral.

Pedernal Section - Mafic Rocks

P10

The rock is a dark green, holocrystalline breccia composed of unstable lithic fragments (40 %) and a matrix of epidote (23.3 %), chlorite (13.7 %), amphibole (12.1 %), quartz-feldspar (1 %), epidote (trace), opaques (trace), carbonate (trace), and metamorphic plagioclase (trace). The unstable lithic clasts are 1 to 10 mm wide and 2 to 25 mm long, equant to elongated, and recrystallized to mosaics of chlorite, epidote, amphibole, quartz-feldspar, muscovite, sericite, and opaques. The minerals are 0.05 to 0.5 mm in size, xenoblastic to idioblastic, and generally granoblastic, though the micas in some fragments have lepidoblastic textures. The matrix minerals are xenoblastic to idioblastic, generally granoblastic with some chlorite having lepidoblastic texture, and are 0.05 to 0.7 mm in size. Matrix epidote is rarely twinned. Carbonate occurs as 0.1 to 0.9 mm sized, equant crystals with polygonal grain boundaries replacing quartzose lithic grains and as single, equnat crystals, 0.05 to 0.1 mm in size, in the matrix. There are several epidote veins with xenoblatic, granoblastic grains up to 1.6 mm in size.

P86

The rock is a dark green, holocrystalline breccia composed of subangular to round, equant to elongated, unstable lithic (38 %), quartzose lithic (15 %) grains, and plagioclase grains (trace) and a matrix of amphibole (26.2 %), quartz-feldspar (11 %), chlorite (3.8 %), epidote (3.5 %), opaques (2 %), and biotite (trace). The quartzose lithic clasts are equant to elongated, 0.3 to 3.7 mm wide and 0.3 to 4.3 mm long, have inclusions of matrix minerals, and have corroded grain boundaries replaced by matrix minerals. The quartz crystals within the quartzose clasts are xenoblastic, granoblastic, 0.05 to 1.4 mm in size, show undulatory extinction, and have polygonal, interlobate, or sutured grain boundaries. The unstable lithic grains have

been recrystallized to mosaics of amphibole, chlorite, epidote, quartz-feldspar, muscovite-sericite, and opaques. The minerlas are 0.05 to 0.6 mm in size, xenoblastic to idioblastic, and generally are granoblastic, but micas in some clasts have lepidoblastic textures. The plagioclase grains are anhedral, elongated, show carlsbad twins, are 0.15 to 0.9 mm in size, and are replaced by matrix alonga grain boundaries. The matrix minerals are generally granoblastic, xenoblastic to idioblastic, and 0.05 to 0.7 mm in size. Some of the opaque minerals are embayed to skeletal and have cryptocrystalline alteration halos, 0.05 to 0.1 mm wide. There is one quartz-epidote vein that is up to 0.2 mm thick.

P743

The rock is a dark green holocrystalline breccia composed of subangular to subround clasts (27 %) and a matrix of amphibole (41 %), quartz-feldspar (12 %), muscovite-sericite (10 %), epidote (4.8 %), chlorite (4 %), biotite (1 %), and opaques (trace). The clasts range in size from 0.5 mm wide by 0.5 mm long to 1.5 mm wide and 6 mm long, are equant to elongated, and can be divided into unstable lithic and quartzose lithic varieties. The quartzose clasts are subangular, 0.2 to 1 mm wide and 0.5 to 2 mm long, have inclusions of matrix minerals, and have corroded grain bounderies that have been recrystallized to matrix minerals. The quartz crystals are 0.05 to 0.4 mm in size, xenoblastic, granoblastic, show undulatory extinction, and have polygonal, interlobate, or sutured grain boundaries. The unstable lithic grains have been recrystallized to mosaics of amphibole, epidote, chlorite, quartz-feldspar, muscovite-sericite, and opaques. The minerals are 0.05 to 0.5 mm in size, xenoblastic to idioblastic, and generally are granoblastic though micas in some clasts have lepidoblastic texture. The matrix minerals are xenoblastic to idioblastic, generally granoblastic, and 0.05 to 0.4 mm in size.

P744

The rock is a dark green, holocrystalline breccia composed of angular to round clasts (67 %) and a matrix of quartz-feldspar (13 %), epidote (9 %), amphibole (6 %), chlorite (2 %), muscovite-sericite (2 %), and opaques (trace). The clasts are 2 to 10 mm in size, equant to elongated, and include quartzose and unstable lithic varieties. The quartzose lithic clasts are equant to elongated, subangular to round, 0.6 to 0.9 mm wide and 0.6 to 1.3 mm long, have corroded clast boundaries that have recrystallized to matrix minerals, and have inclusions of matrix minerals. The quartzose lithic clasts are composed of xenoblastic, granoblastic quartz crystals that are 0.05 to 0.5 mm in size and have polygonal to interlobate grain

boundaries. The unstalbe lithic clasts have been recrystallized to mosaics of amphibole, epidote, chlorite, quartz-feldspar, muscovite, sericite, and opaques. The minerals are 0.05 to 0.5 mm in size, xenoblastic to idioblastic and generally granoblastic though micas in some clasts have lepidoblastic textures. The matrix minerals are 0.05 to 0.3 mm in size, are xenoblastic to idioblastic and generally are granoblastic. Some of the opaques have a cryptocrystalline alteration halo.

SEDIMENTARY ROCKS

Manzano Section

M601

The rock is greenish-gray, coarse-grained, and holocrystalline. The sample is very poorly sorted with very elongated to very equant, angular to subround epiclastic grains of quartz (20 %) and feldspar (20 %) set in a recrystallized matrix of quartz-feldspar (50 %), biotite (2 %), opaques (1 %), actinolite (trace), epidote-zoisite (trace), muscovite (trace), hematite (trace), and sericite (trace). The quartz grains are 0.2 to 2.1 mm in size, show moderate to extreme undulatory extinction which in some cases has produced polycrystalline grains, have inclusions of biotite and chlorite, and have corroded grain boundaries that are recrystallized to matrix. Some quartz grains are embayed by matrix. The feldspar grains are dominately plagioclase (An) and are 0.5 to 2.6 mm in size, have albite and carlsbad twins, are highly altered (50-95 %) to very fine-grained mosaics of muscovite, sericite, opaques, and other minerals, and in many cases, grade into the matrix with no distinct grain boundaries. The quartz-feldspar in the matrix are granoblastic, xenoblastic, and 0.05 to 0.1 mm in size. The opaques are xenoblastic, granoblastic, and 0.05 to 0.1 mm in size. The micas are idioblastic to xenoblastic, lepidoblastic, and 0.05 to 0.2 mm in size. The epidote occurs as 0.3 mm, granoblastic and xenoblastic crystals. The hematite, actinolite, sericite, and zoisite are xenoblastic and 0.05 mm and less in size.

M732

The rock is dark gray, holocrystalline, and medium-grained. The sample is very poorly sorted with very elongated to very equant, angular to subround epiclastic grains of quartz (40 %), feldspar (10 %), and chert (trace), set in a recrystallized matrix of quartz-feldspar (39 %), opaques (8 %), muscovite (1 %), chlorite (1 %), carbonate (trace), and epidote (trace). The quartz grains

are 0.1 to 1.0 mm in size, show undulatory extinction which in some cases has produced polycrystalline grains, and have corroded grain bounderies that have been recrystallized to matrix. The feldspar grains are 0.2 to 0.4 mm in size and are altered (50-80 %) to sericite, opaques, and other matrix minerals. The chert grains are 0.4 to 0.7 mm in size and composed of quartz crystals 0.03 mm and less in size with interlobate crystal boundaries. The chert grains are altered to matrix along the grain boundary. The quartz-feldspar in the matrix are 0.05 to 0.2 mm in size, xenoblastic, and granoblastic. The opaques are xenoblastic, granoblastic, and 0.05 to 0.3 mm in size. The micas are idioblastic to xenoblastic, lepidoblastic, and 0.05 to 0.2 mm in size, with some muscovite altered to chlorite. Epidote occurs as small (0.05-0.2 mm), xenoblastic, granoblastic crystals. The carbonate is 0.09 mm in size, xenoblastic, and replaces muscovite and quartz-feldspar matrix.

M753

The rock is tan, holocrystalline, very fine-grained, and composed of quartz-feldspar (70 %), muscovite (15 %), K-feldspar (9 %), biotite (5 %), opaques (trace), zircon (trace), and epidote (trace). The quartz-feldspar is 0.05 to 0.2 mm in size, xenoblastic, and granoblastic. The muscovite is idioblastic to xenoblastic, lepidoblastic, and 0.05 to 0.5 mm in size. K-feldspar occurs as xenoblastic, granoblastic crystals that are 0.05 to 0.1 mm in size. Biotite is brown in color, 0.05 to 0.3 mm in size, and idioblastic to xenoblastic. The opaques are xenoblastic, granoblastic, and 0.05 to 0.7 mm in size. The zircon is subround, elongated, and 0.05 mm in size. The epidote is 0.05 to 0.07 mm in size, xenoblastic and granoblastic.

BOS-1

The rock is holocrystalline, very fine-grsined and composed of quartz-feldspar (68 %), muscovite (20 %), opaques (7 %), chlorite (5 %), and hematite (trace). The quartz-feldspar are equant to elongated, xenoblastic, 0.05 to 0.4 mm in size, and altered to matrix. The muscovite occurs as idioblastic to xenoblastic, lepidoblastic crystals that are 0.05 to 0.3 mm in size. The opaques are euhedral to anhedral, equant to very elongsted, and 0.05 to 0.3 mm in size. The chlorite is xenoblastic to idioblastic and 0.05 to 0.1 mm in size. The hematite is 0.05 mm in size, xenoblastic, and is an alteration product.

BOS-6

The sample is holocrystalline and coarsee-grained. The sample is very poorly sorted and has very elongated to very equant, subangular to rounded epiclastic grains of

quartz (10 %) and feldspar (trace) set in a recrystallized matrix of quartz-feldspar (66 %), muscovite (7 %), opaques (3 %), actinolite (2 %), chlorite (1 %), epidote (trace), zircon (trace), and hematite (trace). The quartz grains are elongated parrallel to the foliation or equant, 0.5 to 0.9 mm long and 0.3 to 0.7 mm wide, monocrystalline to polycrystalline, and they have corroded grain boundaries that are recrystallized to matrix. Some grains are embayed by matrix. All the quartz grains show undulatory extinction which in some cases has produced polycrystalline grains. The feldspar grains are 0.5 mm is size and altered to sericite, epidote, and chlorite. The quartz-feldspar in the matrix are xenoblastic, granoblastic, 0.05 to 0.5 mm in size, have polygonal to interlobate crystal boundaries, and is dominated by quartz with lesser feldspar that is normally altered to sericite. The muscovite is 0.05 to 0.3 mm in size, idioblastic to xenoblastic, and lepidoblastic. The actinolite is xenoblastic and 0.05 to 0.3 mm in size. The zircon is round, equant to elongated, and 0.06 mm and less in size. The other matrix minerals are xenoblastic (some chlorite is idioblastic), generally granoblastic, and 0.05 to 0.6 mm in size.

Pedernal-Northern Boundary Zone Rocks

P745

The rock is a green with red spots, holocrystalline, very fine-grained chlorite-epidote-quartz schist containing quartz (35 %), chlorite (30 %), epidote (30 %), red-brown biotite (5 %), and traces of opaques. Quartz crystals are xenoblastic, equant to elongated parrellel to the foliation, 0.02 to 0.35 mm in size, and have polygonal to interlobate grain boundaries. The chlorite is idioblastic to xenoblastic, lepidoblastic, 0.02 to 0.05 mm in size, and is in part, intergrown with biotite. Epidote is xenoblastic, granoblastic, rarely twinned, and 0.02 to 0.17 mm in size. The biotite is idioblastic to xenoblastic, lepidoblastic, 0.02 to 0.05 mm in size, and is usually intergrown with chlorite. The opaques occur as large 0.5 to 1 mm grains that are equant to embayed, xenoblastic, and granoblastic, or as small (<0.2 mm) crystals concentrated in red spots (in hand speciemen). The opaques are dominated by hematite.

P746

The rock is a dark brown, holocrystalline, very fine-grained epidote-biotite-quartz schist composed of quartz (40 %), red-brown biotite (30 %), epidote (25 %), opaques (5 %), and chlorite (1 %). Quartz crystals are

xenoblastic, equant to elongated parrellel to the foliation, and 0.02 to 0.4 mm in size with polygonal to interlobate grain boundaries. Biotite crystals are idioblastic to xenoblastic, lepidoblastic, and 0.03 to 0.15 mm in size. The epidote is xenoblastic, granoblastic, and 0.02 to 0.2 mm in size. Opaques are xenoblastic and 0.02 to 0.35 mm in size. The chlorite occurs as xenoblastic to idiblastic crystals, 0.02 to 0.35 mm in size, and intergrown with biotite.

P748

The rock is a dark green, holocrystalline, very fine-grained, brecciated, biotite-chlorite-epidote-quartz schist composed of 55 % quartz, 15 % epidote-zoisite, 10 % chlorite, 10 % biotite, 8 % opaques, and 2 % sericite. The quartz is xenoblastic, equant to elongated parellel to the foliation, 0.02 to 0.4 mm in size, and has polygonal, interlobate, or sutured grain boundaries. The epidote-zoisite is xenoblastic, granoblastic, and 0.02 to 0.1 mm in size. The biotite and chlorite are idioblastic to xenoblastic, lepidoblastic, and 0.04 to 0.8 mm in size. The opaques are xenoblastic, equant to elongated, and 0.03 to 0.3 mm in size and appear to be dominated by hematite. The sericite occurs as small (<0.05 mm) crystals in elongated aggrgates, 0.05 to 0.5 mm in size. The brecciated fragments are subangular, elongated, rotated, 2 to 7 mm long and 1 to 3 mm wide, and generally have concnetrations of opaques minerals along the fragment boundaries. The brecciation has rotated the foliation in the fragments and this is evidence the brecciation is a post-metamorphic event.

P749

The rock is a bluish-gray, holocrystalline, very fine-grained biotie-muscovite-quartz schist compsed of quartz (43 %), muscovite (35 %), green biotite (20 %), and opaques (2 %). The quartz is xenoblastic, equant to elongated parrellel to the foliation, may show undulatory extinction, is 0.05 to 1 mm in size, and has polygonal to interlobate grain boundaries. The muscovite is idioblastic to xenoblastic, lepidoblastic, and up to 4 mm in size. The biotite is idioblastic, lepidoblastic, and 0.1 to 0.5 mm in size. The micas are bent by microscopic folds. The opaques are xenoblastic, equant, embayed, or elongated, and 0.05 to 1.8 mm in size.

P-88

The rock is a grayish-green, holocrystalline, very fine-grained, epidote-chlorite quartzite composed of quartz (90 %), chlorite (5 %), epidote (4 %), and traces of opaques, zircon, carbonate, and tourmaline (?). Quartz crystals are 0.02 to 0.8 mm in size, xenoblastic, equant to elongated parrellel to the foliation, and have polygonal, interlobate, or sutured grain boundaries. The chlorite is idioblastic to xenoblastic, lepidoblastic, and 0.05 to 0.2 mm in size. Epidote occurs as xenoblastic, granoblastic crystals, 0.03 to 0.15 mm in size that are dominately concentrated in bands, 0.5 mm thick that are parrellel to the foliation. The zircon, tourmaline, carbonate, and opaques occur as small (0.02 to 0.4 mm), anhedral, equant to elongated crystals. The opaques appear to be dominated by hematite.

Quartzite
P-84

The quartzite is gray to white, holocrystalline, medium grained, and is composed of 97 % quartz, 1 % muscovite, 1 % opaques, and traces of biotite, zircon, and tourmaline. The quartz crystals are seriate, have polygonal to interlobate grain boundaries, moderate to extreme undulatory extinction, and some grains show motar textures. Most grains are equant to elongated and 0.1 to 0.9 mm in size, but in the areas that exhibt cataclastic tecture, grain size is reduced to less than 0.05 mm with some larger grains having survived granulation. The muscovite is suhedral to anhedral, less than 0.05 to 6 mm long, may be bent, and occur as single grains alone quartz grain boundaries and within quartz grains and as crystal aggregates along quartz grain boundaries. The muscovite and elongated quartz define the foliation. The opaques are euhedral and equant to anhedral and elongated and 0.05 to 0.15 mm in size. They occur as single crystal and as crystal trains parrellel to the foliation. Zircon occurs as single, equant, anhedral crystals, 0.1 mm in size. A red-brown alteration product surrounds some of the zircon grains. The biotite is pleochroic, light green to green, anhedral, equant, and 0.05 mm in size. Tourmaline occurs as small (0.1 mm), single grains that are equant, anhedral, and clear to slightly pleochroic.

POST-TECTONIC SYENITE DIKE
P747

The syenite is brick red, holocrystalline, medium grained, and composed of 85 % alkali feldspar that is highly altered (40-90%) to clay, 10 % hypidiomorphic quartz, and 5 % hematite. The feldspar are lath shaped, anhedral to subhedral, 0.01 to 1 mm in length, show

periclase and Carlsbad twins, and have a trachytic texture. The quartz has straight, sharp to gradational boundaries with the feldspar crystals. Some quartz crystals contain abundant inclusions (<0.01 mm) near boundaries with feldspar crystal. There is a trace of a subhedral, colorless mineral with high relief and birefringence that occurs as small (0.30 mm), single crystals.

APPENDIX C

SAMPLING AND SAMPLE PREPARATION

Over 100 samples were collected from the Manzano succession and more than 200 from the Pedernal succession. Outcrops that lacked obvious alteration and/or veining were selected for sampling, but exceptions arose due to lack of unaltered outcrops for some units. Sampling was done to include all rock types and be representative of their relative abundances. Generally, samples were collected in triplicate: hand sample, geochemical sample, and thin section sample. Single samples were collected in some cases to show textural variation of units along strike or if analysis was not going to be preformed on them.

In the field, geochemical samples were broken down to 4 cm pieces. Geochemical samples selected for analysis were ground into sand size material using a jaw-crusher and a rotary-mill at New Mexico Tech. Both machines have alumina grinding plates to help reduce contamination. Final grinding into a powder was preformed using an automatic agate motar and pestle. A split of each sample was than taken for both INAA and XRF.

APPENDIX D

X-RAY FLOURESCENCE ANALYSIS

INTRODUCTION

Major elements and some trace elements are analyzed for by X-ray flourescences. Analyses are preformed on a Rigaku 3064 XRF Spectrometer with a rhodeum tube. A PDP 1123 computer controls the spectrometer and reduces the raw data. The spectrometer is located at and run by the New Mexico Bureau of Mines and Mineral Resources (NMBMMR).

MAJOR ELEMENTS

A fused disc method based on Norrish and Chappel (1967) and Norrish and Hutton (1969) was used for the major elements. Spectroflux type 105, a powder lithium-borate glass, was used as the flux. Some samples and standards were analyzed several times as a check on analytical procedures and machine calibration. Instrument settings are given in table D1.

A variety of USGS, international, and inhouse standards were run to calibrate the machine. Linear calibration curves were calculated and placed into the computer program that controlled the major element analyses.

Data for major elements was collected in two different

TABLE D1. SETTINGS FOR XRF.

Major Elements

	Absor	Time	Crystal	Angle	Order	Window	Slit	Filter	Step
Fe2O3T	1	40	LiF3	57.52	1st	1-1	1s	out	1/100
MnO	1	20	LiF3	62.93	1st	1-1	3s	out	1/100
TiO2	1	20	LiF3	86.14	1st	2-1	3s	out	1/100
CaO	1	20	LiF3	113.08	1st	2-1	3s	out	1/100
K2O	1	20	LiF3	136.67	1st	1-1	3s	out	1/100
P2O5	1	40	GE	140.96	1st	2-2	3s	out	1/100
SiO2	1	40	PET	109.00	1st	1-1	3s	out	1/100
Al2O3	1	80	PET	144.76	1st	1-1	3s	out	1/100
MgO	1	200	TAP	45.19	1st	1-3	3s	out	1/100
Na2O	1	200	TAP	55.10	1st	2-2	3s	out	1/100

Kv = 35 Detector was a flow proportional counter
mA =75

Time is the time counts were collected, in seconds.
LiF3 = Lithium floride 200
GE = Germanium 111
PET = Pentaerythitol 002
TAP = Thalium Acid
Angle is two-theta in degrees
Order is the analytical peak which is the K-alpha peak.

runs. MA-N and NMR-1 were analyzed several times to check precision and accuracy of analyses: MA-N monitored the first run and NMR-1 the second run. MA-N is a French granite standard (GIT-IWG) and NMR-1 is an inhouse rhyolite standard for NMBMMR. Analyses, precision and accuracy are given in tables D2 (MA-N) and D3 (NMR-1).

The precision for most elements in MA-N was good, except for TiO2 and MnO. The TiO2 concentration in MA-N (0.01 wt. %) is the same as the detectability limit of the machine (0.01 wt. %) and precision and accuracy for TiO2 would not be expected to be good at this concentration level. MnO and MgO had poor accuracy and the rest of the elements (other than TiO2) had good accuracy.

In NMR-1, the precision for most elements was good, except for MnO (66.3 %). The accuracy was good in NMR-1, except for MnO and Na2O. The precision and accuracy is better for some elements and worse for other elements in NMR-1 relative to MA-N. MnO had poor precision and accuracy in both runs. MgO and Na2O had similar precision in both runs while the accuracy was better for Na2O in run one (MA-N) while the accuracy was better for MgO in run two (NMR-1).

In addition to NMR-1, P765 was run in triplicate in the second run. The analyses and statistics for P765 are given in table D4. The precision for all elements was good in P765 and in fact better for all but K2O and P2O5 in P765 relative to NMR-1. The better precision in P765 in

TABLE D2. ANALYSIS AND STATISTICS OF MA-N.

SiO2	67.1	67.2	67.2	67.1	67.1	67.1
TiO2	0.0	0.0	0.0	0.0	0.0	0.0
Al2O3	18.0	18.0	18.1	18.0	18.0	18.0
Fe2O3-T	0.50	0.50	0.50	0.50	0.50	0.51
MnO	0.037	0.036	0.032	0.039	0.036	0.031
MgO	0.12	0.13	0.13	0.15	0.12	0.12
CaO	0.60	0.60	0.60	0.60	0.60	0.59
Na2O	6.13	6.05	5.88	6.11	6.17	5.97
K2O	3.20	3.20	3.21	3.20	3.20	3.19
P2O5	1.40	1.40	1.41	1.41	1.41	1.40
LOI	3.08	3.08	3.08	3.08	3.08	3.08
TOTAL	100.167	100.196	100.142	100.189	100.216	99.991

					Mean	St. Dev.
SiO2	67.2	67.3	67.2	67.1	67.16	0.0711
TiO2	0.0	0.0	0.0	0.0	0.0	---
Al2O3	18.0	18.0	18.0	18.0	18.01	0.0334
Fe2O3-T	0.50	0.50	0.49	0.50	0.500	0.00500
MnO	0.034	0.035	0.036	0.034	0.035	0.0247
MgO	0.13	0.12	0.13	0.13	0.128	0.00972
CaO	0.60	0.60	0.60	0.59	0.598	0.00346
Na2O	6.06	5.99	6.00	5.96	6.032	0.0905
K2O	3.18	3.20	3.20	3.19	3.197	0.00837
P2O5	1.42	1.41	1.40	1.40	1.406	0.0428
LOI	3.08	3.08	3.08	3.08	3.08	
TOTAL	100.204	100.235	100.136	99.984	100.146	

	Prec. %	True Value	Accracy %
SiO2	0.106	66.74	0.839
TiO2	---	0.01	---
Al2O3	0.185	17.66	2.49
Fe2O3-T	1.00	0.47	8.51
MnO	70.7	0.04	22.5
MgO	7.59	0.04	275
CaO	0.579	5.85	1.69
Na2O	1.50	3.19	5.47
K2O	0.262	1.08	0.627
P2O5	3.04	1.39	2.16

Fe2O3-T recalculated from FeO and Fe2O3
Analyses were recalculated absorbed water free.

TABLE D3. ANALYSIS AND STATISTICS OF NMR-1.

SiO2	71.8	71.5	71.9	71.6	71.6	71.7
TiO2	0.45	0.45	0.45	0.44	0.44	0.45
Al2O3	14.2	14.1	14.3	14.1	14.1	14.1
Fe2O3-T	2.58	2.58	2.59	2.57	2.58	2.56
MnO	0.067	0.059	0.070	0.061	0.058	0.060
MgO	0.42	0.44	0.46	0.43	0.39	0.40
CaO	1.59	1.59	1.59	1.59	1.59	1.58
Na2O	3.62	3.61	3.69	3.70	3.62	3.63
K2O	4.75	4.73	4.75	4.73	4.71	4.70
P2O5	0.12	0.12	0.12	0.12	0.12	0.12
LOI	0.628	0.628	0.628	0.628	0.628	0.628
TOTAL	100.23	99.81	100.55	99.97	99.84	99.93

	Mean	St. Dev.	Precision %	True Value	Accuracy %
SiO2	71.7	0.148	0.207	72.42	1.27
TiO2	0.45	0.00775	1.72	0.43	4.56
Al2O3	14.2	0.100	0.704	14.30	1.40
Fe2O3-T	2.58	0.0110	0.425	2.63	2.66
MnO	0.063	0.0418	66.3	0.053	32.1
MgO	0.42	0.0261	6.21	0.42	9.52
CaO	1.59	0.00447	0.281	1.59	0.629
Na2O	3.65	0.0397	1.09	3.16	16.5
K2O	4.73	0.0205	0.433	4.80	2.08
P2O5	0.12	0.0	0.0	0.13	8.33
LOI	0.628				
TOTAL	100.13				

Analyses were recalculated absorbed water free.
Iron analyzed as Fe2O3-T.
The assumed true value is from M. Tuff
(personal communication, 1985).

TABLE D4. ANALYSIS AND STATISTICS FOR P765.

				Mean	St. Dev.	Precision
SiO2	54.01	54.04	53.91	54.00	0.0707	0.131
TiO2	1.62	1.61	1.60	1.61	0.0100	0.621
Al2O3	13.85	13.90	13.86	13.87	0.0265	0.191
Fe2O3-T	15.06	15.05	15.06	15.06	0.00707	0.0470
MgO	3.82	3.87	3.85	3.85	0.0255	0.662
CaO	6.76	6.76	6.73	6.75	0.0173	0.257
Na2O	2.04	2.10	2.03	2.06	0.0381	1.85
K2O	0.53	0.54	0.54	0.54	0.00707	1.31
MnO	0.25	0.24	0.25	0.25	0.00707	2.83
P2O5	0.32	0.32	0.32	0.32	0.0	0.0
LOI	2.61	2.61	2.61			
Total	100.87	101.04	100.76			

Analysis recalculated absorbed water free.
Iron analyzed as Fe2O3-T.

comparision to NMR-1 may be related to one or more of four possibilities. One, some of the elements in P765 have higher concentrations than in NMR-1 and the analysis of these elements would be more precise. Second, the author measured a different LOI on NMR-1 than the average LOI used for analysis of NMR-1. A different LOI could change the actual concentrations of the elements, but would not alter the precision significantly. The third possibility is the fact that NMR-1 is a new standard and the values used to compare to may be modified as the standard is better characterised. Fourth, P765 analyses were run in three consecative loads where NMR-1 was analyzed over the entire run and instrumental drift would affect NMR-1 more than P765.

TRACE ELEMENTS

Trace elements were analyzed for in three sets using pressed powder pellets. The pellets are 5-8 grams, depending on the major element composition of the samples, to ensure the pellets are infinitely thick. Polyvinyl alchol was used to help in adhesion of the pellets and to ensure an even distribution of pressure during pressing. Samples were pressed to 20 tons per square inch with boric acid used for backing.

H22, a glass standard, was run to identify peaks and background locations. Scans were run over the appropriate

angle with the desired crystal to identify the peaks and backgrounds with backgrounds chosen as close to the analytical peaks as possible. After peak and background positions were selected, they were place in the appropriate computer program. Ultrapure glass standards and USGS and international standards were run to calculate interference and background factors and these factors were also placed in the computer program. A second set of USGS, international, and inhouse standards were than run and linear calibration curves calculated and place in the appropriate computer program. Settings were adjusted until a good calibration curve for each element of interest was obtained. Settings are given for each set of analyses in tables D5, D6, and D7.

The trace elements Y, Zr, Sr, Rb, Nb, U, Pb, and Th were analyzed for in the first set. There are several interferences that the computer program corrects for: Y on Nb, Sr on Zr, Rb on Y, and Th on U. Matrix effects were also corrected for by the computer program by using the Rh compton peak.

Due to lack of time, only two standards were analyzed in the first set of trace element analyses: BCR-1 twice and G-2 once (table D8). For BCR-1, the U, Th, and Pb values for the two analyses are not accurate. The presicion for these elements are not very good at the low concentrations present in BCR-1. The accuracy for the other elements is good for the two analyses of BCR-1. The

TABLE D5. SETTINGS FOR XRF

Trace Elements
Y, Sr, Nb, Zr, Rb, and Pb

	Time	Crystal	Angle	Order	Window	Slit	Filter	Step
BKG1	40	LiF1	23.08	1st	1-1	3s	out	1/100
Y	100	LiF1	23.70	1st	1-1	3s	out	1/100
BKG2	40	LiF1	24.54	1st	1-1	3s	out	1/100
Sr	100	LiF1	25.06	1st	1-1	3s	out	1/100
BKG3	40	LiF1	25.62	1st	1-1	3s	out	1/100
RhC	100	LiF2	26.42	1st	1-1	3s	out	1/100
BKG4	100	LiF2	27.71	1st	1-1	3s	out	1/100
Nb	200	LiF2	30.33	1st	1-1	3s	out	1/100
Zr	100	LiF2	32.00	1st	1-1	3s	out	1/100
BKG5	100	LiF2	32.85	1st	1-1	3s	out	1/100
BKG6	100	LiF2	36.68	1st	1-1	3s	out	1/100
U	200	LiF2	37.25	1st	1-1	3s	out	1/100
Rb	100	LiF2	37.91	1st	1-1	3s	out	1/100
Th	200	LiF2	39.19	1st	1-1	3s	out	1/100
Pb	200	LiF2	40.34	1st	1-1	3s	out	1/100
BKG7	100	LiF2	40.98	1st	1-1	3s	out	1/100

Kv = 60
mA = 40

Used both the flow-proportional and the scintillation counters.

Time is the time counts were collected, in seconds.
LiF1 = Lithium fluoride 200
LiF2 = Lithium fluoride 220
Angle is two-theta in degrees.
Order is the analytical peak, which is the K-alpha peak.

TABLE D6. SETTINGS FOR XRF.

Trace Elements
Ba, V, and Cr

	Absor	Time	Crystal	Angle	Order	Window	Slit	Filter	Step
BKG1	1	40	LiF3	88.80	1st	3-2	1s	out	1/100
Ba	1	100	LiF3	87.22	1st	3-2	1s	out	1/100
Ti	1	100	LiF3	86.16	1st	3-2	1s	out	1/100
BKG2	1	40	LiF3	80.50	1st	3-2	1s	out	1/100
V	1	100	LiF3	76.96	1st	3-2	1s	out	1/100
BKG3	1	40	LiF3	76.00	1st	3-2	1s	out	1/100
BKG4	1	40	LiF3	70.75	1st	3-2	1s	out	1/100
Cr	1	100	LiF3	69.34	1st	3-2	1s	out	1/100
BKG5	1	40	LiF3	68.2	1st	3-2	1s	out	1/100
RhC	1	20	LiF3	26.5	1st	3-2	1s	out	1/100

Kv = 40 Used the flow proportional counter.
mA = 60

Time is the time counts were collected, in seconds.
LiF3 = Lithium floride 200
Angle is two-theta in degrees.
Order is the analytical peak which is the K-alpha peak.

TABLE D7. SETTINGS FOR XRF.

Trace Elements
Ga, Zn, and Cu

	Absor	Time	Crystal	Angle	Order	Window	Slit	Filter	Step
Rh1	1	40	LiF1	17.49	1st	2-2	1s	out	2/100
RhC	1	1	LiF1	18.61	1st	2-2	1s	out	2/100
Ga	1	100	LiF1	38.82	1st	2-2	1s	out	2/100
BKG1	1	40	LiF1	39.52	1st	2-2	1s	out	2/100
Zn	1	100	LiF1	41.72	1st	2-2	1s	out	2/100
BKG2	1	40	LiF1	42.67	1st	2-2	1s	out	2/100
Cu	1	100	LiF1	44.95	1st	2-2	1s	out	2/100
BKG3	1	40	LiF1	46.85	1st	2-2	1s	out	2/100

Kv = 60
mA = 40

Time is the time counts were collected, in seconds.
LiF1 = Lithium fluoride 200
Angle is two-theta in degrees.
Order is the analytical peak which is the K-alpha peak.

TABLE D8. ANALYSES OF STANDARDS FOR Y, SR, NB, ZR, U, RB, TH, AND PB

	Y	Sr	Nb	Zr	U	Rb	Th	Pb
BCR-1								
Anal-1	36.6	341	16.2	192	2.88	52.7	9.38	18.6
Anal-2	36.6	342	16.1	193	1.61	52.0	6.80	15.0
True Val.	40	330	19	185	1.70	47	6.1	14
G-2								
Anal-1	12.9	478	11.4	299	2.13	166	25.9	33.5
True Val.	11	480	13	300	2.1	170	25	30

True values are from Abbey (1983).

accuracy in G-2 for Sr, Zr, U, Rb, and Th is good, but for Y, Nb, and Pb the accracy is poor.

In the second set of analyses, Ba, V, Cr, and Ti were analyzed for. Mass absoption coefficients were calculated from major element compositions using a computer program and than the coefficients were entered into the computer along with the sample names before analysis. There are interferences in the second set that the computer program corrects for: V on Cr and Ti on Ba and V.

Five rock standards were analyzed along with the samples: QLO-1, PCC-1, and G-2 in triplicate and BCR-1 and BHVO-1 in duplicate (table D9). From this compilation, the precision and accuracy for Cr and Ba was very poor at low concentrations, but improved at higher concentrations. The presicion for V was good for all standards, but the accuracy was poor. Ti was analyzed for since it interfers on the Ba and V peaks, but the Ti concentrations from the major elements are used in this thesis.

The third set of trace elements analyzed for were Ga, Zn, and Cu. Cu and Zn are contaminates in the X-ray tube and so the precision and accuracy at low values is generally poor.

With the third set of trace elements, four rock standards were analyzed: BCR-1 and W-2 four times, BHVO-1 three times, and QLO-1 twice (table D10). All three elements had good precision. The accuracy for Zn was good, but variable for Cu and Ga. The accuracy for Cu and Ga was

TABLE D9. ANALYSIS AND STATISTICS OF STANDARDS FOR BA, V, AND CR

QLO-1	Ba	V	Cr
Anal-1	1326	39	5.1
Anal-2	1318	45	ND
Anal-3	1298	45	ND
Mean	1314	43	---
St. Dev.	14.4	3.46	---
Precision	1.10	8.06	---
True Val.	1400	61	4.2
Accuracy	7.29	36.1	---

PCC-1	Ba	V	Cr
Anal-1	8.7	25	2525
Anal-2	4.2	21	2528
Anal-3	ND	20	2552
Mean	---	22	2535
St. Dev.	---	2.65	14.8
Precision	---	12.0	0.584
True Val.	4	29	2800
Accuracy	---	31.0	9.82

G-2	Ba	V	Cr
Anal-1	1766	30	4.2
Anal-2	1743	33	8.5
Anal-3	1736	34	5.4
Mean	1749	32	6.0
St. Dev.	4.40	2.12	2.39
Precision	0.251	6.63	39.9
True Val.	1900	36	8
Accuracy	8.63	16.7	47.5

BCR-1	Ba	V	Cr
Anal-1	723	376	5.8
Anal-2	711	387	9.1
True Val.	680	420	15

BHVO-1	Ba	V	Cr
Anal-1	161	282	298
Anal-2	159	286	305
True Val.	135	320	300

True values from Abbey (1983).

TABLE D10. ANALYSES AND STATISTICS OF STANDARDS FOR GA, ZN, AND CU.

BCR-1	Ga	Zn	Cu
Anal-1	23	129	12
Anal-2	22	130	11
Anal-3	22	130	13
Anal-4	23	132	14
Mean	22.5	129.5	12.5
St. Dev.	0.577	2.52	1.29
Precision	2.56	1.95	10.3
True Val.	22	125	16
Accuracy	4.55	5.60	31.3

W-2	Ga	Zn	Cu
Anal-1	16	77	106
Anal-2	19	80	104
Anal-3	17	79	103
Anal-4	19	77	104
Mean	17.8	78.3	104
St. Dev.	1.50	1.50	1.29
Precision	8.43	1.92	1.24
True Val.	16	80	105
Accuracy	18.8	3.75	1.90

BHVO-1	Ga	Zn	Cu
Anal-1	20	103	155
Anal-2	20	106	155
Anal-3	23	107	163
Mean	21	105	158
St. Dev.	1.73	2.12	4.64
Precision	8.43	2.02	2.93
True Val.	21	105	140
Accuracy	9.52	1.90	16.4

QLO-1	Ga	Zn	Cu
Anal-1	15	62	27
Anal-2	14	66	29
True Val.	18	64	27

True values from Abbey (1983).

not dependent on their concentration in the standard.

APPENDIX E

NEUTRON ACTIVATION ANALYSIS

Approximately 0.05 grams of each sample and two standards were weighed out and placed in polyethelene vials. The vials were heat sealed and than washed, first in acetone and finally in distilled water to remove any salt deposited on the vials from the hands. Plastic gloves were worn during washing. Finally, the samples were sent to Sandia National Laboratory reactor for irradiation with thermal neutrons.

A computerized Nuclear Data 6600 model, 4096 channel, gamma-ray spectrometer, with a high resolution germanium detector was used for analysis. Raw data was digitalized and stored on magnetic tape. Nuclear Data software was used to reduce the raw data and print the data out. The software calculated the unknown concentration by comparing the peak area of each element of each sample with that of the standards. The computer corrected for errors due to dead time, weight differences between samples and standards, and for radioactive decay between the time a sample was analyzed and the time the standards were analyzed. Analytical methods are similar to Gordon, et al. (1968) and Gibson and Jagan (1980).

Analytical peak parameters are given in table E1. Some peaks have interferences and need correction before their data can be used. The appropriate peaks and the

TABLE E1. ANALYTICAL PEAKS FOR INAA.

ISOTOPE	ENERGY	COUNT	ISOTOPE	ENERGY	COUNT
239-Np	98.44	7	175-Yb	396.32	7
153-Sm	103.18	7	181-Hf	482.16	40
177-Lu	112.95	7	140-La	487.02	7
152-Eu	121.78	40	152-Eu	778.90	40
141-Ce	145.45	40	134-Cs	795.76	40
169-Yb	177.18	7,40	58-Ni	810.9	40
169-Yb	197.97	7	160-Tb	879.37	40
177-Lu	208.36	7	46-Sc	889.26	7,40
239-Np	228.19	7	46-Sc	1120.52	7,40
152-Eu	244.70	40	60-Co	1173.22	7,40
175-Yb	282.52	7	160-Tb	1177.95	40
160-Tb	298.57	7,40	182-Ta	1221.42	40
233-Pa	311.98	7,40	60-Co	1332.5	7,40
51-Cr	320.08	7,40	152-Eu	1408.08	40
152-Eu	344.30	40	140-La	1596.20	7

Count is the number of days the samples were cooled before analysis.
Each sample was analyzed for 3000 seconds for the 7 day count and 10000 seconds for the 40 day count.
239-Np is the analytical peak for uranium.
233-Pa is the analytical peak for thorium.

method used are listed in table E2.

Two standards were analyzed to calibrate the machine: BCR-1, two samples and G-2, three samples. After the seven day count, the standards were check for any irregularities. The analyses did not look good, especially for G-2 (see table E3). It was decided to rerun the data using only BCR-1 as a standard and treat G-2 as an unknown. There was improvement in accuracy, especially for Cr, Th, and Nd, with only U having less accuracy. For the forty day run, only BCR-1 was used as a standard.

The reason for the poor analyses when using G-2 are unknown, but several possibilities exist. The container were G-2 was stored may have been mis-labeled or contaminated. The G-2 samples could have been contaminated during sample preparation. Also, there may have been flux inhomogenities at the reactor during irradation or machine error during analyses of G-2. Since the sample wieghts were low, the poor analyses for G-2 could be due to low sample wieght.

Some of the peaks still have poor precision and accuracy (table E4). Some of this poor precision and accuracy is probably due to the low sample wieghts. The present practice at New Mexico Tech is to use about 0.3 grams of powder when using ploye thelene vials. Flux inhomogenities could also have contributed to the poor statistics. Some of the peaks have poor analytical precision and accuracy in INAA.

TABLE E2. INAA INTERFERENCES.

Isotope	Energy	Interferring Isotope	Energy	Clean Peak Energy	Interference Ratio
			7-Day Count		
153-Sm	103.18	239-Np	103.7	228.1	1.260
169-Yb	177.18	182-Ta	179.4	222.1	0.384
177-Lu	208.36	239-Np	209.73	228.1	.318
175-Yb	282.52	239-Np	285.41	277.6	.045
160-Tb	298.57	233-Pa	300.11	311.9	.183
175-Yb	396.32	233-Pa	398.5	311.9	.035
			40-Day Count		
141-Ce	145.45	233-Pa	145.4	311.9	0.011
169-Yb	177.18	182-Ta	179.4	222.1	0.384
160-Tb	298.57	233-Pa	300.11	311.9	0.183

INTERFERENCE CORRECTIONS

Clean peak area (counts) = CPA

Interference ratio = IR

Number of counts at interference = IC

Total interference area = IA
(Isotope + interferring isotope)

Net corrected counts = NCC

1) CPA * IR = IC

2) IA - IC = NCC

3) (NCC/IA) * Concentration = Corrected concentration of the element

TABLE E3. STATISTICS FOR 7 DAY COUNT

BCR-1

	Mean	St. Dev.	N	Precision %	True Value	Accuracy %
Sc	32.24	0.7314	8	2.27	32.8	5.76
Cr	116.1	4.983	4	4.29	16	706
Co	36.41	1.763	8	4.84	36.3	7.81
Th	4.446	0.1937	4	4.36	6.04	26.3
U	1.703	0.2890	8	17.0	1.71	26.5
Sm	6.376	0.09055	4	1.42	6.58	3.65
Lu	0.4984	0.06974	8	14.0	0.512	20.1
La	23.93	0.7980	8	3.34	25.0	15.6
Tb	0.8789	0.1221	4	13.9	1.05	28.6
Yb	3.308	0.3678	16	11.1	3.39	23.2

G2

	Mean	St. Dev.	N	Precision %	True Value	Accuracy %
Sc	3.797	0.1947	12	5.13	3.5	17.3
Cr	---	---	1	---	9	66.3
Co	5.300	0.9121	9	17.2	4.6	35.6
Th	27.36	0.7211	6	2.64	24.6	12.6
U	2.180	0.3632	9	16.7	2.04	38.7
Sm	11.59	0.3195	6	2.76	7.2	66.8
Lu	0.09942	0.02879	10	29.0	0.113	62.0
La	187	7.903	12	4.23	86	116
Tb	2.459	0.1647	6	6.70	0.48	426
Yb	0.7708	0.3589	8	46.6	0.78	59.0

N is the number of data points.
True values are from Gladney, et al. (1983).

TABLE E4. STATISTICS FOR BCR-1 ONLY: 7 AND 40 DAY COUNTS.

	Mean	St. dev.	N	Precision %	True value	Accuracy %
U	1.785	0.3143	8	17.6	1.71	34
Sm	6.409	0.1118	4	1.74	6.58	3.63
Lu	0.5122	0.05809	8	11.3	0.512	18.2
La	24.92	0.5547	8	2.23	25.0	11.2
Sc	32.82	0.6407	16	1.95	32.8	3.79
Cr	16.05	0.6935	8	4.32	16	12.6
Co	36.38	1.445	16	3.97	36.3	7.97
Th	6.043	0.1962	8	3.25	6.04	5.34
Tb	1.002	0.113	12	11.3	1.05	21
Yb	3.358	0.3303	20	9.84	3.39	22.9
Cs	0.983	0.09582	4	9.75	0.97	11.2
Ta	0.7966	0.08188	4	10.3	0.79	14.1
Ce	53.08	0.9231	4	1.74	53.7	2.11
Eu	1.961	0.054	12	2.75	1.96	5.95
Ni	13.25	1.528	4	11.5	13	14.6

N is the number of data points.
True values from Gladney, et al. (1983).

APPENDIX F

INDIVIDUAL SAMPLE COMPOSITIONS

This appendix lists the compositon of individual rock samples. Samples are grouped by type and geographical location in the tables: F1, tholeiitic volcanic samples from the Pedernal Hills; F2, mafic calc-alkalic volcanic samples from the Pedernal Hills; F3, felsic volcanic samples from the Pedernal Hills; F4, felsic volcanic samples from the Manzano Mountains; F5, mafic volcaniclastic sample from the Pedernal Hills; F6, felsic volcaniclastic samples from the Pedernal Hills; F7, felsic volcaniclastic sample from the Manzano Mountains; and F8, epiclastic sedimentary rocks from the Manzano Mountains.

In the tables, Fe2O3-T is total iron expressed as Fe2O3, LOI is loss on ignition, and ND is not determined or below the detectability limit. The major elements are in weight percent and were recalculated after subtraction of H2O-. Trace elements are in ppm. Mg numbers were claculated from the equation

$$(MgO/40.32)/((MgO/40.32)+(FeO/71.85))$$

with the FeO value derived from a Fe2O3/FeO ratio of 0.15 for the mafic rocks and a Fe2O3/FeO ratio of 0.50 for the felsic rocks.

In addition to the individual sample compositions, a table listing the chondrite values used to construct REE diagrams is included (table F9).

TABLE F1. COMPOSITION OF THOLEIITE VOLCANIC ROCKS FROM THE PEDERNAL HILLS

SAMPLE	P762	P760
SiO2	49.0	50.4
TiO2	0.55	0.72
Al2O3	16.0	13.5
Fe2O3-T	9.74	12.0
MgO	8.57	7.77
CaO	10.8	9.21
Na2O	2.32	3.11
K2O	0.097	0.20
MnO	0.15	0.17
P2O5	0.086	0.061
LOI	2.71	2.07
TOTAL	100.023	99.211
Mg No.	66.4	59.3
Sr	139	87
Ba	91	182
Rb	2.7	7.4
Th	2.3	1.7
U	ND	ND
Pb	7.8	9.6
Cs	ND	0.24
Zr	56	48
Hf	1.7	1.2
Nb	5.4	5.0
Ta	ND	ND
Y	22	23
Sc	48	45
V	227	311
Cr	66	49
Co	63	57
Ni	25	21
La	15	4.9
Ce	36	13
Sm	4.0	3.1
Eu	1.2	1.0
Tb	0.68	ND
Yb	2.8	2.4
Lu	0.43	0.43
Ga	15	12
Zn	77	99
Cu	121	185

TABLE F1. CONTINUED.

SAMPLE	P762	P760
CIPW norms		
orthoclase	0.594	1.230
albite	20.352	27.385
anorthite	34.168	23.192
diopside		
wollastinite	9.997	8.683
enstatite	5.377	5.180
ferrosilite	4.287	3.055
hypersthene		
enstatite	11.183	12.317
ferrosilite	8.915	7.265
olivine		
forsterite	2.507	3.245
faylite	2.203	2.109
magnetite	1.744	2.158
ilmenite	0.206	1.423
apatite	1.083	0.147
Niggli Numbers		
SI	112.530	120.771
AL	21.654	19.064
FM	46.464	49.759
C	26.574	23.646
ALK	5.307	7.531
K	0.027	0.041
MG	0.631	0.558
TI	0.950	1.297
P	0.084	0.062

TABLE F2. COMPOSITION OF MAFIC CALC-ALKALIC VOLCANICS FROM THE PEDERNAL HILLS.

SAMPLE	P792	P772	P775	P765
SiO2	50.7	52.8	52.9	54.0
TiO2	0.54	0.76	0.70	1.61
Al2O3	19.5	16.8	15.0	13.9
Fe2O3-T	8.78	12.5	9.08	15.1
MgO	4.86	5.81	6.78	3.85
CaO	8.46	3.84	5.86	6.75
Na2O	2.87	2.21	1.71	2.06
K2O	0.86	1.85	2.31	0.54
MnO	0.12	0.18	0.13	0.25
P2O5	0.11	0.070	0.16	0.32
LOI	3.97	3.60	3.67	2.61
TOTAL	100.77	100.42	98.30	100.99
Mg No.	55.4	51.1	62.8	36.8
Sr	287	68	264	201
Ba	334	371	403	148
Rb	29	88	119	32
Th	4.6	6.6	9.1	4.1
U	1.2	1.3	2.1	1.0
Pb	16	15	22	14
Cs	1.2	3.4	0.72	2.1
Zr	99	90	149	101
Hf	2.9	3.1	4.6	2.8
Nb	7.4	9.3	11	8.6
Ta	0.60	0.80	1.8	0.58
Y	28	30	33	44
Sc	31	48	28	40
V	201	219	199	243
Cr	11	53	48	ND
Co	13	71	55	35
Ni	9.3	22	21	ND
La	41	33	51	28
Ce	75	75	107	66
Sm	7.2	6.3	8.2	8.0
Eu	1.8	1.6	1.8	2.6
Tb	0.87	1.8	1.1	1.4
Yb	2.8	3.3	3.1	4.1
Lu	0.40	0.52	0.44	0.58
Ga	16	21	15	17
Zn	77	120	101	151
Cu	23	127	118	ND

TABLE F2. CONTINUED.

SAMPLE	P792	P772	P775	P765
CIPW norms				
quartz	1.334	9.267	7.634	13.624
corundum	---	4.542	---	---
orthoclase	5.292	11.421	14.546	3.287
albite	25.290	19.535	15.418	17.954
anorthite	39.350	19.424	28.165	27.900
diopside				
wollastinite	1.507	---	0.710	1.854
enstatite	0.763	---	0.408	0.652
ferrosilite	0.709	---	0.270	1.249
hypersthene				
enstatite	11.842	15.116	17.585	9.224
ferrosilite	11.009	16.763	11.629	17.657
magnetite	1.570	2.257	1.823	2.688
ilmenite	1.068	1.508	1.417	3.150
apatite	0.265	0.169	0.395	0.763
Niggli Numbers				
SI	133.994	148.478	149.851	153.815
AL	30.371	27.841	25.041	23.333
FM	36.869	51.245	48.303	49.397
C	23.956	11.570	17.786	20.600
ALK	8.804	9.344	8.871	6.670
K	0.165	0.355	0.471	0.147
MG	0.519	0.475	0.593	0.331
TI	1.073	1.607	1.491	3.449
P	0.123	0.083	0.192	0.386

TABLE F2. CONTINUED.

SAMPLE	P740	P901	P774
SiO2	55.4	56.1	56.9
TiO2	0.92	0.70	0.97
Al2O3	16.1	17.7	15.8
Fe2O3-T	9.85	9.30	8.89
MgO	4.23	3.45	3.99
CaO	6.88	4.51	6.45
Na2O	3.34	4.43	3.36
K2O	0.65	0.94	1.67
MnO	0.14	0.14	0.11
P2O5	0.19	0.096	0.25
LOI	2.49	2.87	1.77
TOTAL	100.19	100.236	100.16
Mg No.	49.1	45.5	50.2
Sr	324	183	248
Ba	196	378	466
Rb	22	38	64
Th	8.6	6.2	12
U	2.0	1.5	2.3
Pb	19	15	17
Cs	1.5	0.61	3.2
Zr	136	132	189
Hf	4.4	4.2	6.1
Nb	9.6	9.7	12
Ta	1.1	1.6	1.3
Y	34	32	40
Sc	34	27	28
V	251	176	243
Cr	9.4	8.8	12
Co	45	31	36
Ni	6.9	6.5	10
La	41	34	40
Ce	99	74	116
Sm	10	6.9	12
Eu	2.1	1.8	2.8
Tb	1.3	1.1	1.5
Yb	3.7	2.9	4.1
Lu	0.55	0.52	0.52
Ga	17	18	16
Zn	95	105	88
Cu	342	ND	116

TABLE F2. CONTINUED.

SAMPLE	P740	P901	P774
CIPW norms			
quartz	9.013	7.102	8.826
corundum	---	1.476	---
orthoclase	3.967	5.753	10.110
albite	29.185	38.820	29.125
anorthite	27.902	22.522	23.663
diopside			
wollastinite	2.532	---	3.109
enstatite	1.167	---	1.479
ferrosilite	1.342	---	1.588
hypersthene			
enstatite	9.712	8.899	8.702
ferrosilite	11.170	12.157	9.346
magnetite	1.752	1.667	1.575
ilmenite	1.805	1.377	1.887
apatite	0.454	0.230	0.593
Niggli Numbers			
SI	161.286	173.005	170.973
AL	27.622	32.168	27.978
FM	40.283	37.837	38.267
C	21.461	14.902	20.766
ALK	10.634	15.094	12.989
K	0.114	0.123	0.246
MG	0.456	0.419	0.467
TI	2.014	1.623	2.192
P	0.234	0.125	0.318

TABLE F3. COMPOSITION OF FELSIC VOLCANIC ROCKS FROM THE PEDERNAL HILLS.

SAMPLE	P719	P769	P710	P767
SiO2	67.7	69.4	70.5	72.0
TiO2	0.54	0.42	0.40	0.22
Al2O3	13.4	14.3	13.2	13.8
Fe2O3-T	5.59	3.86	4.19	2.82
MgO	0.60	0.81	1.11	1.39
CaO	2.80	1.66	0.94	4.15
Na2O	3.35	4.42	3.69	1.83
K2O	1.79	2.02	2.94	1.93
MnO	0.071	0.054	0.084	0.063
P2O5	0.090	0.11	0.071	0.037
LOI	1.08	1.27	1.47	1.61
TOTAL	97.01	98.32	98.60	99.85
Mg No.	23.6	37.6	43.2	58.6
Sr	144	117	72	172
Ba	1007	678	599	938
Rb	43	78	147	53
Th	10	20	18	18
U	2.0	3.3	2.8	4.7
Pb	16	22	14	23
Cs	0.67	3.4	3.6	0.86
Zr	102	267	240	132
Hf	3.4	9.1	8.9	5.5
Nb	11	14	14	19
Ta	1.7	2.1	2.2	3.1
Y	40	44	59	66
Sc	18	14	16	17
V	21	30	40	35
Cr	ND	5.9	4.1	13
Co	4.5	5.2	9.4	12
Ni	ND	ND	ND	5.8
La	38	81	85	54
Ce	90	181	135	123
Sm	8.3	13	12	12
Eu	4.8	2.6	2.6	1.6
Tb	1.4	1.8	1.8	2.3
Yb	4.2	5.4	7.3	7.8
Lu	0.68	0.79	0.93	1.0
Ga	ND	ND	ND	ND
Zn	ND	ND	ND	ND
Cu	ND	ND	ND	ND

TABLE F3. CONTINUED.

SAMPLE	P719	P769	P710	P767
CIPW norms				
quartz	33.130	30.392	33.033	42.325
corundum	1.128	2.158	2.489	1.269
orthoclase	11.084	12.342	17.955	11.637
albite	29.702	38.669	32.269	15.800
anorthite	13.940	7.772	4.341	20.761
hypersthene				
enstatite	1.566	2.086	2.857	3.532
ferrosilite	7.156	4.803	5.352	3.659
magnetite	1.003	0.690	0.749	0.503
ilmenite	1.075	0.825	0.785	0.426
apatite	0.218	0.263	0.170	0.087
Niggli Numbers				
SI	331.167	348.075	368.763	362.916
AL	38.629	42.267	40.689	40.992
FM	25.223	20.857	25.519	21.446
C	14.675	8.921	5.268	22.413
ALK	21.473	27.955	28.523	15.149
K	0.260	0.231	0.344	0.410
MG	0.173	0.290	0.339	0.487
TI	1.986	1.584	1.573	0.834
P	0.186	0.234	0.157	0.079

TABLE F3. CONTINUED.

SAMPLE	P720	P969	P753
SiO2	76.1	76.6	76.8
TiO2	0.14	0.16	0.56
Al2O3	12.1	11.9	9.06
Fe2O3-T	2.54	2.57	5.07
MgO	0.16	0.13	2.72
CaO	0.77	0.78	0.61
Na2O	4.01	3.69	1.11
K2O	3.68	4.04	1.93
MnO	0.078	0.039	0.055
P2O5	0.017	0.015	0.088
LOI	0.24	0.253	1.78
TOTAL	99.84	100.18	99.783
Mg No.	15.3	12.7	60.6
Sr	50	51	49
Ba	723	738	491
Rb	131	148	73
Th	20	18	11
U	4.2	4.4	2.1
Pb	22	21	14
Cs	1.7	1.4	2.0
Zr	321	325	186
Hf	10	9.9	6.9
Nb	16	16	9.3
Ta	2.5	2.3	1.1
Y	84	85	28
Sc	9.3	7.9	12
V	ND	ND	76
Cr	ND	ND	25
Co	0.41	0.35	17
Ni	ND	ND	15
La	103	91	54
Ce	204	177	103
Sm	18	16	7.7
Eu	3.0	2.7	2.3
Tb	2.9	2.5	1.1
Yb	8.8	8.7	3.3
Lu	1.4	1.6	0.43
Ga	ND	ND	7.3
Zn	ND	ND	52
Cu	ND	ND	ND

TABLE F3. CONTINUED.

SAMPLE	P720	P969	P753
CIPW norms			
quartz	35.552	36.462	56.466
corundum	0.162	0.075	4.353
orthoclase	21.885	23.944	11.691
albite	34.146	31.314	9.627
anorthite	3.733	3.783	2.513
hypersthene			
enstatite	0.401	0.325	6.944
ferrosilite	3.378	3.308	6.215
magnetite	0.438	0.451	0.892
ilmenite	0.268	0.305	1.090
apatite	0.040	0.035	0.209
Niggli Numbers			
SI	463.954	473.727	473.628
AL	43.473	43.371	32.927
FM	13.482	13.397	48.812
C	5.030	5.168	4.031
ALK	38.015	38.064	14.230
K	0.377	0.419	0.534
MG	0.108	0.089	0.512
TI	0.642	0.744	2.597
P	0.044	0.039	0.230

TABLE F4. COMPOSITION OF FELSIC VOLCANIC ROCKS FROM THE MANZANO MOUNTAINS.

SAMPLE	M742	M601	M723	M758	M743
SiO2	72.2	73.2	73.7	77.7	80.1
TiO2	0.37	0.29	0.32	0.28	0.17
Al2O3	13.7	13.1	12.5	11.2	10.3
Fe2O3-T	3.87	3.59	3.62	2.92	1.95
MgO	1.03	0.79	0.75	0.61	0.30
CaO	2.48	2.02	1.98	2.24	1.13
Na2O	3.52	4.06	2.38	3.21	3.99
K2O	1.62	1.49	3.63	1.03	1.10
MnO	0.15	0.10	0.073	0.11	0.064
P2O5	0.08	0.061	0.070	0.066	0.043
LOI	1.07	1.18	0.95	1.00	1.01
TOTAL	100.09	99.88	99.97	100.37	100.20
Mg No.	43.3	38.7	37.3	35.5	30.6
Sr	353	210	155	340	112
Ba	811	908	721	443	406
Rb	70	55	172	41	43
Th	11	13	13	8.6	13
U	2.4	2.7	2.6	1.7	3.4
Pb	25	24	24	20	25
Cs	2.6	1.5	5.5	1.7	1.3
Zr	288	260	269	231	202
Hf	9.4	8.4	9.7	7.9	6.5
Nb	11	12	12	8.4	9.0
Ta	1.4	1.6	1.5	1.1	1.4
Y	47	51	57	39	50
Sc	18	18	19	16	10
V	30	25	25	22	3.6
Cr	1.7	1.5	ND	ND	ND
Co	6.0	6.1	6.4	5.2	1.2
Ni	ND	ND	ND	ND	ND
La	73	77	80	57	67
Ce	140	155	164	115	139
Sm	13	14	14	9.7	12
Eu	4.9	4.1	4.9	4.1	2.3
Tb	1.8	1.9	2.0	1.4	1.9
Yb	4.9	4.8	6.2	3.8	4.8
Lu	0.75	0.82	0.84	0.56	0.70
Ga	ND	14	ND	ND	ND
Zn	ND	98	ND	ND	ND
Cu	ND	10	ND	ND	ND

TABLE F4. CONTINUED.

SAMPLE	M742	M601	M723	M758	M743
CIPW norms					
quartz	37.152	37.060	39.254	48.302	49.306
corundum	1.863	1.303	1.239	0.898	0.600
orthoclase	9.701	8.949	21.732	6.141	6.567
albite	30.182	34.914	20.402	27.402	34.109
anorthite	11.938	9.780	9.489	10.777	5.380
hypersthene					
enstatite	2.599	2.000	1.892	1.533	0.755
ferrosilite	4.991	4.660	4.581	3.746	2.520
magnetite	0.676	0.634	0.632	0.512	0.337
ilmenite	0.712	0.560	0.616	0.537	0.326
apatite	0.188	0.144	0.164	0.154	0.101
Niggli Numbers					
SI	365.511	390.596	409.105	486.363	579.531
AL	40.873	41.194	40.891	41.315	43.917
FM	23.167	21.182	21.670	20.069	14.259
C	13.452	11.549	11.776	15.023	8.760
ALK	22.508	26.075	25.663	23.593	33.064
K	0.232	0.195	0.501	0.174	0.154
MG	0.336	0.297	0.286	0.284	0.227
TI	1.409	1.164	1.336	1.318	0.925
P	0.171	0.138	0.164	0.175	0.132

TABLE F5. COMPOSITION OF MAFIC VOLCANICLASTIC FROM THE PEDERNAL HILLS.

SAMPLE	P742-A	P742-B
SiO2	52.4	50.2
TiO2	0.66	0.85
Al2O3	14.2	13.6
Fe2O3-T	11.7	12.9
MgO	6.14	7.53
CaO	10.2	8.98
Na2O	3.23	2.79
K2O	0.18	0.27
MnO	0.15	0.17
P2O5	0.049	0.062
LOI	1.57	1.65
TOTAL	100.48	99.002
Sr	121	94
Ba	46	40
Rb	4.5	8.2
Th	ND	ND
U	ND	ND
Pb	11	7.4
Cs	0.06	1.2
Zr	43	55
Hf	1.4	2.0
Nb	5.1	5.2
Ta	ND	ND
Y	23	27
Sc	51	60
V	311	319
Cr	26	60
Co	58	67
Ni	11	17
La	8.5	6.1
Ce	15	15
Sm	3.2	3.9
Eu	1.1	1.6
Tb	0.84	0.76
Yb	2.8	3.4
Lu	0.41	0.51
Ga	14	13
Zn	75	100
Cu	63	68

TABLE F6. COMPOSITION OF FELSIC VOLCANICLASTIC ROCKS FROM THE PEDERNAL HILLS.

SAMPLE	P900		P739	
	A	B	A	B
SiO2	66.1	69.8	72.3	71.8
TiO2	0.31	0.43	0.15	0.34
Al2O3	16.7	13.0	14.9	14.2
Fe2O3-T	3.69	5.84	2.20	3.71
MgO	0.66	1.36	0.46	0.83
CaO	3.23	2.61	2.39	2.37
Na2O	4.64	3.66	4.56	4.32
K2O	2.17	2.09	1.77	1.89
MnO	0.057	0.073	0.030	0.045
P2O5	0.016	0.095	0.021	0.055
LOI	1.60	0.97	1.10	1.09
TOTAL	99.17	99.93	99.88	100.70
Sr	209	118	133	129
Ba	ND	491	720	626
Rb	58	54	53	77
Th	24	15	20	16
U	4.9	3.4	4.4	3.2
Pb	15	12	13	13
Cs	1.6	4.4	0.58	2.8
Zr	394	253	305	274
Hf	12	8.2	11	7.0
Nb	15	16	14	17
Ta	3.1	1.9	2.3	1.8
Y	98	68	72	66
Sc	14	18	9.7	16
V	ND	64	49	62
Cr	3.4	7.2	ND	3.7
Co	6.9	16	3.2	11
Ni	ND	3.9	ND	ND
La	96	105	75	72
Ce	200	284	169	137
Sm	19	17	13	13
Eu	3.9	3.1	3.1	2.4
Tb	3.2	2.3	2.4	2.0
Yb	11	7.3	9.0	5.9
Lu	1.7	1.1	1.2	0.88
Ga	ND	ND	14	14
Zn	ND	ND	21	31
Cu	ND	ND	ND	ND

TABLE F7. COMPOSITION OF FELSIC VOLCANICLASTIC ROCK FROM THE MANZANO MOUNTAINS.

SAMPLE	M734
SiO2	68.1
TiO2	0.45
Al2O3	16.1
Fe2O3-T	4.17
MgO	1.07
CaO	2.07
Na2O	3.74
K2O	2.56
MnO	0.12
P2O5	0.095
LOI	1.65
TOTAL	100.13
Sr	423
Ba	705
Rb	115
Th	12
U	2.8
Pb	34
Cs	3.5
Zr	338
Hf	11
Nb	11
Ta	1.6
Y	56
Sc	21
V	38
Cr	2.7
Co	8.4
Ni	ND
La	85
Ce	167
Sm	15
Eu	6.3
Tb	2.0
Yb	5.3
Lu	0.71
Ga	ND
Zn	ND
Cu	ND

TABLE F8. COMPOSITION OF EPICLASTIC SEDIMENTARY ROCKS FROM THE MANZANO MOUNTAINS.

SAMPLE	M709	M605	M733	M724
SiO2	68.5	71.3	73.7	78.5
TiO2	0.75	0.58	0.62	0.45
Al2O3	15.6	13.8	12.6	10.1
Fe2O3-T	5.62	4.76	5.14	3.62
MgO	1.04	1.03	1.27	0.69
CaO	0.29	0.90	0.75	2.13
Na2O	1.62	1.87	1.33	2.89
K2O	3.94	2.87	2.72	0.68
MnO	0.054	0.065	0.075	0.12
P2O5	0.12	0.077	0.07	0.065
LOI	2.11	2.90	3.53	0.71
TOTAL	99.64	100.152	101.81	99.96
Sr	63	109	96	104
Ba	711	540	539	278
Rb	192	137	133	44
Th	18	18	17	15
U	4.0	3.8	3.3	3.1
Pb	24	28	26	24
Cs	5.1	3.7	3.9	2.4
Zr	231	249	223	299
Hf	7.6	11	7.6	11
Nb	17	15	17	11
Ta	2.5	2.5	2.6	1.9
Y	45	41	41	36
Sc	16	15	14	8.9
V	72	58	58	49
Cr	7.8	8.5	7.2	6.7
Co	16	15	17	9.7
Ni	2.8	4.8	4.9	2.7
La	81	96	79	73
Ce	104	191	158	152
Sm	13	13	12	11
Eu	2.2	2.6	2.0	1.9
Tb	1.7	1.7	1.6	1.4
Yb	3.9	4.7	3.6	3.8
Lu	0.69	0.76	0.62	0.61
Ga	20	ND	ND	ND
Zn	91	ND	ND	ND
Cu	23	ND	ND	ND

TABLE F9. CHONDRITE VALUES FOR REE

ELEMENT	CHONDRITE VALUE
La	0.3150
Ce	0.8130
Sm	0.1920
Eu	0.0722
Tb	0.0490
Yb	0.2080
Lu	0.0323

Reference: Langmuir, et al. (1977).

APPENDIX G

CLASSIFICATION

A modified version of PETCAL from Bingler, et al. (1976), written by R. Koch at NMIMT, is used to help classify the volcanic rocks. Several classification schemes are incorprorated in PETCAL: Macdonald and Katsura (1964), Irvine and Baragar (1971), Middlemost (1972), Miyashiro (1974), and Peccerillo and Taylor (1976). CIPW norms, Niggli numbers, oxide ratios, and petrochemical indices are also calculated by the PETCAL program. The CIPW norms and Niggli numbers are presented in Appendix F along with the compositional data. Some of the petrochemical indices can be used for classification. Also, other classification schemes not contained in PETCAL are presented.

The first step is to assign the volcanic samples to either the alkaline or subalkaline group. The first four diagrams use major element data to assign samples. Figure G1 is a alkalies-silica diagram with dividing lines of Macdonald and Katsura (1964) and Irving and Baragar (1971). All of the samples plot in the subalkaline field using both dividing lines.

On a Ol′-Ne′-Q′ diagram of Irving and Baragar (1971), all the volcanic samples from both sections, except P760 and P762, would plot at the Q′ apex, indicating all of these samples are subalkaline. P760 and P762 would plot at

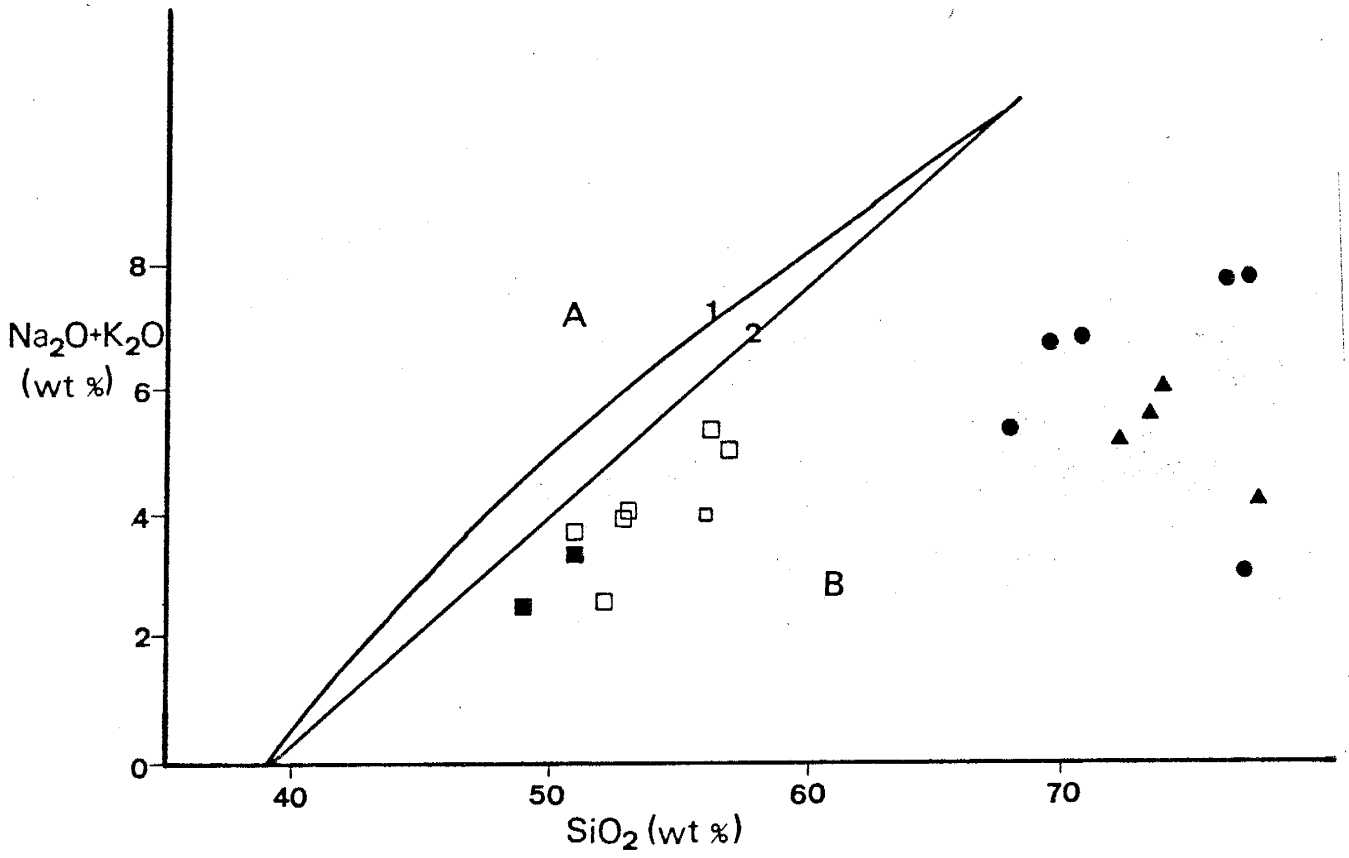

Figure G1. (Na2O+K2O)-SiO2 diagram showing the distribution of volcanic rocks from the Pedernal and the Manzano successions. IB is the dividing line of Irving and Baragar (1971) and MK is the dividing line of Macdonald and Katsura (1964). Fields are A, alkaline and B, subalkaline. Open squares are calc-alkaline basalt and andesites, closed squares are tholeiitic basalts, circles are felsic volcanics, all from the Pedernal section and triangles are felsic volcanics from the Manzano section.

the Ol′ apex, one of the ends of the dividing line between alkaline and subalkaline rock types. Since P760 and P762 are Opx normative, having niether Q or Ne in the CIPW norm (Irving and Baragar, 1971), they can be plotted on the Cpx-Opx-Ol diagram (figure G2) of Chayes (1965 and 1966). On this diagram, P760 and P762 fall in the subalkaline field. G3 is a total alkalies-differential index diagram, with all the volcanics falling in the subalkaline field.

Wright (1969) proposed an alkalinity ratio to use in differentiating subalkaline from alkaline rocks. Figure G4 is a SiO2-alkalinity ratio diagram with all the samples falling in the subalkaline field except P710, P720, P969, and M743, which fall in the alkaline field.

Floyd and Winchester (1975) proposed several diagrams for mafic rocks using trace elements. G5 and G6 show all the mafic volcanics plot in the subalkaline fields as defined by Floyd and Winchester (1975).

From figures G1-G6, the volcanic samples all appear to be subalkaline. The next step is to divide the samples into tholeiitic and calc-alkaline groups if possible.

G7 is a alumina-normative plagioclase diagram with all of the mafic and andesitic volcanic data plotted on it. P760, P762, and P765 all plot in the tholeiitic field and the rest of the mafic and andesitic volcanics fall in the calc-alkaline field. This diagram is not useful for felsic rocks (Irving and Baragar, 1971).

Miyashiro (1974) proposed the SiO2-FeO*/MgO diagram to

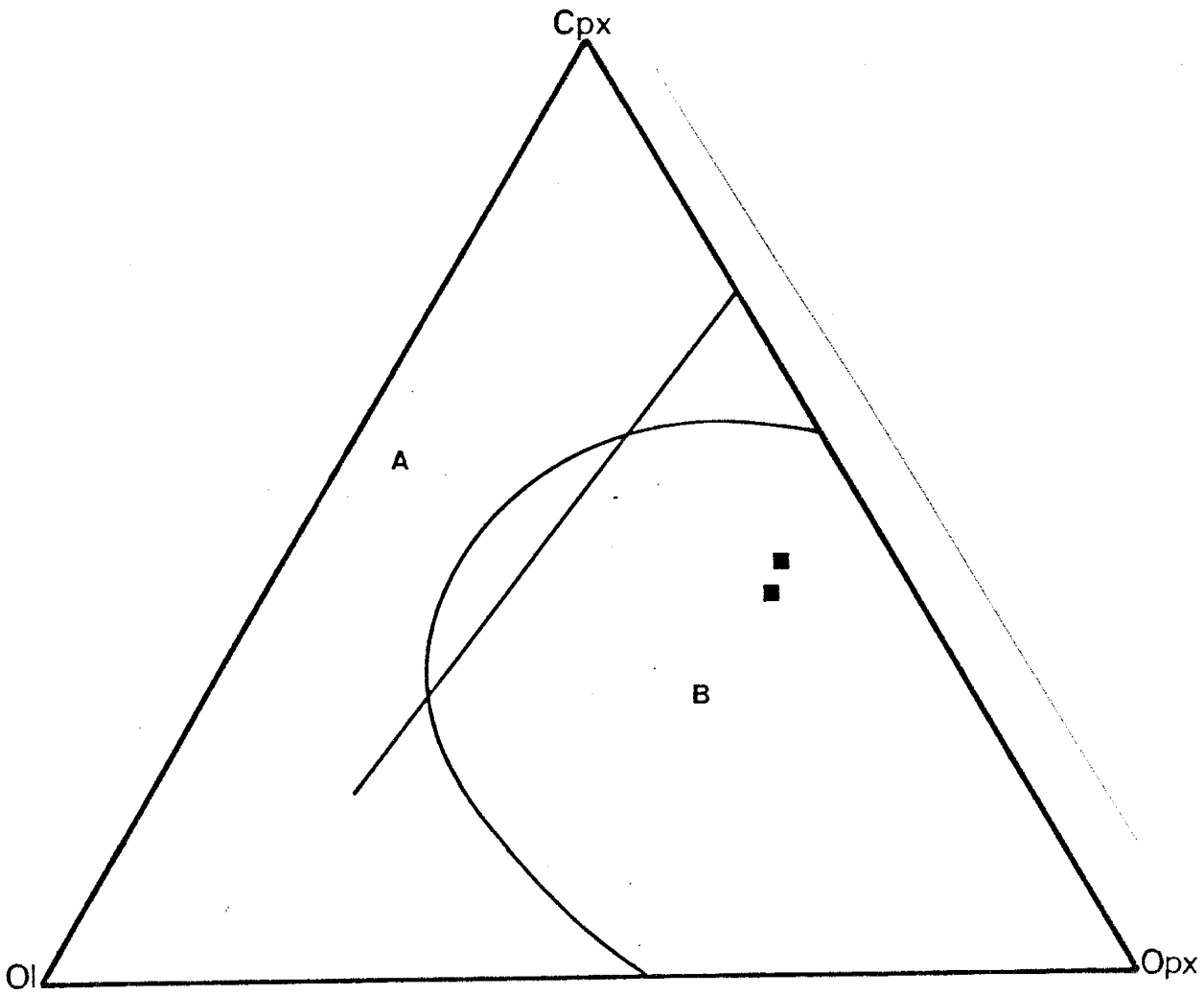

Figure G2. Cpx-Ol-Opx diagram showing the distribution of the tholeiitic basalts from the Pedernal succession. Fields are A, alkaline and B, subalkaline. Dividing lines and fields from Chayes (1965 and 1966).

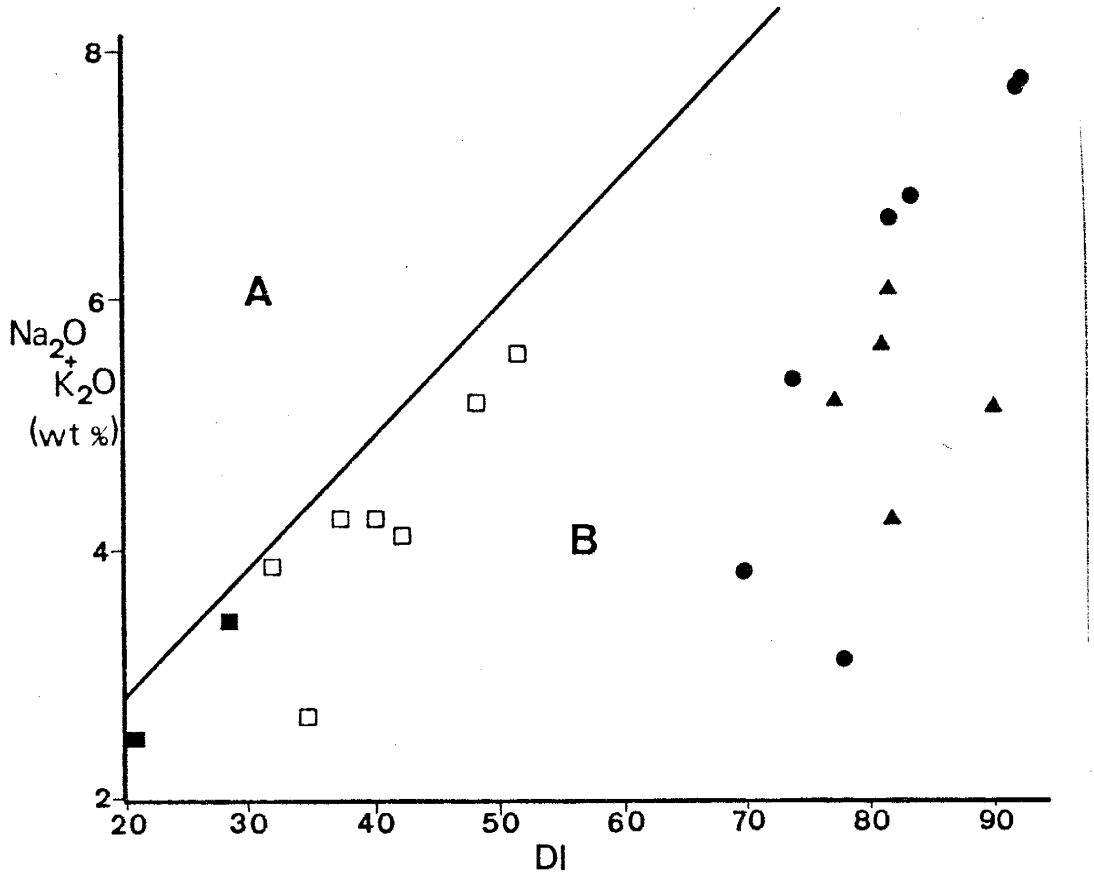

Figure G3. (Na2O+K2O)-DI diagram showing the distribution of volcanic rocks from the Pedernal and the Manzano successions. DI is differential index. Fields from Stewart and Thorton (1975). Symbols and fields as in figure G1.

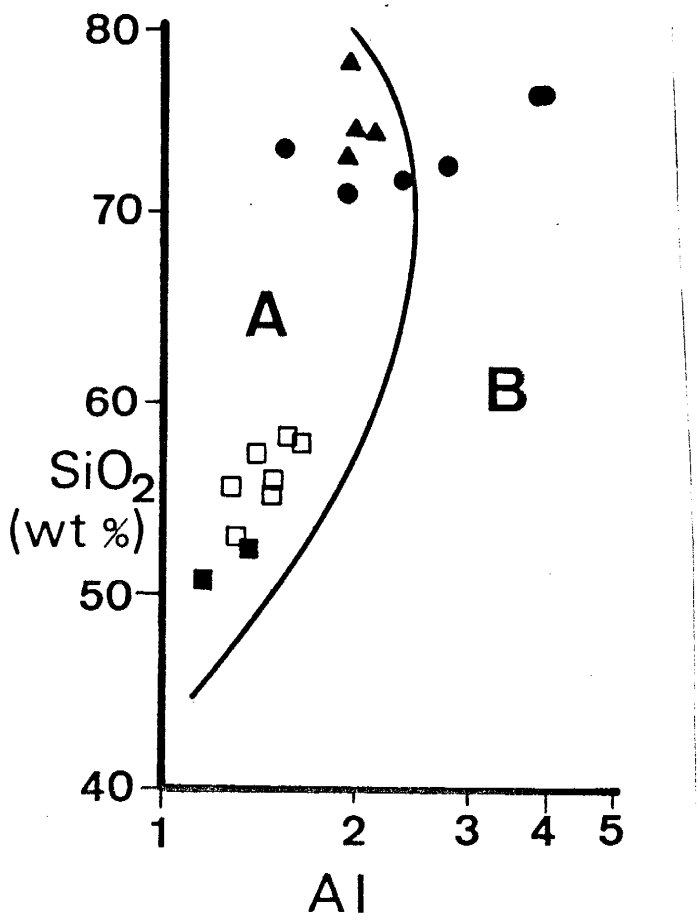

Figure G4. SiO2-Alkalinity index (AI) diagram showing the distribution for volcanic rocks from both the Pedernal and the [illegible] intrusions. Fields are A, subalkaline and B, alkaline (Wright, 1969). Symbols as in figure G1.

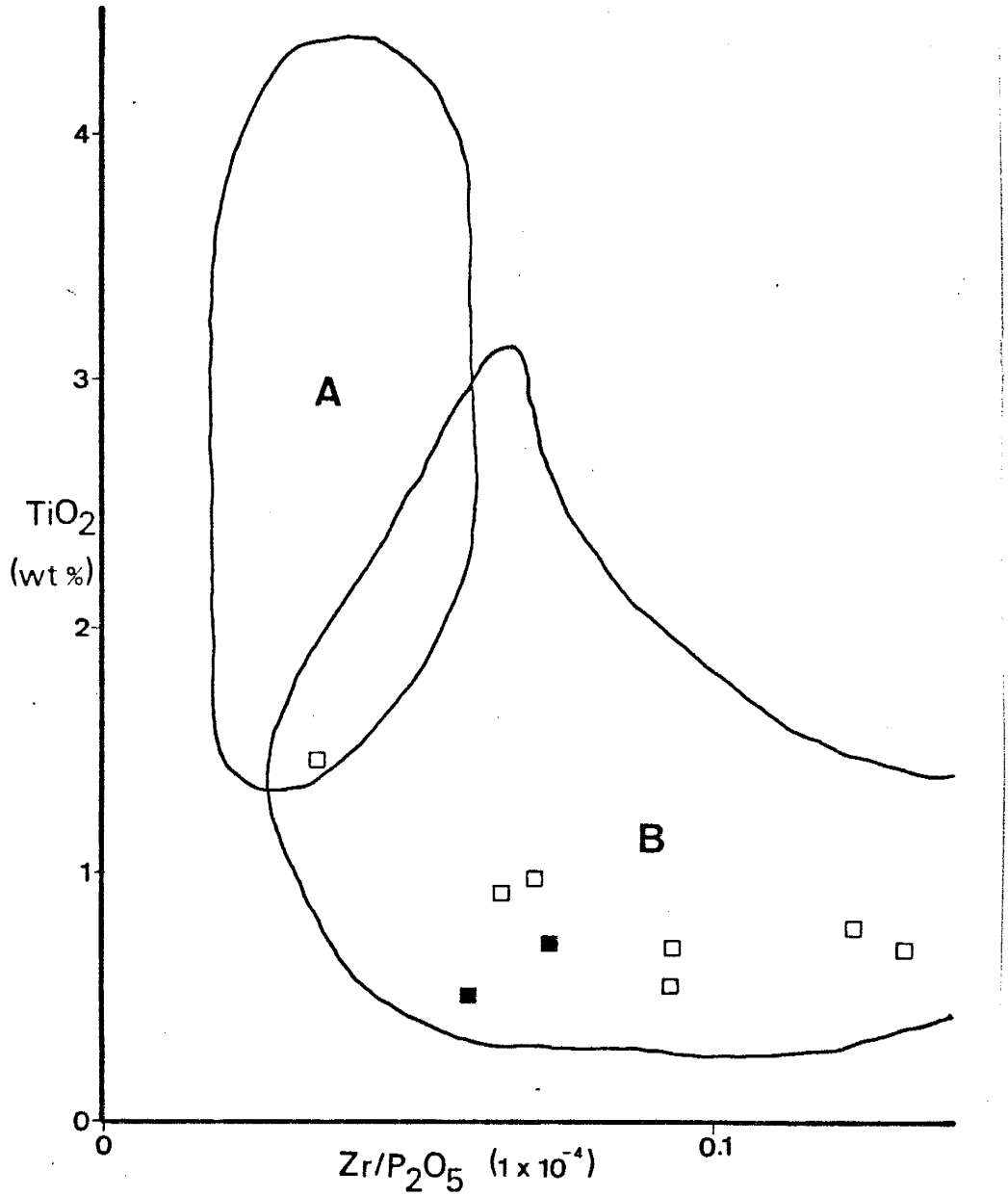

Figure G5. TiO2-(Zr/P2O5) diagram showing the distribution for mafic rocks from the Pedernal succession. Fields from Floyd and Winchester (1975). Symbols and fields as in figure G1.

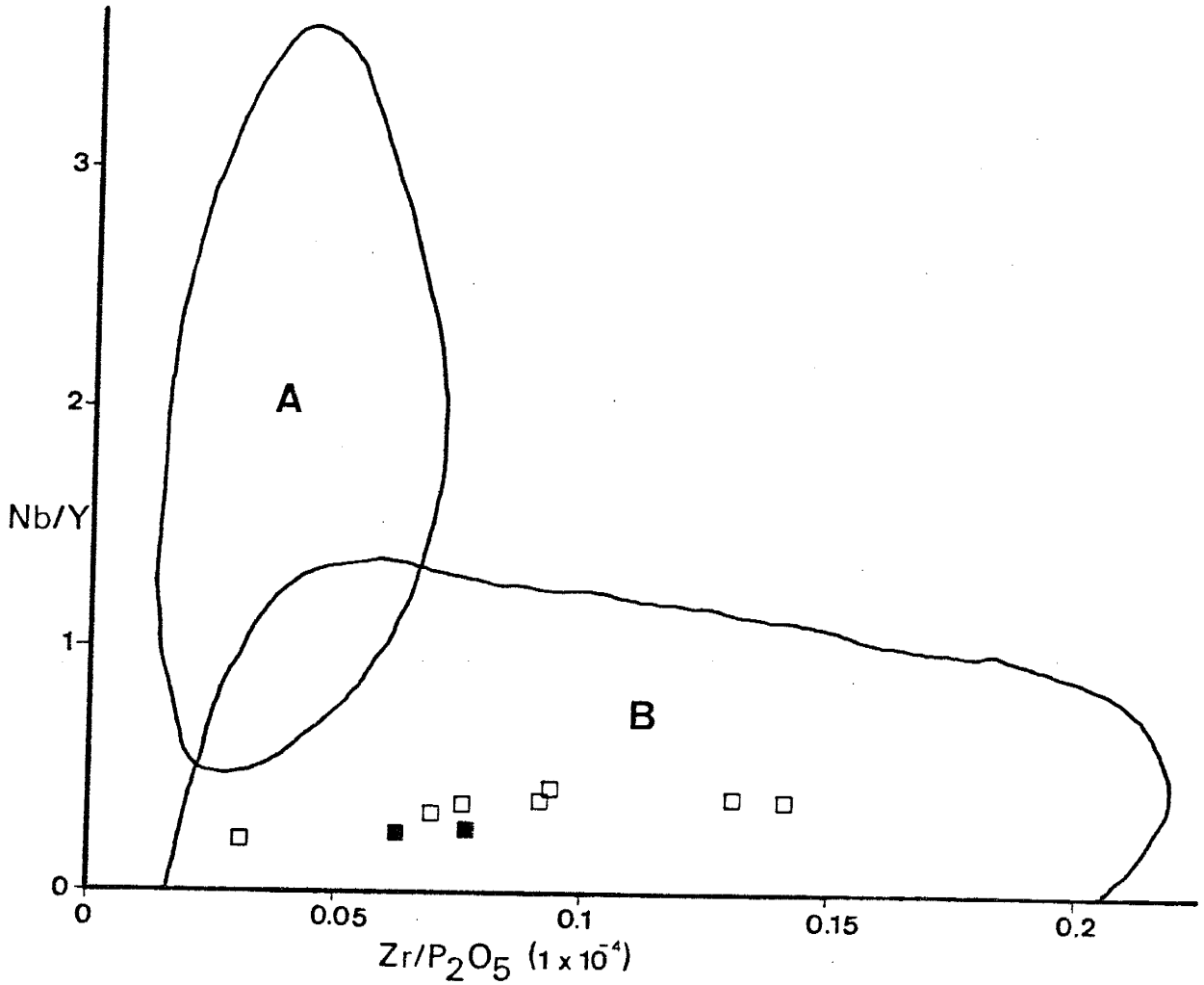

Figure G6. (Nb/Y)-(Zr/P205) diagram showing the distribution for mafic rocks from the Pedernal succession. Fields from Floyd and Winchester (1975). Symbols and fields as in figure G1.

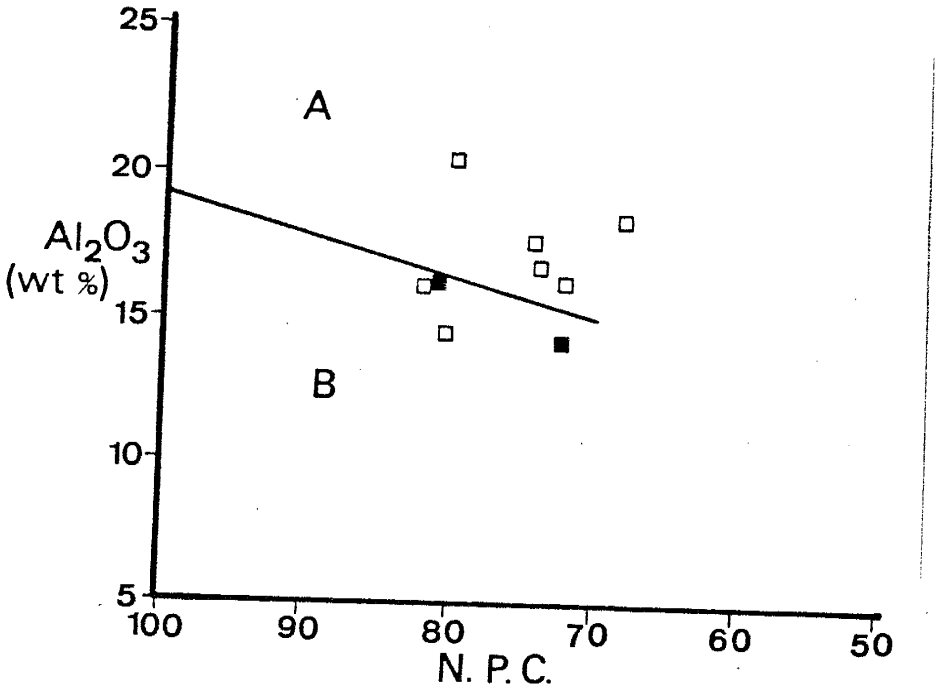

Figure G7. Al2O3-Normative plagioclase composition (NPC) diagram showing the distribution of mafic rocks from the Pedernal succession. Fields are A, calc-alkaline and B, tholeiitic (Irvine and Baragar, 1971). Symbols as in figure G1.

differentiate tholeiitic rocks from calc-alkaline rocks. This diagram holds best for individual samples that have a FeO*/MgO ratio of 2.0 to 5.0 (Miyashiro, 1974). Of the samples with the FeO*/MgO ratio of 2-5, P765 and P901 fall in the tholeiitic field and P740, P774, P769, P710, M742, M601, M723, and M758 plot in the calc-alkaline field. Below the FeO*/MgO ratio of 2.0 samples tend to converge into one area and discrimination is not as efficient (Miyashiro, 1974). P760 and P762 plot in the calc-alkline field and P772 and P792 fall in the tholeiitic field though all four samples plot close to the dividing line. Two more samples have low FeO*/MgO ratios, but also have high silica and so plot in the calc-alkaline field: P753 and P767. Above the FeO*/MgO ratio of 5.0, the fields are not well defined. M743 plots in the calc-alkaline field and P719, P720, and P969 all fall in the tholeiitic field.

Another useful diagram is the AFM plot (G9). P719, P760, P762, and P765 all plot in the tholeiitic field with P772 falling on the dividing line. P720, P969, and M743 plot towards the alkali apex were differentiation of the two series is not efficient. The rest of the samples from both sections fall in the calc-alkaline part of the diagram.

Mafic tholeiitic rocks generally have La/Yb ratios of 0.7 to 3.5 (Coulon and Thorpe, 1981). P760 has a La/Yb ratio of 2.04 and is classed as a tholeiite by the La/Yb ratio. P762 is interpreted as a tholeiite, but has a La/Yb

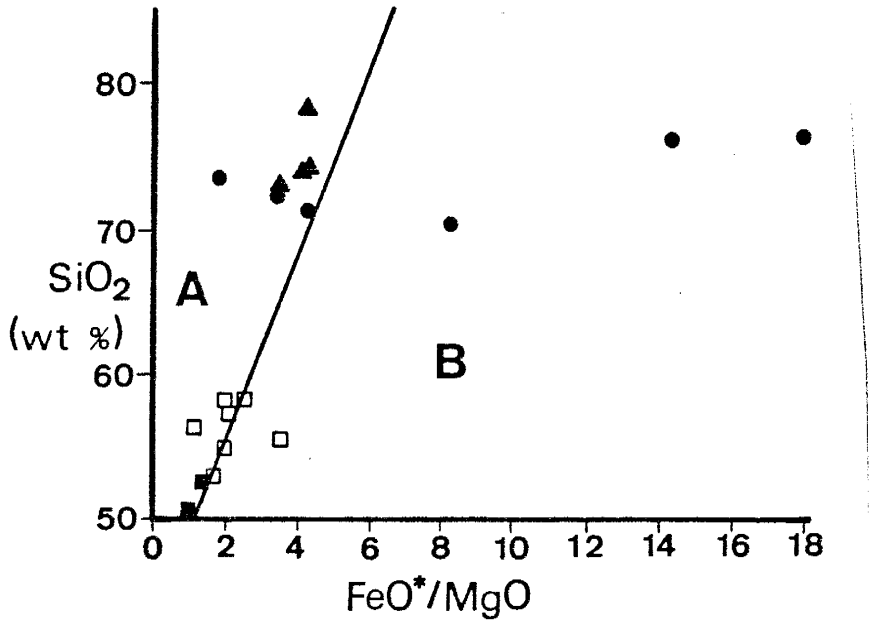

Figure G8. SiO2-(FeO*/MgO) diagram showing the distribution of volcanic rocks from both the Pedernal and the Manzano successions. Fields are A, calc-alkaline and B, tholeiitic (Miyashiro, 1974). Symbols as in figure G1.

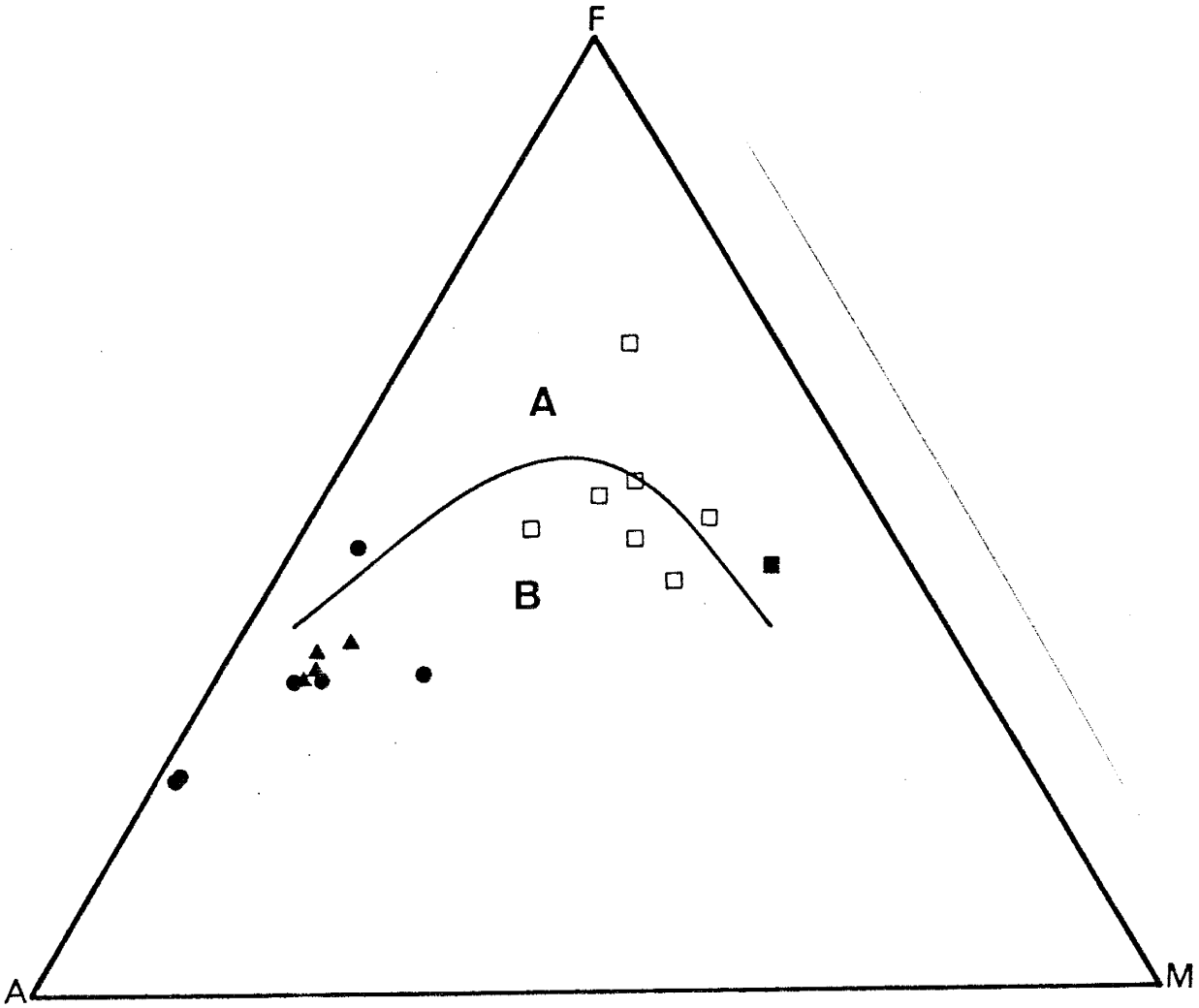

Figure G9. AFM diagram of volcanic rocks from the Pedernal and the Manzano successions. Fields are A, tholeiitic and B, calc-alkaline v(Irvine and Baragar, 1971). Symbols as in figure G1.

ratio of 5.36 and so P762 may be a trasitional rock type with characteristics of both tholeiites and calc-alkaline rocks. The other mafic and andesitic rocks have La/Yb ratios typical of calc-alkaline rocks (Coulon and Thorpe, 1981). Donnelly and Rodgers (1980) used trace elements to classify mafic rocks into tholeiitic and calc-alkaline groups. According to Donnelly and Rodgers classification, P760 is a tholeiite, P762 seems to be a transitional rock type, and the rest of the mafic and andesitic rocks from the Pedernals are calc-alkaline.

Using the last three diagrams, P719, P760, P762, and P765 are tholeiitic rock types. P719 has high modal plagioclase content (see petrographic section) and these diagrams are not strictly applicable. P765 is believed to be a calc-alkaline rock since its trace element content is similar to the other calc-alkaline andesites in the Pedernals. P720 and P969 also plot in the tholeiitic field in G8, but they have similar trace element concentrations as the other felsic calc-alkaline volcanics from the Pedernals. Only P760 and P762 are believed to be true tholeiites. The rest of the samples from both the Pedernal and Manzano sections are believed to be calc-alkaline rocks.

The next step was to assign a more specific rock name to each of the volcanic samples if possible. Several different classification schemes are used and both major element and trace element diagrams are included.

G10 is a normative color index-normative plagioclase diagram. All of the mafic and andesitic volcanics, except for P901, plot in the basalt field, with P901 falling in the andesite field. Most of the felsic volcanics from both the Pedernal and the Manzano sections plot in the dacite field, except for P720, P969, and M743, which fall in the rhyolite field, and P767, which plots in the andesite field.

Another scheme used in PETCAL is from Middlemost (1972). Middlemost divides rocks into classes based on silica: basalt class, 45-53.5%; andesite class, 53.5-62%; dacite class, 62-70%; and rhyolite class, 70% and over. The PETCAL program recalculates the major element analyses of each sample to 100 % on a volatile free basis. By this method, P760, P762, and P792 are classed as basalts. Using the Na2O+K2O contents of the samples, all three basalts are subalkaline. Based on Al2O3 content, P792 is a high-alumina basalt and P760 and P762 are both tholeiitic basalts. P740, P765, P772, P774, P775, and P901 all fall in the andesite class and are all subalkaline according to their total alkalies content. P765, P774, and P775 are icelandites and P740, P772, and P901 are andesites, all by the alumina contents of each sample. The felsic volcanics from both sections fall in the rhyolite class. The rhyolite class can be further divided into high and low lime rhyolites by CaO content (1 % CaO is the dividing line). All of the felsic volcanics from the Manzano

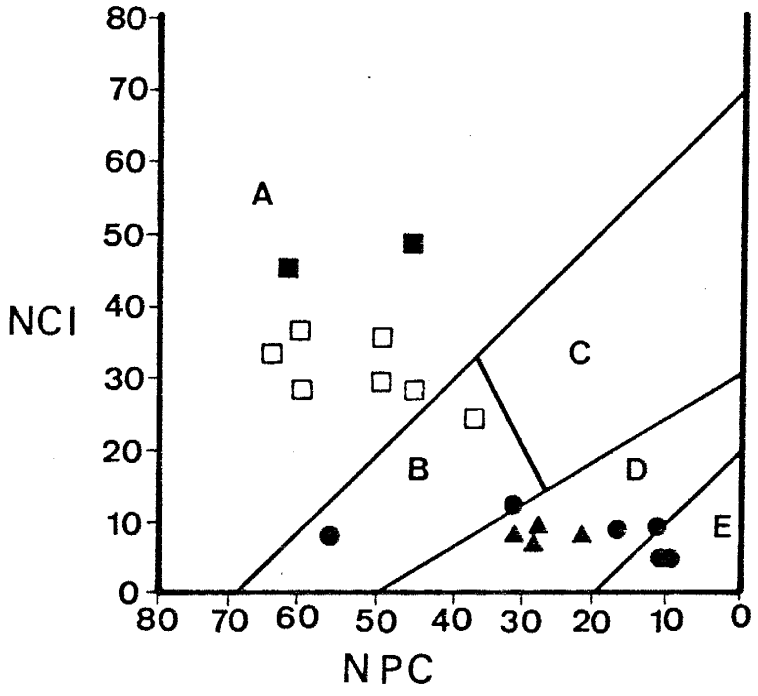

Figure G10. Normative color index (NCI)-Normative plagioclase composition (NPC) diagram showing the distribution of volcanic rocks from both the Pedernal and the Manzano successions. Fields are A, basalt; B, andesite; C, tholeiitic andesite; D, dacite; and E, rhyolite (Irvine and Baragar, 1971). Symbols as in figure G1.

section and samples P719, P767, and P769 from the Pedernal section are high-lime rhyolites. P710, P720, P753, and P969 are all low-lime rhyolites.

Figure G11 is based on Peccerillo and Taylor (1976). P762 plots in the low-K basalt field, P760 and P765 plot in the low-K basaltic-andesite field, and P740 plots in the low-K andesite field. P792 falls in the basaltic andesite field, P774 and P901 fall in the andesite field, P772 falls in the high-K basaltic-andesite field and P775 falls in the high-K andesite field. M601, M743, and M758 all plot in the low-K rhyolite field and the rest of the felsic volcanics from both the Manzano and the Pedernal sections plot in the rhyolite field.

G12 to G14 are trace element diagrams from Winchester and Flyod (1977). In G12, volcanic samples plot in the basaltic-andesite to rhyolite fields and in G13 and G14, samples fall in the basalt to rhyolite fields. P792 plots in the alkaline basalt field and P775 falls in the trachyandesite fields in G14. Since both samples are subalkaline, P792 would classed as a basalt and P775 as an andesite using this diagram. By looking at all three diagrams (G12-G14), the volcanic samples can be assigned a specific rock name: P760, P762, P792 are basalts; P740, P765, P772, P774, P775, and P901 are andesites; P719, P769, P710, P767, and M742 are rhyodacite; and P720, P753, P969, M743, M758, M723, and M601 are rhyolites.

G15 is a Jensen cation diagram that can be used for

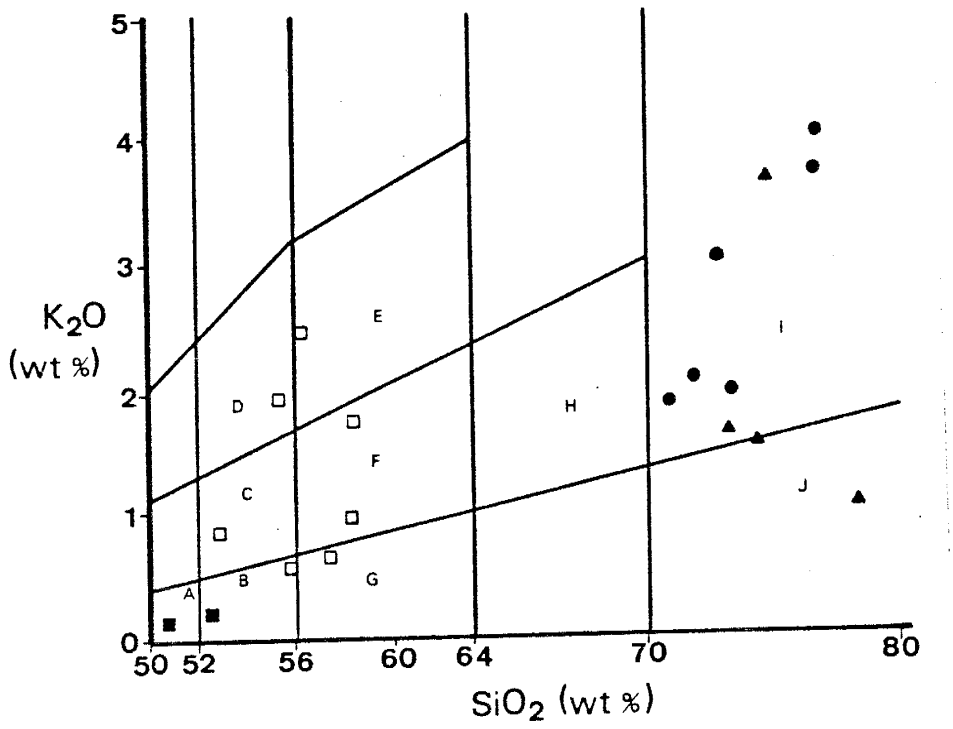

Figure G11. K2O-SiO2 diagram showing the distribution of volcanic rocks from the Pedernal and the Manzano successions. Fields are A, low K basalt; B, low K basaltic andesite; C, basaltic andesite; D, high K basaltic andesite; E, high K andesite; F, andesite; G, low K andesite; H, dacite; I, rhyolite; and J, low K rhyolite (Peccerillo and Taylor, 1976). Symbols as in figure G1.

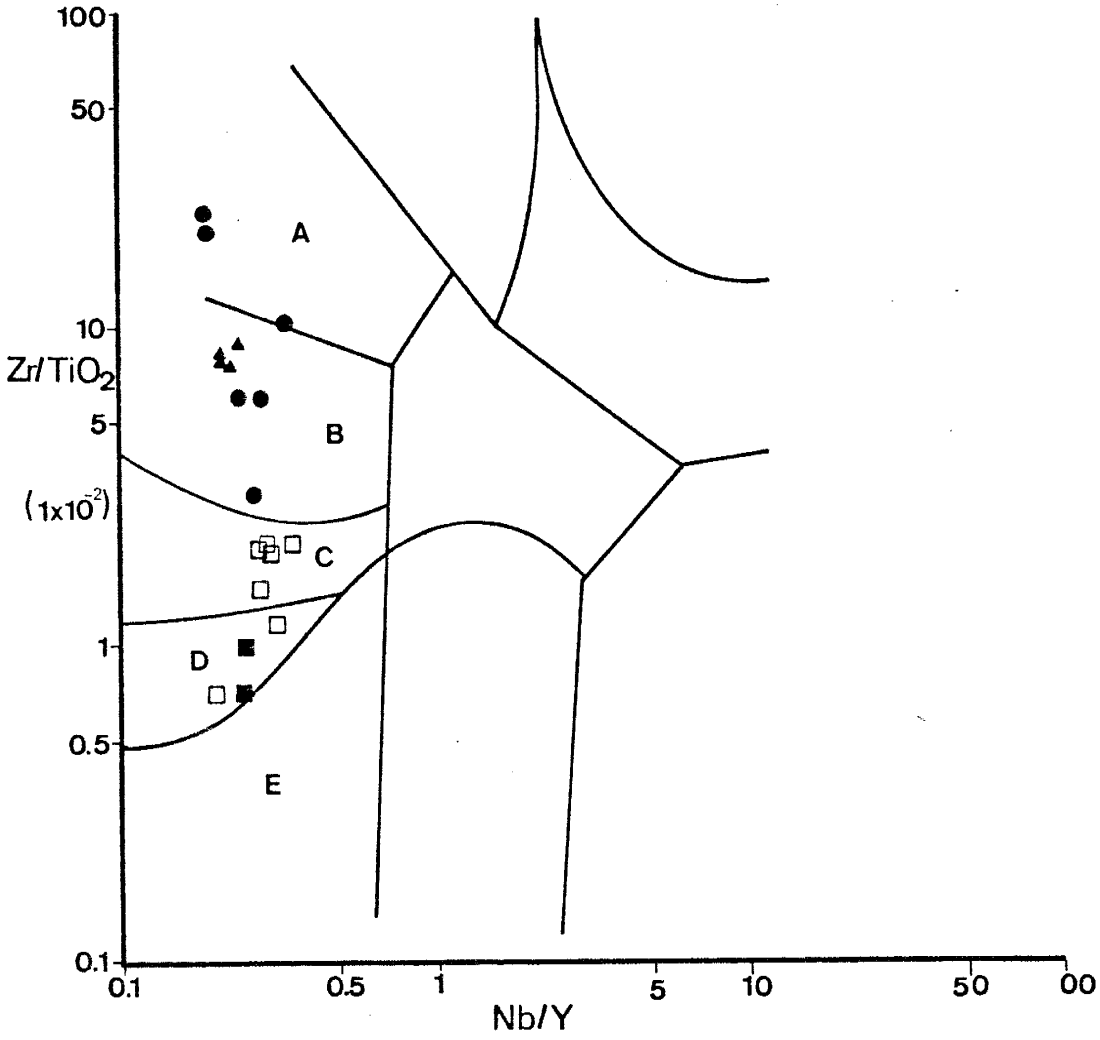

Figure G12. (Zr/TiO2)-(Nb/Y) diagram showing the distribution of volcanic rocks from both the Pedernal and the Manzano successions. Fields are A, rhyolite; B, dacite; C, andesite; D, basaltic andesite; and E, basalt (Winchester and Floyd, 1977). Symbols as in figure G1.

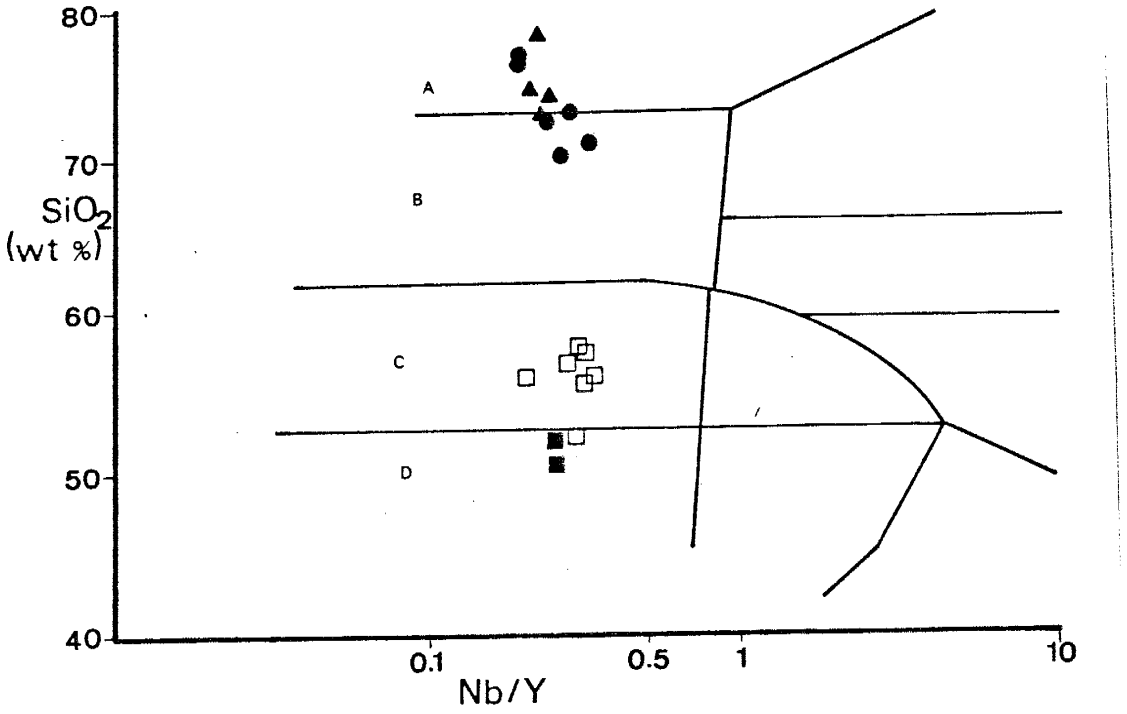

Figure G13. SiO2-(Nb/Y) diagram showing the distribution of volcanic rocks from the Pedernal and the Manzano successions. Fields are A, rhyolite; B, dacite; C, andesite; and D, basalt (Winchester and Floyd, 1977). Symbols as in figure G1.

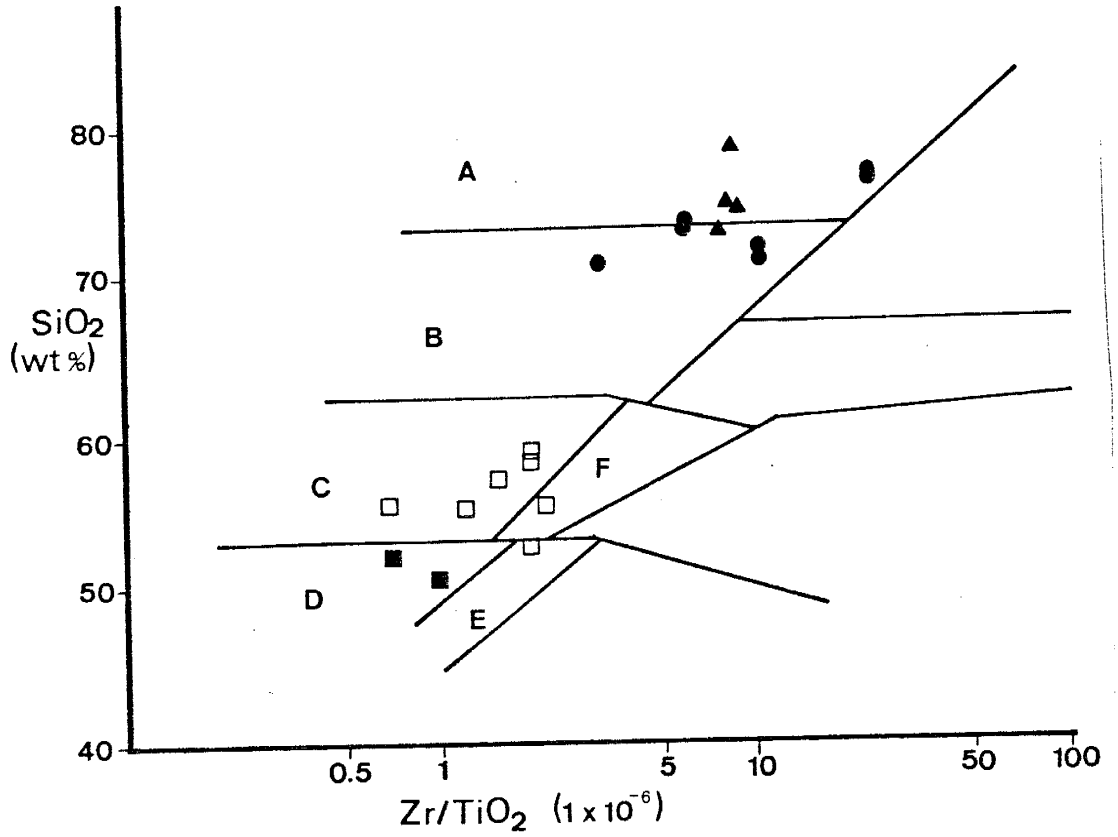

Figure G14. SiO2-(Zr/TiO2) diagram showing the distribution of volcanic rocks from both the Pedernal and the Manzano successions. Fields are A, rhyolite; B, dacite; C, andesite; D, subalkaline basalt; E, alkaline basalt; and F, trachyandesite (Winchester and Floyd, 1977). Symbols as in figure G1.

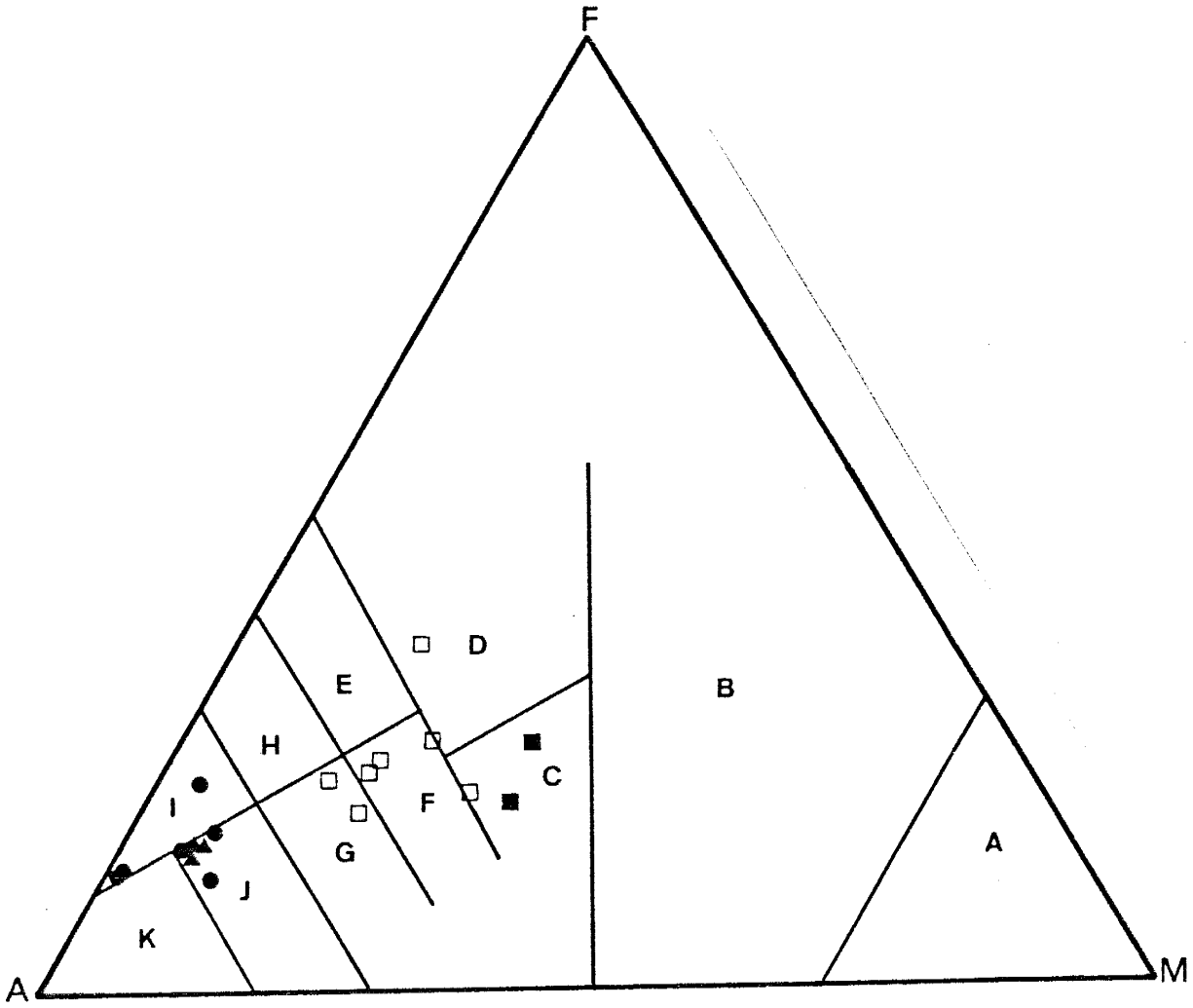

Figure G15. Jensen cation diagram showing the distribution of volcanic rocks from the Pedernal and the Manzano successions. A is Al2O3, F is FeO+Fe2O3+TiO2, and M is MgO. Fields are A, ultramafic komatiite; B, basaltic komatiite; C, high-Mg tholeiitic basalt; D, high-Fe tholeiitic basalt; E, tholeiitic basalt; F, calc-alkaline basalt; G, calc-alkaline andesite; H, tholeiitic andesite; I, tholeiitic rhyolite; J, calc-alkaline dacite; and K, calc-alkaline rhyolite (Jensen, 1976). Symbols as in figure G1.

subalkaline volcanic rocks. Three samples plot in the high-Mg tholeiite field (P760, P762, and P775) and one sample plots in the high-Fe tholeiite field (P765). Four samples fall in the calc-alkaline basalt field: P753, P774, P740, and P772. P753 is believed to be an altered sample (see discusion in Geochemistry section). P792 and P901 plot in the calc-alkaline andesite field. Seven samples fall in the calc-alkaline dacite field: P710, P767, P769, M601, M723, M742, and M758. M743 plots in the calc-alkaline rhyolite field and P719, P720, and P969 plot in the tholeiitic rhyolite field.

On figure G16 not all of the samples plot within the defined fields. The fields encompass two thirds of the data points used to construct this diagram and it should be expected that some samples would fall outside the fields (Church, 1975). The basalts and andesites from the Pedernal section plot in or near the basalt field and extend into the upper part of the andesite field. The felsic volcanics from the Manzano and Pedernal sections plot in or near the dacite, rhyolite, andesite, and trachyte fields. Since the rocks are subalkaline, none of the samples are classified as trachytes.

G17 is an An-Ab'-Or diagram used to distinguish K-poor, K-rich, and normal K rocks. The data from the Pedernals and Manzanos is scattered thourghout the diagram. The scatter may be related to the mobility of K or it may be a primary feature of the rocks.

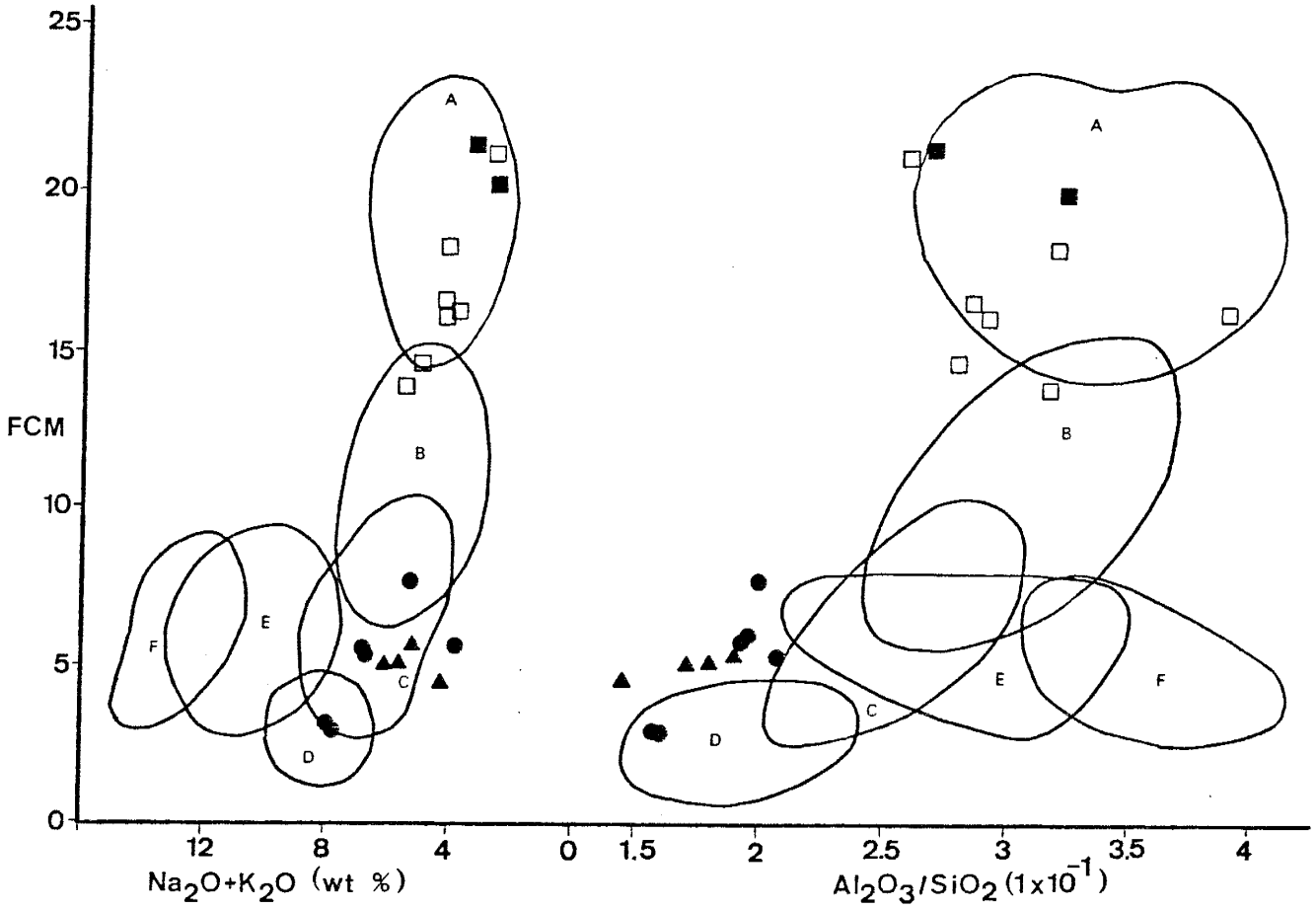

Figure G16. a.) (Fe2O3*+1/2(CaO+MgO))-(Na2O+K2O) diagram. b.)(Fe2O3*+1/2(CaO+ MgO))-(Al2O3/SiO2) diagram. Both diagrams show the distribution of volcanic rocks from the Pedernal and the Manzano successions. Fields are A, basalt; B, andesite; C, dacite; D, rhyolite; E, trachyte; and F, phonolite (Church, 1975). Symbols as in figure G1.

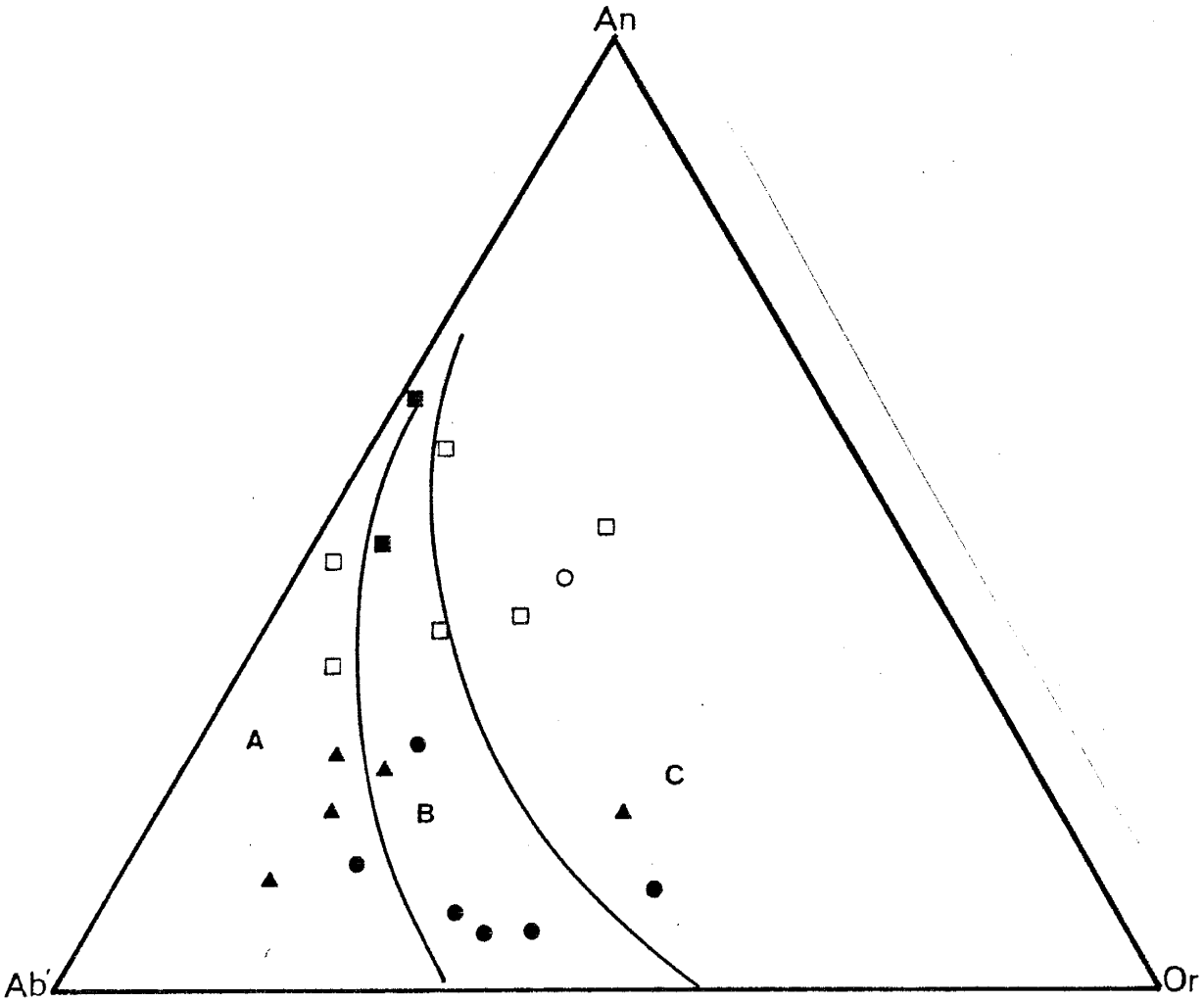

Figure G17. An-Ab'-Or diagram showing the distribution of volcanic rocks from both the Pedernal and the Manzano successions. Fields are A, K-poor; B, normal; and C, K-rich (Irvine and Baragar, 1971). Symbols as in figure G1.

APPENDIX H

MORB NORMALIZED GRAPHS OF MODERN VOLCANICS

This appendix presents graphs for modern volcanics from known tectonic environments: mid-ocean ridge, within plate, island-arc, and continental-arc. The normalizing values are from Pearce (1983). Data was compiled from the literature and sources are listed in a Table (H1) at the end of this appendix.

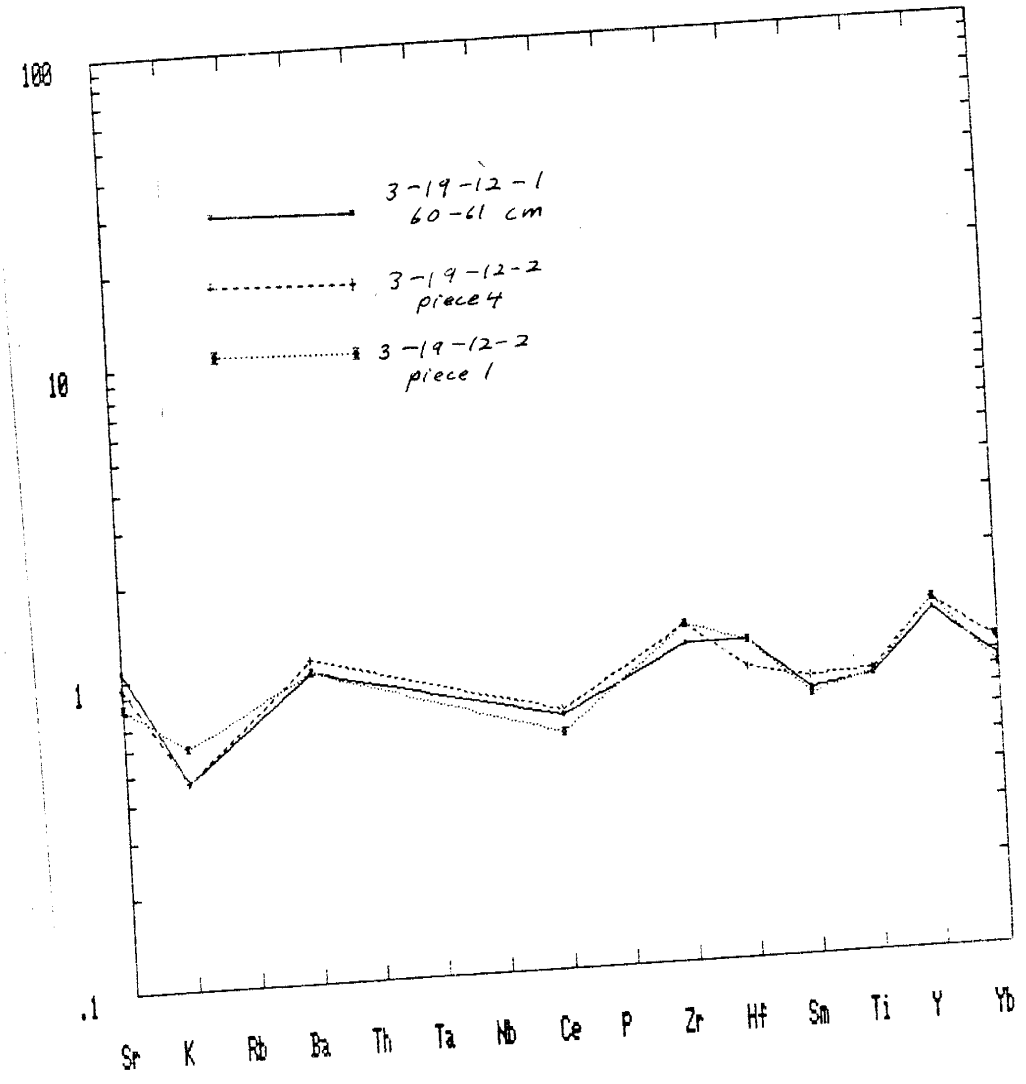

Figure H1. MORB samples. MORB-normalized spider diagram of three samples from the Mid-Atlantic Ridge.

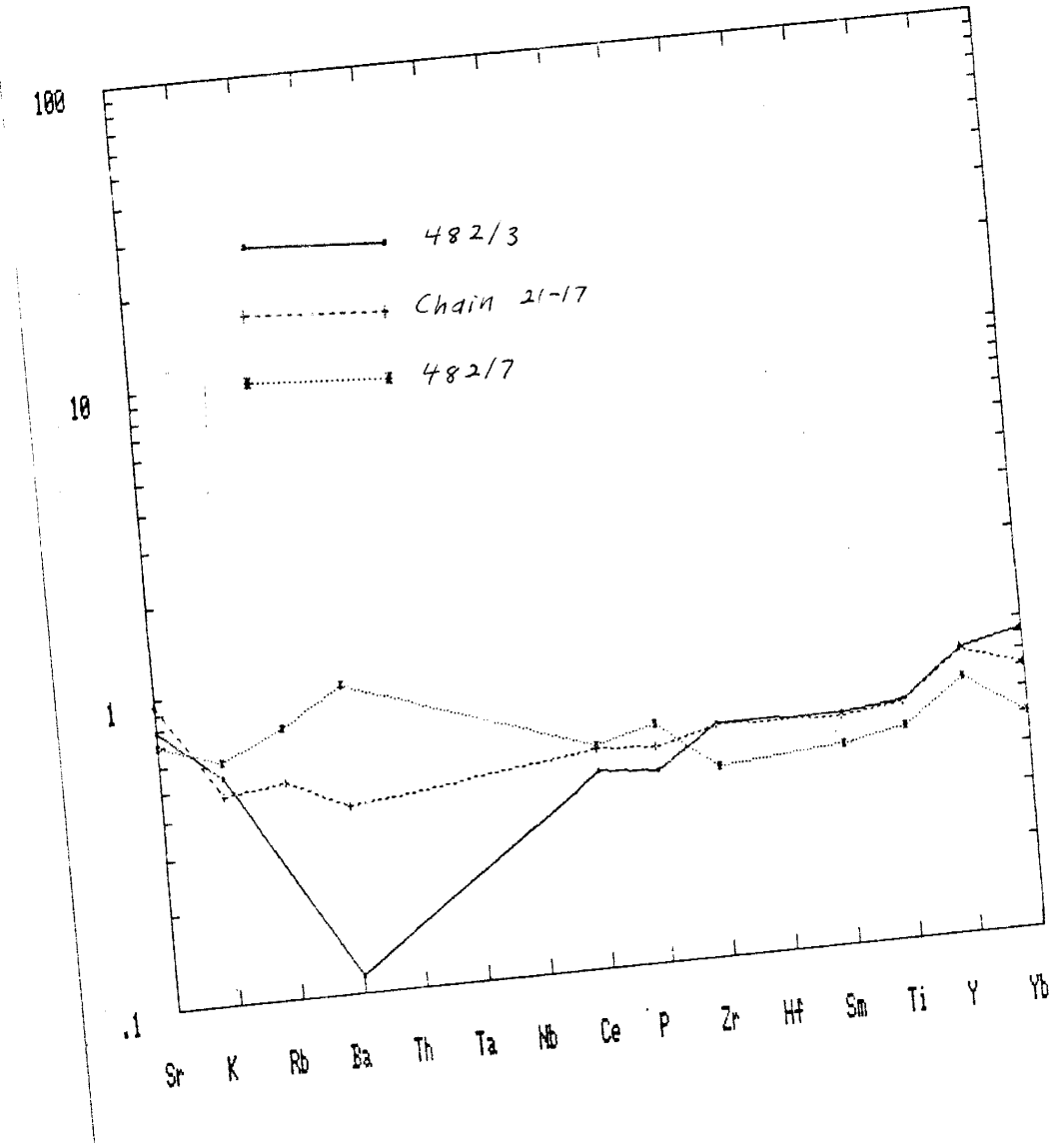

Figure H2. MORB samples. MORB-normalized spider diagram of three samples from the Mid-Atlantic Ridge.

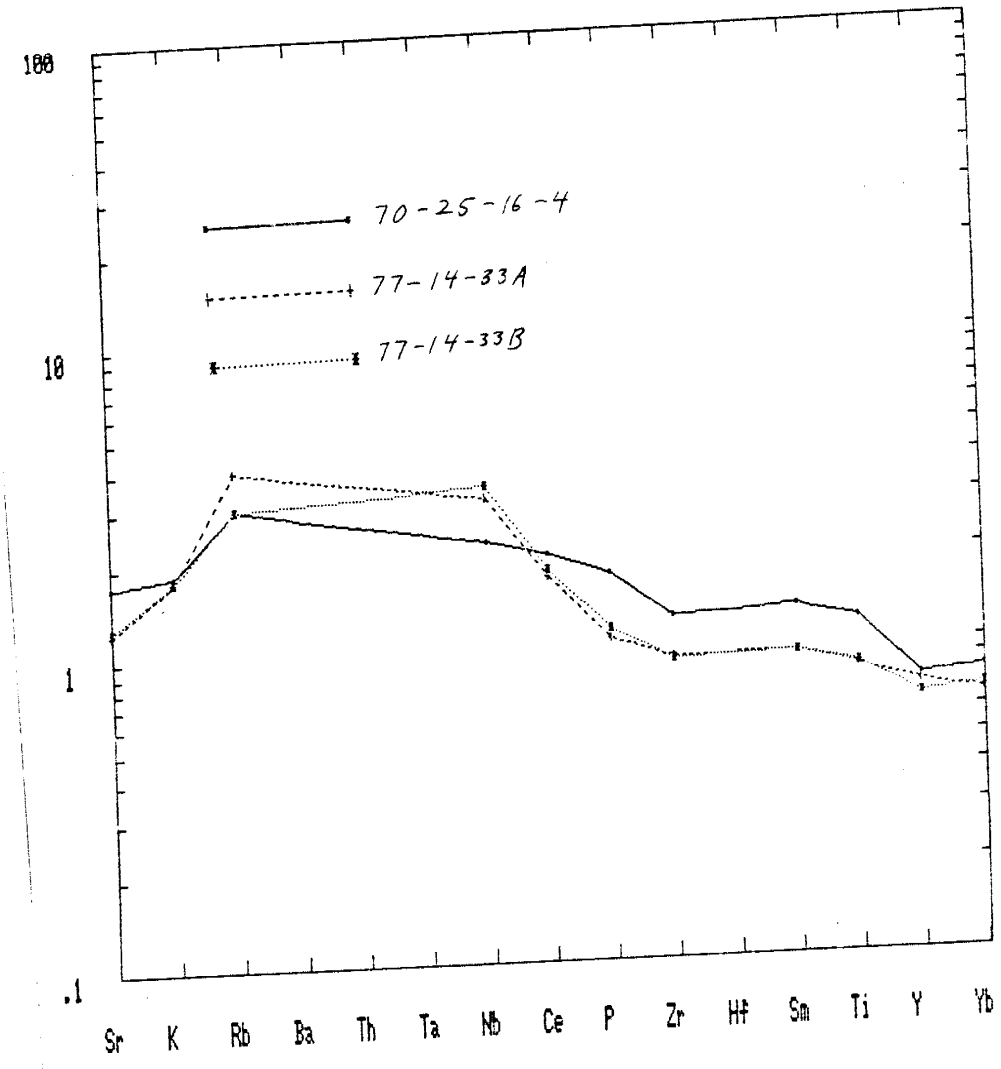

Figure H3. MORB samples. MORB-normalized spider diagram of three samples from Explorer Ridge, Pacific Ocean.

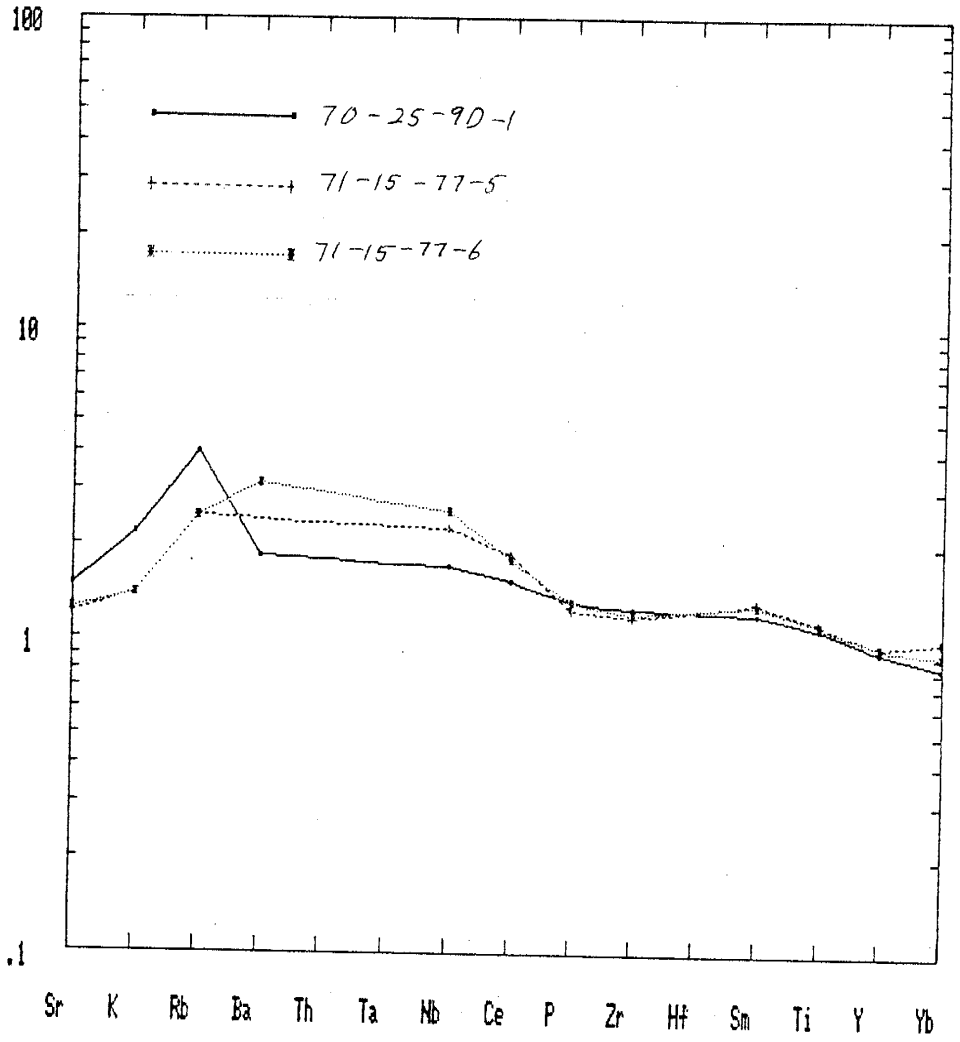

Figure H4. MORB samples. MORB-normalized spider diagram of three samples from Explorer Ridge, Pacific Ocean.

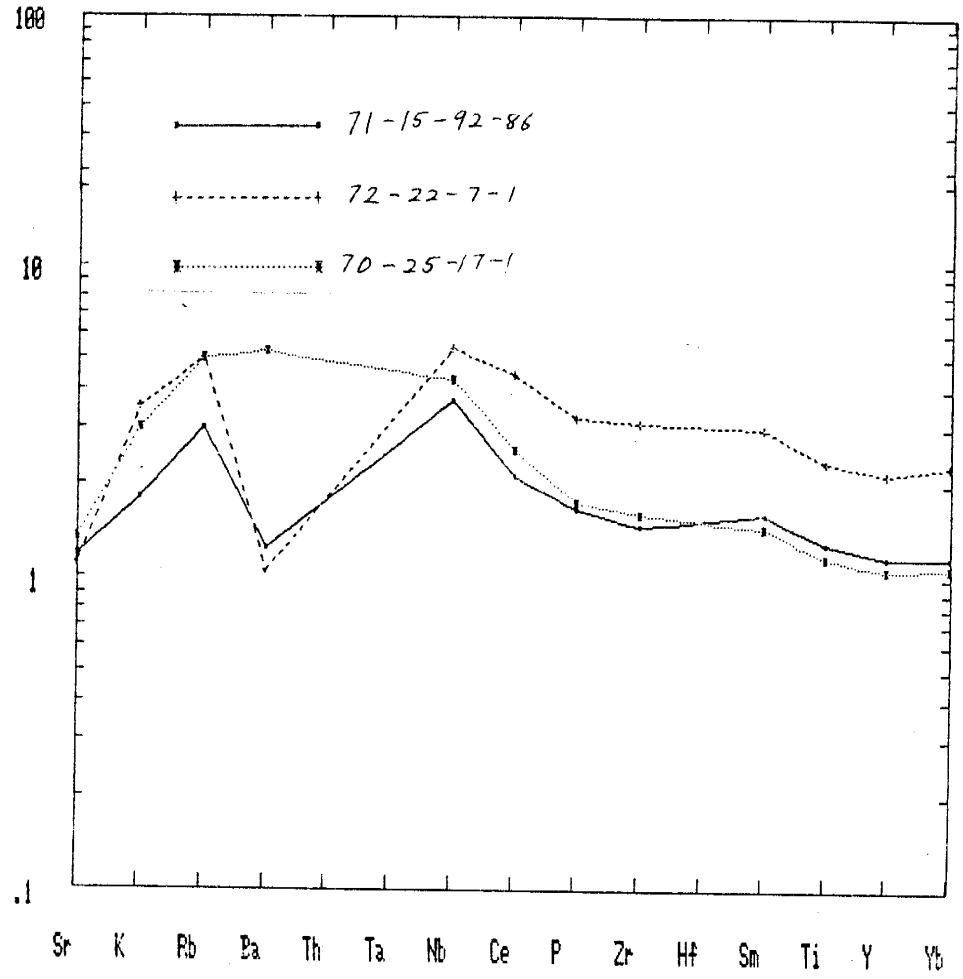

Figure H5. MORB samples. MORB-normalized spider diagram of three samples from Explorer Ridge, Pacific Ocean.

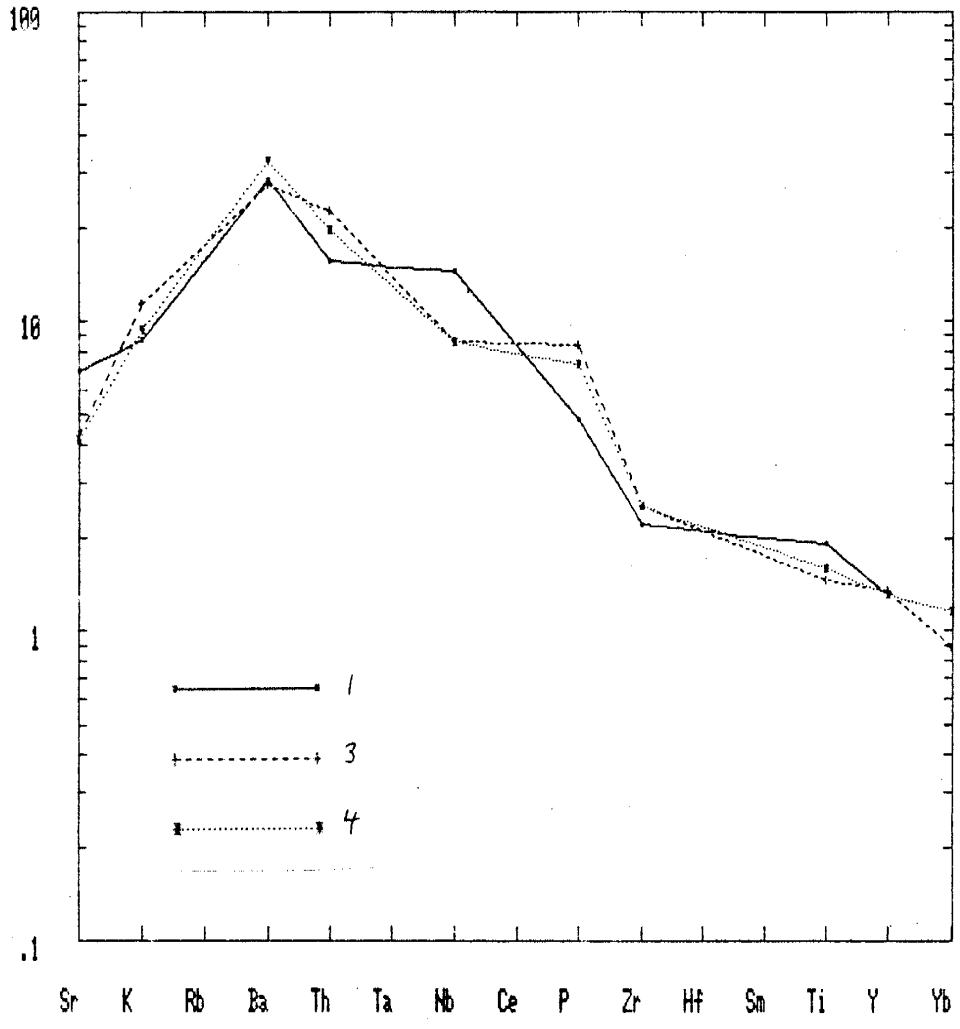

Figure H6. Within plate samples. MORB-normalized spider diagram of three samples from Mount Taylor, New Mexico.

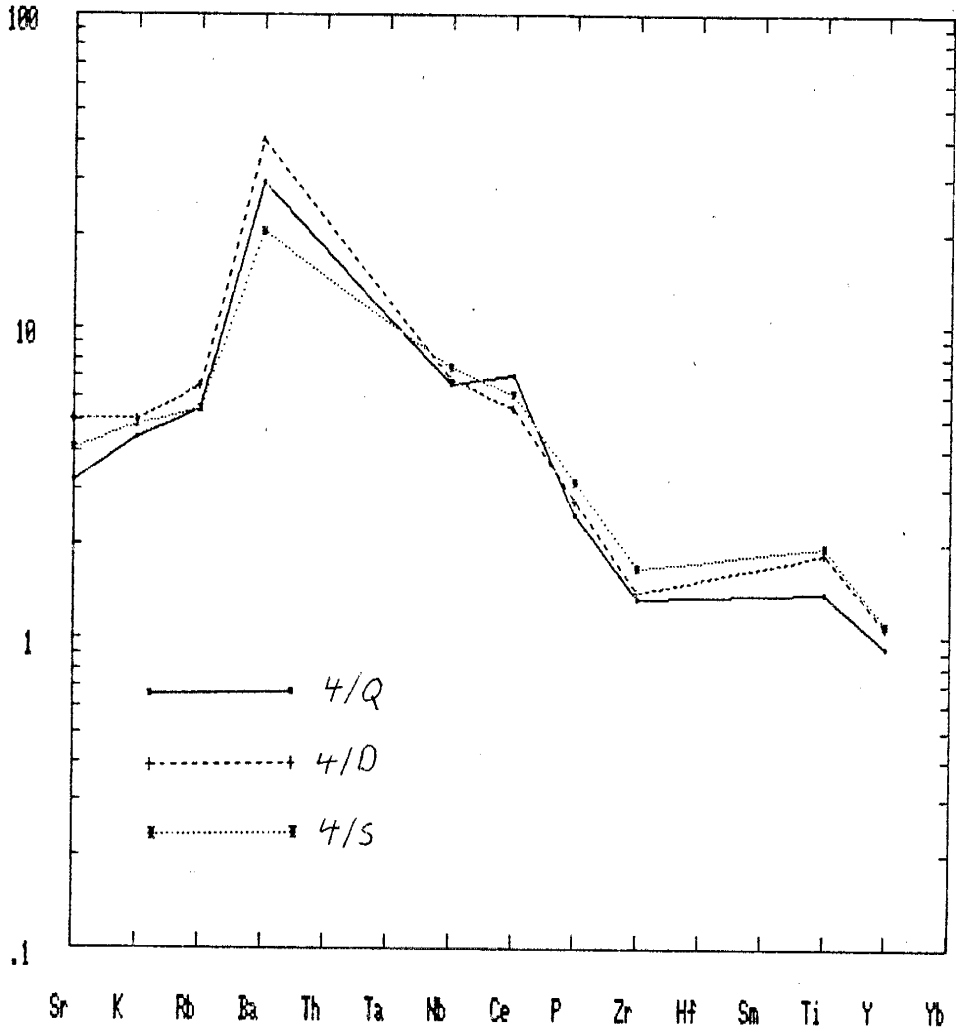

Figure H7. Within plate samples. MORB-normalized spider diagram of three samples from Gregory Rift, Kenya.

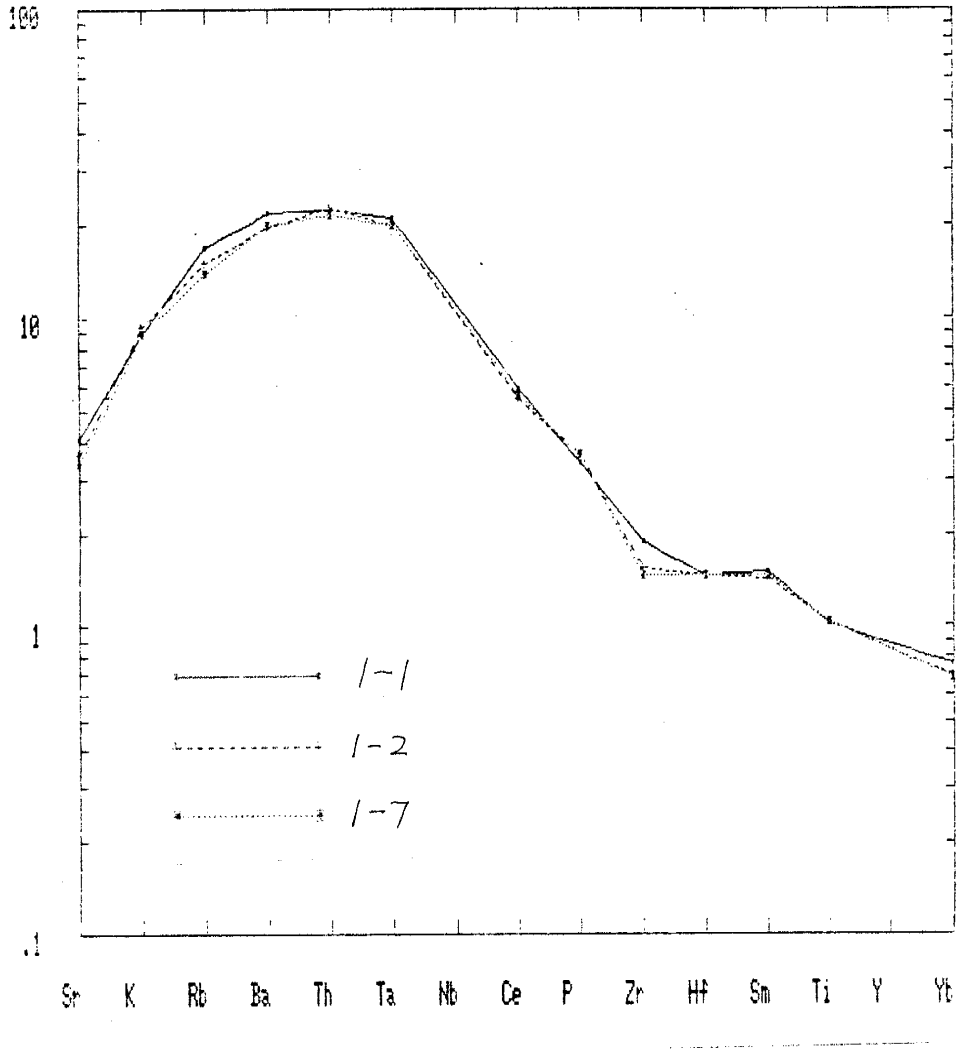

Figure H8. Within plate samples. MORB-normalized spider diagram of three samples from Mathematician Ridge, Indian Ocean.

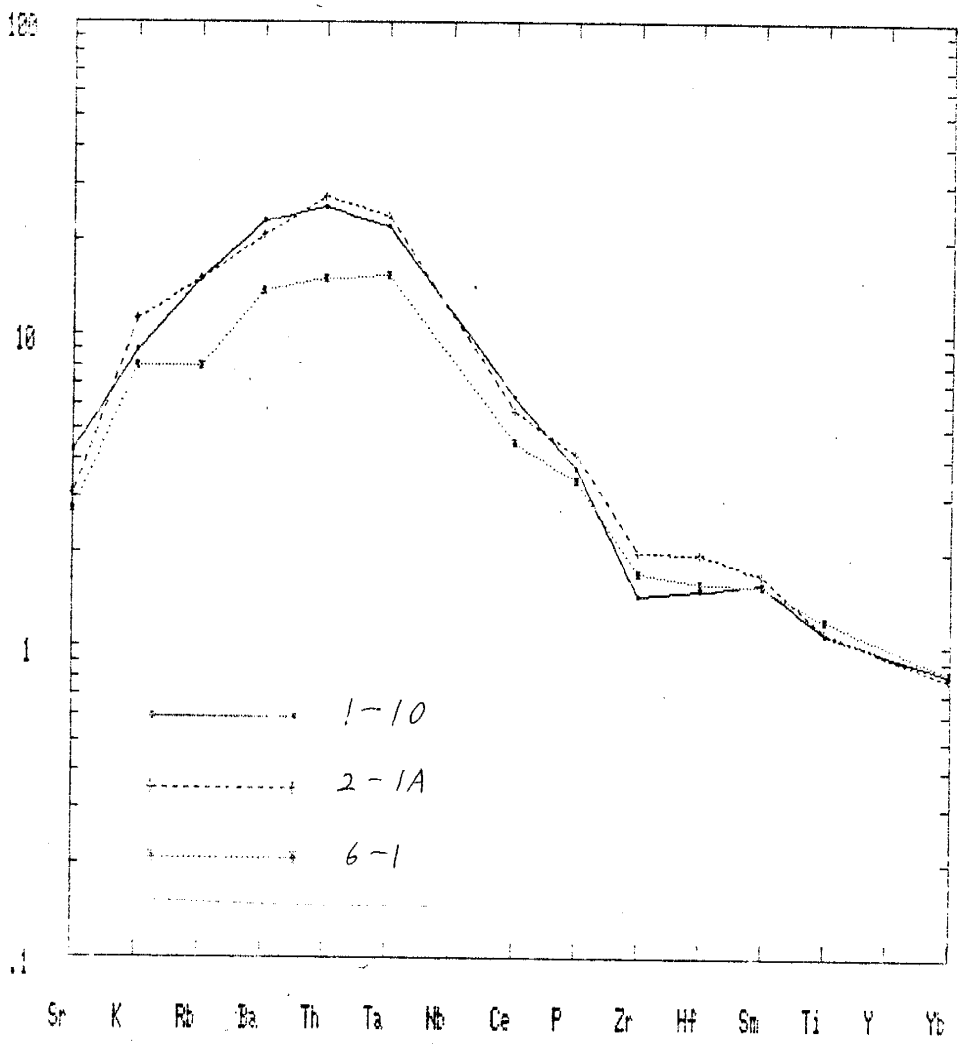

Figure H9. Within plate samples. MORB-normalized spider diagram of three samples from Mathematician Ridge, Indian Ocean.

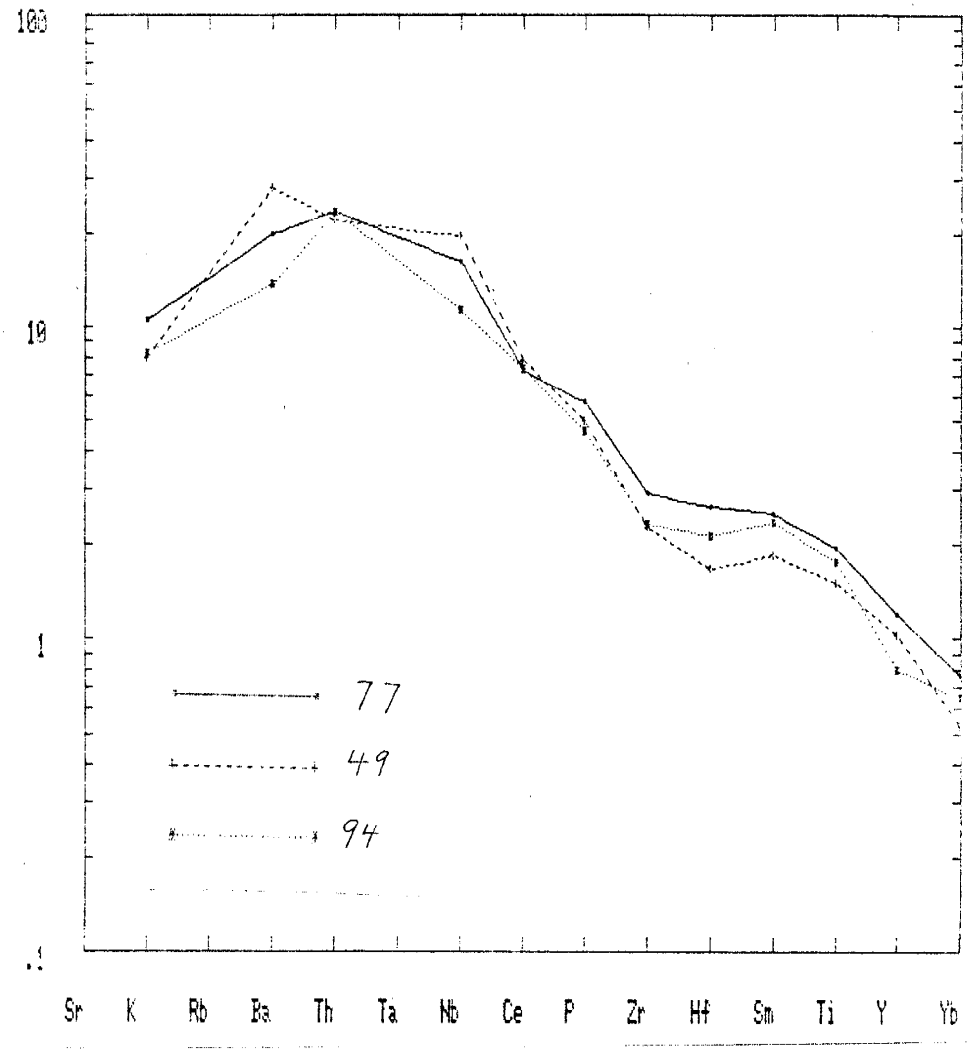

Figure H10. Within plate samples. MORB-normalized spider diagram of three samples from South Island New Zealand.

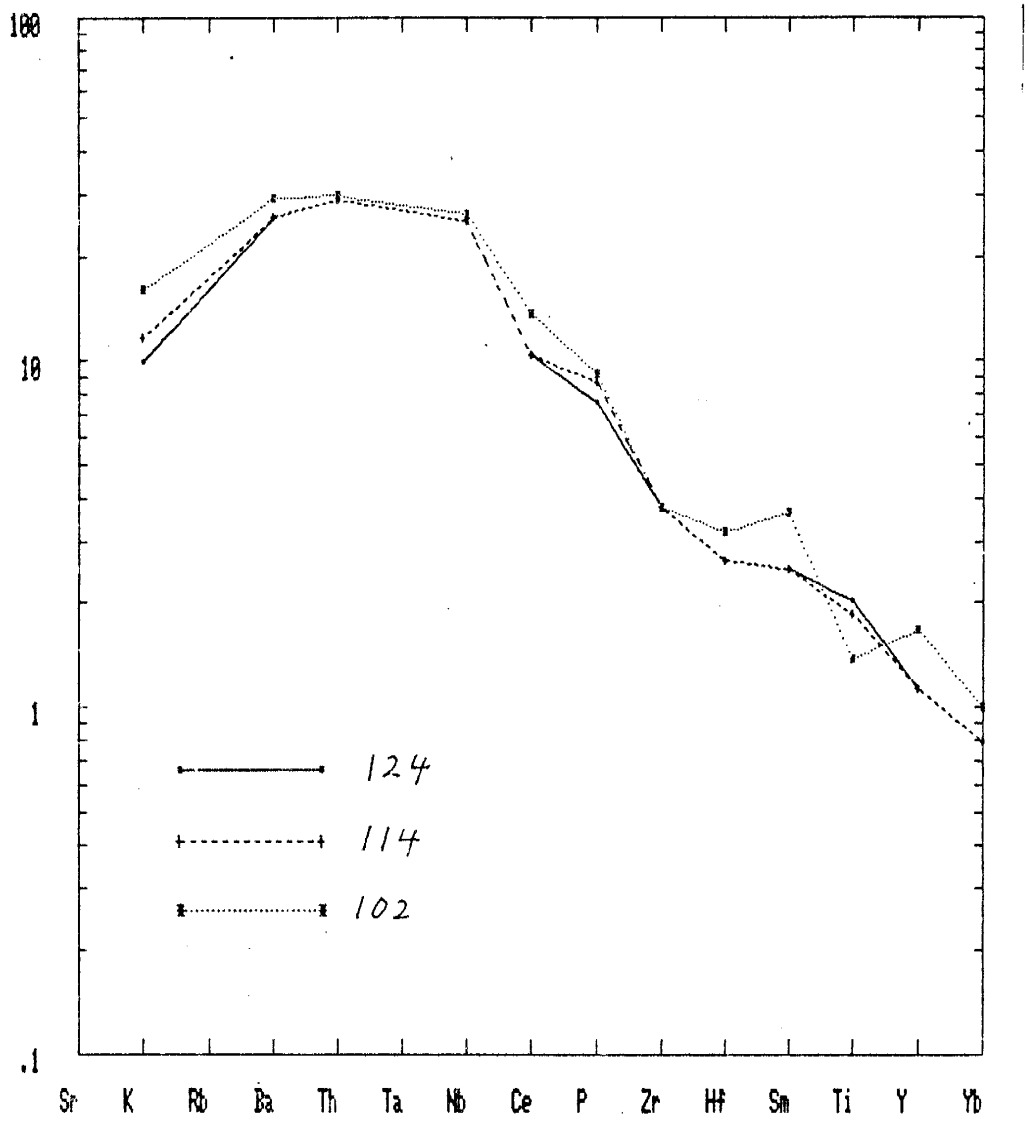

Figure H11. Within plate samples. MORB-normalized spider diagram of three samples from South Island, New Zealand.

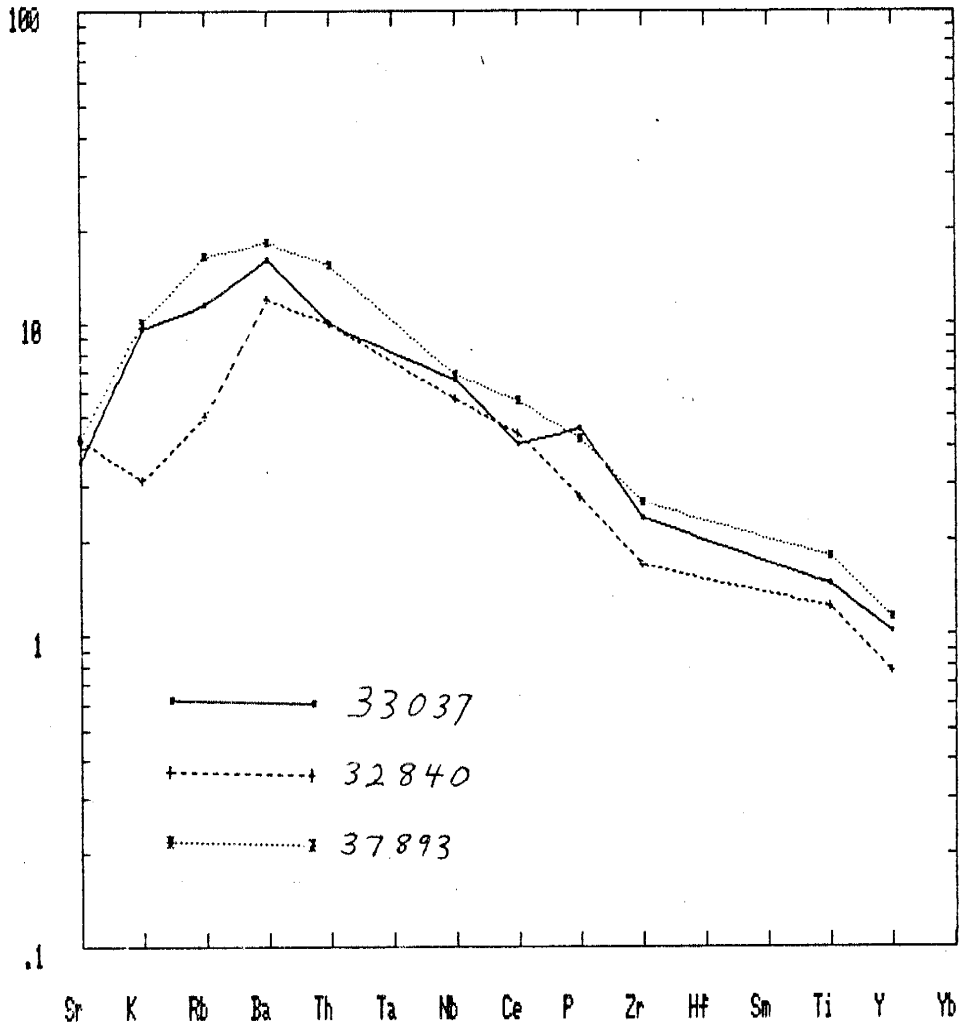

Figure H12. Within plate samples. MORB-normalized spider diagram of three samples from South Queensland, Australia.

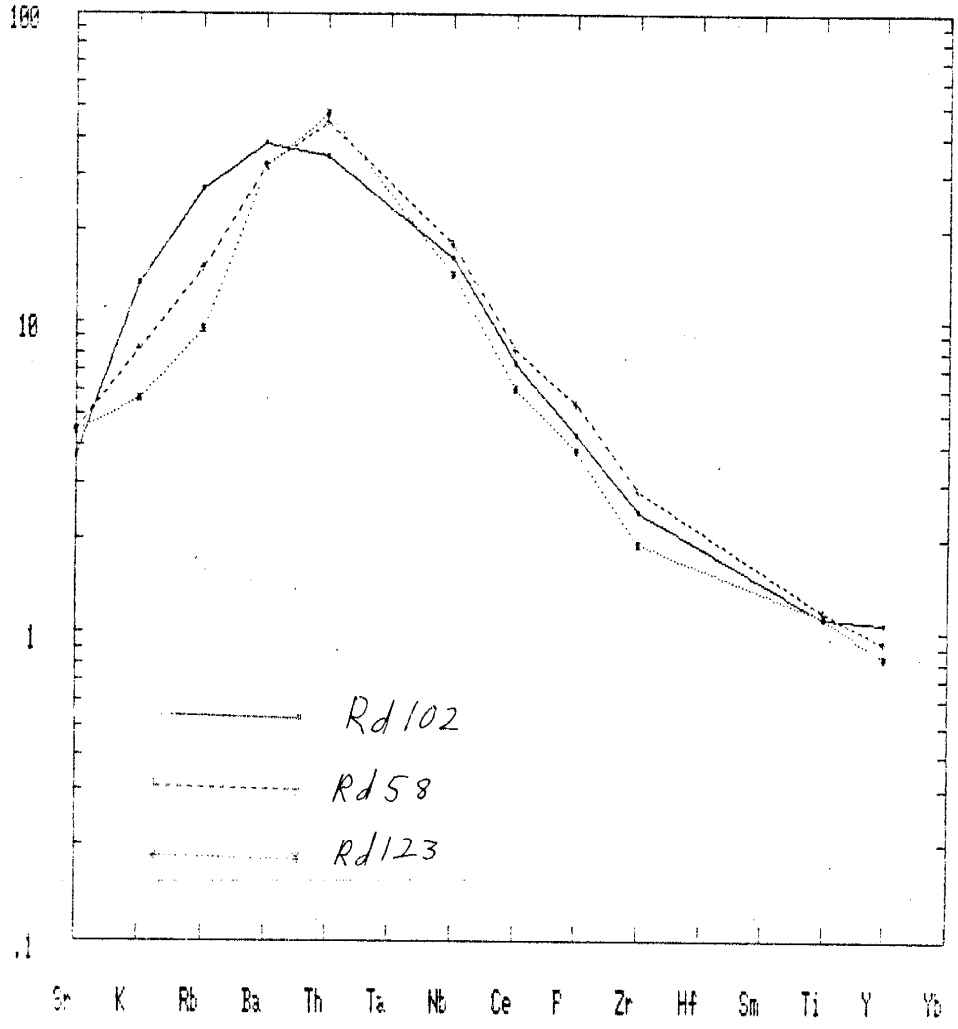

Figure H13. Within plate samples. MORB-normalized spider diagram of three samples from Rodrigues Island, Indian Ocean.

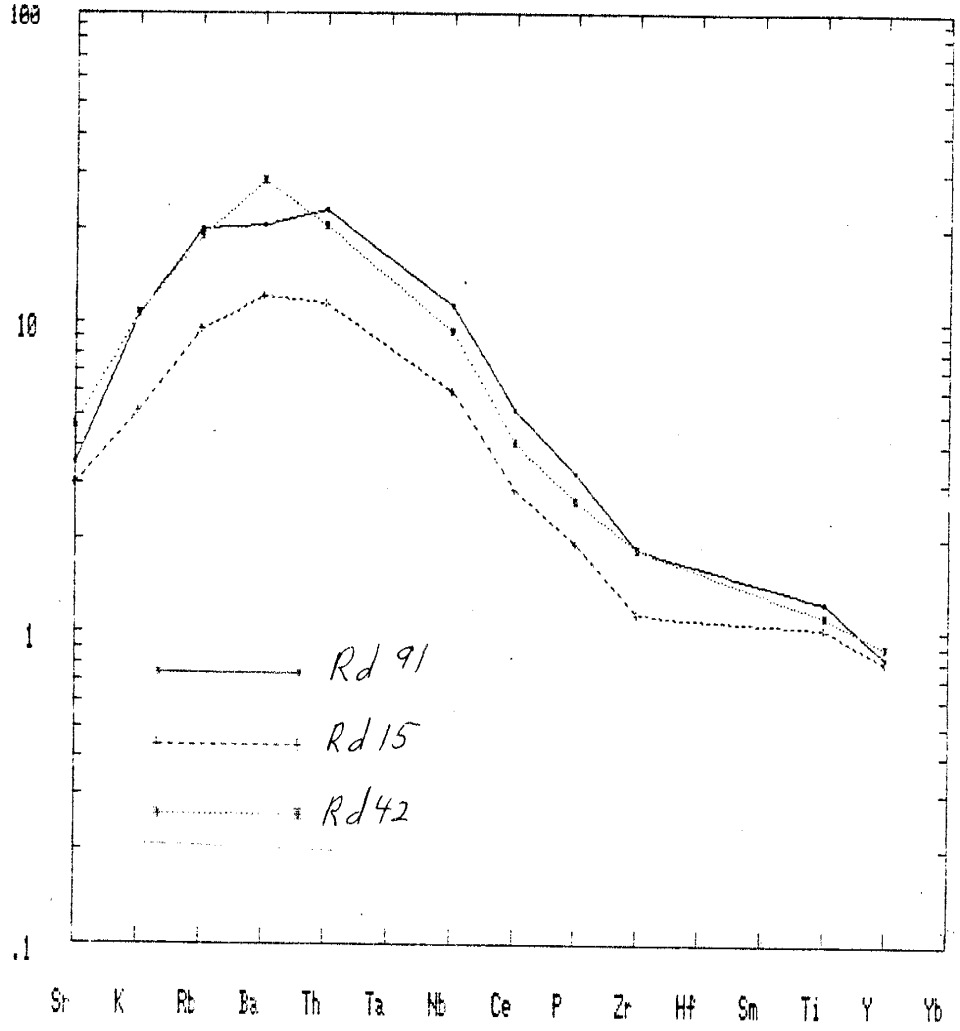

Figure H14. Within plate samples. MORB-normalized spider diagram of three samples from Rodrigues Island, Indian Ocean.

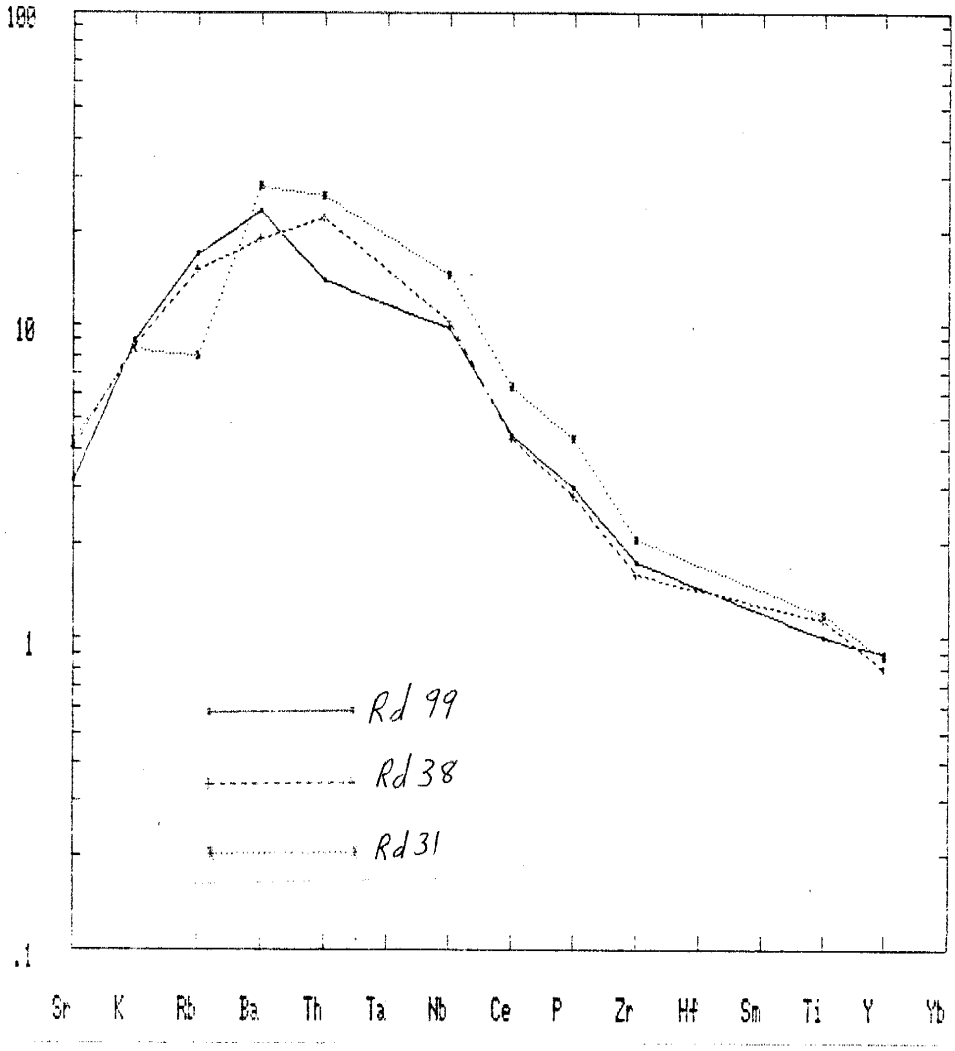

Figure H15. Within plate samples. MORB-normalized spider diagram of three samples from Rodrigues Island, Indian Ocean.

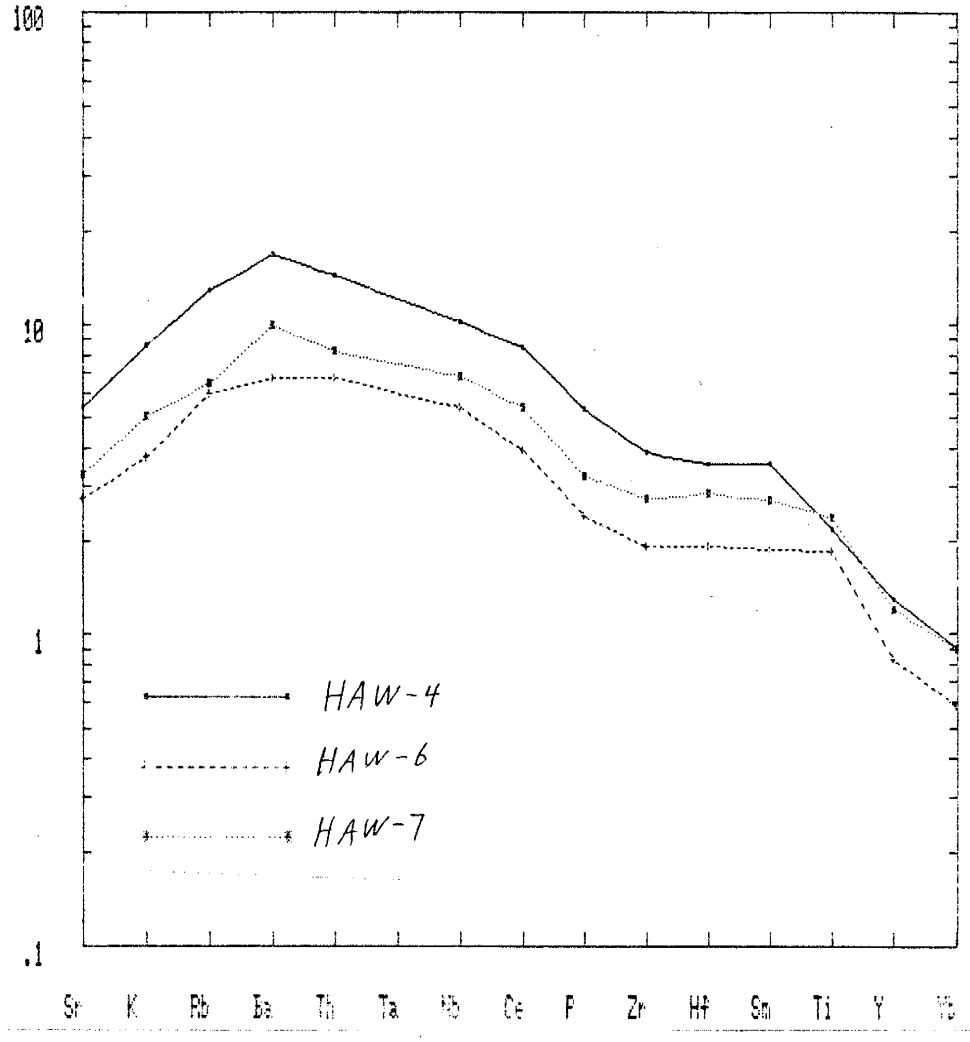

Figure H16. Within plate samples. MORB-normalized spider diagram of three samples from Hawaii.

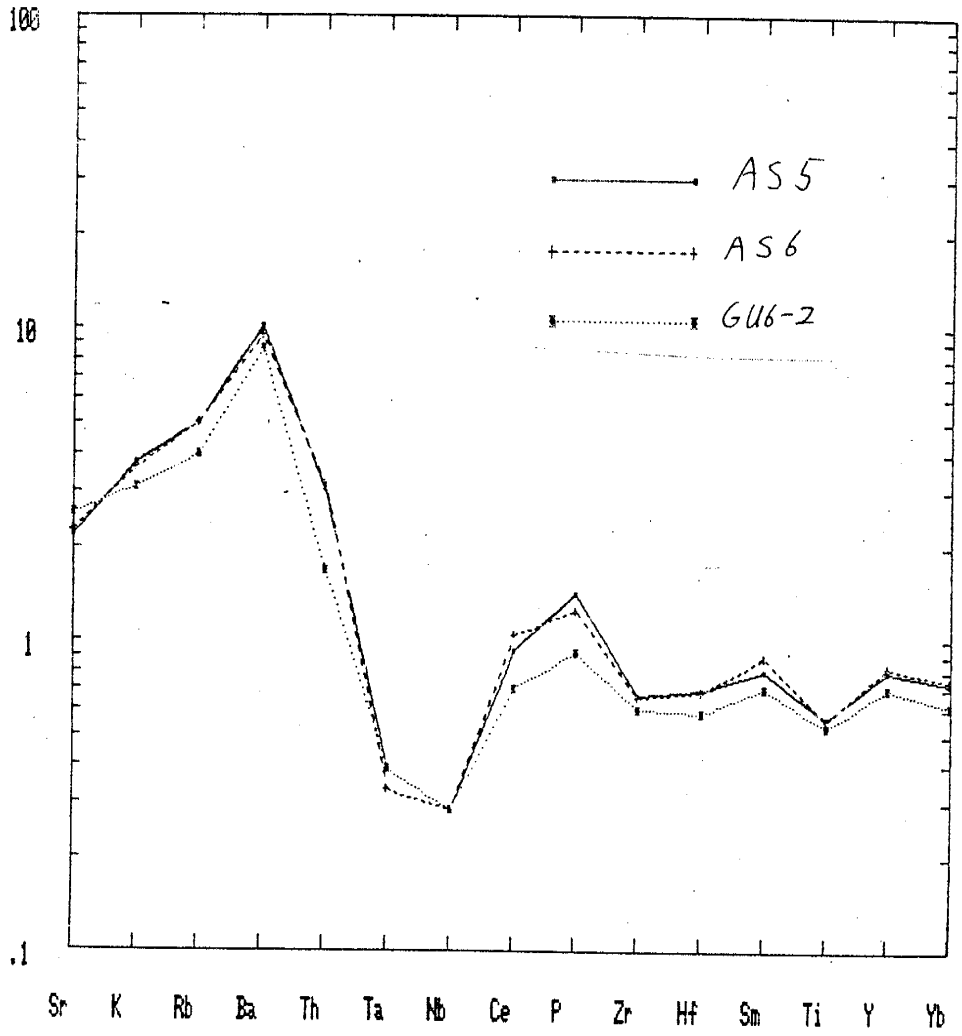

Figure H17. Island-arc samples. MORB-normalized spider diagram of three samples from Mariana Islands.

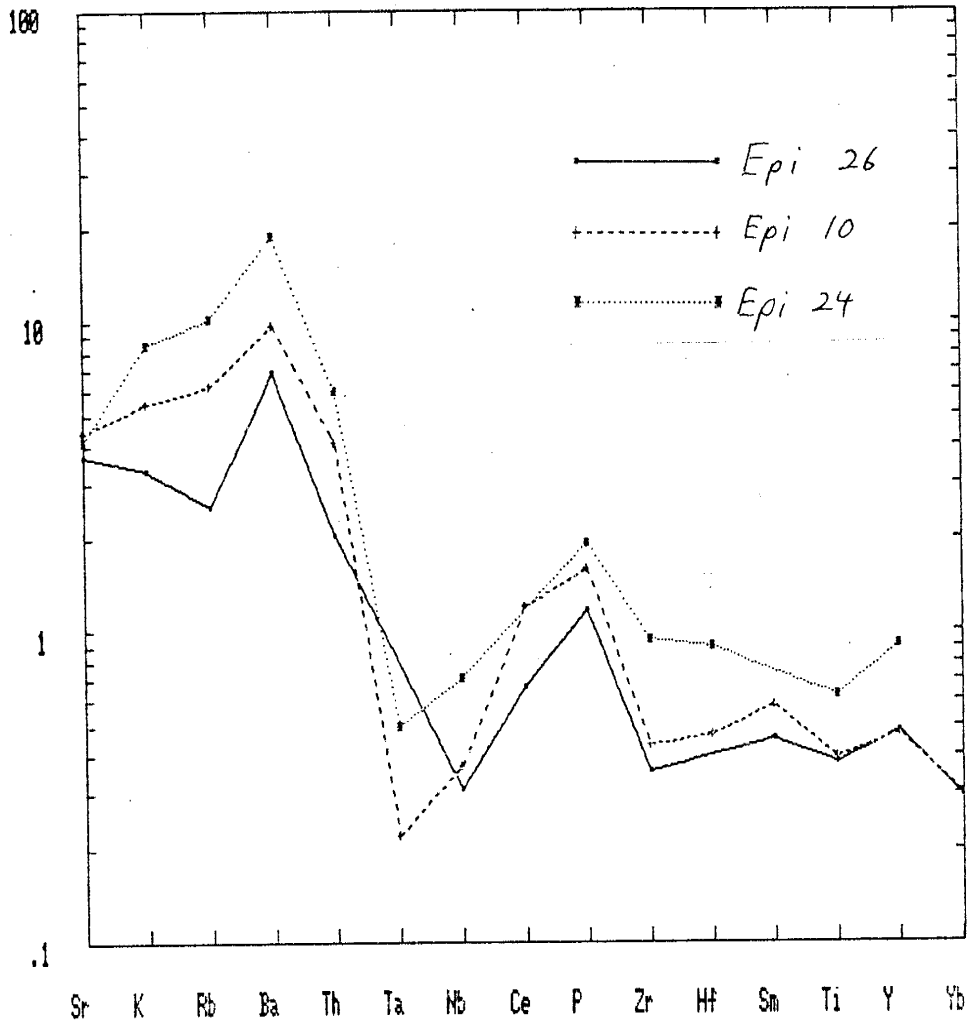

Figure H18. Island-arc samples. MORB-normalized spider diagram of three samples from New Hebrides Islands.

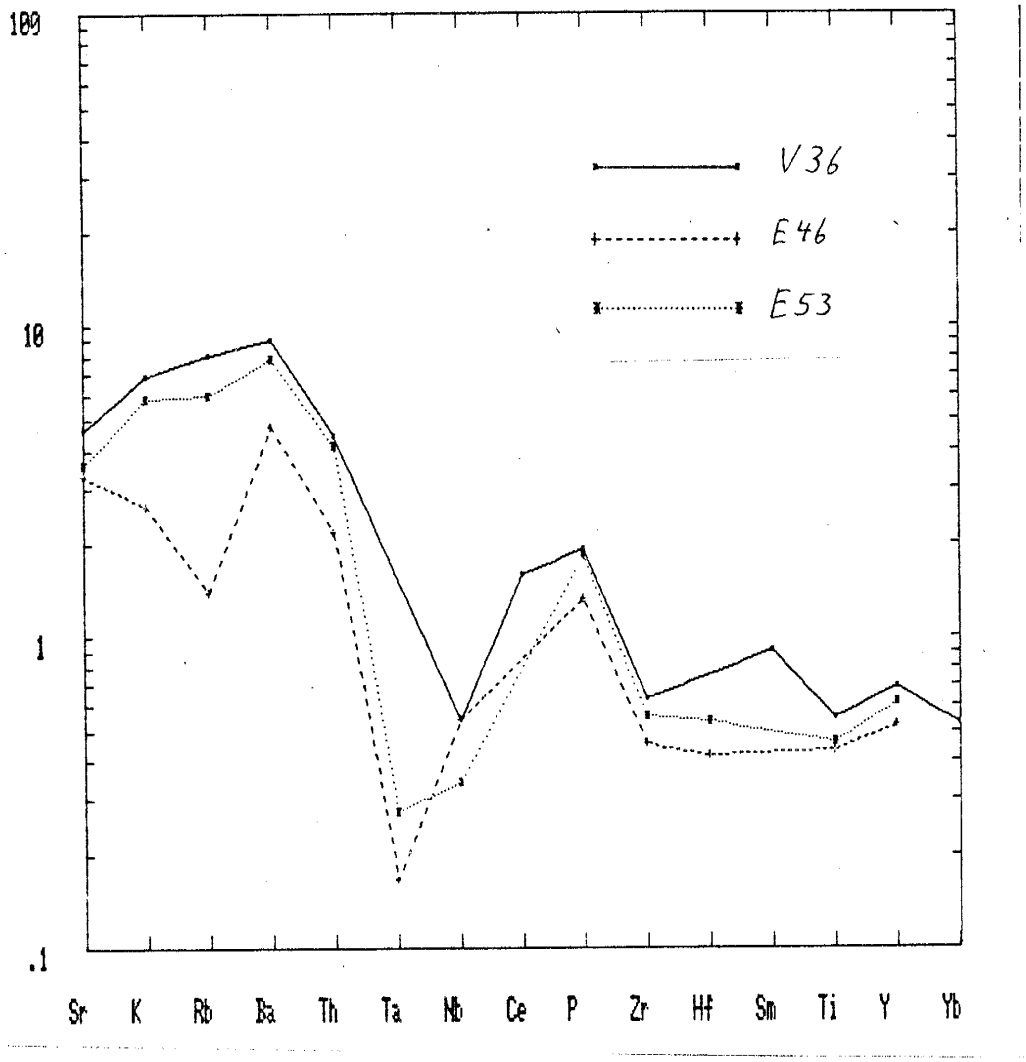

Figure H19. Island-arc samples. MORB-normalized spider diagram of three samples from New Hebrides Islands.

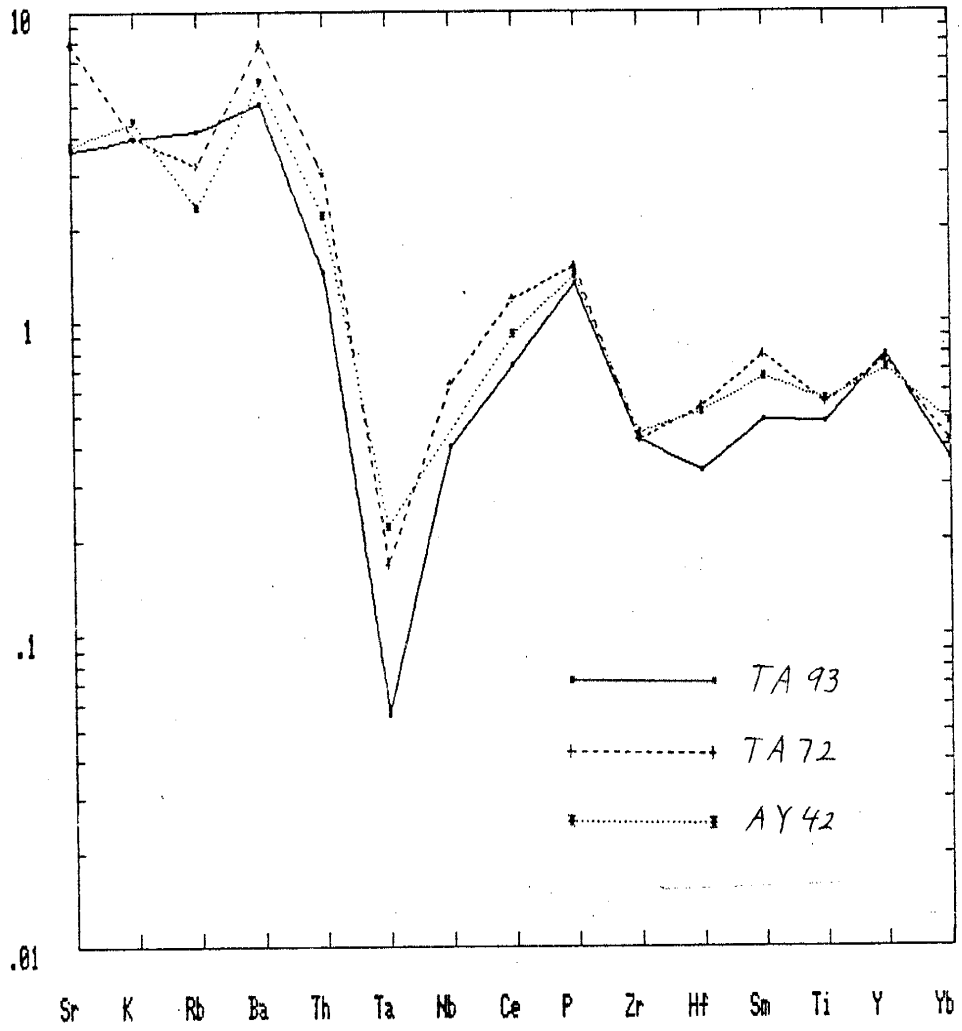

Figure H20. Island-arc samples. MORB-normalized spider diagram of three samples from New Hebrides Islands.

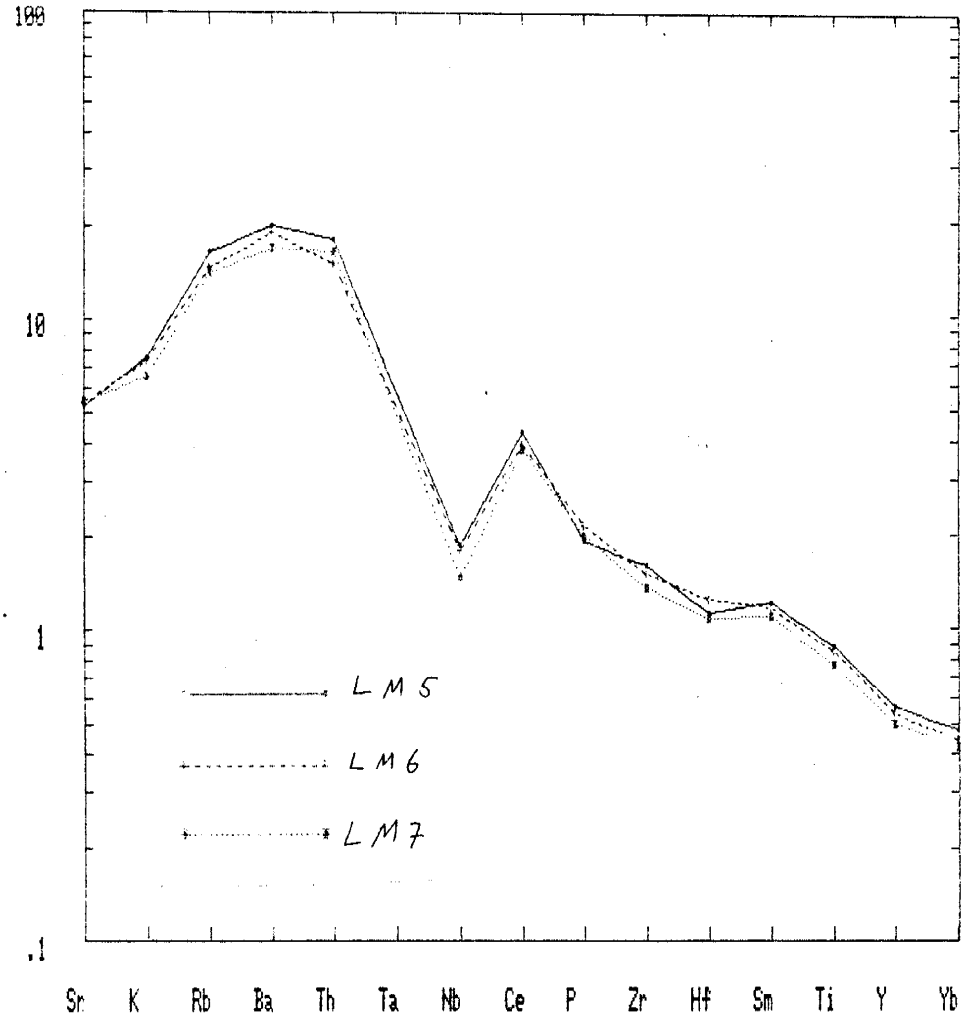

Figure H21. Continental-arc samples. MORB-normalized spider diagram of three samples from Chile.

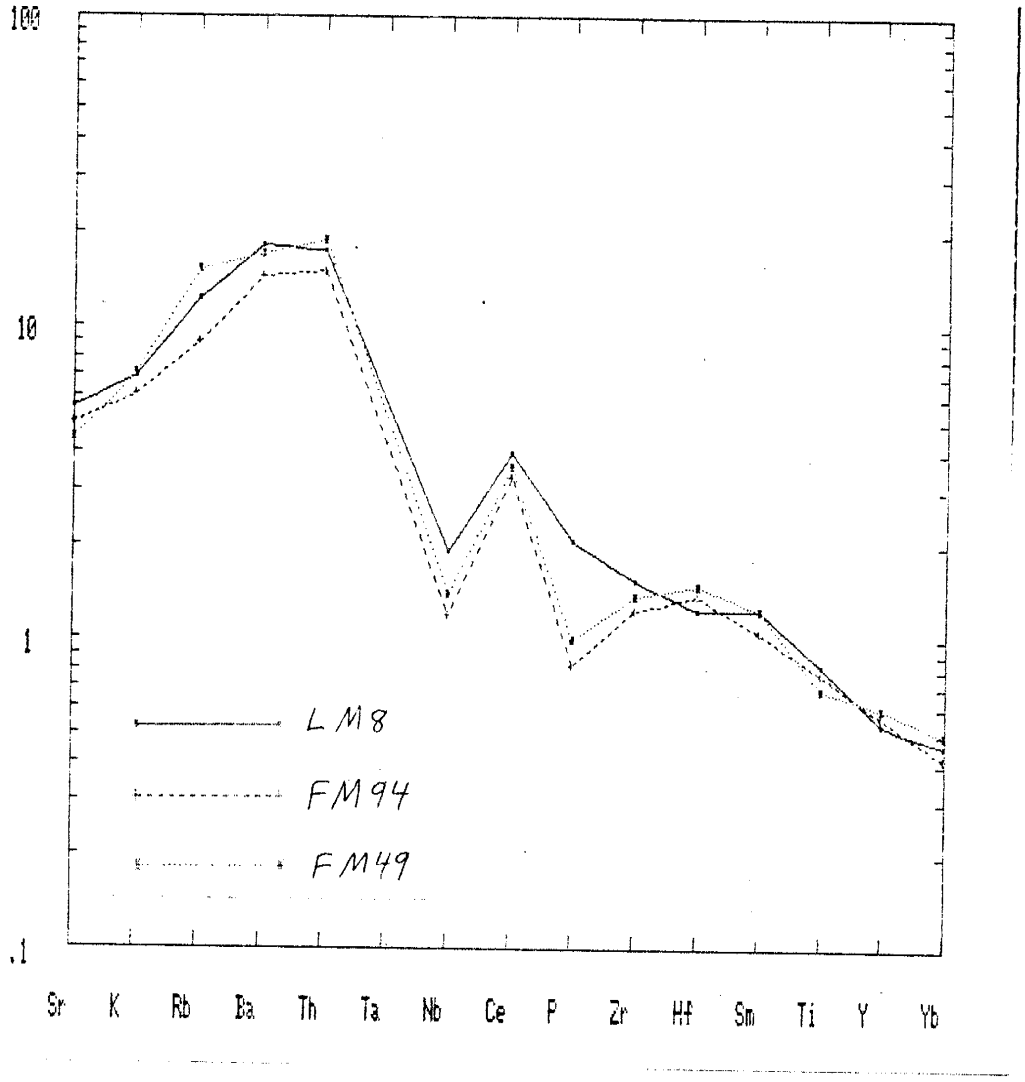

Figure H22. Continental-arc samples. MORB-normalized spider diagram of three samples from Chile.

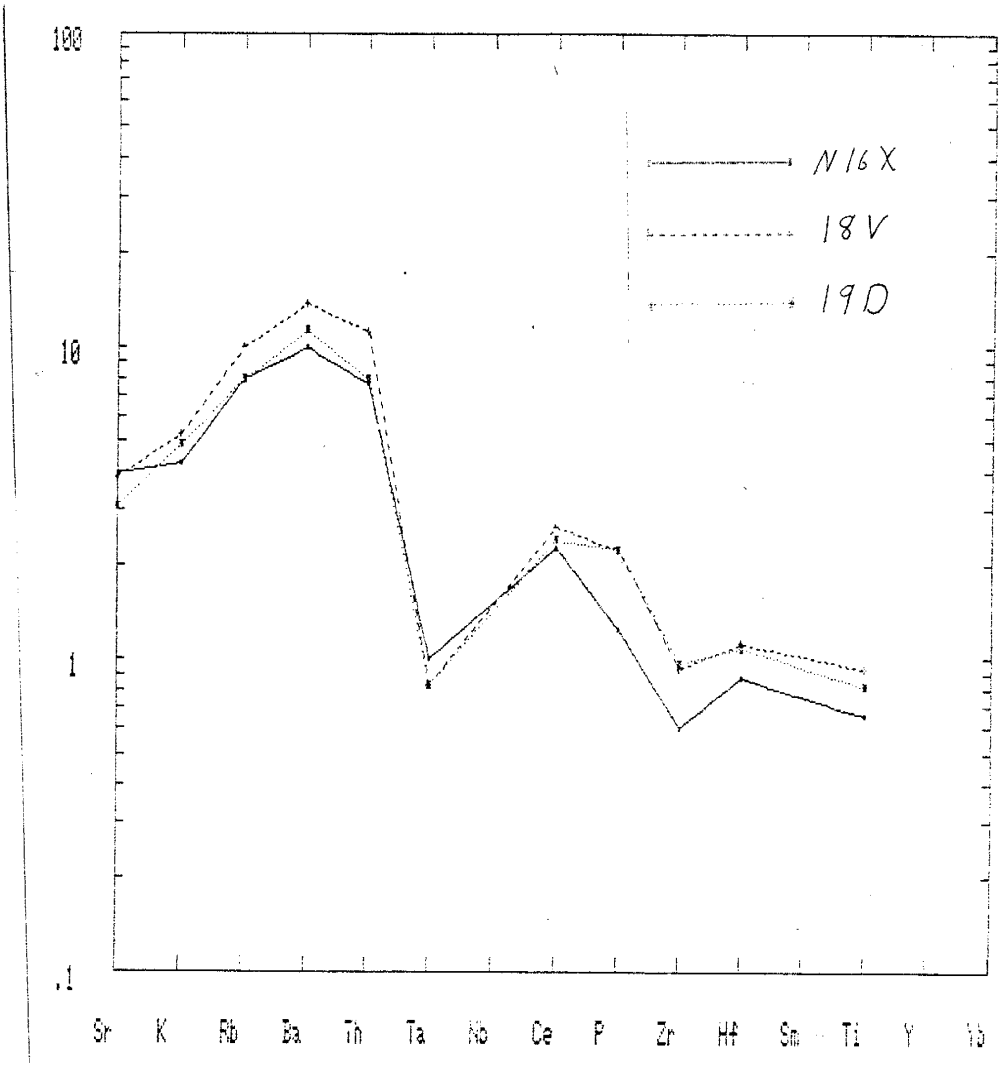

Figure H23. Continental-arc samples. MORB-normalized spider diagram of three samples from south-central Andes.

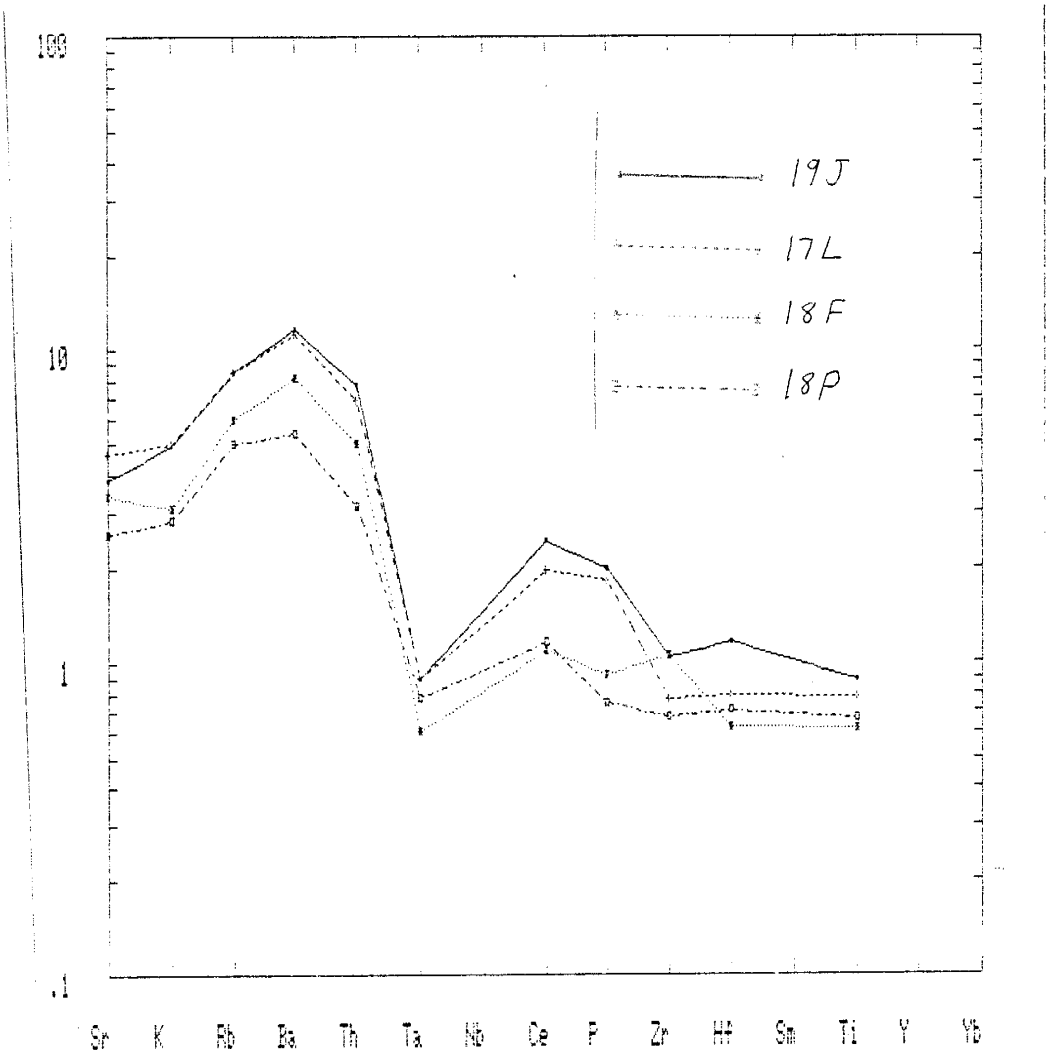

Figure H24. Continental-arc samples. MORB-normalized spider diagram of four samples from south-central Andes.

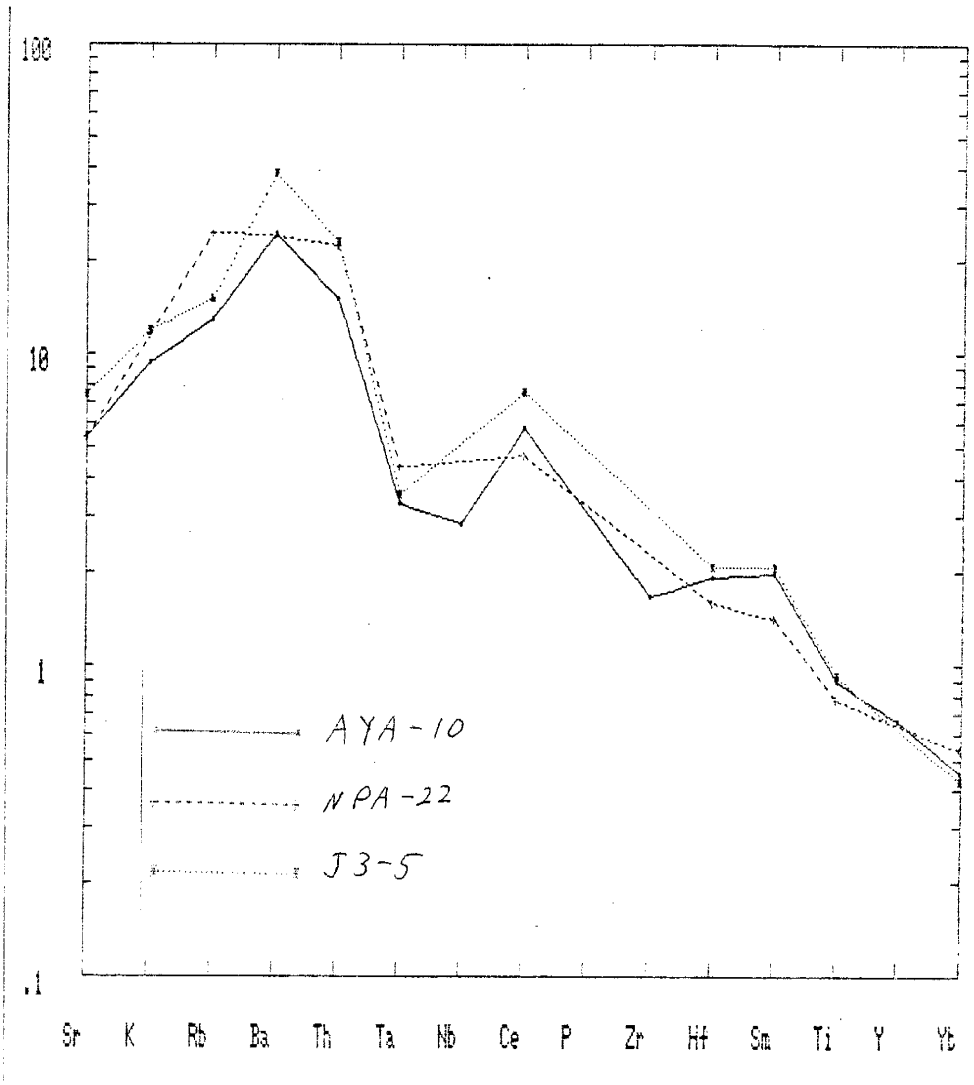

Figure H25. Continental-arc samples. MORB-normalized spider diagram of three samples from Peru.

TABLE H1. REFERENCES FOR MORB-NORMALIZED SPIDER DIAGRAMS.

Location	Refernces
MORB	
Mid-Atlantic Ridge	Frey, et al., 1974
Mid-Atlantic Ridge	Sun, et al., 1979
Explorer Ridge	Cousens, et al., 1984
Within Plate	
Mount Taylor	Lipman and Moench, 1972
Gregory Rift	Sceal and Weaver, 1971
Mathematician Ridge	Batiza and Vanko, 1985
South Island	Price and Taylor, 1980
South Queensland	Ewart, 1982
Rodrigues Island	Baxter, et al., 1985
Hawaii	Basaltic Volcanism Volume
Island-Arc	
Mariana Islands	Hole, et al., 1984
New Hebrides Islands	Dupuy, et al., 1982
Continental-Arc	
Chile	Frey, et al., 1984
South-Central Andes	Deruelle, 1982
Peru	Noble, et al., 1975

APPENDIX I

MODAL ANALYSIS

Work on the sedimentary rocks included modal analysis of four volcanic breccias from the Pedernal section. Modal analysis are preformed using a microscope equiped with a point counting stage and register. Results are tabulated according to several categories of Dickinson and Suczek (1980) along with several other categories (table I1). All quartz grains that are one continous grain are counted as monocrystalline quartz grains (Qm) while all quartz grains made up of multiple crystals are counted as polycrystalline quartz grains (Qp). Polycrystalline quartz grains include grains of igneous origin, metamorphic origin, epiclastic origin, and chert. Plagioclase grains are divided into primary (P) and metamorphic (MP) grains based on crystal shapes, alteration, and relation to surrounding matrix. No potassium feldspars are present in the samples. Lithic grains (L) cannot be separated into volcanic and sedimentary groups due to extensive alteration and recrystallization.

There is no completely reliable method for resolving the problems of distinguishing the various grain types and so there is a certain amount of uncertainty associated with results of point counting. The four samples have extensive alteration and recrystallization and some grain boundaries grade into matrix. This is especially true for the lithic

grains. Also, certain fine-grained volcanic grains may have a similar appearance as chert grains, but in the Pedernal samples, unstable lithic grains are highly altered and recrystallized while chert grains do not show any evidence of alteration and so these two rock types can be distinguished.

The counts for each category and percent of total counts of the categories for each sample are presented in table I2.

Modal analyses can be used for tectonic discrimination. The method of Dickinson and Suczek (1979) is to divide framework grains types into categories and plot the data on triangular diagrams. The detrital modes primarily reflect tectonic setting (Dickinson, et al., 1983), but various other sedimentological factors also influence the compositions of framework grains, including relief, climate, transportation mechanism, depositional environment, and diagenetic change (Dickinson, 1985). The diagrams proposed by Dickinson and Suczek (1979) show consistent patterns for modern sediments and can therefore be used for tectonic interpretation.

Some of the provenance diagrams of Dickinson and Suczek (1980) and Dickinson, et al., (1983) cannot be used for the Pedernal samples. Since no potassium feldspar (K) is present in the samples, the QmPK diagram cannot be used. Also, the QpLvLs diagram cannot be used since the unstable lithic grains cannot be separated into volcanic

(Lv) and sedimentary (Ls). Only the QmFLt and QFL diagrams are useful.

TABLE I1. CATEGORIES FOR POINT COUNTING.

SYMBOL	DESCRIPTION
Qm	Monocrystalline quartz grains
Qp	Polycrystalline quartz grains
Q	Total quartzose grains (Qm+Qp)
L	Unstable polycrystalline lithic grains
Lt	Total lithic grains (L+Qp)
P	Monocrystalline plagioclase grains
MP	Metamorphic plagioclase
Bi	Biotite in the matrix
Ch	Chlorite in the matrix
Amp	Amphibole in the matrix
Ep	Epidote in the matrix and as grains
Sr	Sericitic matrix
Op	Opaques as grains and in the matrix
Ma	Quartzo-feldspathic matrix

TABLE I2. MODAL ANALYSES OF PEDERNAL VOLCANIC SAMPLES.

SYMBOL	P743 COUNTS	P743 PERCENT	P744 COUNTS	P744 PERCENT
Qm	3	0.2	0	0.0
Qp	17	1.4	43	4.2
L	315	25.3	644	62.7
P	0	0.0	0	0.0
MP	0	0.0	0	0.0
Bi	14	1.1	0	0.0
Amp	507	42.8	62	6.0
Ch	52	4.2	15	1.5
Ep	59	4.7	95	9.3
Sr	125	10.0	23	2.2
Op	5	0.4	3	0.3
Ma	147	11.8	130	12.7
TOTAL	1244	99.9	1027	100.0

SYMBOL	P86 COUNTS	P86 PERCENT	P10 COUNTS	P10 PERCENT
Qm	1	0.1	0	0.0
Qp	150	14.9	0	0.0
L	380	37.8	416	40.0
P	4	0.4	0	0.0
MP	0	0.0	7	0.7
Bi	5	0.5	0	0.0
Amp	263	26.2	126	12.1
Ch	38	3.8	138	13.7
Ep	35	3.5	242	23.3
Sr	0	0.0	0	0.0
Op	20	2.0	11	1.1
Ma	109	10.8	75	7.2
TOTAL	1005	100	1039	100

APPENDIX J

DISTRIBUTION COEFFICIENTS

This appendix lists the distribution coefficients used for modelling and the literature sources the Kds were compiled from. Distribution coefficients were compiled for mafic, intermediate, dacitic, rhyolitic, and high-silica rhyolitic rocks. Ni, Cr, and Co are temperature and/or compositionally dependent in olivine, clinopyroxene, orthopyroxene, and garnet in a mafic system. Values were assumed to be constant and average values in a mafic system were selected for modelling.

TABLE J1. DISTRIBUTION COEFFICIENTS FOR A MAFIC SYSTEM.

Elem.	Amp	Opx	Oliv	Mgt	Cpx	Plag	Ilm	Gar
Rb	0.2	0.02	0.01	0.0	0.02	0.13	0.47	0.04
Ba	0.70	0.013	0.01	0.0	0.005	0.25	0.4	0.02
K	0.96	0.014	0.007	0.0	0.011	0.17	0.0	0.02
Sr	0.60	0.02	0.015	0.0	0.1	2.0	0.68	0.012
Th	0.05	0.13	0.02	0.0	0.02	0.05	0.05	0.0
U	0.0	0.007	0.04	0.0	0.05	0.06	0.0	0.0
Zr	1.5	0.03	0.01	0.1	0.1	0.01	0.28	0.3
Nb	0.8	0.15	0.01	0.4	0.1	0.01	0.8	0.1
Hf	0.4	0.04	0.04	0.4	0.3	0.01	0.38	0.15
Ta	0.4	0.0	0.03	0.5	0.06	0.04	0.04	0.0
Y	1.0	0.2	0.01	0.2	0.5	0.03	0.2	2.0
Ti	1.5	0.1	0.02	7.5	0.3	0.04	50	0.3
V	3.5	0.0	0.05	25	1.2	0.0	0.0	0.0
Sc	1.5	1.0	0.3	2.0	2.0	0.04	0.04	5.0
La	0.20	0.007	0.00001	0.0	0.07	0.15	0.39	0.03
Ce	0.25	0.008	0.00001	0.0	0.1	0.12	0.035	0.03
Sm	0.50	0.02	0.0006	0.0	0.4	0.067	0.05	0.22
Eu	48.00	0.02	0.001	0.0	0.4	0.35	0.05	1.0
Tb	0.5	0.05	0.002	0.0	0.5	0.06	0.02	3.0
Yb	0.48	0.15	0.02	0.0	0.6	0.07	0.05	5.0
Lu	0.49	0.18	0.016	0.0	0.5	0.06	0.04	5.5
Ni	7.0	3.1	18	29	7	0.0	2	3.5
Cr	10	5	0.8	150	4.8	0.0	5	0.5
Co	3	1.35	3.7	7.4	1.4	0.0	2	4

Amp = amphibole
Opx = orthopyroxene
Oliv = olivine
Mgt = magnetite
Cpx = clinopyroxene
Plag = plagioclase
Ilm = ilmenite
Gar = garnet

TABLE J2. DISTRIBUTION COEFFICIENTS FOR INTERMEDIATE ROCKS.

Elements	Amp	Opx	Mgt	Cpx
Rb	0.05	0.02	0.0	0.02
Ba	0.09	0.02	0.0	0.02
K	0.33	0.15	0.0	0.02
Sr	0.23	0.15	0.15	0.08
Th	0.15	0.05	0.1	0.01
U	0.1	0.006	0.1	0.0
Zr	1	0.09	0.3	0.25
Nb	1.3	0.35	2.5	0.3
Hf	0.4	0.1	0.4	0.25
Ta	1.3	0.35	1	0.3
Y	2.5	0.45	0.5	1.5
Ti	3	0.3	9	0.4
V	32	1.1	20	1.3
Sc	10	1.8	2	3.5
La	0.5	0.025	0.2	0.4
Ce	0.8	0.035	0.2	0.3
Sm	1.8	0.06	0.3	0.63
Eu	1.5	0.07	0.25	0.5
Tb	2	0.5	0.25	0.7
Yb	1.8	0.6	0.25	0.9
Lu	1.7	0.7	0.25	0.7
Ni	8	9	20	6
Cr	13	5.5	8	2
Co	30	20	25	30

Amp = amphibole Mgt = magnetite
Opx = orthopyroxene Cpx = clinopyroxene

TABLE J2. CONTINUED.

Elements	Plag	Biot	Gar	Ap
Rb	0.051	2.2	0.01	0.0
Ba	0.2	6	0.02	0.0
K	0.11	6	0.01	0.0
Sr	1.5	0.12	0.02	1.35
Th	0.01	0.5	0.02	2
U	0.007	0.02	0.0	0.0
Zr	0.03	2	0.5	0.1
Nb	0.025	5	0.1	0.1
Hf	0.01	2	0.57	0.1
Ta	0.025	1	0.1	0.0
Y	0.06	0.03	11	20
Ti	0.05	2.5	0.5	0.1
V	0.01	50	8	0.0
Sc	0.01	15	3	0.0
La	0.15	0.11	0.37	3.5
Ce	0.13	0.32	0.53	5
Sm	0.085	0.25	1.5	7.8
Eu	0.4	0.25	1.45	30
Tb	0.06	0.35	15	5
Yb	0.05	0.44	35	3
Lu	0.036	0.3	40	2.9
Ni	0.0	13	0.6	0.0
Cr	0.0	25	1.8	0.0
Co	0.0	17	22	0.0

Plag = plagioclase Gar = garnet
Biot = biotite Ap = apatite

TABLE J3. DISTRIBUTION COEFFICIENTS FOR DACITIC ROCKS.

Elements	Amp	Opx	Mgt	Plag
Rb	0.01	0.003	0.0	0.05
Ba	0.04	0.003	0.0	0.3
K	0.07	0.002	0.0	0.26
Sr	0.02	0.01	0.0	5
Th	0.01	0.15	0.4	0.05
U	0.01	0.006	0.1	0.007
Zr	1.4	0.08	0.2	0.03
Nb	1.3	0.35	1	0.03
Hf	1.4	0.03	0.5	0.05
Ta	1.5	0.5	5	0.08
Y	4.7	0.45	0.5	0.06
Ti	3	0.45	10	0.05
V	32	1.7	30	0.01
Sc	15	3.5	3.9	0.1
La	0.6	0.1	0.0	0.08
Ce	0.9	0.15	0.0	0.2
Sm	4	0.25	0.0	0.11
Eu	4.5	0.17	0.0	1.5
Tb	6	0.65	0.1	0.085
Yb	4.9	0.85	0.1	0.08
Lu	4.9	0.9	0.1	0.06
Ni	6	7	15	0.0
Cr	10	8	12	0.0
Co	25	4	20	0.0

Amp = amphibole Mgt = magnetite
Opx = orthopyroxene Plag = plagioclase

TABLE J3. CONTINUED.

Elements	Biot	Gar	Ap	Zir
Rb	3.3	0.01	0.0	0.0
Ba	10	0.015	0.0	0.0
K	10	0.02	0.0	0.0
Sr	0.12	0.15	2	0.0
Th	0.3	0.02	2	100
U	0.02	0.01	0.01	0.01
Zr	1.2	1.2	0.1	1000
Nb	5	0.5	0.1	50
Hf	2	0.5	0.1	800
Ta	1	0.5	0.0	50
Y	0.03	35	20	60
Ti	1.5	1.2	0.1	50
V	50	8	0.0	0.0
Sc	10	20	0.0	60
La	0.03	0.35	20	2
Ce	0.04	0.35	35	2.5
Sm	0.06	2.6	63	3.1
Eu	0.15	1	30	3.5
Tb	0.16	35	20	100
Yb	0.18	40	25	200
Lu	0.2	30	25	200
Ni	15	0.6	0.0	0.0
Cr	13	3	0.0	0.0
Co	10	3.7	0.0	0.0

Biot = biotite Ap = apatite
Gar = garnet Zir = zircon

TABLE J4. DISTRIBUTION COEFFICIENTS FOR RHYOLITIC ROCKS.

Elements	Amp	Opx	Kf	Mgt	Sph
Rb	0.01	0.003	0.35	0.0	0.0
Ba	0.04	0.003	6	0.0	1
K	0.07	0.002	1.5	0.0	0.0
Sr	0.02	0.01	4	0.15	100
Th	0.01	0.15	0.01	0.4	130
U	0.0	0.006	0.005	0.1	0.0
Zr	4	0.2	0.1	0.8	0.0
Nb	4	0.8	0.05	2.5	0.0
Hf	1.4	0.1	0.1	0.5	65
Ta	1.5	0.15	0.05	5	800
Y	6	1	0.1	2	0.0
Ti	7	0.4	0.05	60	0.0
V	32	6	0.01	30	0.0
Sc	10	7	0.02	8	40
La	0.33	0.1	0.05	0.0	32
Ce	1.5	0.15	0.04	0.0	60
Sm	7.8	0.25	0.02	0.0	200
Eu	5	0.17	1.1	0.0	120
Tb	12	0.65	0.006	0.1	210
Yb	8	0.85	0.01	0.1	190
Lu	5.5	0.9	0.006	0.1	115

Amp = amphibole
Opx = orthopyroxene
Kf = potassium feldspar
Mgt = magnetite
Sph = sphene

TABLE J4. CONTINUED.

Elements	Plag	Ilm	Cpx	Biot	Gar
Rb	0.04	0.0	0.03	2.2	0.01
Ba	0.3	0.0	0.13	6	0.015
K	0.1	0.0	0.002	6	0.02
Sr	5	0.0	0.52	0.12	0.15
Th	0.05	0.4	0.03	0.5	0.02
U	0.006	0.0	0.01	0.02	0.0
Zr	0.1	1.0	0.6	2	1.2
Nb	0.06	3.0	0.8	5	0.5
Hf	0.04	0.7	0.3	2	0.5
Ta	0.05	30	0.4	1	0.5
Y	0.1	0.0	4.0	0.03	35
Ti	0.05	50	0.7	2.5	1.2
V	0.01	12	1.1	50	8
Sc	0.04	8	22	15	20
La	0.08	0.0	0.3	0.11	0.35
Ce	0.25	0.0	0.5	0.32	0.35
Sm	0.13	0.0	1.67	0.25	2.6
Eu	4	0.0	1.5	0.25	1
Tb	0.6	0.1	1.8	0.35	35
Yb	0.05	0.1	1.5	0.44	40
Lu	0,05	0.1	1.5	0.3	30

Plag = plagioclase
Ilm = ilmenite
Cpx = clinopyroxene
Biot = biotite
Gar = garnet

TABLE J4. CONTINUED.

Elements	Zir	Ap	All
Rb	0.0	0.0	0.0
Ba	0.0	0.0	0.0
K	0.0	0.0	0.0
Sr	0.0	2	100
Th	100	2	1500
U	0.0	0.0	1
Zr	1000	0.1	2
Nb	50	0.1	2
Hf	450	0.1	10
Ta	50	0.0	2
Y	60	40	100
Ti	50	0.1	50
V	0.0	0.0	0.0
Sc	60	0.0	60
La	2	20	2500
Ce	2.5	35	2000
Sm	3.1	63	1300
Eu	3.5	30	800
Tb	100	20	500
Yb	200	25	100
Lu	200	25	100

Zir = zircon
Ap = apatite
All = allanite

TABLE J5. DISTRIBUTION COEFFICIENTS FOR HIGH-SILICA RHYOLITES.

Elements	Amp	Opx	Kf	Mgt	Ilm	Plag
Rb	0.01	0.003	0.4	0.0	0.0	0.15
Ba	0.04	0.3	6	0.0	1	1.5
K	0.07	0.002	2.1	0.0	0.0	0.22
Sr	0.02	0.01	4	0.15	0.0	8
Th	0.01	5.5	0.02	10	0.43	0.2
U	0.0	0.3	0.015	0.1	0.06	0.15
Zr	4	0.2	0.1	0.8	0.0	0.1
Nb	4	0.8	0.05	2.5	0.0	0.06
Hf	1.4	0.1	0.02	10	0.65	0.15
Ta	1.5	0.1	0.02	1.0	18	0.15
Y	6	1	0.1	2	0.0	0.1
Ti	7	0.7	0.1	100	380	0.05
V	32	6	0.01	30	0.0	0.01
Sc	10	19	0.04	9	40	0.15
La	0.33	10	0.07	12	1.3	0.5
Ce	1.5	9	0.04	11	1.2	0.4
Sm	7.8	6.4	0.02	7	0.68	0.2
Eu	5	2.4	2.5	2	0.4	5.0
Tb	12	4.8	0.02	3.5	0.36	0.2
Yb	8	2.1	0.02	2	0.55	0.15
Lu	5.5	2.1	0.015	2	0.74	0.10

Amp = amphibole
Opx = orthopyroxene
Kf = potassium feldspar
Mgt = magnetite
Ilm = ilmenite
Plag = plagioclase

TABLE J5. CONTINUED.

Elements	Cpx	Biot	Gar	Zir	Ap	All
Rb	0.03	2.2	0.01	0.0	0.0	0.0
Ba	2.3	6	0.015	0.0	0.0	0.0
K	0.002	1.8	0.02	0.0	0.0	0.0
Sr	0.52	0.12	0.15	0.0	2	100
Th	4.0	1.7	0.02	100	2	450
U	0.5	0.2	0.0	300	0.0	14
Zr	0.6	2	1.2	1000	0.1	2
Nb	0.8	5	0.5	50	0.1	2
Hf	0.3	0.65	0.5	2700	0.1	10
Ta	0.70	1.3	0.5	50	0.0	2
Y	4.0	0.03	35	60	40	100
Ti	2.5	30	1.2	50	0.1	50
V	1.1	50	8	0.0	0.0	0.0
Sc	120	15	20	60	0.0	50
La	15	3	0.35	10	20	2500
Ce	12	2.5	0.35	12	35	2000
Sm	11	1.6	2.6	13	63	750
Eu	6	1.0	1	15	30	400
Tb	10	0.8	35	40	20	240
Yb	5.0	0.5	40	500	25	30
Lu	5.0	0.5	30	600	25	15

Cpx = clinopyroxene
Biot = biotite
Gar = garnet
Zir = zircon
Ap = apatite
All = allanite

BIBLOGRAPHY

Abbey, S.; 1983. Studies in 'Standard Samples' of Silicate Rocks and Minerals: 1969-1982. Geol. Sur. Can. Pap., 83-15, 114 pp.

Alabaster, T.; Pearce, J. A.; and Malpas, J.; 1982. The Volcanic Stratigraphy and Petrogenesis of the Oman Ophiolite Complex. Contrib. Mineral. Petrol., 81, p. 168-183.

Albuquerque, C. A. R. De; 1977. Geochemistry of the Tonalitic and Granitic Rocks of the Nova Scotia Southern Plutons. Geochim. Cosmochim. Acta 41, p. 1-13.

Allegre, C. J. and Turcotte, D. L.; 1985. Geodynamic Mixing in the Mesosphere Boundary Layer and the Origin of Oceanic Islands. Geophy. Rev. Lett., 12, p. 207-210.

Allen, J. C.; Boettcher, A. L.; and Marland, G.; 1975. Amphiboles in Andesite and Basalt: I. Stability as a Function of P-T-fO2. Am. Mineral., 60, p. 1069-1085.

Allen, P.; 1985. The Geochemistry of the Amphibolite-Granulite Facies Transition in Central South Asia. Unpubl. Ph. D. dissert., New Mex. Inst. Mining Tech., 386 pp.

Anderson, A. T.; 1976. Magma Mixing: Petrological Process and Volcanological Tool. J. Vol. Geother. Res., 1, p. 3-33.

Anderson, A. T. and Gottfried, D.; 1971. Contrasting Behaviour of P, Ti, and Nb in a Differentiated High-Alumina Olivine Tholeiite and a Calcalkaline Andesite Suite. Geol. Soc. Am. Bull., 82, p. 1929-1942.

Arculus, R. J. and Willis, K. J. A.; 1980. The Petrology of Plutonic Blocks and Inclusions from the Lesser Antilles Island Arc. J. Petrol., 21, p. 743-799.

Armstrong, D. G.; 1977. Unpubl. map of the Pedernal Hills.

Armstrong, D. G. and Holcombe, R. J.; 1982. Precambrian Rocks of a Portion of the Pedernal Highlands, Torrance County, New Mexico. New Mex. Geol. Soc. Guidebk., 33, p. 203-210.

Armstrong, R. L.; 1968. A Model for the Evolution of Strontium and Lead Isotopes in a Dynamic Earth. Rev. Geophy., 6, p. 175-199.

Armstrong, R. L.; 1971. Isotopic and Chemical Constraints on Models of Magma Genesis in Volcanic Arcs. Earth Planet. Sci. Lett., 12, p. 137-142.

Arndt, N. T.; 1977. Partitioning of Nickel Between Olivine and Ultrabasic and Basic Komatiitic Liquids. CIW Yearbk., 76, p. 553-557.

Arth, J. G.; 1976. Behavior of Trace Elements During Magmatic Processes - A Summary of Theoretical Models and Their Applications. J. Res. U. S. Geol. Sur., 4, p. 41-47.

Arth, J. G. and Barker, F.; 1976. Rare-Earth Partitioning Between Hornblende and Dacitic Liquid and Implications for the Genesis of Trondhjemitic-Tonalitic Magmas. Geol., 4, p. 534-536.

Arth, J. G.; Barker, F.; Peterman, Z. E.; and Friedman, I.; 1978. Geochemistry of the Gabbro-Diorite-Tonalite-Trondhjemite Suite of Southwest Finland and Its Implications for the Origin of Tonalitic and Trondhjemitic Magmas. J. Petrol., 19, p. 289-316.

Arth, J. G. and Hanson, G. N.; 1975. Geochemistry and Origin of the Early Precambrian Crust of Northeastern Minnesota. Geochim. Cosmochim Acta 39, p. 325-362.

Atherton, M. P.; McCourt, W. J.; Sanderson, L. M.; and Taylor, W. P.; 1979. The Geochemical Character of the Segmented Peruvian Coastal Batholith and

Associated Volcanics. p. 45-64 in Origin of Granite Batholiths: Geochemical Evidence ed. by M P. Atherton and J. Tarney, Shiva Publ. Ltd., Kent, UK.

Bacon, C. R.; 1983. Eruptive History of Mount Mazama and Crater Lake Caldera, Cascade Range, USA. J. Volcan. Geotherm. Res., 18, 57-115.

Baer, A. J.; 1977. Speculations on the Evolution of the Lithosphere. Precam. Res., 5, p. 249-260.

Bailey, J. C.; 1981. Geochemical Criteria for a Refined Tectonic Discrimination of Orogenic Andesites. Chem. Geol., 31, p. 139-154.

Barker, P. E.; 1982. Evolution and Classification of Orogenic Volcanic Rocks. p. 11-23 in Andesites ed. by R. S. Thorpe, John Wiley and Sons.

Barker, P. E.; 1984. Geochemical Evolution of St. Kitts and Montserrat, Lesser Antilles. J. geol. Soc. London 141, p. 401-411.

Basaltic Volcanism on the Terrestrial Planets. 1981. Lunar and Planetary Instit., Pergamon Press, 1286 pp.

Batiza, R. and Vanko, D. A.; 1985. Petrologic Evolution of Large Failed Rifts in the Eastern Pacific: Petrology of Volcanic and Plutonic Rocks from the Mathematician Ridge Area and the Gaadalupe Trough. J. Petrol., 26, p. 564-602.

Bauer, P. W.; 1982a. Precambrian Geology and Tectonics of the Southern Manzano Mountains, Central New Mexico. New Mex. Geol. Soc. Guidebk., 33, p. 211-216.

Bauer, P. W.; 1982b. Geology of the Precambrian Rocks of the Southern Manzano Mountains, New Mexico. Unpul. Masters thesis, U. New Mex., 133 pp.

Bauer, P. W. and Williams, M. L.; 1985. Structural Relationships and Mylonites in Proterozoic Rocks of the Northern Pedernal Hills, Central New Mexico. New Mex. Geol. Soc. Guidebk., 36, p. 141-145.

Baxter, A. N.; Upton, B. G. J.; and White, W. M.; 1985. Petrology and Geochemistry of Rodrigues Island, Indian Ocean. Contrib. Mineral. Petrol., 89, p. 90-101.

Bellieni, G.; Peccerillo, A.; and Poli, G.; 1981. The Vedrette di Ries (Rieserferner) Plutonic Comples: Petrological and Geochemical Data Bearing on Its Genesis. Contrib. Mineral. Petrol., 78, p. 145-156.

Berlin, R. and Henderson, C. M. B.; 1969. The Distribution of Sr and Ba Between the Alkali Feldspar, Plagioclase and Groundmass Phases of Porphyritic Trachytes and Phonolites. Geochim. Cosmochim. Acta 33, p. 247-255.

Best, M. G.; 1975. Migration of Hydrous Fluids in the Upper Mantle and Potassium Variation in Calc-alkaline Rocks. Geol., 3, p. 429-432.

Beswick, A. E. and Carmichael, I. S. E.; 1978. Constraints on Mantle Source Compositions Imposed by Phosphorus and the Rare-Earth Elements. Contrib. Mineral. Petrol., 67, p. 317-330.

Beswick, A. E. and Soucie, G.; 1978. A Correction Procedure for Metasomatism in an Archean Greenstone Belt. Precam. Res., 6, p. 235-248.

Bhatia, M. R.; 1983. Plate Tectonics and Geochemical Composition of Sandstones. J. Geol., 91, p. 611-627.

Bhatia, M. R. and Crook, K. A. W.; 1986. Trace Element Characteristics of Graywackes and Tectonic Setting Discrimination of Sedimentary Basins. Contr. Mineral. Petrol., 92, p. 181-193.

Bischoff, J. L. and Dickson, F. W.; 1975. Seawater-Basalt Interaction at 200 C and 500 Bars: Implications for Origin of Sea-Floor, Heavy Metal Deposits and Regulation of Seawater Chemistry. Earth Planet. Sci. Lett., 25, p. 385-397.

Blount, W.; 1982. The Contact Between the Sais Quartzite and the Lower Metaclastics of Ojo Da Casa, New Mexico. New Mex. Geol. Soc. Guidebk., 33, p. 26.

Boardman, S. J.; 1976. Geology of the Precambrian Metamorphic Rocks of the Salida Area, Chaffee County, Colorado, Moun. Geol., 13, p. 89-100.

Boetlcher, A. L.; 1977. The Role of Amphiboles and Water in Circum-Pacific Volcanism. p. 107-125 in High Pressure Research: Applications in Geophysics ed. by M. H. Manghnani and S. I. Akimoto, Academic Press, Inc., New York.

Bolton, W. R.; 1976. Precambrian Geochronology of the Sevilleta Metarhyolite and Los Pinos, Sepultura, and Priest Plutons of the Southern Sanadia Uplift, New Mexico. Unpubl. Masters thesis, New Mex. Inst. Mining Tech., 45 pp.

Bougault, H.; Joron, J. L.; and Treuil, M.; 1980. The Primordial Chondritic Nature and Large-Scale Heterogeneities in the Mantle: Evidence from High and Low Partition Coefficient Elements in Oceanic Basalts. Phil. Trans. R. Soc. Lond., A297, p. 203-213.

Bowen, N. L.; 1928. The Evolution of Igneous Rocks. Princeton Univ. Press, 332 pp.

Brenchley, P. J.; 1969. Origin of Matrix in Ordovician Greywackes, Berwyn Hills, North Wales. J. Sed. Pet., 39, p. 1297-1301.

Breyer, J. A. and Ehlmann, A. J.; 1981. Mineralogy of Arc-Derived Sediment: Siliclastic Sediment on the Insular Shelf of Puerto Rico. Sediment., 28, p. 61-74.

Briqueu, L.; Bougault, H.; and Joron, J. L.; 1984. Quantification of Nb, Ta, Ti and V Anamolis in Magmas Associated with Subduction Zones: Petrogenetic Implications. Earth Planet. Sci. Lett., 68, p. 297-308.

Briqueu, L. and Lancelot, J. R.; 1983. Sr Isotopes and K, Rb, Sr Balance in Sediments and Igneous Rocks from the Subducted Plate of the Vanuata (New Hebrides) Active Margin. Geoch. Cosmochim. Acta 47, p. 191-200.

Brookins, D. G.; 1974. Summary of Recent Rb-Sr Age Determinations from Precambrian Rocks of North-Central New Mexico. New Mex. Geol. Soc. Guidebk., 25, p. 119-121.

Brookins, D. G.; 1982. Radiometric Ages of Precambrian Rocks from Central New Mexico. New Mex. Geol. Soc. Guidebk., 33, p. 187-189.

Brown, G. C. and Fyfe, W. S.; 1970. The Production of Granitic Melts During Ultrametamorphism. Contrib. Mineral. Petrol., 28, p. 310-318.

Burt, D. M.; Sheridan, M. F.; Bikun, J. V.; and Christiansen, E. H.; 1982. Topaz Rhyolites: Distribution, Origin and Significance for Exploration. Econ. Geol., 77, p. 1818-1836.

Busby-Spera, C.; 1985. A Sand-Rich Submarine Fan in the Lower Mesozoic Mineral King Caldera Complex, Sierra Nevada, California. J. Sed. Pet., 55, p. 376-391.

Busby-Spera, C. J.; 1986. Depositional Features of Rhyolitic and Andesitic Volcaniclastic Rocks of the Mineral King Sumarine Caldera Complex, Sierra Nevada, California. J. Vol. Geother. Res., 27, p. 43-76.

Byers, Jr., F. M.; 1959. Geology of Umnak and Bogoslof Islands, Aleutian Islands, Alaska. U. S. Geol. Sur. Bull., 1028-L, p. 267-369.

Byers, Jr., F. M.; 1961. Petrology of Three Volcanic Suites, Umnak and Bogoslof Islands, Aleutian Islands, Alaska. Geol. Soc. Am. Bull., 72, p. 93-128.

Callender, J.; 1983. Transposition Structures in

Precambrian Rocks of New Mexico. New Mex. Geol. Soc. Guidebk., 34, p. 143-146.

Cameron, K. L. and Cameron, M.; 1985. Rare Earth Element, 87Sr/86Sr, and 143Nd/144Nd Compositions of Cenozoic Orogenic Dacites from Baja California, Northwestern Mexico, and Adjacent West Texas: Evidence for the Predominance of a Subcrustal Component. Contrib. Mineral. Petrol., 91, p. 1-11.

Cameron, M.; Bagby, W. L.; and Cameron, K. L.; 1980. Petrogenesis of Voluminous Mid-Tertiary Ignimbrites of the Seirra Madre Occidental, Chihuahua, Mexico. Contrib. Mineral. Petrol., 74, p. 271-284.

Cann, J. R.; 1970. Rb, Sr, Y, Zr, and Nb in Some Ocean Floor Basaltic Rocks. Earth Planet. Sci. Lett., 10, p. 7-11.

Cavin, W. J.; Connolly, J. R.; Woodward, L. A.; Edwards, D. L.; and Parchman, M.; 1982. Precambrian Stratigraphy of Manzanita and North Manzano Mountains, New Mexico. New Mex. Geol. Soc. Guidebk., 33, p. 191-196.

Cawthorn, R. G.; 1976. Melting Relations in Part of the System CaO-MgO-Al2O3-SiO2-Na2O-H2O Under 5 Kb Pressure. J. Petrol. 17, p. 44-72.

Cawthorn, R. G.; Curran, E. B.; and Arculus, R. J.; 1978. A Petrogenetic Model for the Origin of the Calc-Alkaline Suite of Grenada, Lesser Antilles. J. Petrol., 14, p. 327-337.

Cawthorn, R. G. and O'Hara, M. J.; 1976. Amphibole Fractionation in Calc-Alkaline Magma Genesis. Am. J. Sci., 276, p. 309-329.

Chayes, F.; 1965. Statistical Petrography. C. I. W. Yearbk., 64, p. 153-165.

Chayes, F.; 1966. Alkaline and Sub-alkaline Basalts. Am. J. Sci., 26, p. 128-145.

Christiansen, E. H.; Burt, D. M.; Sheridan, M. F.; and Wilson, R. T.; 1983. Petrogenesis of Topaz Rhyolites from the Western USA. Contrib. Mineral. Petrol., 83, p. 16-30.

Church, B. N.; 1975. Quantitative Classification and Chemical Comparison of Common Volcanic Rocks. Geol. Soc. Am. Bull., 86, p. 257-263.

Clarke, D. B. and O'Hara, M. J.; 1979. Nickel, and the Existence of High-MgO Liquids in Nature. Earth Planet. Sci. Lett., 44, p. 153-158.

Coats, A. R.; 1962. Magma Type and Crustal Structure in the Aleutian Arc. p. 92-109 in The Crust of the Pacific Basin ed. by G. A. Macdonald and H. Kuno, Am. Geophy. U. Mon. Ser., 9.

Coats, R. R.; 1952. Magmatic Differentiation in Tertiary and Quaternary Volcanic Rocks from Adak and Kanaga Islands, Aleutian Islands, Alaska. Geol. Soc. Am. Bull., 63, p. 485-514.

Coats, R. R.; 1953. Geology of Buldir Island, Aleutian Islands, Alaska. U. S. Geol. Sur. Bull., 989-A, p. 1-26.

Coats, R. R.; 1956. Geology of Northern Adak Island, Alaska. U. S. Geol. Sur. Bull., 1028-C, p. 45-67.

Coats, R. R.; Nelson, W. H.; Lewis, R. Q.; and Powers, H. A.; 1961. Geologic Reconnaissance of Kiska Island, Aleutian Islands, Alaska. U. S. Geol. Sur. Bull., 1028-D, p. 563-581.

Cole, J. W.; 1979. Structure, Petrology, and Genesis of Cenozoic Volcanism, Taupo Volcanic Zone, New Zealand - A Review. N. Z. J. Geol. Geophy., 22, p. 631-657.

Cole, J. W.; 1981. Genesis of Lavas of the Taupo Volcanic Zone, North Island, New Zealand. J. Vol. Geother. Res., 10, p. 317-337.

Condie, K. C.; 1978. Geochemistry of Proterozoic Granitic Plutons from New Mexico, U. S. A. Chem. Geol., 21, p. 131-149.

Condie, K. C.; 1980. Precambrian Rocks of Red River - Wheeler Peak Area, New Mexico. New Mex. Bur. Mines Min. Res. Geol. Map 50.

Condie, K. C.; 1981a. Precambrian Rocks of the Southwestern United States and Adjacent Areas of Mexico. New Mex. Bur. Mines Min. Res. Res. Map 13.

Condie, K. C.; 1981b. Geochemical and Isotopic Constraints on the Origin and Source of Archean Granites. Spec. Publs. geol. Soc. Aust., 7, p. 469-479.

Condie, K. C.; 1982a. Plate-Tectonics Model for Proterozoic Continental Accretion in the Southwestern United States. Geol., 10, p. 37-42.

Condie, K. C.; 1982b. Early and Middle Proterozoic Supracrustal Successions and Their Tectonic Settings. Am. J. Sci., 282, p. 341-357.

Condie, K. C.; 1985. Variation in the Composition of Basalts: An Index to Mantle Evolution. J. Petrol., 26, p. 545-563.

Condie, K. C.; 1986. Geochemistry and Tectonic Setting of Early Proterozoic Supracrustal Rocks in the Southwestern United States. J. Geol., 94, p. 845-864.

Condie, K. C. and Budding A. J.; 1979. Geology and Geochemistry of Precambrian Rocks, Central and South-Central New Mexico. New Mex. Bur. Mines Min. Res. Mem., 35, 58 pp.

Condie, K. C. and McCrink, T. P.; 1982. Geochemistry of Proterozoic Volcanic and Granitic Rocks from the Gold Hill-Wheeler Peak Area, Northern New Mexico. Precam. Res., 19, p. 141-166.

Condie, K. C. and Nuter, J. A.; 1981. Geochemistry of the Dubois Greenstone Succession: An Early Proterozoic Bimodal Volcanic Association in West-Central Colorado. Precam. Res., 15, p. 131-155.

Condie, K. C. and Shadel, C. A.; 1984. An Early Proterozoic Volcanic Arc Succession in Southeastern Wyoming. Can. J. Earth Sci., 21, p. 415-427.

Condie, K. C.; Viljoen, M. J.; and Kable, E. J. D.; 1977. Effects of Alteration on Element Distributions in Archean Tholeiites from the Barberton Greenstone Belt, South Africa. Contrib. Mineral. Petrol., 64, p. 75-89.

Coulon, C. and Thorpe, R. S.; 1981. Role of Continental Crust in Petrogenesis of Orogenic Volcanic Associations. Tectonophy., 77, p. 79-93.

Cousens, B. L.; Chase, R. L.; and Schilling, J. -G.; 1984. Basalt Geochemistry of the Explorer Ridge Area, Northeast Pacific Ocean. Can. J. Earth Sci., 21, p. 157-170.

Crandell, D. R.; 1971. Postglacial Lahars from Mount Rainer Volcano, Washington. U. S. Geol. Sur. Prof. Pap., 677, p. 1-75.

Crook, K. A. W.; 1974. Lithogenesis and Geotectonics: The Significance of Compositional Variation in Flysch Arenites (Graywackes). Soc. Econ. Paleo. Mineral. Spec. Paper 19, p. 304-310.

Cummins, W. A.; 1962. The Greywacke Problem. Geol. J., 3, p. 51-72.

Darton, N. H.; 1928. 'Red Beds' and Associated Formations in New Mexico. U. S. Geol. Sur. Bull., 794, 356 pp.

Davy, R. and Lewis, J. D.; 1981. The Geochemistry of the Mount Edgar Batholith, Pilbara Area, Western Australia. Spec. Publ. geol. Soc. Aust., 7, p. 373-383.

De Boer, J.; Odom, L. A.; Ragland, P. C.; Snider, F. G.; and Tilford, N. R.; 1980. The Bataan Orogene: Eastward Subduction, Tectonic Rotations, and Volcanism in the Western Pacific (Philippines). Tectonophy., 67, p. 251-282.

Delaney, J. M. and Helgeson, H. C.; 1978. Calculation of the Thermodynamic Consequences of Dehydration in Subducting Oceanic Crust to 100 Kb. and >800 C. Am. J. Sci., 278, p. 638-686.

DePalo, D. J.; 1981. Neodymium Isotopes in the Colorado Front Range and Crust-Mantle Evolution in the Proterozoic. Nature 291, p. 193-196.

DePaolo, D. J.; 1983. The Mean Life of Continents: Estimates of Continent Recycling Rates from Nd and Hf Isotopic Data and Implications for Mantle Structure. Geophy. Res. Lett., 10, p. 705-708.

DePaolo, D. J. and Wasserburg, G. J.; 1977. The Sources of Island Arcs as Indicated by Nd and Sr Isotopic Studies. Geophy. Res. Lett., 4, p. 465-468.

Deruelle, B.; 1982. Petrology of the Plio-Quaternary Volcanism of the South-Central and Meridional Andes. J. Vol. Geother. Res., 14, p. 77-124.

Dickinson, W. R.; 1970. Interpreting Detrital Modes of Greywacke and Arkose. J. Sed. Pet., 40, p. 695-707.

Dickinson, W. R.; 1985. Interpreting Provenance Relations from Detrital Modes of Sandstones. p. 333-361 in Provenance of Arenites ed. by G. G. Zuffa, D. Reidel Publ. Co.

Dickinson, W. R.; Beard, L. S.; Brakenridge, G. R.; Erjavec, J. L.; Ferguson, R. C.; Inman, K. F.; Knepp, R. A.; Linberg, F. A.; and Ryberg, P. T.; 1983. Provenance of North America Phanerozoic Sandstones in Relation to Tectonic Setting. Geol. Soc. Am. Bull., 94, p. 222-235.

Dickinson, W. R. and Suczek, C. A.; 1979. Plate Tectonics and Sandstone Compositions. Am. Assoc. Pet. Geol., 63, p. 2164-2182.

Dietrich, V.; Emmermann, R.; Oberhansli, R.; and Puchelt, H.; 1978. Geochemistry of Basaltic and Gabbroic Rocks from the West Mariana Basin and the Mariana Trench. Earth Planet. Sci. Lett., 39, p. 127-144.

Dixon, T. H. and Batiza, R.; 1979. Petrology and Chemistry of Recent Lavas in the Northern Marianas: Implications for the Origin of Island Arc Basalts. Contrib. Mineral. Petrol., 70, p. 167-181.

Donnelly, T. W. and Rogers, J. J. W.; 1980. Igneous Series in Island Areas: The Northeastern Caribbean Compared with Worldwide Island-Arc Assemblages. Bull. Volcan., 43, p. 347-382.

Donnelly, T. W.; Rogers, J. J. W.; Pushkar, P.; and Armstrong, R. L.; 1971. Chemical Evolution of the Igneous Rocks of the Eastern West Indies: An Investigation of Thorium, Uranium, and Potassium Distributions, and Lead and Strontium Isotopic Ratios. Geol. Soc. Am. Mem., 130, p. 181-224.

Dostal, J. and Capedri, S.; 1975. Partition Coefficients of Uranium for Some Rock-Forming Minerals. Chem. Geol., 15, p. 223-233.

Dostal, J.; Capedri, S.; and Dupuy, C.; 1976. Uranium and Potassium in Calc-Alkaline Volcanic Rocks from Sardinia. Lithos 9, p. 179-183.

Dostal, J.; Dupuy, C.; Carron, J. P.; Le Guen De Kerneizon, M.; and Maury, R. C.; 1983. Partition Coefficients of Trace Elements: Applications to Volcanic Rocks of St. Vincent, West Indies. Geochim. Cosmochim. Acta 47, p. 525-533.

Dostal, J. and Strong, D. F.; 1983. Trace-Element Mobility During Low-Grade Metamorphism and Silicification of Basaltic Rcoks from Saint John, New Brunswick. Can. J. Earth Sci., 20, p. 431-435.

Drake, M. J.; 1976. Evolution of Major Mineral Compositions and Trace Element Abundances During Fractional Crystallization of a Model Lunar Composition. Geochim. Cosmochim. Acta 40, p. 401-411.

Drury, S. A.; 1983. The Petrogenesis and Setting of Archean Metavolcanics from Karnataka State, South India. Geochim. Cosmochim. Acta 47, p. 317-329.

Dupuy, C.; Dostal, J.; Marcelot, G.; Bougault, H.; Joron, J. L.; and Treuil, M.; 1982. Geochemistry of Basalts from Central and Southern New Hebrides Arc: Implications for Their Source Rock Composition. Earth Planet. Sci. Lett., 60, p. 207-225.

Eggler, D. H.; 1972. Water-Saturated and Undersaturated Melting Relations in a Paricutin Andesite and an Estimate of Water Content in the Natural Magma. Contrib. Mineral. Petrol., 34, p. 261-271.

Eggler, D. H. and Burnham, C. W.; 1973. Crystallization and Fractionation Trends in the System Andesite-H2O-CO2-O2 at Pressures to 10 Kb. Geol. Soc. Am. Bull., 84, p. 2512-2532.

Ehmann, W. D. and Rebagay, T. V.; 1970. Zirconium and Hafnium in Meteroites by Activation Analysis. Geochim. Cosmochim. Acta 34, p. 649-658.

Eichelberger, J. C.; 1975. Origin of Andesite and Dacite: Evidence of Mixing at Glass Mountain in California and the Other Circum-Pacific Volcanoes. Geol. Soc. Am. Bull., 86, p. 1381-1391.

Eichelberger, J. C.; 1978. Andesite Volcanism and Crustal Evolution. Nature 275, p. 21-27.

Elliott, R. B.; 1973. The Chemistry of Gabbro/Amphibolite Transitions in South Norway. Contrib. Mineral. Petrol., 38, p. 71-79.

Engel, A. E. J.; 1963. Geologic Evolution of North America. Science 140, p. 143-152.

Ewart, A.; 1979. A Review of the Mineralogy and Chemistry of Teriary-Recent Dacitic, Latitic, Rhyolitic, and Related Salic Volcanic Rocks. p. 13-121 in Trondhjemites, Dacites, and Related Rocks ed. by F. Barker, Elsevier Sci. Publ. Co.

Ewart, A.; 1981. The Mineralogy and Chemistry of the Anorogenic Tertiary Silicic Volcanics of S. E. Queensland and N. E. New South Wales, Australia. J. Geophy. Res., 86, p. 10242-10256.

Ewart, A.; 1982a. The Mineralogy and Petrology of Tertiary-Recent Orogenic Rocks: With Special Reference to the Andesitic-Basaltic Compositional Range. p. 25-95 in Andesites ed. by R. S. Thorpe, John-Wiley and Sons.

Ewart, A.; 1982b. Petrogenesis of the Tertiary Anorogenic Volcanic Series of Southern Queensland, Australia, in the Light of Trace Element Geochemistry and O, Sr and Pb Isotopes. J. Petrol., 23, p. 344-382.

Ewart, A.; Brothers, R. N.; and Mateen, A.; 1977. An Outline of the Geology and Geochemistry, and the Possible Petrogenetic Evolution of the Volcanic Rocks of the Tonga-Kermadec-New Zealand Island Arc. J. Volc. Geother. Res., 2, p. 205-250.

Ewart, A. and Bryan, W. B.; 1973. The Petrology and Geochemistry of the Tongan Islands. p. 503-522 in The Western Pacific: Island Arcs, Marginal Seas, Geochemistry ed. by P. J. Coleman, Crane, Russak and Co., Inc. New York.

Ewart, A.; Bryan, W. B.; and Gill, J. B.; 1973. Mineralogy and Geochemistry of the Younger Volcanic Islands of Tonga, S. W. Pacific. J. Petrol., 14, p. 429-465.

Ewart, A.; Hildreth, W.; and Carmichael, I. S. E.; 1975. Quaternary Acid Magma in New Zealand. Contrib. Mineral. Petrol., 51, p. 1-27.

Ewart, A. and Taylor, S. R.; 1969. Trace Element Geochemistry of the Rhyolitic Volcanic Rocks, Central

North Island, New Zealand. Phenocryst Data. Contrib. Mineral. Petrol., 22, p. 127-146.

Ewart, A.; Taylor, S. R.; and Capp, A. C.; 1968. Trace and Minor Element Geochemistry of the Rhyolitic Volcanic Rocks, Central North Island, New Zealand. Contrib. Mineral. Petrol., 18, p. 76-104.

Fairbrothers, G. E.; Carr, M. J.; and Mayfield, D. G.; 1978. Temporal Magmatic Variation at Boqueron Volcano, El Salvador. Contrib. Mineral. Petrol., 67, p. 1-9.

Fallis, Jr., J. F.; 1958. Geology of the Pedernal Hills Area, Torrance County, New Mexico. Unpubl. Masters thesis, U. New Mex., 50 pp.

Fernandez, A.; Hormann, P. K.; Kussmaul, S.; Meave, J.; Pichler, H.; and Subieta, T.; 1978. First Petrologic Data on Young Volcanic Rocks of S. W. Bolivia. Tscher. Mineral. Petrogr. Mitt., 19, p. 149-172.

Field, D. and Elliott, R. B.; 1974. The Chemistry of Gabbro/Amphibolite Transitions in South Norway. II. Trace Elements. Contrib. Mineral. Petrol., 47, p. 63-76.

Field, D.; Drury, S. A.; and Cooper, D. C.; 1980. Rare-Earth and LIL Element Fractionation in High-Grade Charnokitic Gneisses, South Norway. Lithos 13, p. 281-289.

Field, M. E. and Pilkey, O. H.; 1969. Feldspar in Atlantic Continental Margin Sands off the Southeastern United States. Geol. Soc. Am. Bull., 80, p. 2097-2102.

Fisher, R. V.; 1979. Models of Pyroclastic Surges and Pyroclastic Flows. J. Volcan. Geotherm. Res., 6, p. 305-318.

Fisher, R. V. and Schmincke, H. U.; 1984. Pyroclastic Rocks. Springer-Verlag, Berlin, 472 pp.

Fiske, R. S.; 1963. Subaqueous Pyroclastic Flows in the Ohanapecoh Formation, Washington. Geol. Soc. Am. Bull., 74, p. 391-406.

Fitton, J. G.; 1971. The Generation of Magmas in Island Arcs. Earth Planet. Sci. Lett., 11, p. 63-67.

Fitzsimmons, J. P.; 1961. Precambrian Rocks of the Albuquerque Country. New Mex. Geol. Soc. Guidebk., 12, p. 90-96.

Floyd, P. A. and Winchester, J. A.; 1975. Magma Type and Tectonic Setting Discrimination Using Immobile Elements. Earth Planet. Sci. Lett., 27, p. 211-218.

Folk, R. L.; 1965. Petrology of Sedimentary Rocks. U. Texas, 170 pp.

Francis, E. H. and Howells, M. F.; 1973. Transgressive Welded Ash-Flow Tuffs Among the Ordovician Sediments of NE Snowdonia, N. Wales. J. geol. Soc. Lond., 129, p. 621-641.

Frey, F. A.; Bryan, W. B.; and Thompson, G.; 1974. Atlantic Ocean Floor: Geochemistry and Petrology of Basalts from Legs 2 and 3 of the Deep-Sea Drilling Project. J. Geophy. Res., 79, p. 5507-5527.

Frey, F. A.; Gerlach, D. C.; Hickey, R. L. Lopez-Escobar, L.; and Munizaga-Villavicencio, F.; 1984. Petrogensis of the Laguna del Maule Volcanic Complex, Chile (36 S). Contrib. Mineral. Petrol., 88, p. 133-149.

Frey, F. A. and Green, D. H.; 1974. The Mineralogy, Geochemistry and Origin of Lherzolite Inclusions in Victorian Basanites. Geochim. Cosmochim. Acta 38, p. 1023-1059.

Frey, F. A.; Haskin, M. A.; Poetz, J. A.; and Haskin, L. A.; 1968. Rare Earth Abundances in Some Basic Rocks. J. Geophy. Res., 73, p. 6085-6098.

Garcia, M. O.; 1978. Criteria for the Identification of Ancient Volcanic Arcs. Earth Sci. Rev., 14, p. 147-165.

Gelinas, L.; Mellinger, M.; and Trudel, P.; 1982. Archean Mafic Metavolcanics from the Rouyn-Noranda District, Abitibi Greenstone Belt, Quebec. 1. Mobility of the Major Elements. Can. J. Earth Sci., 19, p. 2258-2275.

Gibson, I. L. and Jagan, P.; 1980. Instrumental Neutron Activation Analysis of Rocks and Minerals. p. 109-131 in Short Course in Neutron Activation Analysis in Geosciences ed. by G. K. Muecke, Min. Assoc. Can., Halifax.

Gill, J.; 1981. Orogenic Andesites and Plate Tectonics. Springer, 390 pp.

Gill, J. B.; 1984. Sr-Pb-Nd Isotopic Evidence That Both MORB and OIB Sources Contribute to Oceanic Island Arc Magmas in Fiji. Earth Planet. Sci. Lett., 68, p. 443-458.

Gladney, E. S.; Burns, C. E.; and Roelandts, I.; 1983. 1982 Compliation of Elemental Concentrations in Eleven United States Geological Survey Rock Standards. Geostand. Newslett., 7, p. 3-226.

Goldich, S. S.; Hanson, G. N.; Hallford, C. R.; and Mudrey, Jr., M. G.; 1972. Early Precambrian Rocks in the Saganaga Lake - Northern Light Lake Area, Minnesota - Ontario Part I. Petrology and Structure. Geol. Soc. Am. Mem., 135, p. 151-177.

Gonzalez, R. A.; 1968. Petrography and Structure of the Pedernal Hills, Torrance County, New Mexico. Unpubl. Masters thesis, U. New Mex., 78 pp.

Gonzalez, R. A. and Woodward, L. A.; 1972. Petrology and Structure of Precambrian Rocks of the Pedernal Hills, New Mexico. New Mex. Geol. Soc. Guidebk. 23, p. 144-147.

Gordon, G. E.; Randle, K.; Goles, G.; Corliss, J.; Beeson, M.; and Oxley, S.; 1968. Instumental Neutron Activation Analysis of Standard Rocks with High Resolution Gamma-Ray Detectors. Geochim. Cosmochim. Acta 32, p. 369-396.

Graham, A. L. and Mason, B.; 1972. Niobium in Meteorites. Geochim. Cosmochim. Acta 36, p. 917-922.

Grambling, J. A.; 1982. Precambrian Structures in Canon del Trigo, Manzano Mountains, New Mexico. New Mex. Geol. Soc. Guidebk. 33, p. 217-220.

Green, D. H.; 1971. Composition of Basaltic Magmas as Indicators of Conditions of Origin: Application to Oceanic Volcanism. Phil. Trans. R. Soc. Lond., 268A, p. 707-725.

Green, D. H.; 1973. Magmatic Consequences of Plate Tectonics. abst., p. 455-457 in The Western Pacific: Island Arcs, Marginal Seas, Geochemistry ed. by P. J. Coleman, Crane, Russak and Co., Inc., New York.

Green, D. H. and Ringwood, A. E.; 1967. An Experimental Investigation of the Gabbro to Eclogite Transformation and Its Petrological Applications. Geochim. Cosmochim. Acta 31, p. 767-833.

Green, T. H. and Ringwood, A. E.; 1968. Genesis of the Calc-Alkaline Igneous Rock Suite. Contrib. Mineral. Petrol., 18, p. 105-162.

Greenberg, J. K. and Brown, B. A.; 1983. Lower Proterozoic Volcanic Rocks and Their Setting in the Southern Lake Superior District. Geol. Soc. Am. Mem., 160, p. 67-84.

Grove, T. L. and Donnelly-Nolan, J. M.; 1986. The Evolution of Young Silicic Lavas at Medicine Lake Volcano, California: Implications for the Origin of Compositional Gaps in Calc-alkaline Series Lavas. Contr. Mineral. Petrol., 92, p. 281-302.

Hajash, A.; 1975. Hydrothermal Processes Along Mid-Ocean Ridges: An Experimental Investigation. Contrib. Mineral. Petrol., 53, p. 205-226.

Hajash, Jr., A.; 1984. Rare Earth Element Abundances and Distribution Patterns in Hydrothermally Altered Basalts: Experimental Results. Contrib. Mineral. Petrol., 85, p. 409-412.

Hajash, A. and Archer, P. L.; 1980. Experimental Seawater/Basalt Interactions: Effect of Cooling. Cantrib. Mineral. Petrol., 75, p. 1-3.

Hajash, A. and Chandler, G. W.; 1981. An Experimental Investigation of High Temperature Interactions Between Seawater and Rhyolite, Andesite, Basalt, and Peridotite. Contrib. Mineral. Petrol., 81, p. 240-254.

Hamilton, W.; 1969. Mesozoic California and the Underflow of Pacific Mantle. Geol. Soc. Am. Bull., 80, p. 2409-2430.

Hanson, G. N.; 1978. The Application of Trace Elements to the Petrogenesis of Igneous Rocks of Granitic Composition. Earth Planet. Sci. Lett., 38, p. 26-43.

Hanson, G. N.; 1980. Rare Earth Elements in Petrogenetic Studies of Igneous Systems. Ann. Rev. Earth Planet. Sci., 8, p. 371-406.

Hanson, G. N. and Langmuir, C. H.; 1978. Modelling of Major Elements in Mantle-Melt Systems Using Trace Element Approaches. Geochim. Cosmochim. Acta 42, p. 725-741.

Harris, P. G.; Kennedy, W. O.; and Scarfe, C. M.; 1970. Volcanism Versus Plutonism - The Effect of Chemical Composition. p. 187-200 in Mechanisms of Igneous Intrusion ed. by G. Newall and N. Rust, Geol. J. Spec. Issue 2.

Harrison, W. J.; 1981. Partition Coefficients for REE Between Garnets and Liquids: Implications of Non-

Henry's Law Behavior for Models of Basalt Origin and Evolution. Geochim. Cosmochim. Acta 45, p. 1529-1544.

Harrison, T. M. and Watson, E. B.; 1984. The Behavior of Apatite During Crustal Anatexis: Equilibrium and Kinetic Considerations. Geochim. Cosmochim. Acta 48, p. 1467-1477.

Hart, S. R.; 1969. K, Rb, Cs Contents and K/Rb, K/Cs Ratios of Fresh and Altered Submarine Basalts. Earth Planet. Sci. Lett., 6, p. 295-303.

Hart, R.; 1970. Chemical Exchange Between Sea Water and Deep Ocean Basalts. Earth Planet. Sci. Lett., 9, p. 269-279.

Hart, S. R. and Davis, K. E.; 1978. Nickel Partitioning Between Olivine and Silicate Melt. Earth Planet. Sci. Lett., 40, p. 203-220.

Hart, S. R.; Erlank, A. J.; and Kable, E. J. D.; 1974. Sea Floor Basalt Alteration: Some Chemical and Sr Isotopic Effects. Contrib. Mineral. Petrol., 44, p. 219-230.

Hawkesworth, C. J.; 1979. 143Nd/144Nd, 87Sr/86Sr and Trace Element Characteristics of Magmas Along Destructive Plate Margins. p. 76-89 in Origin of Granite Batholiths: Geochemical Evidence ed. by M. P. Atherton and J. Tarney, Shiva Publ. Ltd., Kent, U. K.

Hawkesworth, C. J.; O'Nions, R. K.; and Arculus, R. J.; 1979. Nd- and Sr-Isotope Geochemistry of Island Arc Volcanics, Grenada, Lesser Antilles. Earth Planet. Sci. Lett., 45, p. 237-248.

Hawkesworth, C. J.; O'Nions, R. K.; Pankhurst, R. J.; Hamilton, P. J.; and Evensen, N. M.; 1977. A Geochemical Study of Island-Arc and Back-Arc Tholeiites from the Scotia Sea. Earth Planet. Sci. Lett., 36, p. 253-262.

Hawkesworth, C. J. and Powell, M.; 1980. Magma Genesis

in the Lesser Antilles Island Arc. Earth Planet. Sci. Lett., 51, p. 297-308.

Hawkesworth, C. J.; Rogers, N. W.; van Calsteren, P. W. C.; and Menzies, M. A.; 1984. Mantle Enrichment Processes. Nature 311, p. 331-335.

Hawkins, Jr., J. W. and Whetten, J. T.; 1969. Graywacke Matrix Minerals: Hydrothermal Reactions with Columbia River Sediments. Science 66, p. 868-870.

Heiken, G. and Eichelberger, J. C.; 1980. Eruption of Chaos Crage, Lassen Volcanic National Park, California. J. Volcan. Geotherm. Res., 7, p. 443-481.

Hekinian, R.; 1971. Chemical and Mineralogical Differences Between Abyssal Hill Basalts and Ridge Tholeiites in the Eastern Pacific Ocean. Marine Geol., 11, p. 77-91.

Hellman, P. L. and Henderson, P.; 1977. Are Rare Earth Elements Mobile During Spilitisation? Nature 267, p. 38-40.

Hellman, P. L.; Smith, R. E.; and Henderson, P.; 1977. Rare Earth Element Investigation of the Cliefden Outcrop, N. S. W., Australia. Contrib. Mineral. Petrol., 65, p. 155-164.

Hellman P. L.; Smith, R. E.; and Henderson, P.; 1979. The Mobility of the Rare Earth Elements: Evidence and Implications from Selected Terrains Affected by Burial Metamorphism. Contrib. Mineral. Petrol., 71, p. 23-44.

Helz, R. T.; 1973. Phase Relations of Basalts in Their Melting Range at PH2O = 5 kb as a Function of Oxygen Fugacity. Part I. Mafic Phases. J. Petrol., 14, p. 249-302.

Helz, R. T.; 1976. Phase Relations of Basalts in Their Melting Ranges at PH2O = 5 Kb. Part II. Melt Compositions. J. Petrol., 17, p. 139-193.

Hildreth, W.; 1979. The Bishop Tuff: Evidence for the Origin of Compostional Zonation in Silicic Magma Chambers. Geol. Soc. Am. Spec. Pap., 180, p. 43-75.

Hildreth, W.; 1981. Gradients in Silicic Magma Chambers: Implications for Lithospheric Magmatism. J. Geophy. Res. 86, p. 10153-10192.

Hoffman, P. H.; 1980. Wopmay Orogen: A Wilson-Cycle of Early Proterozoic Age in the Northwest of the Canadian Shield. Geol. Assoc. Canada Spec. Pap. 20, p. 523-549.

Hole, M. J.; Saunders, A. D.; Marriner, G. F.; and Tarney, J.; 1984. Subduction of Pelagic Sediments: Implications for the Origin of Ce-Anomalous Basalts from the Mariana Islands. J. geol. Soc. Lond., 141, p. 453-472.

Holloway, J. R. and Burnham, C. W.; 1972. Melting Relations of Basalt with Equilibrium Water Pressure Less than Total Pressure. J. Petrol., 13, p. 1-29.

Holm, P. E.; 1982. Non-Recognition of Continental Tholeiites Using the Ti-Y-Zr Diagram. Contrib. Mineral. Petrol., 79, p. 308-310.

Holm, P. M. and Munksgaard, N. C.; 1982. Evidence for Mantle Metasomatism: An Oxygen and Strontium Isotope Study of the Vulsianian District, Central Italy. Earth Planet. Sci. Lett., 60, p. 276-388.

Howells, M. F.; Campbell, S. D. G.; and Reedman, A. J.; 1985. Isolated Pods of Subaqueous Welded Ash-Flow Tuff: A Distal Facies of the Capel Curing Volcanic Formation (Ordovician), North Wales. Geol. Mag., 122, p. 175-180.

Humphris, S. E. and Thompson, G.; 1978. Trace Element Mobility During Hydrothermal Alteration of Oceanic Basalts. Geochim. Cosmochim. Acta 42, p. 127-136.

Hynes, A.; 1980. Carbonatization and Mobility of Ti, Y, and Zr, in Ascot Fromation Metabasalts, SE Quebec. Contrib. Mineral. Petrol., 75, p. 79-87.

Irvine, T. N. and Baragar, W. R.; 1971. A Guide to the Chemical Classification of the Common Igneous Rocks. Can. J. Earth Sci., 8, p. 523-548.

Irving, A. J.; 1978. A Review of Experimental Studies of Crystal/Liquid Trace Element Partitioning. Geochim. Cosmochim. Acta 42, p. 743-770.

Irving, A. J. and Frey, F. A.; 1978. The Distribution of Trace Elements Between Garnet Megacrysts and Volcanic Liquids of Kimberlitic to Rhyolitic Compositions. Geochim. Cosmochim. Acta 42, p. 771-787.

Ishizaka, K. and Tatsumi, Y.; 1980. On Trace Element Contents of Some Ryozen Volcanic Rocks from the Northeastern Part of Fukushima Prefecture - A Preliminary Report. J. Japan Assoc. Min. Petr. Econ. Geol., 75, p. 10-13.

Jacob, K. H.; Nakamura, K.; and Davies, J. N.; 1977. Trench-Volcano Gap Along the Alaska-Aleutian Arc: Facts, and Speculations on the Role of Terrigenous Sediments for Subduction. p. 243-258 in Island Arcs, Deep Sea Trenches, and Back-Arc Basins ed. by M. Talwani and W. C. Pitman III, Am. Geophy. U., Maurice Ewing Ser., 1.

Jakes, P. and White, A. J. R.; 1969. Structure of the Melanesian Arcs and Correlation with Distribution of Magma Types. Tectonophy., 8, p. 223-236.

Jakes, P. and White, A. J. R.; 1972. Major and Trace Element Abundances in Volcanic Rocks of Orogenic Areas. Geol. Soc. Am. Bull., 83, p. 29-40.

James, D. E.; 1982. Combined O, Sr, Nd, Pb Isotopic and Trace Element Study of Crustal Contamination in Central Andean Lavas. I. Local Chemical Variation. Earth Planet. Sci. Lett., 57, p. 47-62.

Jensen, L. S.; 1976. A New Cation Plot for Classifying Subalkaline Volcanic Rocks. Ontario Division of Mines Misc. Pap., 66, 22 pp.

Jezek, P. A. and Noble, D. C.; 1978. Natural Hydration and Ion Exchange of Obsidian: An Electon Microprobe Study. Am. Mineral., 63, p. 266-273.

Johnson, D. W.; 1902. Notes of a Geological Reconnoissance in Eastern Valencia County, New Mexico. The Amer. Geol., 29, p. 80-87.

Johnson, S. C.; 1986. Structural Analysis of the Contact Between Precambrian Lower Metaclastics and Sais Quartzite, Comanche Canyon, Central Manzano Mountains, Central New Mexico. abst in New Mex. Geol., 8, p. 21.

Jones, N. W. and Bloss, F. D.; 1980. Laboratory Manual for Optical Mineralogy. Burgess Publ. Co., Minneapolis, Minn., 192 pp.

Katsui, Y.; 1963. Evolution and Magmatic History of Some Krakatoan Calderas in Hokkaido, Japan. J. Fac. Sci. Hokkaido Univ., Ser. 4., 11, p. 631-650.

Kay, R. W.; 1977. Geochemical Constraints on the Origin of Aleutian Magmas. p. 229-242 in Island Arcs, Deep Sea Trenches, and Back-Arc Basins ed. by M. Talwani and W. C. Pitman III, Am. Geophy. U., Maurice Ewing Ser., 1.

Kay, R. W.; 1980. Volcanic Arc Magmas: Implications of a Melting-Mixing Model for Element Recycling in the Crust-Upper Mantle System. J. Geol., 88, p. 497-522.

Kay, R. W.; 1984. Elemental Abundances Relevant to Identification of Magma Sources. Phil. Trans. R. Soc. Lond., A310, p. 535-547.

Kay, S. M.; Kay, R. W.; and Citron, G. P.; 1982. Tectonic Controls on Tholeiitic and Calc-Alkaline Magmatism in the Aleutian Arc. J. Geophy. Reas.,

87, p. 4051-4072.

Kelley, V. C.; 1972. Geology of the Fort Sumner Sheet, New Mexico. New Mex. Bur. Mines Min. Res. Bull., 98, 55 pp.

Kennedy, G. C.; 1955. Some Aspects of the Role of Water in Rock Melts. Geol. Soc. Am. Spec. Pap., 62, p. 489-504.

Kluth, C. F. and Coney, P. J.; 1981. Plate Tectonics of the Ancestral Rocky Mountains. Geol., 9, p. 10-15.

Kokelaar, B. P.; Howells, M. F.; Bevins, R. E.; and Rouch, R. A.; 1984. Volcanic and Associated Sedimentary and Tectonic Processes in the Ordovician Margianl Basin of Wales: A Field Guide. p. 291-322 in Margin Basin Geology ed. by B. P. Kokelaar and M. F. Howells, Geol. Soc. Spec. Publ., 16.

Kokelaar, B. P.; Howells, M. F.; Bevins, R. E.; Rouch, R. A.; and Dunkley, P. N.; 1984. The Ordovician Marginal Basin of Wales. p. 245-269 in Margin Basin Geology ed. by B. P. Kokelaar and M. F. Howells, Geol. Soc. Spec. Publ., 16.

Kuno, H.; 1959. Origin of Cenozoic Petrographic Provinces of Japan and Surrounding Areas. Bull. Volc., 20, p. 37-76.

Kuno, H.; 1960. High-Alumina Basalt. J. Petrol., 1, p. 121-145.

Kuno, H.; 1968. Origin of Andesite and Its Bearing on the Island Arc Structure. Bull. Volc., 32, p. 141-176.

Kushiro, I.; 1972. Effect of Water on the Composition of Magmas Formed at High Pressures. J. Petrol., 13, p. 311-334.

Kushiro, I. and Sato, H.; 1978. Origin of Calc-alkaline Andesites in Japanese Island: Critical Review and Discussion. abst., p. 284-285 in International

Geodynamics Conference Western Pacific and Magma Genesis.

Kushiro, I.; Shimizu, N.; and Nakamura, Y.; 1972. Compositions of Coexisting Liquid and Solid Phases Formed Upon Melting of Natural Garnet and Spinal Lherzolites at High Pressures: A Preliminary Report. Earth Planet. Sci. Lett., 14, p. 19-25.

Langmuir, C. H.; Bender, J. F.; Bence, A. E.; and Hanson, G. N.; 1977. Petrogenesis of Basalts from the Famous Area: Mid-Atlantic Ridge. Earth Planet. Sci. Lett., 36, p. 133-156.

Lewis, J. F.; 1969. Composition, Physical Properties and Origin of Sodic Anorthosites from the Ejected Plutonic Blocks of the Soufriere Volcano, St. Vincent, West Indies. Contrib. Mineral. Petrol., 21, p. 272-294.

Lewis, J. F.; 1970. Chemical Composition and Physical Properties of Magnetite from the Ejected Plutonic Blocks of the Soufriere Volcano, St. Vincent, West Indies. Amer. Mineral., 55, p. 793-807.

Lewis, J. F.; 1971. Composition, Origin, and Differentiation of Basalt Magma in the Lesser Antilles. p. 159-179 in Caribbean Geophysical, Tectonic, and Petrologic Studies, ed. by T. W. Donnelly, Geol. Soc. Am. Mem., 130.

Lewis, J. F.; 1973a. Mineralogy of the Ejected Plutonic Blocks of the Soufriere Volcano, St. Vincent: Olivine, Pyroxene, Amphibole and Magnetite Paragenesis. Contrib. Mineral. Petrol., 38, p. 197-220.

Lewis, J. F.; 1973b. Petrology of the Ejected Plutonic Blocks of the Soufriere Volcano, St. Vincent, West Indies. J. Petrol., 14, p. 81-112.

Lindstrom, D. J.; 1983. Kinetic Effects on Trace Element Partitioning. Geochem. Cosmochim. Acta 47, p. 617-622.

Lipman, P. W.; 1965. Chemical Compositon of Glassy and Crystalline Volcanic Rocks. U. S. Geol. Sur. Bull., 1201-D, D1-D24.

Lipman, P. W.; 1969. Alkalic and Tholeiitic Basaltic Volcanism Related to the Rio Grande Depression, Southern Colorado and Northern New Mexico. Geol. Soc. Am. Bull., 80, p. 1343-1354.

Lipman, P. W.; 1967. Mineral and Chemical Variations Within an Ash-Flow Sheet from Aso Caldera, Southwestern Japan. Contr. Mineral. Petrol., 16, p. 300-327.

Lipman, P. W. and Moench, R. H.; 1972. Basalts of the Mount Taylor Volcanic Field, New Mexico. Geol. Soc. Am. Bull., 83, p. 1335-1344.

Lloyd, B. P. and Bailey, D. K.; 1975. Light Element Metasomatism of the Continental Mantle: The Evidence and the Consequences. Phys. Chem. Earth 9, p. 389-416.

Lopez-Escobar, L.; Frey, F. A.; and Vergara, M.; 1977. Andesites and High-Alumina Basalts from Central-South Chile High Andes: Geochemical Evidence Bearing on Their Petrogenesis. Contrib. Mineral. Petrol., 63, p. 199-228.

Lopez-Escobar, L.; Vergara, M.; and Frey, F. A.; 1981. Petrology and Geochemistry of Lavas from Antaco Volcano, a Basaltic Volcano of the Southern Andes. J. Volcan. Geotherm. Res., 11, p. 329-352.

Loring, A. K.; and Armstrong, D. G.; 1982. Cambrian-Ordovician Syenites of New Mexico, Part of a Regional Alkalic Intrusive Episode. Geol., 8, p. 344-348.

Ludden, J. N. and Thompson, G.; 1978. Behaviour of Rare Earth Elements During Submarine Weathering of Tholeiitic Basalt. Nature 274, p. 147-149.

Ludden, J. N. and Thompson, G.; 1979. An Evaluation of the Behaviour of the Rare Earth Elements During the Weathering of Sea-Floor Basalt. Earth Planet. Sci.

Lett., 43, p. 85-92.

Ludden, J.; Gelinas, L.; and Trudel, P.; 1982. Archean Metavolcanics from the Rouyn-Noranda District, Abitibi Greenstone Belt, Quebec. 2. Mobility of Trace Elements and Petrogenetic Constraints. Can. J. Earth Sci., 19, p. 2276-2287.

Luhr, J. F. and Carmichael, I. S. E.; 1980. The Colima Volcanic Complex, Mexico. I. Post-Caldera Andesites from Volcan Colima. Contrib. Mineral. Petrol., 71, p. 343-372.

Luhr, J. F. and Carmichael, I. S. E.; 1985. Jorullo Volcano, Michoacan, Mexico (1759-1774): The Earliest Stages of Fractionation in Calc-alkaline Magmas. Contrib. Mineral. Petrol., 90, p. 142-161.

Maaloe, S. and Wyllie, P. J.; 1975. Water Content of a Granite Magma Deduced from the Sequence of Crystallization Determined Experimentally with Water-Undersaturated Conditions. Contrib. Mineral. Petrol., 52, p. 175-191.

McCarthy, T. S. and Hasty, R. A.; 1976. Trace Element Distibution Patterns and Their Relationship to the Crystallization of Granite Melts. Geochim. Cosmochim. Acta 40, p. 1351-1358.

McCulloch, M. T. and Prefit, M. R.; 1981. 143Nd/144Nd, 87Sr/86Sr and Trace Element Constraints on the Petrogenesis of Aleutian Island Arc Magmas. Earth Planet. Sci. Lett., 50, p. 167-179.

Macdonald, G. A. and Katsura, T.; 1964. Chemical Composition of Hawaiian Lavas. J. Petrol., 5, p. 82-133.

MacGeehan, P. J. and MacLean, W. H.; 1980. An Archean Sub-Seafloor Geothermal System, 'Calc-Alkali' Trends, and Massive Sulphide Genesis. Nature 286, p. 767-771.

Mack, G. H.; 1984. Exceptions to the Relationship Between Plate Tectonics and Sandstone Compositions. J. Sed.

Petrol., 54, p. 212-220.

McLennan, S. M. and Taylor, S. R.; 1981. Role of Subducted Sediments in Island-Arc Magmatism: Constraints from REE Patterns. Earth Planet. Sci. Lett., 54, p. 423-430.

Mann, A. C.; 1983. Trace Element Geochemistry of High Alumina Basalt-Andesite-Dacite-Rhyodacite Lavas of the Main Volcanic Series of Santorini Volcano, Greece. Contrib. Mineral. Petrol., 84, p. 43-57.

Magaritz, M.; Whitford, D. J.; and James D. E.; 1978. Oxygen Isotopes and the Origin of High - 87Sr/86Sr Andesites. Earth Planet. Sci. Lett., 40, p. 220-230.

Mallory, W. W.; 1975. Middle Southern Rocky Mountains, Northern Colorado Plateau, and Eastern Great Basin. U. S. Geol. Sur. Prof. Pap., 853, p. 265-278.

Marsh, B. D.; 1973. Island Arc Magmatism. abstr. in Am. Geophy. U. Trans., 54, p. 1206.

Marsh, B. D.; 1976. Some Aleutian Andesites: Their Nature and Source. J. Geol., 84, p. 27-45.

Marsh, B. D. and Carmichael, I. S. E.; 1974. Benioff Zone Magmatism. J. Geophy. Res., 79, p. 1196-1206.

Marsh, B. D. and Leitz, R. E.; 1978. Geology of Amak Island, Aleutian Islands, Alaska. J. Geol., 87, p. 715-723.

Masuda, Y. and Aoki, K. -I.; 1978. Two Types of Island Arc Tholeiite in Japan. Earth Planet. Sci. Lett., 39, p. 298-302.

Masuda, Y. and Aoki, K.; 1979. Trace Element Variations in the Volcanic Rocks from the Nasu Zone, Northeastern Japan. Earth Planet. Sci. Lett., 44, p. 139-149.

Maxwell, C. H.; 1982. Geochemical and Geophysical Maps of the Manzano Wilderness, Valencia and Torrance Counties, New Mexico. U. S. Geol. Sur. Miscell. Field Studies Map MF1464-C.

Maxwell, C. H. and Wobus R. A.; 1982a. Geologic Map of the Manzano Wilderness, Valencia and Torrance Counties, New Mexico. U. S. Geol. Sur. Miscell. Field Studies Map MF1464-A.

Maxwell, C. H. and Wobus, R. A.; 1982b. Mineral Resource Potential of the Manzano Wilderness, Valencia and Torrance Counties, New Mexico. U. S. Geol. Sur. Miscell. Field Studies Map MF1464-B.

Maynard, J. B.; Vallanoi, R.; and Yu, H. -S.; 1982. Composition of Modern Deep-Sea Sands from Arc-Related Basins. Geol. Soc. Lond. Spec. Publ., 10, p. 551-561.

McBirney, A. R. and Williams, H.; 1969. Geology and Petrology of the Galapagos Islands. Geol. Soc. Am. Mem., 118, 197 pp.

Meijer, A.; 1976. Pb and Sr Isotopic Data Bearing on the Origin of Volcanic Rocks from the Mariana Island-Arc System. Geol. Soc. Am. Bull., 87, p. 1358-1369.

Meijer, A.; 1983. The Origin of Low-K Rhyolites from the Mariana Frontal Arc. Contrib. Mineral. Petrol., 83, p. 45-51.

Meinzer, O. E.; 1911. Geology and Water Resources of Estancia Valley, New Mexico: With Notes on Ground-Water Conditions in Adjacent Parts of Central New Mexico. U. S. Geol. Sur. Water-Supply Pap., 275, 89 pp.

Menzies, M. and Seyfried, Jr., W.; 1979. Experimental Evidence of Rare Earth Element Immobility in Greenstones. Nature 282, p. 398-399.

Mertzman, Jr., S. A.; 1978. A Tschermakite-Bearing High-Alumina Olivine Tholeiite from the Southern Cascades, California. Contrib. Mineral. Petrol., 67, p. 261-

265.

Mitchell, A. H. and Reading H. G.; 1971. Evolution of Island Arcs. J. Geol., 79, p. 253-284.

Miyashiro, A.; 1972. Metamorphism and Related Magmatism in Plate Tectonics. Am. J. Sci., 272, p. 629-656.

Miyashiro, A.; 1973. Paired and Unpaired Mobile Belts. Am. J. Sci., 273, p. 321-355.

Miyashiro, A. and Shido, F.; 1975. Tholeiitic and Calc-Alkalic Series in Relation to the Behaviors of Titanium, Vanadium, Chromium, and Nickel. Am. J. Sci., 275, p. 265-277.

Moore, J. C.; 1973. Complex Deformation of Cretaceous Trench Deposits, Southeastern Alaska. Geol. Soc. Am. Bull., 84, p. 2005-2020.

Moore, J. C.; 1975. Selective Subduction. Geol., 3, p. 530-532.

Morice, M. G.; Jezek, P. A.; Gill, J. B.; Whitford, D. J.; and Monoarfa, M.; 1983. An Introduction to the Sangihe Arc: Volcanism Accompanying Arc-Arc Collision in the Molucca Sea, Indonesia. J. Volc. Geotherm. Res., 19, p. 135-165.

Morris, J. D. and Hart, S. R.; 1983. Isotopic and Incompatible Element Constraints on the Genesis of Island Arc Volcanics from Cold Bay and Amak Island, Aleutians, and Implications for Mantle Structure. Geochim. Cosmochim. Acta 47, p. 2015-2030.

Morrison, M. A.; 1978. The Use of "Immobile" Trace Elements to Distinquish the Paleotectonic Affinities of Metabasalts: Applications to the Paleocene Basalts of Mull and Skye, Northwest Scotland. Earth Planet. Sci. Lett., 39, p. 407-416.

Mottl, M. J.; 1983. Metabasalts, Axial Hot Springs, and the Structure of Hydrothermal Systems at Mid-Ocean

Ridges. Geol. Soc. Am. Bull., 94, p. 161-180.

Mottl, M. J. and Holland, H. D.; 1978. Chemical Exchange During Hydrothermal Alteration of Basalt by Seawater. I. Experimental Results for Major and Minor Components of Seawater. Geochim. Cosmochim. Acta 43, p. 869-884.

Mukhopadhyay, B.; 1974. Rubidium-Strontium Whole-Rock Geochronology and Strontium Isotope Geology of the Madera Formation near Albuquerque, New Mexico. unpubl. Ph. D. thesis, U. New Mex.

Mukhopadhyay, B.; Brookins, D. G.; and Bolivar, S. L.; 1975. Rb-Sr Whole-Rock Study of the Precambrian Rocks of the Pedernal Hills, New Mexico. Earth Planet. Sci. Lett., 27, p. 283-286.

Mullen, E. D.; 1983. MnO/TiO2/P2O5: A Minor Element Discriminant for Basaltic Rocks of Oceanic Environments and Its Implications for Petrogenesis. Earth Planet. Sci. Lett., 62, p. 53-62.

Myers, D. A. and McKay, E. J.; 1971. Geological Map of the Bosque Peak Quadrangle, Torrance, Valencia, and Bernalillo Counties, New Mexico. U. S. Geol. Sur. Geol. Quad. Map GQ948.

Myers, D. A. and McKay, E. J.; 1972. Geologic Map of the Capilla Peak Quadrangle, Torrance and Valencia Counties, New Mexico. U. S. Geol. Sur. Geol. Quad. Map GQ1008.

Mysen, B. O.; 1977. Partitioning of Cerium, Samrium and Thulium between Pargasite, Garnet Peridotite Minerals and Hydrous Silicate Melts at High Temperatures and Pressures. CIW Yb., 76, p. 588-594.

Mysen, B. O.; 1978a. Experimental Determination of Rare Earth Element Partitioning Between Hydrous Silicate Melt, Amphibole and Garnet Peridotite Minerals at Upper Mantle Pressures and Temperatures. Geochim. Cosmochim. Acta 42, p. 1253-1263.

Mysen, B. O.; 1978b. Limits of Solution of Trace Elements

in Minerals According to Henery's Law: Review of Experimental Data. Geochim. Cosmochim. Acta 42, p. 871-885.

Mysen, B. O.; 1979. Trace Element Partitioning Between Garnet Peridotite Minerals and Water-Rich Vapor: Experimental Data from 5 to 30 Kbar. Am. Mineral., 64, p. 274-287.

Mysen, B. O.; 1981. Rare Earth Element Partitioning Between Minerals and (CO2+H2O) Vapor as a Function of Pressure, Temperature, and Vapor Composition. CIW Yb., 80, p. 347-349.

Mysen, B. O. and Kushiro, 1979. The Effect of Pressure on the Partitioning of Nickel Between Olivine and Aluminosilicate Melt. Earth Planet. Sci. Lett., 42, p. 383-389.

Mysen, B. O.; Kushiro, I.; Nicholls, I. A.; and Ringwood, A. E.; 1974. A Possible Mantle Origin for Andesitic Magmas: Discussion of a Paper by Nicholls and Ringwood. Earth Planet. Sci. Lett., 21, p. 221-229.

Mysen, B. O. and Virgo, D.; 1979. Influence of Melt Structure on Crystal-Liquid Trace-Element Partitioning. CIW Yb., 78, p. 326-327.

Mysen, B. O. and Virgo, D.; 1980. Trace Element Partitioning and Melt Structure: An Experimental Study at 1 Atm Pressure. Geochim. Cosmochim. Acta 44, p. 1917-1930.

Mysen, B. O.; Virgo, D.; and Seifert, F.; 1979. Influence of Melt Structure on Element Partitioning Between Olivine and Melt and Between Clinopyroxene and Melt at 1 Atm. CIW Yb., 78, p. 542-547.

Nelson, B. K. and DePaolo, D. J.; 1985. Rapid Production of Continental Crust 1.7 to 1.9 b. y. ago: Nd Isotopic Evidence from the Basement of the North American Mid-Continent. Geol. Soc. Am. Bull., 96, p. 746-754.

Nelson, C. H.; Meyer, A. W.; Thor, D.; and Larsen, M.; 1986. Crater Lake, Oregon: A Restricted Basin with Base-of-slope Aprons of Nonchannelized Turbidites. Geol., 14, p. 238-241.

Neumann, H.; Mead, J.; and Vitaliano, C. J.; 1954. Trace Element Variation During Fractional Crystallization as Calculated from the Distribution Law. Geochim. Cosmochim. Acta 6, p. 90-99.

Nicholls, I. A.; 1974. Liquids in Equilibrium with Peridotite Mineral Assemblages at High Water Pressures. Contrib. Mineral. Petrol., 45, p. 289-316.

Nicholls, I. A.; 1978. Primary Basaltic Magmas for the Pre-Caldera Volcanic Rocks of Santorini. p. 109-120 in Thera and the Aegean World I. ed. by C. Doumas, Thera and the Aegean World, London.

Nicholls, I. A. and Ringwood, A. E.; 1972. Production of Silica-Saturated Tholeiitic Magmas in Island Arcs. Earth Planet. Sci. Lett., 17, p. 243-246.

Nicholls, I. A. and Ringwood, A. E.; 1973. Effect of Water on Olivine Stability in Tholeiites and the Production of Silica-Saturated Magmas in the Island-Arc Environment. J. Geol., 81, p. 285-300.

Nickolds, S. R. and Allen, R.; 1953. The Geochemistry of Some Igneous Rock Series. Geochim. Cosmochim. Acta 4, p. 105-142.

Nickolds, S. R. and Allen, R.; 1954. The Geochemistry of Some Igneous Rock Series. Pt. 2. Geochim. Cosmochim. Acta 5, p. 245-285.

Nickolds, S. R. and Allen, R.; 1956. The Geochemistry of Some Igneous Rock Series. Pt. 3. Geochim. Cosmochim. Acta 9, p. 34-77.

Noble, D. C.; 1965. Ground-Water Leaching of Sodium from Quickly Cooled Volcanic Rocks. abst. in Am. Mineral., 50, p. 289.

Noble, D. C.; 1966. Comendites in the Western United States. abst. in Geol. Soc. Am. Spec. Pap., 87, p. 117-118.

Noble, D. C.; 1967a. Stress-Corrision Failure and the Hydration of Glassy Silicic Rocks. Am. Mineral., 53, p. 1756-1759.

Noble, D. C.; 1967b. Sodium, Potassium, and Ferrous Iron Contents of Some Secondary Hydrated Natural Silicic Glasses. Am. Mineral., 52, p. 280-286.

Noble, D. C.; Bowman, H. R.; Hebert, A. J.; Silberman, M. L.; Heropoulos, C. E.; Fabbi, B. P.; and Hedge, C. E.; 1975. Chemical and Isotopic Constraints on the Origin of Low-Silica Latite and Andesite from the Andes of Central Peru. Geol., 3, p. 501-504.

Nohda, S.; 1984. Classification of Island Arcs by Nd-Sr Isotopic Data. Geochem. J., 18, p. 1-9.

Norrish, K. and Chappell, B. W.; 1967. X-ray Fluorescence Spectrography. p. 161-214. in Physical Methods in Determinative Mineralogy ed. by J. Zussman, Academic Press Inc., Oxford.

Norrish, K. and Hutton, J. T.; 1969. An Accurate X-ray Spectrographic Method for the Analysis of a Wide Range of Geological Samples. Geochim. Cosmochim. Acta 33, p. 431-454.

Notsu, K.; Kita, I.; and Yamaguchi, T.; 1985. Mantle Contamination Under Akagi Volcano, Japan, As Inferred from Combined Sr-O Isotope Relationships. Geophy. Rev. Lett., 12, p. 365-368.

Nystrom, J. O.; 1984. Rare Earth Element Mobility in Vesicular Lave During Low-Grade Metamorphism. Contrib. Mineral. Petrol., 88, p. 328-331.

Odom, I. E.; 1975. Felspar-Grain Size Relations in Cambrian Arenites, Upper Mississippi Valley, J. Sed. Pet., 45, p. 636-650.

O'Nions, R. K.; Hamilton, P. J.; and Evenson, N. N.; 1977. Variations in 143Nd/144Nd and 87Sr/86Sr Ratios in Oceanic Basalts. Earth Planet. Sci. Lett., 34, p. 13-22.

Osburn, E. F., 1959. Role of Oxygen Pressure in the Crystallization and Differentiation of Basaltic Magma. Am. J. Sci., 257, p. 609-647.

Osburn, E. F.; 1962. Reaction Series for Subalkaline Igneous Rocks Based on Different Oxygen Pressure Conditions. Am. Mineral., 47, p. 211-226.

Oversby, V. M. and Ewart, A.; 1972. Lead Isotopic Composition of Tonga-Kermadec Volcanics and Their Petrogenetic Significance. Contr. Mineral. Petrol., 37, p. 181-210.

Pankhurst, R. J.; 1979. Isotope and Trace Element Evidence for the Origin and Evolution of Caledonian Granites in the Scottish Highland. p. 18-33 in Origin of Granite Batholiths: Geochemical Evidence ed. by M. P. Atherton and J. Tarney, Shiva Publ. Ltd., Kent, U. K.

Parson, W. H.; 1969. Criteria for the Recognition of Volcanic Breccias: Review. Geol. Soc. Am. Mem., 115, p. 263-304.

Patchett, P. J. and Arndt, N. T.; 1986. Nd Isotopes and Tectonics of 1.9-1.7 Ga Crustal Genesis. Earth Planet. Sci. Lett., 78, p. 329-338.

Pearce, J. A.; 1982. Trace Element Characteristics of Lavas from Destructive Plate Boundaries. p. 525-548 in Andesites ed. by R. S.Thorpe, John Wiley and Sons.

Pearce, J. A.; 1983. Role of the Sub-Continental Lithosphere in Magma Genesis at Active Continental Margins. p. 230-272 in Continental Basalts and Mantle Xenoliths ed. by C. J. Hawkesworth and M. J. Norry, Shiva Geology Series.

Pearce, J. A. and Cann. J. R.; 1973. Tectonic Setting of Basic Volcanic Rocks Determined Using Trace Element Analyses. Earth Planet. Sci. Lett., 19, p. 290-300.

Pearce, J. A. and Norry, M. J.; 1979. Petrogenetic Implications of Ti, Zr, Y and Nb Variations in Volcanic Rocks. Contrib. Mineral. Petrol., 69, p. 33-47.

Peccerillo, A. and Taylor, S. R.; 1976. Geochemistry of Eocene Calc-alkaline Volcanic Rocks from the Kastamonu Area, Northern Turkey. Contrib. Mineral. Petrol., 58, p. 63-81.

Perfit, M. R.; and Gast, D. A.; Bence, A. E.; Arculus, R. J.; and Taylor, S. R.; 1980. Chemical Characteristics of Island-Arc Basalts: Implications for Mantle Sources. Chem. Geol., 30, p. 227-256.

Peterson, D. W.; 1970. Ash-Flow Deposits - Their Character, Origin, and Significance. J. Geol. Educa., 18, p. 66-67.

Pettijohn, F. J.; 1983. Chemical Composition of Sandstones - Excluding Carbonate and Volcanic Sands. U. S. Geol. Surv. Prof. Paper 440-S, 21pp.

Pettijohn, F. J.; Potter, P. E.; and Siever, R.; 1972. Sand and Sandstone. Springer-Verlag, New York, 617 pp.

Pharaoh, T. C. and Pearce, J. A.; 1984. Geochemical Evidence for the Geotectonic Setting of Early Proterozoic Metavolcanic Sequences in Lapland. Precam. Res., 25, p. 283-308.

Phelps, D.; 1979. Petrology, Geochemistry and Origin of the Sparta Quartz Diorite-Trondhjemite Complex, Northeastern Oregon. p. 547-579 in Trondhjemites, Dacites and Related Rocks ed. by F. Barker, Elsevier Scien. Publ. Co.

Philpotts, J. A.; Schnetzler, C. C.; and Hart, S. R.; 1969. Submarine Basalts: Some K, Rb, Sr, Ba, Rare-

Earth, H2O and CO2 Data Bearing on Their Alteration, Modification by Plagioclase and Possible Source Materials. Earth Planet. Sci. Lett., 7, p. 293-299.

Pichler, H. and Zeil, W.; 1972. The Cenozoic Rhyolite-Andesite Association of the Chilean Andes. Bull. Volc., 35, p. 424-452.

Poldervaart, A.; 1956. Zircons in Rocks. 2. Igneous Rocks. Am. J. Sci., 254, p. 521-554.

Poldervaart, A. and Elston, W.; 1954. The Calc-Alkaline Series and the Trend of Fractional Crystallization of Basaltic Magma. A New Approach at Graphical Representation. J. Geol. 62, p. 150-162.

Potter, P. E.; 1978. Petrology and Chemistry of Modern Big River Sands. J. Geol., 86, p. 423-449.

Potter, P. E.; 1984. South African Modern Beach Sand and Plate Tectonics. Nature 311, p. 645-648.

Powell, M.; 1978. Crystallization Conditions of Low-Pressure Cumulate Nodules from the Lesser Antilles Island Arc. Earth Planet. Sci. Lett., 39, p. 162-172.

Prefit, M. R.; Gast, D. A.; Bence, A. E.; Arculus, R. J.; and Taylor, S. R.; 1980. Chemical Characteristics of Island-Arc Basalts: Implications for Mantle Sources. Chem. Geol., 30, p. 227-256.

Prestvik, T.; 1982. Basic Volcanic Rocks and Tectonic Setting. A Discussion of the Zr-Ti-Y Discrimination Diagram and Its Suitability for Classification Purposes. Lithos 15, p. 241-247.

Price, R. C. and Taylor, S. R.; 1980. Petrology and Geochemistry of the Banks Peninsula Volcanoes, South Island, New Zealand. Contrib. Mineral. Petrol., 72, p. 1-18.

Pushkar, P.; Steuber, A. M.; Tomblin, J. F.; and Julian,

G. M.; 1973. Strontium Isotopic Ratios in Volcanic Rocks from St. Vincent and St. Lucia, Lesser Antilles. J. Geophy. Res., 78, p. 1279-1287.

Rajamani, V.; Shivkumar, K.; Hanson, G. N.; and Shirey, S. B.; 1985. Geochemistry and Petrogenesis of Amphibolites, Kolar Schist Belt, South India: Evidence for Komatiitic Magma Derived by Low Percentages of Melting of the Mantle. J. Petrol., 26, p. 92-123.

Ramsay, W. R. H.; Crawford, A. J.; and Foden, J. D.; 1984. Field Setting, Mineralogy, Chemistry, and Genesis of Arc Picrites, New Georgia, Solomon Islands. Contrib. Mineral. Petrol., 88, p. 386-402.

Rea, W. J.; 1974. The Volcanic Geology and Petrology of Montserrat, West Indies. J. geol. Soc. Lond., 130, p. 341-355.

Reiche, P.; 1949. Geology of the Manzanita and North Manzano Mountains, New Mexico. Geol. Soc. Am. Bull., 60, p. 1183-1212.

Reid, F. W.; 1983. Origin of the Rhyolitic Rocks of the Taupo Volcanic Zone, New Zealand. J. Vol. Geother. Res., 15, p. 315-338.

Reeves, R. D. and Brook, R. R.; 1978. Trace Element Analysis of Geological Material John Wiley and Sons, New York, 421pp.

Ridley, W. I.; Rhodes, J. M.; Reid, A. M.; Jakes, P.; Shih, C.; and Bass, M. N.; 1974. Basalts from Leg 6 of the Deep-Sea Drilling Project. J. Petrol., 15, p. 140-159.

Ringwood, A. E.; 1974. The Petrological Evolution of Island Arc Systems. J. geol. Soc. Lond., 130, p. 193-204.

Ringwood, A. E.; 1977. Petrogenesis in Island Arc Systems. p. 311-324 in Island Arcs, Deep Sea Trenches, and Back-Arc Basins ed. by M. Talwani and

W. C. Pitman III, Am. Geophy. U., Washington D. C., Maurice Ewing Ser., 1.

Ritchey, J. L.; 1980. Divergent Magmas at Crater Lake, Oregon: Products of Fractional Crystallization and Vertical Zoning in a Shallw, Water-Understaturated Chamber. J. Vol. Geotherm. Res., 7, p. 373-386.

Robertson, J. M.; 1981. Bimodal Volcanism in the Early Proterozoic Pecos Greenstone Belt, Southern Sangre De Cristo Mountains, New Mexico. Geol. Soc. Am. Abst Prog., 13, p. 103.

Roeder, D. L. and Emslie, R. F.; 1970. Olivine-Liquid Equilibrium. Contrib. Mineral. Petrol., 29, p. 275-289.

Rose, Jr., W. I. and Bornhorst, J. J.; 1981. Uranium and Thorium in Selected Quaternary Volcanic Rocks of Guatemala and Sumatra: Evidence of Uranium Redistribution. p. 13-21 in Uranium in Volcanic and Volcaniclastic Rocks ed. by P. C. Goodell and A. C. Waters, A. A. P. G. Studies in Geol., 13.

Roser, B. P. and Korsch, R. J.; 1985. Plate Tectonics and Geochemical Compositions of Sandstones: A Discussion. J. Geol., 93, p. 81-84.

Ross, C. S. and Smith, R. L.; 1955. Water and Other Volatiles in Volcanic Glass. Am. Mineral., 40, p. 1071-1089.

Ross, C. S. and Smith, R. L.; 1961. Ash-Flow Tuffs: Their Origin, Geological Relations and Identification. U. S. Geol. Sur. Prof. Pap., 366, p. 1-81.

Rudnick, R. L.; 1983. Geochemistry ano Tectonic Affinities of a Proterozoic Bimodal Igneous Suite, West Texas. Geol., 11, p. 352-355.

Rutherford, M J.; Sigurdsson, H.; Carey, S.; and Davis, A.; 1985. The May 18, 1980 Eruption of Mount St. Helens 1. Melt Composition and Experimental

Phase Equilibria. J. Geophys. Res., 90, p. 2929-2947.

Sakuyama, M.; 1979. Evidence of Magma Mixing: Petrological Study of Shirouma-Oike Calc-Alkaline Andesite Volcano, Japan. J. Volc. Geothermal. Res., 5, p. 197-208.

Sakuyama, M. 1981. Petrological Study of the Myoko and Kurohime Volcanoes, Japan: Crustallization Sequence and Evidence for Magma Mixing. J. Petrol., 22, p. 553-583.

Sakuyama, M., 1983. Petrology of Arc Volcanic Rocks and Their Origin by Mantle Diapirs. J. Volc. Geothermal. Res., 18, p. 297-320.

Sano, Y., Nakamura, Y., and Wakita, H., 1985. Areal Distribution of 3He/4He Ratios in the Tohoku District, Northeastern Japan. Chem. Geol., 52, p. 1-8.

Sato, H.; 1977. Nickel Content of Basaltic Magmas Identification of Primary Magmas and a Measure of the Degree of Olivine Fractionation. Lithos 10, p. 113-120.

Saunders, A. D. and Tarney, J., 1979. The Geochemistry of Basalts from a Back-Arc Spreading Centre in the East Scotia Sea. Geochim. Cosmochim. Acta 43, p. 555-572.

Saunders, A. D.; Tarney, J.; and Weaver, S. D.; 1980. Transverse Geochemical Variations Across the Antarctic Peninsula: Implications for the Genesis of Calc-alkaline Magmas. Earth Planet. Sci. Lett., 46, p. 344-360.

Sceal, J. S. C. and Weaver, S. D.; 1971. Trace Element Data Bearing on the Origin of Salic Rocks from the Quaternary Volcano Paka, Gregory Rift, Kenya. Earth Planet. Sci. Lett., 12, p. 327-331.

Schmincke, H. -U., 1967. Fused Tuff and Peperites in South-Central Washington. Geol. Soc. Am. Bull., 78, p. 319-330.

Sekine, T.; Katsura, T., and Aramaki, S.; 1979. Water Saturated Phase Relations of Some Andesites with Application to the Estimation of the Initial Temperature and Water Pressure at the Time of Eruption. Geochim. Cosmochim. Acta 43, p. 1367-1376.

Seyfried, W. and Bishcoff, J. L.; 1977. Hydrothermal Transport of Heavy Metals by Seawater: The Role of the Seawater/Basalt Ratios. Earth Planet. Sci. Lett., 34, p. 71-77.

Seyfried, W. and Bishcoff, J. L.; 1981. Experimental Seawater-Basalt Interaction at 300 C, 500 Bars, Chemical Exchange, Secondary Mineral Formation and Implications for the Transport of Heavy Metals. Geochim. Cosmochim. Acts 45, p. 135-147.

Seyfried, W. and Mottl, M. J.; 1982. Hydrothermal Alteration of Basalt by Seawater under Seawater-Dominated Conditions. Geochim. Cosmochim. Acta 46, p. 985-1002.

Shaw, D. M.; 1978. Trace Element Behaviour During Anatexis in the Presence of a Fluid Phase. Geochim. Cosmochim. Acta 42, p. 933-943.

Shervais, J. W.; 1982. Ti-V Plots and the Petrogenesis of Modern and Ophiolitic Lavas. Earth Planet. Sci. Lett., 59, 101-118.

Silver, L. T.; 1978. Precambrian Formations and Precambrian History in Cochise County, Southeastern Arizona. New Mex. Geol. Soc. Guidebk., 29, p. 157-163.

Smith, R. E.; 1957. Geology and Ground-Water Resources of Torrance County, New Mexico. New Mex. Bur. Mines Min. Res. Ground-Water Rept., 5, 186 pp.

Smith, R. E. and Smith S. E.; 1976. Comments on the Use of Ti, Zr, Y, Sr, K, P, and Nb in Classification of Basaltic Magmas. Earth Planet. Sci. Lett., 32, p. 114-120.

Smith R. L.; 1960. Zones and Zonal Variations in Welded Ash Flows. U. S. Geol. Sur. Prof. Pap., 354-F, p. 149-159.

Smith, R. L.; 1979. Ash Flow Magmatism. Geol. Soc. Am. Spec. Pap., 180, p. 5-27.

Snyder, G. L.; 1959. Geology of Little Sitkin Island, Alaska. U. S. Geol. Surv. Bull., 1028-H, p. 169-210.

Soegaard, K. and Eriksson, K. A.; 1985. Evidence of Tide, Storm, and Wave Interaction on a Precambrian Siliclastic Shelf: The 1,700 m. y. Ortega Group, New Mexico. J. Sed. Pet., 55, p. 672-684.

Soegaard, K. and Eriksson, K. A.; 1986. Transition from Arc Volcanism to Stable-Shelf and Subsequent Convergent-Margin Sedimentation in Northern New Mexico From 1.76 GA. J. Geol., 94, p. 47-66.

Sparks, R. S. J.; 1976. Grain Size Variations in Ignimbrites and Implications for the Transport of Pyroclastic Flows. Sediment., 23, p. 147-188.

Sparks, R. S. J.; Self, S.; and Walker, G. P. L.; 1973. Products of Ignimbrite Eruptions. Geol., 1, p. 115-118.

Sparks, R. S. J.; Sigurdsson, H.; and Carey, S. N.; 1980. The Entrance of Pyroclastic Flows Into the Sea: II. Theoritical Considerations on Subaqueous Emplacement and Welding. J. Volcan. Geother. Res., 7, p. 97-105.

Spulber, S. D. and Rutherford, M. J.; 1983. The Origin of Rhyolite and Plagiogranite in Oceanic Crust: An Experimental Study. J. Petrol., 24, p. 1-25.

Stacey, J. S. and Hedlund, D. C.; 1983. Lead-Isotopic Compositions of Diverse Igneous Rocks and Ore Deposits from Southwestern New Mexico and Their Implications for Early Proterozoic Crustal Evolution in the Western

United States. Geol. Soc. Am. Bull., 94, p. 43-57.

Stark, J. T.; 1956. Geology of the South Manzano Mountains, New Mexico. New Mex. Bur. Mines Min. Res. Bull., 34, 46 pp.

Stark, J. T. and Dapples, E. C.; 1946. Geology of the Los Pinos Mountains, New Mexico. Geol. Soc. Am. Bull., 57, p. 1121-1172.

Staudigel, H.; Hart, S. R.; and Richardson, S. H.; 1981. Alteration of the Oceanic Crust: Processes and Timing. Earth Planet. Sci. Lett., 52, p. 311-327.

Stern, R. J.; 1979. On the Origin of Andesite in the Northern Mariana Island Arc: Implications from Agrigan. Contrib. Mineral. Petrol., 68, p. 207-219.

Stewart, D. C.; 1975. Crystal Clots in Calc-Alkaline Andesites as Breakdown Products of High-Al Amphiboles. Contrib. Mineral. Petrol., 53, p. 195-204.

Stewart, D. C. and Thornton, C. P.; 1975. Andesite in Oceanic Regions. Geol., 3, p. 565-568.

Sun, S. -S.; Nesbitt, R. W.; and Sharaskin, A. Y.; 1979. Geochemical Characteristics of Mid-Ocean Ridge Basalts. Earth Planet. Sci. Lett., 44, p. 119-138.

Tanaka, T. and Nishizawa, O.; 1975. Partitioning of REE, Ba and Sr Between Crystal and Liquid Phases for a Natrual Silicate System at 20 kb Pressure. Geochem. J., 9, p. 161-166.

Tarney, J. and Saunders, A. D.; 1979. Trace Element Constraints on the Origin of Cordilleran Batholiths. p. 90-105 in Origin of Granite Batholiths: Geochemical Evidence, ed. by M. B. Atherton and J. Tarney, Shiva Publ., Kent, U. K.

Tatsumi, Y.; Sakuyama, M.; Fukuyama, H.; and Kushiro, I.; 1983. Generation of Arc Basalt Magmas and Thermal Structure of the Mantle Wedge in Subduction Zones. J. Geophy. Res., 88, p. 5815-5825.

Taylor, S. R.; Capp, A. C.; Graham, A. L.; and Blake, D. H.; 1969. Trace Element Abundances in Andesite II. Siapan, Bougainville and Fiji. Contr. Mineral. Petrol., 23, p. 1-26.

Taylor, S. R.; Kaye, M.; White, A. J. R.; Duncan, A. R.; and Ewart, A.; 1969. Genetic Significance of Co, Cr, Ni, Sc, and V Content of Andesites. Geochem. Cosmochim. Acta 33, p. 275-286.

Thomas, J. J.; Shuster, R. D.; and Bickford, M. E.; 1984. A Terrane of 1,350 to 1,400-m.y.-old Silicic Volcanic and Plutonic Rocks in the Buried Proterozoic of the Mid-Continent and in the Wet Mountains, Colorado. Geol. Soc. Am. Bull., 95, p. 1150-1157.

Thompson, G.; 1973. A Geochemical Study of the Low-Temperature Interaction of Sea-Water and Oceanic Igneous Rocks. EOS 54, p. 1015-1019.

Thompson, G. and Humphris, S. E.; 1984. Petrology and Geochemistry of Rocks from the Walvis Ridge: Deep Sea Drilling Project Leg 74, Sites 525, 527, and 528. Initial Rept. of DSDP, 74, p. 755-764.

Thompson, R. N.; Dickin, A. P.; Gibson, I. L.; and Morrison, M. A.; 1982. Elemental Fingerprints of Isotopic Contamination of Hebridean Palaeocene Mantle-Derived Magmas by Archean Sial. Contrib. Mineral. Petrol., 79, p. 159-168.

Thompson, R. N.; Morrison, M. A.; Mattey, D. P.; Dickin, A. P.; and Moorbath, S.; 1080. An Assessment of the Th-Hf-Ta Diagram as a Discriminant for Tectonomagmatic Classification and in the Detection of Crustal Contamination of Magmas. Earth Planet. Sci. Lett., 50, p. 1-10.

Thorpe, R. S.; Francis, P. W.; and Moorbath, S.; 1979.

Rare Earth and Strontium Isotope Evidence Concerning the Petrogenesis of North Chilean Ignimbrites. Earth Planet. Sci. Lett., 42, p. 354-367.

Thorpe, R. S.; Potts, P. J.; and Francis, P. W.; 1976. Rare Earth Data and Petrogenesis of Andesite from North Chilean Andes. Contr. Mineral. Petrol., 54, p. 65-78.

Tilley, C. E.; 1950. Some Aspects of Magmatic Evolution. Quart. J. Geol. Soc. Lond., 106, p. 37-61.

Titus, F. B., Jr.; 1963. Geology and Ground-Water Conditions in Eastern Valencia County, New Mexico. New Mex. Bur. Mines Mineral. Resour. Rept., 7, 113pp.

Uto, K.; 1986. Variation of Al2O3 Content in Late Cenozoic Japanese Basalts: A Re-Examination of Kuno's High-Alumina Basalt. J. Volcan. Geotherm. Res., 29, p. 397-411.

Valloni, R.; 1985. Reading Provenance from Modern Marine Sands. p. 309-332 in Provenance of Arinites ed. by G. G. Zaffa, D. Reidel Publ. Co.

Valloni, R. and Mezzadri, G.; 1984. Compositional Suites of Terrigenous Deep-Sea Sands of the Present Continental Margins. Sediment., 31, p. 353-364.

van de Kamp, P. C. and Leake, B. E.; 1986. Petrography and Geochemistry of Feldspathic and Mafic Sediments of the Northeastern Pacific Margin. Trans. R. Soc. Edinburgh, Earth Sci., 76, p. 411-449.

Van Schmus, W. R. and Bickford, M. E.; 1981. Proterozoic Chronology and Evolution of the Midcontinent Region, North America p. 261-296 in Precambrian Plate Tectonics ed. by A. Kroner, Elsevier, Amsterdam.

Velbel, M. A.; 1985. Mineralogically Mature Sandstones in Accretionary Prisms. J. Sed. Petrol., 55, p. 685-690.

Villemant, B.; Jaffrezic, H.; Joron, J. L. and Treuil, M.; 1981. Distribution Coefficients of Major and Trace Elements: Fractional Crystallization in the Alkali Basalt Series of Chaine des Puys (Massif Central, France). Geochim. Cosmochim. Acta 45, p. 1997-2016.

Wada, K.; 1981. Contrasted Petrological Relations Between Tholeiitic and Calc-alkalic Series from Funagata Volcano, Northeast Japan. J. Jap. Assoc. Min. Petr. Econ. Geol., 76, p. 215-232.

Waldron, H. H.; 1961. Geologic Reconnaissance of Frosty Peak Volcano and Vicinity, Alaska. U. S. Geol. Surv. Bull., 1028-F, p. 677-708.

Walker, J. P. L.; 1971. Grain-Size Characteristics of Pyroclastic Deposits. J. Geol., 79, p. 696-714.

Walker, R. G.; 1976. Facies Models 1. General Introduction. Geosci. Can., 3, p. 21-24.

Wang, C.; 1980. Sediment Subduction and Frictional Sliding in a Subduction Zone. Geology 8, p. 530-533.

Watson, E. B.; 1976. Two-Liquid Partition Coefficients: Experimental Data and Geochemical Implications. Contr. Mineral. Petrol., 56, p. 119-134.

Watson, E. B.; 1977. Partitioning of Manganese Between Forsterite and Silicate Liquid. Geochem. Cosmochim. Acta 41, p. 1363-1374.

Watson, E. B.; 1979. Sircon Saturation in Felsic Liquids: Experimental Results and Applications to Trace Element Geochemistry. Contrib. Mineral. Petrol., 70, p. 407-413.

Watson, E. B.; 1980a. Apatite and Phosphorus in Mantle Source Regions: An Experimental Study of Apatite/Melt Equilibria at Pressures to 25 Kbar. Earth Planet. Sci. Lett., 51, p. 322-335.

Watson, E. B.; 1980b. Some Experimentally Determined Zircon/Liquid Partition Coefficients for the Rare Earth Elements. Geochim. Cosmochim. Acta 44, p. 895-897.

Watson, E. B.; 1985. Henry's Law Behaviour in Simple Systems and in Magmas: Criteria for Discerning Concentration-Dependent Partition Coefficients in Nature. Geochem. Cosmochim. Acta 49, p. 917-923.

Watson, E. B. and Harrison, T. M.; 1983. Zircon Saturation Revisited: Temperature and Compostion Effects in a Variety of Crustal Magma Types. Earth Planet. Sci. Lett., 64, p. 295-304.

Weaver, B. L. and Tarney, J.; 1981. Lewisian Gneiss Geochemistry and Archean Crustal Development Models. Earth Planet. Sci. Lett., 55, p. 171-180.

Weill, D. F. and Drake, M. J.; 1973. Europium Anomaly in Plagioclase Feldspar: Experimental Results and Semiquantitative Model. Science 180, p. 1059-1060.

Wendlandt, R. F. and Harrison, W. J.; 1978. Phase Equilibria and Rare Earth Element Partitioning Between Coexisting Immiscible Carbonate and Silicate Liquids and CO2 Vapor in the System K2O-Al2O3-SiO2-CO2 CIW Yearbk., 77, p. 695-703.

Whetten, J. T. and Hawkins, J. W.; 1970. Diagenetic Origin of Graywacke Matrix Minerals. Sediment., 15, p. 347-361.

White, D. L.; 1978. Rb-Sr Isochron Ages of Some Precambrian Plutons in South-Central New Mexico. Isochron/West 21, p. 8-14.

White, W. M. and Patchett, J.; 1984. Hf-Nd-Sr Isotopes and Incompatible Element Abundances in Island Arcs: Implications for Magma Origins and Crust-Mantle Evolution. Earth Planet. Sci. Lett., 67, p. 167-185.

Whitford, D. J.; Compston, W.; Nicholls, I. A.; and Abbott, M. J.; 1977. Geochemistry of Late Cenozoic

Lavas from Eastern Indonesia: Role of Subducted Sediments in Petrogenesis. Geology 5, p. 571-575.

Whitford, D. J. and Jezek, P. A.; 1979. Origin of Late-Cenozoic Lavas from the Banda Arc, Indonesia: Trace Element and Sr Isotope Evidence. Contrib. Mineral. Petrol., 68, p. 141-150.

Wilcox, R. E.; 1954. Petrology of Particutin Volcano, Mexico. U. S. Geol. Surv. Bull., 965-C.

Williams, H. and McBirney, A.; 1979. Volcanology. Freeman, Cooper and Co., San Fransico, 391pp.

Winchester, J. A. and Floyd, P. A.; 1976. Geochemical Magma Type Discrimination: Application to Altered and Metamorphosed Basic Igneous Rocks. Earth Planet. Sci. Lett., 28, p. 459-469.

Winchester, J. A. and Floyd, P. A.; 1977. Geochemical Discrimination of Different Magma Series and Their Differentiation Products Using Immobile Elements. Chem. Geol., 20, p. 325-343.

Wohletz, K. H. and Sherridan, M. F.; 1979. A Model of Pyroclastic Surge. Geol. Soc. Am. Spec. Pap., 180, p. 177-194.

Wood, B. J.; 1976. Partitioning of Samarium between Garnet and Liquid. CIW Yb., 75, p. 659-662.

Wood, D. A.; 1979. A Variably Veined Suboceanic Upper Mantle - Genetic Significance for Mid-Ocean Ridge Basalts from Geochemical Evidence. Geol., 7, p. 499-503.

Wood, D. A.; 1980. The Applications of a Th-Hf-Ta Diagram to Problems of Tectonomagmatic Classification and to Establishing the Nature of Crustal Contamination of Basaltic Lavas of the British Tertiary Volcanic Province. Earth Planet. Sci. Lett., 50, p. 11-30.

Wood, D. A.; Gibson, I. L.; and Thompson, R. N.; 1976.

Elemental Mobility During Zeolite Facies Metamorphism of the Tertiary Basalts of Eastern Iceland. Contrib. Mineral. Petrol., 55, p. 241-254.

Wood, D. A.; Joron, J. -L.: and Treuil, M.; 1979. A Re-Apprasial of the Use of Trace Elements to Classify and Discriminate Between Magma Series Erupted in Different Tectonic Settings. Earth Planet. Sci. Lett., 45, p. 326-336.

Woodhead, J. D. and Fraser, D. G.; 1985. Pb, Sr, and 10Be Isotopic Studies of Volcanic Rocks from the Northern Mariana Islands. Implications for Magma Genesis and Crustal Recycling in the Western Pacific. Geochem. Cosmochim. Acta 49, p. 1925-1930.

Woodward, L. A.; 1969. Metamorphic and Igneous Rocks of Pedernal Hills Area, Torrance County, New Mexico. abst. in Geol. Soc. Am. Spec. Pap., 121, p. 579-580.

Woodward, L. A. and Fitzsimmons, J. P., 1967. Precambrian Banded Iron Formation, Pedernal Peak, Torrance County, New Mexico. abst. in New Mex. Geol. Soc. Guidebk., 18, p. 228.

Wright, A. V. and Coward, M. P.; 1977. Rootless Vents in Welded Ash-Flow Tuffs from Northern Snowdonia, North Wales, Indicating Deposition in a Shallow Water Environment. Geol. Mag., 114, p. 133-140.

Wright, J. B.; 1969. A Simple Alkalinity Ratio and Its Application to Questions of Non-Orogenic Granite Genesis. Geol. Mag., 106, p. 370-384.

Wright, J. V. and Walker, G. P. L.; 1977. The Ignimbrite Source Problem: Significance of a Co-Ignimbrite Lag-Fall Deposit. Geology 5, p. 729-732.

Wright, J. V.; Smith, A. L.; and Self, S.; 1980. A Working Terminology of Pyroclastic Deposits. J. Volcan. Geotherm. Res., 8, p. 315-336.

Wyllie, P. J.; 1963. Effects of the Changes in Slope

Occuring on Liquidus and Solidus Paths in the System Diopside-Anorthite-Albite. Mineral. Soc. Am. Spec. Paper 1, p. 204-212.

Wyllie, P. J.; Huang, W. -L.; Stern, C. R.; and Maaloe, S.; 1976. Granitic Magmas: Possible and Impossible Sources, Water Contents, and Crystallization Sequences. Can. J. Earth Sci., 13, p. 1007-1019.

Yamada, E.; 1984. Subaqueous Pyroclastic Flows: Their Development and Their Deposits. p. 29-35 in Margin Basin Geology ed. by B. P. Kokelaar and M. F. Howells, Geol. Soc. Spec. Publ., 16.

Yamaguchi, T.; 1984. Fractional Crystallization of the Island Arc Tholeiitic Magma in Hotuka Volcano. J. Jap. Assoc. Min. Petr. Econ. Geol., 79, p. 214-232.

Yoder, H. S.; 1969. Calcalkalic Andesites: Experimental Data Bearing on the Origin of Their Assumed Characteristics. p. 77-89 in Proceedings of the Andesite Conference ed. by A. R. McBirney, Dep. Geol. Mineral. Indust. Oregon Bull., 65.

Yoder, H. S. and Tilley, C. E.; 1962. Origin of Basalt Magmas: An Experimental Study of Natural and Synthetic Rock Systems. J. Petrol., 3, p. 342-532.

Zielinski, R. A.; 1982. The Mobility of Uranium and Other Elements During Alteration of Rhyolite Ash to Montmorillonite: A Case Study in the Troublesome Formation, Colorado, U. S. A. Chem. Geol., 35, p. 185-204.

Zielinski, R. A.; Lipman, P. W.; and Millard, Jr., H. T.; 1977. Minor-Element Abundances in Obsidian, Perlite, and Felsite of Calc-alkaline Rhyolites. Am. Mineral., 62, p. 426-437.